

Design, Analysis and Trajectory Tracking Control of Underactuated Mobile Capsule Robots



Md Nazmul Huda

Faculty of Science and Technology

Bournemouth University

This dissertation is submitted for the degree of
Doctor of Philosophy

2016

© This copy of the thesis has been supplied on condition that anyone who consults it is understood to recognise that its copyright rests with its author and due acknowledgement must always be made of the use of any material contained in, or derived from this thesis.

I would like to dedicate this thesis to my loving mother, my siblings and my departed father.

Declaration

I hereby declare that except where specific reference is made to the work of others, the contents of this thesis are original work of the author.

Md Nazmul Huda
2016

Acknowledgements

The completion of this work has been made possible with the guidance, support and encouragement of many individuals to whom I owe a lot. First of all, I would like to express my gratitude to my first supervisor and mentor Prof. Hongnian Yu who inspired me to become what I am today. I thank him for allowing me to work in his group, for believing in me, for allowing me to see him anytime, for providing constructive feedback during every discussion and above all his kindness and support. I would like to thank my second supervisor Dr. Shuang Cang for providing constructive feedback on my research.

I would like to thank Mr. S.O. Wane, Prof. M.J. Goodwin, Dr. Raian Ali, Dr. Chris Richardson, Prof. Mark Hadfield and Dr. Andrew Main for their support and valuable remarks. I am thankful to my friends Muntaseer Hussain, Rakesh Yedla, Upendra Dayaratne, Pengcheng Liu, Pree Thiengburanathum, Mahbub Mishu, Abu Saifullah and Dr. Mehdi Chowdhury who provided kind advice during my difficult times and ensured my well-being and maintained a homely environment during my stay in UK.

I would like to thank my entire family for their confidence on me, for motivating me to pursue my endeavors, for their love, support, patience and encouragement throughout my life. I would like to thank two countries Bangladesh and UK for providing opportunities to get world-class education.

Finally, I would like to thank almighty Allah and his Rasul for providing me the strength and patience to come this far.

Abstract

The research on capsule robots (capsubots) has received attraction in recent years because of their compactness, simple structure and their potential use in medical diagnosis (e.g. capsule endoscopy), treatment and surgical assistance. The medical diagnostic capability of a capsule endoscope - which moves with the aid of visceral peristalsis - in the GI (gastro-intestinal) tract can be improved by adding propulsion to it e.g. legged, magnetic or capsobot-type propulsion.

Driven by the above needs this thesis presents the design, analysis, trajectory tracking control and implementation of underactuated mobile capsule robots. These capsule robots can be modified and used in in-vivo medical applications. Researches on the capsobot-type underactuated system focus on the stabilization of the robot and tracking the actuated configuration. However trajectory tracking control of an unactuated configuration (i.e. the robot motion) was not considered in the literature though it is the primary requirement of any mobile robot and also crucial for many applications such as in-vivo inspection. Trajectory tracking control for this class of underactuated mechanical systems is still an open issue. This thesis presents a strategy to solve this issue.

This thesis presents three robots namely a one-dimensional (1D) capsule robot, a 2D capsule robot and a 2D hybrid capsule robot with incremental capability. Two new acceleration profiles (utroque and contrarium) for the inner mass (IM) - internal moving part of the capsule robot - are proposed, analysed and implemented for the motion generation of the capsule robots. This thesis proposes a two-stage control strategy for the motion control of an underactuated capsule robot. A segment-wise trajectory tracking algorithm is developed for the 1D capsule robot. Theoretical analysis of the algorithm is presented and simulation is performed in the Matlab/Simulink environment based on the theoretical analysis. The algorithm is implemented in the developed capsule robot, the experimentation is performed and the results are critically analyzed. A trajectory tracking control algorithm combining segment-wise and behaviour-based control is proposed for the 2D capsule robot. Detailed theoretical analysis is presented and the simulation is performed to investigate the robustness of the trajectory tracking algorithm to friction uncertainties. A 2D capsule robot prototype

is developed and the experimentation is performed. A novel 2D hybrid robot with four modes of operation - legless motion mode, legged motion mode, hybrid motion mode and anchoring mode - is also designed which uses one set of actuators in all operating modes. The theoretical analysis, modelling and simulation is performed.

This thesis demonstrates effective ways of propulsion for in-vivo applications. The outer-shape of the 1D and 2D capsule robots can be customized according to the requirement of the applications, as the propulsion mechanisms are completely internal. These robots are also hermetically sealable (enclosed) which is a safety feature for the in-vivo robots. This thesis addresses the trajectory tracking control of the capsubot-type robot for the first time. During the experimentation the 1D robot prototype tracks the desired position trajectory with some error (relative mean absolute error: 16%). The trajectory tracking performance for the 2D capsubot improves as the segment time decreases whereas tracking performance declines as the friction uncertainty increases. The theoretical analysis, simulation and experimental results validate the proposed acceleration profiles and trajectory tracking control algorithms. The designed hybrid robot combines the best aspects of the legless and legged motions. The hybrid robot is capable of stopping in a suspected region and remain stationary for a prolonged observation for the in-vivo applications while withstanding the visceral peristalsis.

Contents

Contents	xi
List of Figures	xv
List of Tables	xix
1 Introduction	1
1.1 Background and Research Motivation	1
1.2 Aims and Objectives	5
1.2.1 Aims	5
1.2.2 Objectives	5
1.3 Research Contributions	6
1.4 Thesis Outline	6
1.5 List of Publications	9
1.5.1 Patent	9
1.5.2 Journals and Conferences	9
2 Literature Review	11
2.1 Introduction	11
2.2 Needs and Challenges of Medical Robots	12
2.2.1 Needs of Medical Robots	12
2.2.2 Challenges	14
2.3 Classification of Minimally Invasive Medical Robots	16
2.4 External Large Medical Robots	17
2.5 Miniature in-vivo Robot: Laparoscopic Robot	18
2.5.1 Background	18
2.5.2 In-vivo Laparoscopic Robots Under Research	19
2.6 Miniature in-vivo Robot: Endoscopic robot	25

2.6.1	Background	25
2.6.2	In-vivo Endoscopic Robots Under Research	26
2.7	Control of Underactuated Mechanical Systems	40
2.7.1	Dynamics of UMS	40
2.7.2	Control Problems	40
2.7.3	Stabilization Control / Set-point Regulation	41
2.7.4	Trajectory Tracking Control	42
2.8	Summary	43
2.9	Scope of Contribution	44
3	1D Capsule Robot	47
3.1	Introduction	47
3.2	Modelling, Problem Statement and Proposed Strategy	47
3.2.1	Dynamic Modelling	47
3.2.2	Problem Statement and Proposed Strategy	48
3.3	Proposed Acceleration Profiles and Motion Generation	49
3.3.1	Proposed Acceleration Profiles	49
3.3.2	Motion Generation	51
3.3.3	Optimum Selection of Acceleration Profile Parameters	56
3.3.4	Comparison with Other Profiles	58
3.4	Proposed Control Approach	59
3.4.1	Preparation Stage: Database creation	60
3.4.2	Stage 1: Desired IM Trajectory Generation	61
3.4.3	Stage 2 : Control of the IM	65
3.5	Simulation, Experiments and Analysis	66
3.5.1	Simulation Setup and Results	66
3.5.2	Experimental Setup and Results	68
3.5.3	Analysis	72
3.6	Summary	79
4	2D Capsule Robot	81
4.1	Introduction	81
4.2	System Description and Defining the Behaviours	83
4.2.1	System Description: 2D Capsubot Model	83
4.2.2	System Description: Motion Generation and Switching	84
4.2.3	System Description: Basis Behaviours	87

4.2.4	Reference Frame Allocation	89
4.3	Trajectory Tracking of 2D Capsubot	91
4.3.1	Proposed Trajectory Tracking Algorithm	91
4.3.2	Methods for Implementing the Proposed Trajectory Tracking Algorithm	93
4.3.3	Simulation Results and Discussion	102
4.4	Experimentation	108
4.4.1	Experimental Setup	108
4.4.2	Control Strategy	110
4.4.3	Experimental Results and Analysis	111
4.5	Summary	115
5	Hybrid Robot	119
5.1	Introduction	119
5.2	Hybrid Robot Design	119
5.3	Working Principle	123
5.3.1	Legless Mode	125
5.3.2	Legged Mode	125
5.3.3	Hybrid Mode	126
5.3.4	Anchoring Mode	127
5.4	Modelling of the Hybrid Robot	128
5.4.1	Modelling of the Legless Mode	128
5.4.2	Modelling of the Legged Mode	128
5.4.3	Modelling of the Hybrid Mode	134
5.4.4	Modelling of the Anchoring Mode	136
5.5	Simulation Results and Discussion	137
5.5.1	Legless Mode	137
5.5.2	Legged Mode	137
5.5.3	Hybrid Mode	139
5.6	Summary	139
6	Conclusions and Future Works	143
6.1	Conclusions	143
6.2	Aims and Objectives Revisited	144
6.3	Future Works	147

Appendix A	151
A.1 Simulink Model of 1D Capsubot	151
Appendix B	157
B.1 Simulink Model of 2D Capsubot	157
References	163

List of Figures

2.1	Fixed-base in vivo laparoscopic robots	21
2.2	Wheeled in vivo laparoscopic robots	23
2.3	In vivo magnetic drive laparoscopic robots	24
2.4	Suction-based in vivo robots	26
2.5	Legged endoscopic robots	28
2.6	Biomimetic endoscopic robots	32
2.7	Electric stimulation propulsion robot and swimming robot	33
2.8	Internal reaction locomotion robot	35
2.9	Magnetic and hybrid propulsion endoscopic robots	38
3.1	Schematic of capsobot with reference line	48
3.2	Schematic diagram of the proposed control system of the capsobot	49
3.3	Acceleration profiles for the IM	52
3.4	Four possible scenarios of the capsobot for motion generation	53
3.5	Accelerations, velocities and positions of the IM and the capsobot for the utroque profile for the scenario of Figs. 3.4(a) and 3.3(a)	55
3.6	Accelerations, velocities and positions of the IM and the capsobot for the contrarium profile for the scenario of Figs. 3.4(c) and 3.3(c)	57
3.7	Desired trajectory for the 1D capsobot trajectory tracking (segment-wise tracking)	62
3.8	Flow chart of the selection algorithm for the 1D capsobot trajectory tracking	63
3.9	Simulated results for the capsobot trajectory tracking using the proposed control	67
3.10	CAD design and implemented capsobot	70
3.11	Experimental results for position trajectory tracking using proposed control approach	73

3.12	Experimental and simulation results for position trajectory tracking using proposed control approach	74
3.13	Experimental and simulation capsobot position trajectory tracking error using proposed control approach	75
4.1	Top view of the 2D capsobot (a) x , y and ϕ are generalised coordinate and measured with respect to the fixed reference frame $O(X_O, Y_O)$ (b) Rotation ϕ_{Mj} is measured with respect to the local frame R_j - frame L_j rotates with the capsobot during rotation (here positive direction of rotational motion is shown) (c) Translation x_{Mj} and x_{mi} are measured with respect to the local frame L_j (here positive direction of linear motion is shown)	82
4.2	Examples of acceleration profile for the (a) Motion modes (linear and rotational) (b) Switching mode	85
4.3	Movements of the IMs for various motion behaviours (a) Linear (FW) (b) Linear (BW) (c) Rotational (CW) (d) Rotational (CCW)	88
4.4	(a) Desired position trajectory with time axis ($x = At, y = B\sin(\Omega t)$); where, $A = \frac{1}{3}, B = 6, \Omega = \frac{1}{10}$ (b) Taking segments from the desired position trajectory (part of the trajectory is shown)	92
4.5	Block diagram of the behaviour-based control of the 2D capsobot (one of the behaviour set from A to I is used to track a segment)	96
4.6	Selection algorithm for Fig. 4.5 (ϵ_1 and ϵ_2 are small positive numbers)	97
4.7	Simulated control forces on the IMs for the segment time, $T=2s$ (a) IM_1 (b) IM_2 ; Trajectories of the 2D capsobot for $T = 2s$ (c) Segment-wise translation trajectory (d) Orientation/ steering angle trajectory	103
4.8	Trajectories of the 2D capsobot for the segment time, $T = 2s$ (a) x trajectory (by using $x_j = x_{j-1} + (d_j - d_{j-1})\cos(\phi_j)$) (b) y trajectory (by using $y_j = y_{j-1} + (d_j - d_{j-1})\sin(\phi_j)$) (c) Position trajectory on $x - y$ plane with time axis	105
4.9	Comparison of the trajectory tracking errors for various segment times (a) steering angle (ϕ) trajectory (b) x trajectory (c) y trajectory	106
4.10	Implemented capsobot	109
4.11	A) Modified linear DC motor (LM) B) Motion controller	110
4.12	Schematic diagram of stage 2 of the control system	111
4.13	Experimental results for the linear motion	113
4.14	Experimental results for the rotational motion	114

4.15	Comparison between the experimental and simulation results for the linear motion	116
4.16	Comparison between the experimental and simulation results for the rotational motion	117
5.1	A perspective view of a hybrid robot having two sets of projecting legs. . .	120
5.2	A partially exploded perspective view of the hybrid robot of Fig. 5.1 where the leg-sets are coupled with the cylindrical rods.	121
5.3	A rear end view of a gripper, leg, and nut assembly of a hybrid robot	122
5.4	A perspective view of a gripper, leg, and nut assembly of a hybrid robot . .	122
5.5	End view of a nut and pin assembly of a hybrid robot	123
5.6	First and second configurations, a side view of a linear actuator, leg, and nut assembly of the hybrid robot when configured for legged motion	124
5.7	A rear end view of one of the linear actuator, leg, and nut assembly in legged mode	124
5.8	Leg and cylindrical rod movements in Legged mode	126
5.9	IM movements in hybrid mode	127
5.10	Hybrid robot in anchoring mode	127
5.11	Leg-opening 140 degrees - the robot is stationary	129
5.12	Leg closing: the leg (red dotted and blue solid) in two positions (140° and 110°) when the leg is not facing any obstacle - the robot does not move . .	130
5.13	Leg closing: the leg (red dotted and blue solid) in two positions (140° and 110°) if the robot moves	132
5.14	Leg opening: the leg (blue solid and red dotted) in two positions (110° and 140°) - the robot remains stationary	134
5.15	Acting forces for one leg when F_{ext} exceeds the limiting value of f_{leg} (applicable to both hybrid and anchoring mode)	136
5.16	Legged movement in one closing cycle -	138
5.17	Simulation results for hybrid translation-clockwise rotation	140
5.18	Simulation results for hybrid translation-anti-clockwise rotation	141
A.1	Simulink model of the 1D capsbot trajectory tracking	152
A.2	Subsystems of the Simulink model of the 1D capsbot trajectory tracking control of A.1	153
A.3	Subsystems of the trajectory tracking controller subsystem of Fig. A.2(a) .	154
A.4	Subsystems of the capsbot model subsystem of Fig. A.2(b)	155

B.1	Simulink model of the 2D capsobot trajectory tracking control	158
B.2	Subsystems of the Simulink model of the 2D capsobot trajectory tracking control of B.1	159
B.3	Subsystems of the trajectory tracking controller subsystem of Fig. B.2(a) . .	160
B.4	Simulink model for equation (4.1) - a subsystem of the capsobot model subsystem of Fig. B.2(b)	161
B.5	Simulink model for equations (4.2) and (4.3) - a subsystem of the capsobot model subsystem of Fig. B.2(b)	161
B.6	Simulink model for equations (4.4) - a subsystem of the capsobot model subsystem of Fig. B.2(b)	162

List of Tables

2.1	Comparison of minimally invasive diagnosis and intervention robots based on key features	16
2.2	Comparison among in-vivo laparoscopic robots based on key features	20
2.3	Comparison among legged endoscopic robots based on key features	29
2.4	Comparison among biomimetic endoscopic robots based on key features	31
2.5	Comparison among external propulsion endoscopic robots based on key features	36
3.1	Parameters of the developed 1D capsobot	66
3.2	Parameters of the developed capsobot to create the database	72
3.3	Database for the utroque profile	72
3.4	Database for the contrarium profile	75
3.5	Comparison of the algorithm performance for simulation and experiments	76
4.1	Comparison of the algorithm performance for various segment times	107
4.2	Comparison of the algorithm performance for various friction changes where the segment time = 1s	108
4.3	Parameter values of the 2D capsobot	112
5.1	Description of the notation used in this chapter	128
5.2	Parameters for the hybrid robot	137

Chapter 1

Introduction

1.1 Background and Research Motivation

Minimally invasive diagnosis and interventions feature safe and reliable techniques and result shorter hospital stays, less pain, more rapid return to daily work, and improved immunological response compared to the conventional ways. Robot-assisted laparoscopic and thoracoscopic surgeries became popular because of its reduced invasiveness and improved reliability [1]. Researches to develop minimally invasive devices for surgical and diagnostic applications are also gaining popularity among the robotics research community [2–9]. Furthermore miniature in-vivo mobile robots are being developed to be utilized in in-vivo diagnosis and surgical procedures [10–16].

In-vivo laparoscopic robots may improve patient experience during and after the surgical procedure by providing the surgeon with vision and surgical task assistance. Researches show promising results in various in-vivo experiments though currently they lack precise control [17, 18]. The ultimate goal of this approach is to develop a multiple cooperative modular robot which together can perform a complete surgery. They are small and easily transportable [19]. They could be life-saving for remote areas e.g. battlefield and even for space mission where large medical equipment are not available. 90% of the battlefield deaths happen within 30 minutes of initial injury, long before the patients can be transported to operation theatre. 50% of deaths happen because of thoracic and abdominal haemorrhage [20]. The wireless in-vivo robots can potentially be used for initial monitoring, treatments and basic surgery before the patient can be transported to the hospital and thus be able to reduce mortality rate. The robots can be deployed by non-medical person and then a surgeon can operate it remotely to provide the medical care [21].

The researchers have developed camera robots [15, 22–24], mobile wheeled robots

[18, 19, 25], magnetic drive robots [14, 26–30] and suction based robots [7, 31] for biopsy and, vision and task assistance during laparoscopic surgery. In-vivo (porcine) tests of the in-vivo laparoscopic robots show impressive results. However in-vivo robots having external moving parts (e.g. wheeled robot) raises the concern of the safety of the internal soft tissue while moving over the abdominal organs (e.g. liver, spleen, intestine, and stomach). The wheeled robots reported in [17] moves over the abdominal organs without causing any visible tissue damage. However microscopic or internal damages have not been investigated. Also amount of tissue losses depends on tissue composition (e.g. fat, muscle), layer thickness and geometry, and histological characteristics [17]. The robots with magnetic drives move either along the abdominal wall [14, 26, 27, 29, 30] or within the abdominal cavity over the abdominal organs [28]. The external magnet could be fixed on a base [28] or could be operated by a human operator [14, 27] or attached to a robotic-arm [26]. The researchers [28] report that the precise robot positioning was not possible and requires further investigation. Although most of the developed robots are tethered for power and communication, the wheeled robot presented in [17] relies on battery for power and communicates wirelessly. An intra-abdominal zigbee wireless network is used to communicate between the anchoring frame and the array of robots used in [29]. The in-vivo porcine experiments using multiple cooperative robots [10, 14, 17] demonstrate the feasibility of using miniature laparoscopic robots to assist in surgical procedures. However, the robots are still in the in-vivo animal evaluation stage. Further improvements are necessary before a clinical trial is possible [10, 14, 17].

In 2000, Given Imaging [32] introduced wireless capsule endoscope (WCE) which has LEDs and a camera in front for the inspection of the GI (gastro-intestinal) track. It is a non-invasive process and easy to perform and thus encourages the patients to go for the inspection of a potential GI disease [33]. However these capsules are moved by the aid of visceral peristalsis and do not have control over their movements and orientations which result low diagnostic accuracy compared to the traditional probe endoscopy [34]. Mobile robots have been being developed to be integrated with the wireless capsule endoscope (WCE) to provide the capsule endoscope self-propulsion capability. It will potentially improve the diagnostic capability and accuracy of wireless capsule endoscope (WCE) [35].

Mobile robots designed for capsule endoscopes i.e. for GI track can be classified based on the locomotion principles/mechanisms as external propulsion robot (magnetic propulsion robot) [28, 36, 37], internal propulsion robot [17, 38–41] and hybrid propulsion robot [11, 42]. Internal propulsion robot has the propulsion embedded with the robot whereas for external propulsion the propulsive force is generated by an external system. A hybrid

propulsion robot uses more than one propulsion mechanisms usually a combination of external and internal propulsions.

The main advantage of the external propulsion is that it does not require onboard actuators and mechanisms and, thus requires less energy compared to internal propulsion. The robot still needs a magnetic component onboard which interacts with the external robot. However this magnetic component takes smaller space compared to the internal propulsion mechanism [43]. The robot can be made hermetically sealable as there are no external moving parts i.e. no limbs or legs. However precise movement and control is not always possible for external magnetic propulsion because of nonlinearity of magnetic field [37]. Also tissue-distending or removal of tissue from the camera is not possible using this mechanism. There is a risk of getting stuck in a collapsed region inside the GI track which inspired to develop a hybrid robot in [42]. Furthermore MRI system [44, 45] and robotic navigation system (e.g. Stereotaxis [46, 47], Yaskawa Motoman [12, 36]) used for many external propulsions are expensive and bulky and, the control is complex. Thus external propulsion robot actuated by MRI or robotic navigation system may not be deployed outside the hospital or by a nonclinical person [12, 36].

The internal propulsion robot can achieve precise position control compared to the external propulsion robot because of having the actuator on board. Some of the internal propulsion robots have the capability to distend lumen to facilitate the movement and to distend away the tissue from the camera lens [40]. However internal propulsion means there is a need of on-board power to drive the actuators. It is a challenge to accommodate the propulsion mechanism, power source (e.g. battery pack) and other relevant components in a capsule body while keeping the robot size within the limit of a standard capsule endoscope. Most of the internal propulsion robots have limbs or legs which may injure the internal soft tissue. A wider leg may reduce the risk of tissue damage [48]. Moreover it is challenging to make a hermetically sealable robot which has legs or limbs. Most of the legged locomotion work was performed before 2011 and the research on this area decreased because of the on-board power requirement and design complexity. Innovations in energy storage or wireless energy transfer may revive the research area [49]. An inchworm principle based robot is developed in [50] which uses wireless power transmission to energise the robot. On the contrary the capsule robot (capsubot)- an internal propulsion robot based on internal reaction force - is simple in construction and have no external legs or wheels [51, 52]. Thus unlike legged robot, capsule robot does not pose threat to the internal soft tissue and could be suitable for in-vivo applications. Furthermore the capsule robot can be made hermetically sealable as there are no external moving parts.

The hybrid robots developed, use external propulsion as primary propulsion and internal mechanism to achieve additional functionality. To achieve the fine positioning capability, the hybrid robot of [53] uses two small internal magnets and one internal motor. To achieve the tissue distending capability, the hybrid robot of [42] uses an internal leg-mechanism. However to achieve additional functionality they introduce new mechanism on-board which requires on-board power to run.

Though plenty of researches have been performed on miniature in-vivo robots for minimally invasive diagnosis and interventions, the developed robots are still in the preclinical phase. The literature presented above suggests that further investigations and new designs may solve issues that existing robots have and will eventually accelerate the process to develop a clinical miniature in-vivo robot. Because of the advantages of capsule robot propulsion principle over other propulsions, this research will investigate the capsule robot propulsion principle further and develop two capsule robots and one hybrid capsule robot with incremental capabilities. The capsobot is an underactuated system - a system which has fewer independent control actuators than degrees of freedom (DOF) to be controlled [54]. Examples of underactuated systems are legged robot with passive joints, pendulum on a cart [55] and helicopters.

Control of underactuated systems can be divided into two classes: stabilization [56–58] and trajectory tracking control [59–62]. Two controllers (wheel velocity controller and vehicle position stabilization controller) were presented in [56] for a wheeled inverted pendulum (wheel movement active and pendulum movement passive) by utilizing partial feedback linearization. In [63] the propulsion principle of a capsobot was analyzed from the viewpoint of physics and a control law and the optimum parameters of the system were proposed. In [64], the motion generation of a single mass capsobot was explained on the basis of a four step velocity profile which is, fast motion for the first two steps and slow motion in the last two steps. In [41], motion of a single mass capsobot was explained on the basis of a novel four step acceleration profile and a stand-alone prototype was developed. However trajectory tracking control of the capsobot-type underactuated systems - such as pendulum on a cart [55] and a capsobot [41] - was not considered in the literature according to the author's knowledge. Though trajectory tracking is the primary requirement of a mobile robot, trajectory tracking control for capsobot-type underactuated mechanical systems is still an open issue. This research will investigate the trajectory tracking control of the capsobot-type robots.

1.2 Aims and Objectives

1.2.1 Aims

This research aims to design and analyse underactuated mobile capsule robots and then it will develop and implement trajectory tracking control for the capsule robots. These capsule robots potentially can be used in in-vivo medical applications such as capsule endoscope.

1.2.2 Objectives

The objectives of this research project are:

- To identify the challenges of the miniature in-vivo robots for the medical diagnosis and interventions.
- To review designs and working principles of miniature in-vivo robots for the medical diagnosis and interventions.
- To propose a design of the miniature in-vivo mobile robot for the medical diagnosis and interventions.
- To develop mathematical models of the underactuated mobile capsule robots (capsubots).
- To propose a control strategy for the trajectory tracking of the capsubot-type underactuated systems.
- To conduct the theoretical analysis of the working principles of the capsule robots.
- To conduct the theoretical analysis of the proposed control strategy.
- To conduct the simulation of the trajectory tracking control and to investigate the robustness of the trajectory tracking control with uncertainties.
- To develop the capsubot prototypes and demonstrate the motion generation of the capsubot.
- To implement the trajectory tracking control in the developed capsubot prototype.
- To perform the experiments to demonstrate the performance of the proposed trajectory tracking control.

1.3 Research Contributions

The main contributions of chapter 3 are to develop a new two-stage control strategy for the trajectory tracking control of a one dimensional (1D) capsule robot (capsubot), to propose a segment-wise trajectory tracking algorithm, to implement the control strategy in a developed prototype and to validate the control strategy through experimental study. Other contributions include the proposal of two new acceleration profiles (utroque and contrarium) for the capsuobot motion generation, the development of a way to optimally select the profile parameters for the proposed acceleration profiles considering the system constraints. Another contribution is the proposal of a novel selection algorithm to select the acceleration profile (i.e utroque or contrarium) and to select the correct acceleration profile parameters (acceleration values).

The main contributions of chapter 4 are proposal of a trajectory tracking control algorithm by combining segment-wise and behaviour-based control for the trajectory tracking control of an underactuated two dimensional (2D) capsule robot (capsubot) and the validation of the algorithm through simulation and rigorous robustness analysis. Other contributions include defining various basis behaviours for the 2D capsuobot, developing a selection algorithm for the selection of the behaviour set, developing the rules for implementing each behaviour and developing a 2D capsuobot prototype, implementing the closed-loop control strategy for the inner masses (IMs) of the 2D capsuobot.

The main contributions of chapter 5 are the design of a novel miniature hybrid robot for in-vivo medical use comprising four modes of operation, the analysis of the working principles of various modes and the modelling of the robot in various modes.

1.4 Thesis Outline

Chapter 2 This chapter presents the needs and challenges of medical robots, classifies the minimally invasive medical robots, provides detailed literature of each of the classes, provides tables comparing among various classes and also presents literature on the control of the underactuated mechanical systems.

Firstly this chapter discusses the needs for medical robots and presents the challenges faced to develop medical robots such as large surgical robots and miniature in-vivo robots. Then this chapter classifies minimally invasive medical robots based on the size and targeted anatomy into external large robots, miniature in-vivo laparoscopic robots and miniature in-vivo endoscopic robots. It presents a comparison among the

above mentioned medical robot classes. Next this chapter presents the background and state-of-the-art of external large medical robots. After that the background of the miniature in-vivo laparoscopic robots are provided. The in-vivo laparoscopic robots are further classified based on propulsion capability and propulsion methods. Details of each of the classes are provided and a comparison is presented based on the key features. Afterwards miniature in-vivo endoscopic robots are presented: firstly the background, secondly the classification based on locomotion principles/mechanisms and finally details of each of the classes and comparisons.

This chapter also reviews the control of underactuated mechanical systems (UMSs). It presents the generalized dynamic equation for UMSs and describes the control problems for UMSs. Then it discusses the stabilization control and the trajectory tracking control of various UMSs. At the end, this chapter presents the summary of the chapter and describes the scope of contribution of this thesis.

Chapter 3 This chapter presents the modelling, theoretical analysis, trajectory tracking, simulation and experimentation of the 1D capsule robot (capsubot). Firstly this chapter introduces the capsule robot. Then this chapter presents the modelling of an 1D capsuobot, explains the problem and proposes a control strategy for the trajectory tracking of the capsuobot-type underactuated systems. It proposes two new acceleration profiles and explains the motion generation of the capsuobot for both the acceleration profiles. The motivation to propose the acceleration profiles are also explained and discussed by comparing with other profiles proposed in the literature. This chapter optimally selects the profile parameters for the newly proposed acceleration profiles considering the system constraints.

After that the proposed control approach is presented in detail: firstly it explains the creation of the database which is required for the controller design; then it discusses the generation of the inner mass (IM) trajectory from the desired capsuobot trajectory; it proposes a novel selection algorithm for the proper selection of the acceleration profile (i.e. utroque or contrarium) and also to select the correct acceleration profile parameters (acceleration values); it describes the tuning of the segment time and finally it presents the low-level control of the inner mass (IM) using partial feedback linearization.

The simulation is performed for the proposed control strategy in the Matlab/Simulink environment and the proposed control is implemented in a developed 1D capsuobot. The details of the developed prototype and physical constraints are presented. The

simulation and experimental results are presented, compared and critically analyzed. It discusses about the repeatability and reproducibility of the simulation, capsbot prototype and the experiments. It explains the drift, overshoot and noise which are present in the experimental results. The chapter also discusses about an attached video which shows the demonstration of the capsbot position trajectory tracking. Finally this chapter presents the scalability of the capsbot.

Chapter 4 This chapter presents a 2D capsule robot, its modelling, motion generation, trajectory tracking and experimentation. Firstly this chapter introduces the 2D capsule robot. Then modelling and motion generation of the 2D capsule robot are discussed. After that this chapter defines nine basis behaviours and discusses reference frame allocation. A trajectory tracking algorithm combining segment-wise and behaviour-based control is proposed and detailed method for implementing the proposed trajectory tracking algorithm is presented. It presents the database creation and discusses the segment generation. It presents an algorithm for the behaviour-based control and rules for implementing the behaviours. It also presents the selection of the acceleration profile parameters for each behaviour and the tuning of the segment time. Low level control of the IMs is also discussed briefly.

This chapter presents the simulation setup and the simulation results. It shows the impact of the segment time change on the performance of the trajectory tracking. The simulation results also show the robustness of the trajectory tracking for various friction uncertainties. This chapter explains the prototyping, programming of the capsule robot prototype and presents the experimentation. It presents the experimental results, compares them with simulation results and analyses them. This chapter concludes with a summary of the chapter.

Chapter 5 This chapter presents the detailed design, working principle, modelling and simulation of a novel hybrid robot. Firstly it presents the detailed design of the hybrid robot where it describes all the components of the robot, their functions and how the rotary motion of the legs are created with the help of the internal mechanism. Then this chapter presents the working principle of the robot in the four operating modes of the hybrid robot using the same set of actuators. It also presents the mathematical modelling of the robot in various operating modes considering internal and external forces while the robot is within a tubular environment. Further this chapter presents the simulation of the robot in various modes showing the position of the robot and actuator forces. Finally this chapter concludes with a summary of the chapter.

1.5 List of Publications

1.5.1 Patent

- H. Yu, M. N. Huda, Yang Liu and S. O.Wane, “Travelling capsule with two drive mechanisms” GB Patent GB2497544.

1.5.2 Journals and Conferences

- M. N. Huda, H. Yu, and S. Cang “Behaviour-based control approach for the trajectory tracking of an underactuated planar capsule robot,” IET Control Theory & Applications, vol. 9, no. 2, pp. 163–175, 2014.
- M. N. Huda and H. Yu "Trajectory tracking control of an underactuated capsobot," Autonomous Robots, vol. 39, no. 2, pp. 183–198, 2015.
- M. N. Huda, H. Yu, and S. Cang “Robots for minimally invasive diagnosis and intervention,” Robotics and Computer-Integrated Manufacturing, vol. 41, pp. 127-144, 2016.
- M. N. Huda, H. Yu and M. J. Goodwin "Experimental study of a capsobot for two dimensional Movements," 2012 UKACC International Conference on Control, 2012, pp. 108-113, IEEE (Best student paper award).
- M. N. Huda and H. Yu "Design, modelling and motion analysis of a pill-sized hybrid endoscopic capsule robot", IEEE Transactions on Biomedical Engineering (Submitted).

Chapter 2

Literature Review

2.1 Introduction

Minimally invasive diagnosis and interventions provide many benefits over conventional way for many procedures. The benefits include safer techniques, higher efficiency, less pain and quick recovery. The large medical robots such as da-Vinci have been being used in this purpose, whereas the research of the miniature in-vivo robots for the laparoscopic and endoscopic use, is growing in the recent years. A comprehensive literature search was performed using keywords 'laparoscopic robot', 'capsule endoscope', 'capsule robot' and 'surgical medical robot' primarily for the time period of 2000-2015. The articles relevant to the theme of this thesis are reviewed and included in this chapter. This chapter concentrates medical robots for minimally invasive diagnosis and intervention in general and propulsions of miniature in-vivo robots in particular.

The robots are classified and compared using critical characteristics and summarized in Tables 2.1 - 2.5. For the miniature robots, each propulsion mechanism has some advantages and some disadvantages. While external magnetic propulsions have potential to provide propulsion without increasing the robot size, they lack of precise position control and many of them require expensive and bulky equipment. On the other hand the internal propulsions have the capability of precise position control but require mechanisms which need substantial amount of power to drive. The capsule robot propulsion, a type of internal propulsion has the advantage of having the propulsion mechanism on-board and of being limbless. The capsule robot would be the focus of this thesis. It is an underactuated mechanical system. Thus this chapter also reviews the control of the underactuated systems in general and control of capsule robot in particular.

2.2 Needs and Challenges of Medical Robots

2.2.1 Needs of Medical Robots

Robotics for healthcare is defined as the systems capable of doing mechatronic actions based on the analysis of sensor information to provide healthcare such as to perform medical diagnosis and interventions, to deliver treatments, to support rehabilitation and to support patients in prevention programs. The requirements and needs of medical robots can be seen from the viewpoints of various stakeholders namely the patients, the professional users (e.g. doctors, nurses), cure and care institutions (e.g. hospitals), insurance companies and researchers. The needs are provided below [65–68]:

1. **Safety:** From the patient point of view safety is the most important requirement. Healthcare professionals (e.g. doctors, nurses) are keen to maintain safety because of their obligation towards the patients and also to maintain their reputation. Thus the procedures performed by with the help of robots need to be safe for the patient and the healthcare professionals. Medical robots offer newer, better and safer treatments compared to the traditional approaches in many procedures. Robot-assisted surgery offers increased safety by creating no-fly zones or virtual fixtures during the surgery to prevent accidental damage/injury to internal soft tissues or organs [65].
2. **Medical care in remote areas and disaster scenarios:** Robots can enable access to medical care in remote areas, space missions, undersea, underground environment and disaster scenarios where medical facilities are not available. A light-weight, flexible and modular co-operative semiautonomous robot-team can be carried to the above mentioned environment and can be tele-operated by surgeons remotely [68].
3. **Quality:** Care institutions and medical professionals are interested in improving the quality of diagnosis and treatments. Medical robots can help in improving the quality of treatments and surgical techniques. The quality of microvascular anastomosis - procedure which connects ultrasmall vessels and neural structures - can be improved by using robot-assisted surgery and thus the requirement of revision surgery can be avoided [65, 69].
4. **Accuracy and recovery time:** Medical robot can significantly improve the accuracy in surgical procedures such as tissue manipulation tasks during microsurgery and bone machining during hip or knee surgery [65, 70]. They are consistent, untiring and stable while performing the surgery. Quick recovery is one of the important requirements

- for both the patients and the healthcare professionals. By using minimally invasive robot systems in medical procedures quicker recovery is possible [65]
5. Enhanced documentation: Robot assisted procedures (computer integrated surgery systems) have enhanced capability to log more detailed information/data about each surgical case than the conventional procedures. This enables easy performance analysis and contributes to the better plan for future surgeries. This information/data further contributes to the research and development of surgical simulators, skill assessment and certification tools for the surgeons. [65].
 6. Minimally invasive procedure: Some traditional medical procedures and treatments are painful and burdensome to the patients. Thus medical robots which introduce minimally invasive procedure are being adopted by the hospitals and doctors. Capsule endoscope is a non-invasive alternative of traditional probe endoscopy which is painful and uncomfortable [34]. Robot-assisted surgery is a minimally invasive option for traditional manual surgery for many procedures such as general surgery, urology, cardiothoracic surgery, orthopedic surgery, neurosurgery and gynaecologic surgery [71].
 7. Inaccessible environment: Medical robots enable the healthcare professionals to perform medical procedures in inaccessible areas without major incisions. Inaccessible areas include space-constrained areas such as inside of a patient [67]. Robot-assisted laparoscopic surgery is performed within abdominal or pelvic cavity using laparoscopic instruments inserted through small trocars (8mm-12mm) [72]. Capsule endoscope enables the inspection of lower small bowel which was impossible with traditional probe endoscope.
 8. Increased ageing population: Because of the post-world war II baby boom the aged population percentage will increase over the next two to three decades with an annual growth rate of 2.8 % [3]. The elderly people will increase approximately 100%, 50% and 40% in Japan, Europe and USA respectively by 2030 [68]. The ageing problem demands increased medical and social care. Medical robotics may offer help to tackle the increased healthcare demands by providing assistance to healthcare professionals.
 9. Economic factors: Historically healthcare spending grows faster than the economy. Innovation is required especially in robotics to impede this spending growth in the near future when healthcare professionals will be outnumbered by the number of aged population. Robotics has the potential to reduce the labour cost by replacing human

carer with medical robots. It may ensure healthcare to larger number of patients without increasing healthcare professionals [66]. Though the initial cost for many robot systems are quite high, the added benefits such as the efficient operation, quick recovery time and less hospital stay may make the overall cost of healthcare cheaper.

This thesis presents three capsule robots. The capsule robots can potentially be used in in-vivo medical applications such as capsule endoscope. Capsule endoscope offers minimally invasive alternative inspection opportunity in the gastro-intestinal track. It also offers inspection in inaccessible environment such as small bowel.

2.2.2 Challenges

Minimally invasive diagnosis and interventions feature safe and reliable techniques and, result in less pain and shorter hospital stays compared to the conventional ways. This motivates the development of minimally invasive devices such as external large robots (e.g. da vinci robot), miniature in-vivo robots for surgical and diagnostic applications [2, 4, 6, 9, 73–76]. The challenges of external large robots and miniature in-vivo robots are individually discussed below:

Challenges of external large robots External large robots (e.g. da vinci robot) used in robot-assisted surgery are expensive, bulky, heavy-weight and, needs a large operating room and significant setup time. The challenge is to make it light weight and add more flexibility to the system so that it can be used outside large operating room. The tools used in the robot-assisted procedures are rigid and effective workspace (points that can be reached by end of the tool) within the patient is limited. The challenge is to develop usable flexible access tools which will increase the workspace of the surgery robot inside the patient. Bio-inspired materials such as artificial muscles can be useful in developing flexible access surgery tools as they can work both as an actuator and sensor [3, 77].

Challenges of miniature in-vivo laparoscopic robots and endoscopic robots Miniature in-vivo endoscopic robots work within the gastro-intestinal (GI) track whereas miniature in-vivo laparoscopic robots work within the abdominal or the thoracic cavity. The following challenges for developing miniature in-vivo robots have been identified [16, 17, 25, 35, 40]:

1. Safety: Contact and movement of a robot should cause no damage to the internal soft-tissues. The overall technology used should be safe for the patient.

2. Size and weight: The size of laparoscopic robots should be small enough so that it can be inserted through a standard laparoscopic port (12 mm in diameter [78]) and the weight of robots should be light enough so that the internal organs can withstand it. The endoscopic robot should be small enough so that it can be integrated with a capsule endoscope ($11\text{mm} \times 26\text{mm}$ [32]).
3. Hermetically sealable (Encapsulation of the robot): The robot should be hermetically sealable so that the patient lumen remains safe from the robot components. This will keep the internal electronics of the robot safe as well. The traditional design of mobile robot with external moving parts such as legs, wheels or tracks makes it challenging to develop a miniature in-vivo mobile robot hermetically sealable
4. Robot control: A control system is required to control and manipulate the robot. To design the control system a model of the robot and the environment is required. The irregularity and complexity of the structure inside human body make the modelling of the environment very challenging.
5. Energy efficient robot: The robot should be energy efficient so that the power required to propel the robot can be supplied with a very small size battery such as a coin cell battery for the total period of investigation (current time of investigation for small bowel is approximately 8 hours [34]). Most of the commercially available capsule endoscope ($11\text{mm} \times 26\text{mm}$ [32]) uses silver-oxide coin battery that has a capacity of 55 mAh with a output voltage of 3V [34]. The legged robot developed in [40] requires a 200 mAh battery for the locomotion to run for an hour.
6. Stopping/anchoring capability: The endoscopic robot is required to have stopping/anchoring capability by overcoming the visceral peristalsis for better and longer inspection of the suspected region. The capsule endoscope available in the market moves with the help of visceral peristalsis and can not stop at any suspected region intentionally if required.
7. Speed: The traveling speed of the robot should be high enough so that it can travel the GI track within a short period of time (less than 1 hr). E.g. a standard colonoscopy is performed within 20 min to 1 hr [40] whereas the standard capsule endoscope takes 8-10 hrs [79] to complete its journey in the GI track.

2.3 Classification of Minimally Invasive Medical Robots

Robots for minimally invasive diagnosis and interventions can be classified based on various perspectives such as based on manipulator design, based on level of autonomy and based on targeted anatomy [65]. In this thesis the robots are primarily classified based on the size as external large robots [2, 9] and miniature in-vivo robots. The miniature in-vivo robots are further classified based on the targeted anatomy into miniature in-vivo laparoscopic robots [17, 19, 80] and miniature in-vivo endoscopic robots [35, 81]. Table 2.1 shows the comparison among the above-mentioned robots.

Table 2.1 Comparison of minimally invasive diagnosis and intervention robots based on key features

Robot / Criteria	External large robot [2, 9, 82] 	Miniature in-vivo robot	
		In-vivo endoscopic robot [40, 81] 	In-vivo laparoscopic robot [17, 19, 25] 
Operating anatomy	any	gastro-intestinal track	abdominal cavity, thoracic cavity
Clinical applications	surgery: general, cardiothoracic, orthopedic, neuro and gynaecologic	diagnosis, biopsy	surgery assistant: vision, task. biopsy
Robot position	outside patient's body	inside patient's body	inside patient's body
Size	large robot having multiple robotic hands	miniature - typical diameter <20mm and length <50mm) e.g. in [40] diameter: 11mm, length: 25mm	miniature - typical diameter <20mm and length <100mm, e.g. in [25] diameter: 15mm and length: 85 mm
Large operating room	requires	internal propulsions do not require, external propulsions may require	magnetic drive may require, other propulsions do not require
Currently operating	medical and research labs	research labs	research labs
Power	mains cable	battery, tethered	tethered

2.4 External Large Medical Robots

External large robots have been used in robot-assisted surgery such as laparoscopic and thoracoscopic surgery since early 1990s [83] which removes some of the limitations of manual laparoscopy namely hand tremor, bulky instrument handling and poor visibility [84]. Robot-assisted surgery is performed by a multi-arm robot which is tele-operated by a surgeon. Each arm of the robot can manipulate a tool or camera according to the command by the surgeon. [9, 75].

The first robot used in surgical procedure is an industrial robot, Unimation PUMA 200, in 1985 in USA. It is used to precisely guide a probe for brain biopsy using CT guidance [85]. The robot is experimentally used for 22 patients and is found to improve the precision but is very crude [66]. Robots has been used in orthopaedic surgery such as hip and knee surgeries since early 1990s [86–89]. Initially industrial robots were used which performed the surgery autonomously with little surgeon involvement where the leg was clamped down rigidly [90]. Later robots such as Caspar were successfully used for total hip and total knee replacement surgeries [91, 92]. The first robot surgical system approved by FDA (Food and Drug Administration) is the Robodoc. Integrated Surgical Systems developed Robodoc in 1992 for orthopaedic surgeries. It demonstrated greater accuracy as compared to the conventional ways. The robot was first used for hip replacement surgery [93, 94]. However it shows poor performance if the patient moves. This system is no more in production [66]. Mechatronics in Medicine Group at Imperial College developed Acrobot which was a special-purpose orthopaedic surgery robot. It was used in knee replacement surgery where it assists the surgeon by providing motion constraints [95, 96]. The Acrobot was further developed into a trolley-mounted system called Acrobat Sculptor where a separate arm was used to dynamically track the knee position. Thus it avoided the need of clamping the leg rigidly and made the surgical procedure less invasive [97, 98].

The other robot systems approved by FDA are AESOP, da-Vinci and Zeus. AESOP (Automated Optical System for Optimal Positioning) developed by Computer Motion, Inc. is a foot-switch or hand-controlled robot arm when it was first introduced. The later versions of AESOP are voice-controlled. The robot arm uses an adapter to hold laparoscope with a video camera to assist the surgeon and replace human camera holder [75]. It enables solo-surgeon laparoscopic surgery in various surgical procedures e.g. cholecystectomies, hernia repairs and colectomy [99, 100]. Though AESOP provides a stable camera platform, the camera movements in voice control are slower as compared to human assistant control. Moreover voice-control might distract other members of the surgical team [75].

Intuitive Surgical, Inc. developed the da-Vinci Surgical System which got FDA approval in 2000. It consists of a surgeons' console, a visualization system, surgical cart with multiple robot arms and proprietary surgical instruments. The surgeons' console comprises of 3D imaging system, hand controlled manipulators and foot-pedals. The surgeon operates using the hand-controlled manipulators and the foot-pedals with the aid of the 3D imaging system. The robot arms are connected to the operating trocars through which the camera and the operating instruments are passed to the operating area inside the patient. The hand, wrist and finger movements of the surgeon are translated to the actions of the instruments inside the patient. The foot-pedals provide further control to camera focus and instrument clutches. The Endowrist technology enables the instruments to have seven degrees of freedom which offers greater range of motion than human hand. The 3D view provides the surgeon the illusion of being in the operating site. The supporting staffs help in preparing the trocars, installing the instruments and tools, supervising the robot arms with the aid of a visualisation system. In the later version of the da-Vinci system, a fourth robot arm is added which enables the surgeon to toggle between three tools while operating [9, 71, 75, 101].

FDA has approved the da-Vinci surgical system for various surgical procedures e.g. general, urologic, gynecologic and cardiac surgeries [101]. The clinical data shows an improved or equal surgical outcome with shorter hospital stays, less pain and more rapid return to daily work for robot assisted surgery. Though the initial cost of the robot system is high (the price of da-Vinci System is approximately 1.5 million Euros), the total hospital cost for a patient is comparable to conventional laparoscopy due to less post-surgery complications. Thus increased usages of robots in surgery are seen in recent years [101]. In USA 36 % of hysterectomy for benign conditions and 83% of prostatectomy were performed by the da-Vinci Surgical System in 2011 as compared to 0% and 23 % respectively in 2005 [102].

2.5 Miniature in-vivo Robot: Laparoscopic Robot

2.5.1 Background

Laparoscopic surgery is a minimally invasive abdominal or pelvic surgery performed using laparoscopic instruments inserted through small trocars. It was introduced in the middle of 1980s [103] and expanded rapidly because of its advantages over traditional open surgery [74, 104]. To further reduce the invasiveness, robot-assisted laparoscopic and thoracoscopic surgeries were introduced in early 1990s [83]. An approach for improving patient experience during and after the surgical procedure is to send a miniature laparoscopic robot/a

team of miniature laparoscopic robots entirely inside the patient body through the laparoscopic trocars to provide the surgeon with vision and surgical task assistance. The ultimate goal of this approach is to develop a multiple cooperative modular robot which together can perform a complete surgery. They are small and easily transportable [19].

2.5.2 In-vivo Laparoscopic Robots Under Research

University of Nebraska-Lincoln develops fixed-base camera robots [15, 24], mobile wheeled robots [18, 19, 25] and magnetic drive robots [14] for biopsy and, vision and task assistance during laparoscopic surgery. BioRobotics Institute, Scuola Superiore Sant'Anna, Italy develops miniature modular in vivo robots including camera robot, retraction unit and manipulator unit [29, 30]. University of South Florida develops MARVEL (Miniature Anchored Robotic Videoscope for Expedited Laparoscopy) and Camera Module [22, 23]. Other research groups working in miniature laparoscopic robots develop magnetic drive robots [26–28] and suction based robots [7, 31] for surgical assistance. Thus the in-vivo laparoscopic robots can be divided based on the propulsion capability and propulsion methods as:

- Fixed base camera robots [15, 22, 23, 105, 106]
- Wheeled robots [17, 25]
- Magnetic drive robots [14, 26, 27, 29, 30] and
- Suction-based robots [31, 107]

Table 2.2 compares the above mentioned in-vivo laparoscopic robots.

Fixed base camera robots

Fixed-base camera robots are further classified based on the method used to mount the robot within the abdominal cavity.

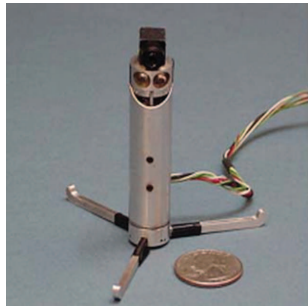
Tripod mounted camera robot A fixed-base tethered camera robot (Fig. 2.1(a)) is developed for augmenting the vision and depth perception of operating area inside the patient's body. The robot consists of a camera, two LEDs, a robot body, 3 legs which works as the tripod stand; the camera allows a 360 degree panning and a '45' degree tilting. The robot is tested during a porcine cholecystectomy. The surgeon gets supplementary vision feedback throughout the process which helps him in planning and placing the trocars and, provides better knowledge about the surgical field [15].

Table 2.2 Comparison among in-vivo laparoscopic robots based on key features

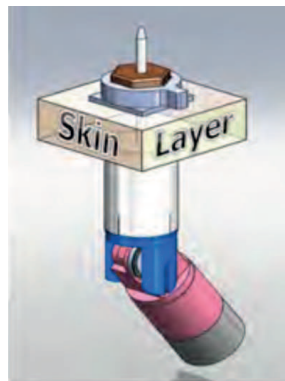
Robot / Criteria	Fixed base robots [15] 	Wheeled robots [25] 	Magnetic drive robots [14] 	Suction-based robots [7, 31] 
Power	tethered	tethered	tethered	tethered
Operating anatomy	abdominal cavity	abdominal cavity	abdominal cavity	abdominal cavity, intra-cardial environment
Locomotion	pan and tilt	wheeled locomotion	magnetic locomotion	inch-worm like locomotion
External moving parts	yes	yes	no	yes
Large operating room	does not require	does not require	may require	does not require
Clinical applications	vision assistant	task and vision assistant, biopsy	vision assistant	navigation
Actuator	brushless DC motor	permanent magnet DC motor	external solenoid	vacuum pressure
In-vivo / Ex-vivo trials	in-vivo test (porcine)	in-vivo test (porcine)	in-vivo test (porcine)	in-vivo test (porcine)

Needle mounted camera robot A system named MARVEL (Miniature Anchored Robotic Videoscope for Expedited Laparoscopy) is developed in [22, 23] which includes multiple fixed-base pan/tilt camera modules, a master control module and a human-machine interface. The camera module (2.1(c)) comprises of five subsystems namely illumination, vision, wireless communication, embedded control and attachment needle power subsystems. The camera module is attached to the abdominal wall with the attachment needle power subsystem which is also used to power the camera module. Two camera modules are tested simultaneously inside the abdominal cavity of a porcine subject demonstrating transmission of images from the camera modules [22, 23].

Suturing mounted camera robot A fixed-base surgical imaging device (Fig. 2.1(b)) with pan, tilt, zoom and lighting is developed in [105, 106]. The length and diameter of the device is 110 mm and 11 mm respectively. In vivo porcine animal experiments are performed using the device which includes cholecystectomy, appendectomy and nephrectomy. The device is inserted into the abdominal cavity through a standard 12 mm trocar and mounted by suturing to the abdominal wall.



(a) Fixed base pan and tilt camera robot (tripod mounted) [15, 108] (b) Fixed base imaging device in abdominal cavity (suturing mounted) [106]



(c) Fixed base MARVEL camera module - Left: CAD design; right: prototype (needle mounted) [22, 23]

Fig. 2.1 Fixed-base in vivo laparoscopic robots

Wheeled Robots

Wheeled robots (Fig. 2.2(a)) are designed and developed for supporting laparoscopic procedure in [25]. The robot consists of two independently controllable wheels, an appendage and a central region for camera. They develop robots with brush, helical, smooth, male and female type wheels. The developed prototype is 15mm in diameter and 85 mm long. The helical wheel performs best during the in-vivo porcine tests in traversing and climbing the

abdominal organs without causing tissue damage [25]. All the wheeled robots developed for surgical assistance have the similar mobility principle but various added functionalities. A mobile in-vivo wheeled camera biopsy robot is developed and tested in a porcine model in [18] shown in Fig. 2.2(d). Traditional biopsy requires two ports (one for camera, one for biopsy tools) for biopsy whereas this robot requires only one port as it integrates an adjustable-focus camera and biopsy tool in one unit. The robot is able to grasp the porcine tissue and free it from the organ during the test [18]. An abdominal cavity simulator is developed by Nebraska University and used in Aquarius underwater habitat where the crew members performed the surgical task (Fig. 2.2(d)) with the aid of a fixed base camera robot and a mobile wheeled camera robot. The crew performed an appendectomy while being telementored via video conference. The results show that a miniature in-vivo camera robot can be a replacement of traditional laparoscopic camera without compromising the task accuracy [19]. In-vivo wheeled robots are developed for clamping, cauterisation and liquid delivery in [109]. Two robots perform a cooperative work - clamping robot grasps and then cautery robot cuts a portion of small bowel - where they use laparoscope for visualisation. These researches suggest that in future several miniature robots which are sent inside the abdominal cavity through single incision can perform surgical procedures cooperatively.

Robots with Magnetic Drives

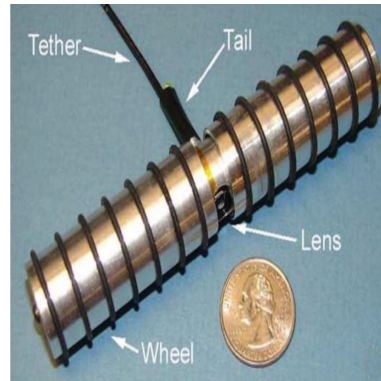
Several robots namely peritoneum-mounted imaging robot (Fig. 2.3(a)), lighting robot, retraction robot (Fig. 2.3(b)) are developed in [14] to cooperatively assist in surgical procedures in laparoscopic, robot-assisted surgery or NOTES (Natural orifice transluminal endoscopic surgery). Magnets at each end of the robots and external magnetic handles are used to attach the robots to the abdominal wall and to maneuver them. Few magnetic drive robots are developed in [28] where a ferromagnetic material is used inside each robot and an external magnet controlled the movement of each robot. This type of robots includes robot with vision capability and, robot with vision and manipulation capabilities.

A camera system (Fig. 2.3(d)) with a dimension of $32\text{mm} \times 29\text{mm} \times 129\text{mm}$ is developed in [27] which is inserted through a 26 mm incision in the umbilicus. A magnet handle is used to suspend and move the camera along the abdominal wall. An alternative way is to mount the camera using a hook and ring arrangement and then to use the magnet handle to move the camera around the incision point [27].

An array of robots (Fig. 2.3(e)) (electro-cutter robot, manipulator robot - diameter: 12mm, length: 95 mm, weight: 12 g, retraction robot - diameter: 12mm, length: 52 mm, weight: 12 g, and camera robot) are developed in [29, 30]. A triangle shaped anchoring



(a) Mobile wheeled robot [25]



(b) Mobile camera robot [19]

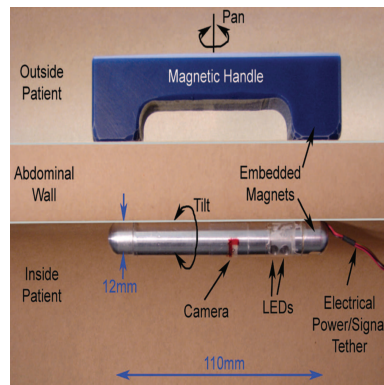


(c) Mobile camera biopsy robot [18]

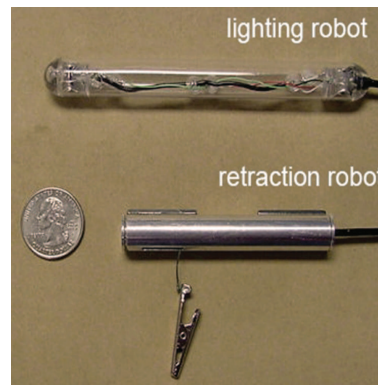


(d) Crew members of Aquarius underwater habitat performing surgical tasks with the assistance of a fixed base camera robot (Fig. 2.1(a)) and a mobile camera robot (Fig. 2.2(b)) [19]

Fig. 2.2 Wheeled in vivo laparoscopic robots



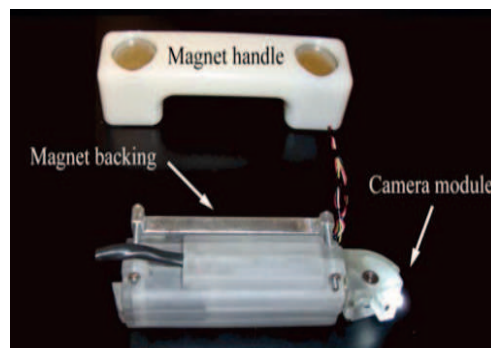
(a) Peritoneum-mounted imaging robot system [14]



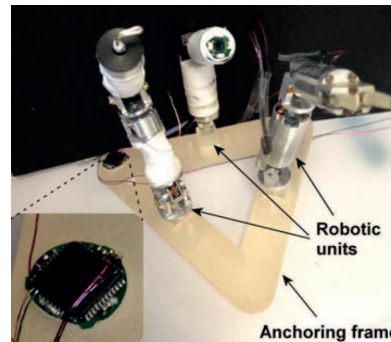
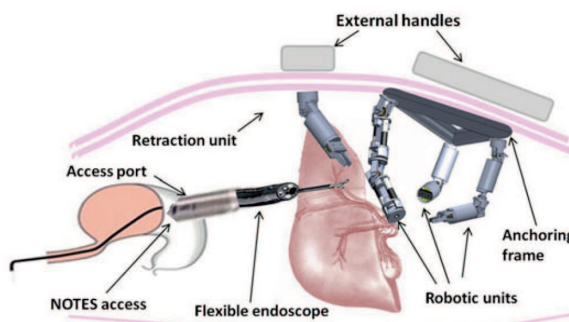
(b) Lighting and retraction robots [14]



(c) In vivo magnetic drive robot: experimental model [28]



(d) In vivo magnetic drive camera module [27]



(e) In vivo magnetic drive array of robots (Left: schematic of robots within the abdominal cavity; right: prototype [29])

Fig. 2.3 In vivo magnetic drive laparoscopic robots

frame with three docking systems is used to support the array of robots inside the abdominal cavity. Two external magnetic handles are used to anchor the anchoring frame and the retraction robot. The magnetic handle can be used to move the retraction robot along the abdominal wall which increases the robot's workspace. The robots can be docked and undocked during the surgical procedures if required. The complete platform is inserted into a phantom abdominal cavity through esophageal access port. Further experiments such as tissue cutting, pick and place are performed to demonstrate the interaction capability of two robots [29, 30].

A robotic system consisting of a camera robot and a robotic grasper is proposed in [26]. The end effectors of two external robotic arms hold two external magnets which control the positions of the robots inside the abdominal cavity.

Suction-based Robot

The suction based HeartLander crawler robot shown in Fig. 2.4(a) is developed in [7] for navigation and fine positioning within intracardial environment. This is a tethered robot with two suction grippers - front and rear - and actuation wires. The robot moves using cycling inchworm like gait of extension and retraction. It uses suction pressure to grip the pericardium with the rear suction gripper and extends the body by actuating front body forward using the drive wires. Then it grips the pericardium using the front gripper, releases the rear gripper and retracts the rear body towards the front gripper. During the path tracking the surgeon defines the final goal point, the robot then autonomously generates an intermediate goal point located 'lookahead distance' ahead from the robot position. When the robot achieves the intermediate goal, the robot repeats the previous process until it is near to the final goal point; it then switches to fine-positioning control mode. This is the only in-vivo robot which had semiautonomous path-tracking feature [7]. Another suction-based robot developed for abdominal cavity in [31] shown in Fig. 2.4(b) uses the abdominal wall for movement surface.

2.6 Miniature in-vivo Robot: Endoscopic robot

2.6.1 Background

Gastrocamera, introduced in 1950s, enabled the inspection of Gastro-intestinal (GI) track [33]. Nowadays, traditional probe endoscopy (PE) is an effective way of diagnosis, treatment and surgery of esophagus, stomach, colon and upper small bowel. However rigidity

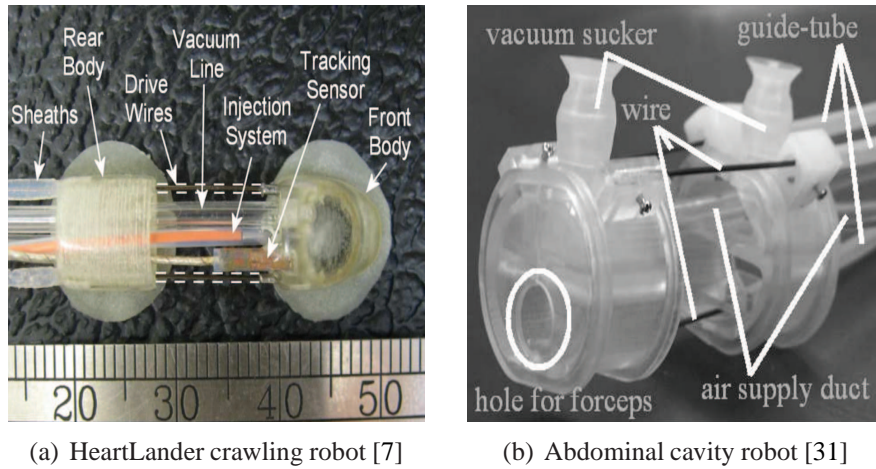


Fig. 2.4 Suction-based in vivo robots

and large diameter (11-13mm) of PE make it inaccessible to major parts of small bowel and, patients found the procedures painful and uncomfortable [34]. In 2000, Given Imaging [32] introduced wireless capsule endoscope (WCE) for the non-invasive inspection of GI track [33]. Several capsules are developed targeting various parts of the GI track e.g. Pillcam SB for small bowel and Pillcam Colon for colon [81]. However these capsules are moved by the aid of visceral peristalsis and do not have control over their movements and orientations which results low diagnostic accuracy [34]. Researches are ongoing to add self-propulsion capability, additional sensors and actuators with the WCE which has the potential to improve the diagnostic accuracy and extend interventional ability [35]. The robots designed and developed in this purpose are reviewed below.

2.6.2 In-vivo Endoscopic Robots Under Research

A complete robot for capsule endoscopy consists of six modules: locomotion, power, vision, telemetry, localization and diagnosis/tissue manipulation tools [34, 35]. The robots can be classified based on each of the modules. However in this thesis we focus on the locomotion of the robot. The robots built for capsule endoscopes can be classified based on the locomotion principles/mechanisms as: (1) internal propulsion robot, (2) external propulsion robot and (3) hybrid propulsion robot. Internal propulsion robot has the propulsion embedded with the robot whereas for external propulsion the propulsive force is generated by an external system. A hybrid propulsion robot uses more than one propulsion mechanisms.

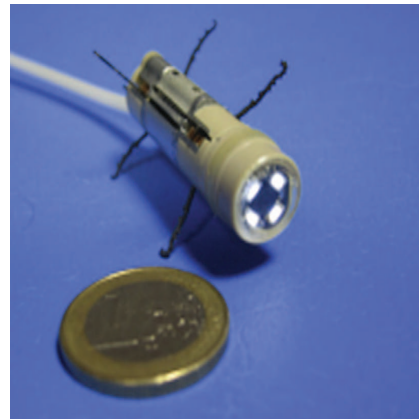
Internal Propulsion Robot

For an internal propulsion robot, the propulsion mechanism (actuators and corresponding mechanism) is totally onboard of the robot. Thus the robot has greater control on its mobility. The significant internal propulsion robots are reviewed below.

Legged Propulsion Robot BioRobotics Institute, Scuola Superiore Sant'Anna, Italy develops legged endoscopic capsule robots that extend from the 3-legged to 12-legged endoscopic capsule robots (Fig. 2.5). Table 2.3 provides the comparison among various legged endoscopic robots. Initially BioRobotics Institute design with SMA wire actuators and develop a 6-legged capsule robot prototype [110]. But design complexity and lack of durability of SMA wire compel them to choose BLDC as an actuator for their later versions of the robot. They develop 4-legged (diameter: 12mm, length: 40mm) [111], 8-legged (diameter: 12mm, length: 40mm) [48, 112] and 12-legged endoscopic capsule robots (diameter: 11mm, length: 25mm) [40]. The 12-legged endoscopic capsule robot has two leg set (LS), one near the front and one near the rear for successful locomotion. Every leg set has 6 legs. The rear LS has the primary function of producing thrust force, while the front LS is used for the dual purposes of bracing the capsule against unwanted backward motion as rear legs retract and also to help propel the capsule around curves. In order to move two LS independently two BLDC motors are used. The capsule can travel a distance equal to colon in a shorter time compared to the WCE [40].



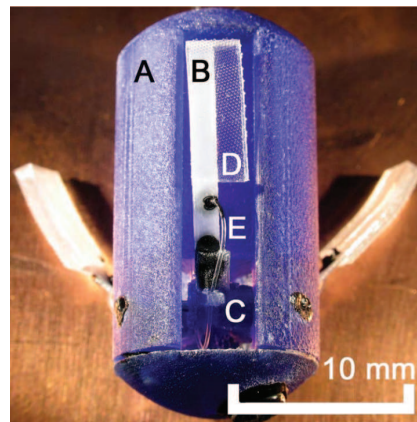
(a) SMA based four-legged robot [111]



(b) Eight-legged robot [48]



(c) Motor-driven twelve-legged robot [40]



(d) Legged anchoring robot [113]

Fig. 2.5 Legged endoscopic robots

Table 2.3 Comparison among legged endoscopic robots based on key features

Criteria/ Robot	Size (Diameter, Length) mm	Power	Locomotion speed (mm/min)	Actuator	External moving parts	Distend tissue	Precise position control	Intended area of work	Large operating room	Practical trial
6-legged [110] 	not reported	tethered	not reported	SMA wires	exists	capable	possible	small bowel, colon	not required	no
4-legged [111] 	12,40	tethered	10-30 (ex-vivo)	BLDC motor	exists	capable	possible	small bowel, colon	not required	ex-vivo
8-legged [48] 	12,40	tethered	50 (in-vivo)	2 BLDC motors	exists	capable	possible	small bowel, colon	not required	in-vivo, LGI phantom
12-legged [40] 	11,25	battery	50 (LGI phantom)	2 BLDC motors	exists	capable	possible	small bowel, colon	not required	ex-vivo, LGI phantom
anchoring [113, 114] 	not reported	not reported	0	SMA wire motor	exists	not capable	not possible	small bowel, colon esophagus	not required	in-vitro

Bio-mimetic/ Bio-inspired Propulsion Robot Several propulsion methods have been designed by mimicking biological systems. The developed propulsion methods include earthworm-like robot, cilia-based robot, flagellar swimming robot and paddling-based robot. Table 2.4 provides the comparison among the bio-mimetic endoscopic robots.

Earthworm-like / Inchworm-like propulsion robot: Several prototypes [115–118] are developed based on earthworm-like or inchworm-like propulsion principle using piezo-actuators or SMA (shape memory alloy) spring. Fig. 2.6(a) shows one of them. The principle is cyclic expansion and compression of the actuator. All of the prototypes consist of one actuation mechanism (SMA or piezo), one or two bodies and insect-claw like directional passive claspers which clamps to prevent backward motion of the robot. The implemented module can travel 2 mm/cycle where the cycle time is 8s [116]. This principle is similar to suction-based propulsion described before except that in earthworm principle passive claspers are used instead of the active suction cup.

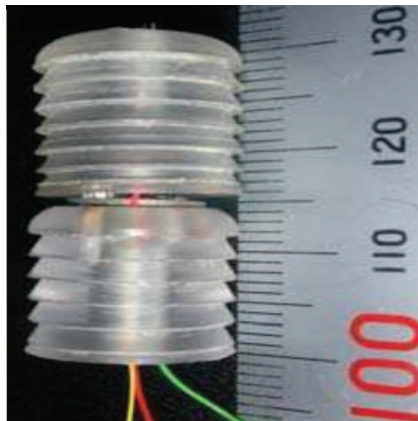
A modular robot system (Fig. 2.6(b)) based on inchworm-like locomotion is developed in [119]. Here all the modules (in this case two modules) are swallowed and the modules are assembled inside the GI track using permanent magnets placed at the end of each module. The assembled robot system moves by using opening/folding of the legs and the pushing/pulling of the connectors between the modules. Modeling and gait generation of a earth-worm like robot is presented in [120]. A motor-based capsule robot with inchworm propulsion principle is developed in [50] which is powered by wireless power transmission. A hollow-cylinder-like three-dimensional coil is proposed for receiving the power. Ex-vivo experiment is performed using the developed prototype.

Cilia-based Robot: The cilia-based robot developed in [121, 122] using SMA spring based actuators is shown in Fig. 2.6(c). It uses two sets of cilia controlled by two groups of SMA springs. By controlling the opening and closing of the cilia sets the robot can produce bidirectional movements.

Flagellar Swimming Robot: A swimming mechanism [123, 124] mimics the swimming action of a flagellum. The micro-robot includes a main body and two tails, each having three segments of piezoelectric material. Traveling waves generated by exciting the segments of the tails with electricity of different phase and amplitude create the propulsive force of the robot. An up-scaled tail for the proposed robot is developed.

Table 2.4 Comparison among biomimetic endoscopic robots based on key features

Criteria/ Robot	Size (Diameter, Length) mm	Power	Locomotion speed (mm/min)	Actuator	External moving parts	Distend tissue	Precise position control	Intended area of work	Large operating room	Practical trial
Earthworm like [116] 	13, 33	tethered	8.5-14.7 (in-vitro)	SMA spring	exists	not capable	possible	small bowel, colon	not required	in-vitro
Cilia-based [121] 	15, 35	tethered	24 (in-vitro)	SMA spring	exists	not capable	possible	small bowel, colon	not required	in-vitro
Paddling based [125] 	13, 30	tethered	197-375 (in-vitro)	linear actuator	exists	not capable	possible	small bowel, colon	not required	in-vitro in-vivo



(a) Earth-worm propulsion robot [116]



(b) Inchworm-like locomotion based modular robot [119]



(c) Cilia-based propulsion robot [121]



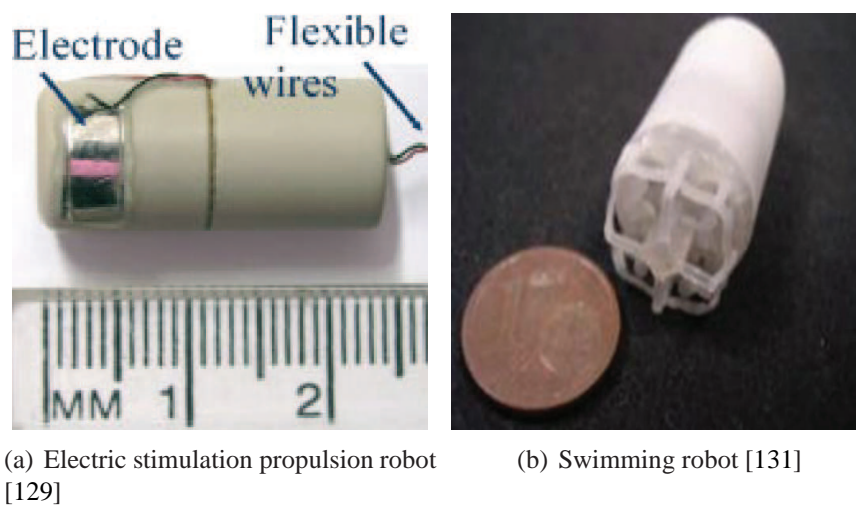
(d) Paddling based propulsion robot [125]

Fig. 2.6 Biomimetic endoscopic robots

Paddling-based Propulsion Robot: This propulsion principle mimics a canoeist paddling a canoe [125, 126] which is a directed propulsion. A linear actuator with two cylinders: inner cylinder and outer cylinder, represents the canoeist. The robot (Fig. 2.6(d)) consists of six legs placed radially to the robot and connected to the inner cylinder of the actuator through grooves. At the beginning of the cycle the legs remain folded and at the furthest most front position. Then the actuator slowly pulls the legs so that legs are protruded and clamp the intestinal wall and thus the legs along with cylinder are locked at one place. The actuator continues to pull the cylinder. As the cylinder is locked and cannot move, rest of the robot body moves forward. Then the actuator pushes the cylinder forward, the legs are released from the wall and folded inside and move forward without resistance and at the end the legs return to their initial position and ready to start the next cycle. By repeating this, the robot could move forward. The developed prototype is 13mm in length and 30mm in

diameter and, 6.5 mm/s velocity is achieved in the in-vitro test.

Electrical Stimuli Propulsion Robot This robot (Fig. 2.7(a)) is propelled by the contraction of intestinal smooth muscle produced by electrical stimuli applied by two electrodes placed on the robot [127–130]. The contraction creates sort of 'artificial' peristalsis which creates propulsive force and the robot moves opposite to the contraction end along the lumen. The propulsion is bidirectional depending on which electrode is activated. Average velocity achieved in the experiment is 2.91 ± 0.99 mm/s (forward) and 2.23 ± 0.78 mm/s (backward).



(a) Electric stimulation propulsion robot [129]

(b) Swimming robot [131]

Fig. 2.7 Electric stimulation propulsion robot and swimming robot

Vibratory Propulsion Robot The Vibratory propulsion robot is investigated in [39, 132]. The robot has an eccentric mass inside the robot which is also the rotor of a motor. When the eccentric mass (rotor) rotates, it generates a centripetal force. The horizontal component of the force propels the robot. The developed robot is 28 mm long and 16 mm in diameter. The robot is tested on various surfaces (sand, liquid soap, solid foam and rubber hose) and moves with an average speed of 3 cm/s (liquid soap) to 12 cm/s (solid foam).

Swimming Robot A swimming gastric capsule robot is shown in Fig. 2.7(b). To use this robot, the stomach has to be prepared with half litre of ingested polyethylene glycol (PEG) solution which enlarges the gastric region. The capsule performs 3D movement within the enlarged stomach with the help of 4 propellers run by four individual DC motors. It uses all four of its propeller while it advances in a rectilinear direction and for steering it uses only

two of its four propellers. The weight/volume ratio of the capsule is made equal to PEG density (1200kg/m^3) to make the robot enable to float, maintain the position & orientation and observe the suspected region when the propellers are stopped. The robot is 15 mm in diameter and 40 mm in length and can be operated remotely by a human operator using joystick. The capsule is tested in a porcine stomach ex-vivo and maximum speed obtained is 21.3 cm/s [131, 133].

A swimming robot modified from [131] is wirelessly powered in [134]. The embedded electronics and the motors of the robot are supplied up to 400mW through inductive wireless power transmission. However only two motors can be operated at a time due to power limitation. Swimming robot of [131, 133] is improved in [38] and a complete functional system is developed consisting of an on-board locomotion system, a tele-operation console, a vision system and a real-time video transmission. A user can remotely control the swimming gastric robot through the user interface by only observing the video stream from the camera.

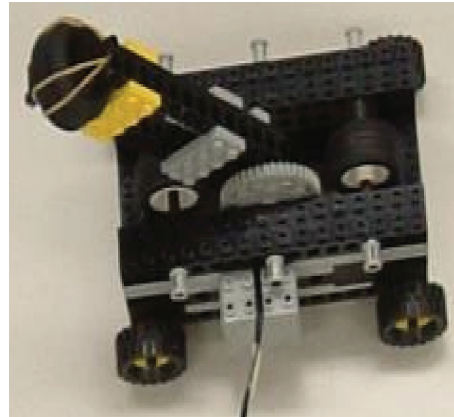
Internal Reaction Propulsion Robot In this principle the robot moves by the reaction force caused by the movement of internal mass. These robots have no external legs or wheels [51, 52]. The structure of the principle is derived from [135]. A mass attached to the main object through a piezoelectric element, is made to move away from the main object rapidly and then to return to the initial position slowly with a sudden stop. The main object moves during the rapid motion and at the stopping moment of the mass and, remains stationary for the rest of the time. The object can move along a straight line by repeating the above process. Linearly moving mass and inverted pendulum which are described below can be used to generate the reaction force.

Using Linearly Moving Mass: In [136] linearly moving mass is used to generate robot motion. Here a permanent magnet is placed in a peripherally coil wound cylindrical body (capsule) (Fig. 2.8(a)). By controlling current flow through the coil the permanent magnet can be moved back and forth within the capsule. The capsule robot completes each motion cycle in four steps. In the first two steps the magnet moves very fast and the reaction force caused the capsule to move in the opposite to the magnets motion. Again in the third and fourth steps the magnet moves slowly while the friction dominates over the reaction and the capsule remains stationary. By repeating the cycle the capsule can move in one dimension.

Using Inverted Pendulum: Here the driving force is created by the reaction of the motion of an inverted pendulum. In [137] a pendulum-driven cart (Fig. 2.8(b)) is developed and tested. The cart consists of passive wheels and a motor driven inverted pendulum on top



(a) Using linearly moving mass [136]



(b) Using inverted pendulum [137]

Fig. 2.8 Internal reaction locomotion robot

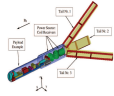
of it which can move in the yz plane. The cart moves forward when the pendulum moves with the counter-clockwise high angular accelerated motion (step 1) and then low angular accelerated motion (step 2). The cart stays stationary when the pendulum moves with low accelerated angular motion counterclockwise (step 3) and then clockwise (step 4) while friction dominates over reaction force. At the end of step 4 the pendulum reaches to its initial position. By repeating the above steps the robot moves in a certain direction.

External Propulsion Robot

By using external propulsion the burden of having internal actuators is eliminated. The robot now have more space for other modules e.g. telemetry and diagnosis modules. External magnetic field that interacts with internal magnetic components is the typical source of propulsion in external propulsion robot. External propulsion robot includes MRI guided robot, permanent magnet actuated robot (using hand-held/motorized magnet or robotic navigation system) and coils actuated robot. Table 2.5 compares among the external propulsion endoscopic robots.

External MRI Guided Propulsion The static and RF magnetic field inherent in the MRI are used in this driving principle. Three swimming tails each consisting of three coils in a row are responsible for the propulsion of the robot. RF magnetic field provides power to generate alternating current in the coils of the tails. The alternating current interacting with the static magnetic field produces a waving movement and thus produces the propulsive force [44].

Table 2.5 Comparison among external propulsion endoscopic robots based on key features

Criteria/ Robot	Size (Diameter, Length) mm	Power	Locomotion speed (mm/min)	Actuator	External moving parts	Distend tissue	Precise position control	Intended area of work	Large operating room	Practical trial
MRI guided propulsion[44] 	complete prototype was not developed	wireless power	complete prototype was not developed	magnetic fields of MRI	exists	not capable	not possible	GI track	required	none
Robotic magnetic navigation [46] 	capsule: 11, 26; shell: 13, 13	none	not reported	magnetic fields	does not exist	not capable	not possible	GI track	required	in-vivo, plastic phantom
Motorized magnet actuated propulsion [138] 	capsule: 11,26 shell: 11,10	battery	90-190 ex-vivo	external magnetic field	does not exist	not capable	not possible	small bowel	not required	PVC pipe, ex-vivo
External coil actuated propulsion [13] 	8, 20	none	180	electro magnetic actuation	does not exist	not capable	not possible	small bowel	not required	ex-vivo

A magnetic guidance system similar to MRI is reported in [45] to control a capsule ($31\text{mm} \times 11\text{mm}$) to examine the stomach of 61 patients. An operator can control the movement of the capsule inside the stomach using two joysticks. Both gastroscopy and the capsule are used for the examination. The diagnostic results using gastroscopy and the capsule are comparable.

External Permanent Magnet Actuated Propulsion The external permanent magnet could be operated by a human operator or by a motor or by a robot arm. They are described below:

Using hand-held/motorized magnet: Given Imaging develops a magnetic actuation system under the project NEMO (Nanobased Capsule-Endoscopy with Molecular Imaging and Optical Biopsy) (Fig. 2.9(a)). They modify their capsule to add a magnetic material inside. They use external hand-held plate permanent magnet to maneuver the capsule [139].

A magnetically actuated soft capsule endoscopic robot (diameter: 15 mm, length: maximum - 40 mm, minimum - 30 mm) is developed in [140, 141]. It is actuated by a motorized external permanent magnet and it is able to navigate in three dimensions by rolling on the stomach surface. External attractive magnetic force is used to anchor the robot on a desired location and external magnetic torque is used to roll the robot to navigate on the stomach surface. The robot can be actively deformed in the axial direction using external magnetic actuation. Rolling locomotion and drug releasing experiment is performed in synthetic stomach. The robot is further developed in [142] and a magnetically actuated multimodal drug release mechanism is integrated where magnetic pulse frequency controls the drug release rate. The robot of [141] is modified to add biopsy functionality in [5] and ex-vivo biopsy experiments using pig stomach are performed. The robot carries and releases micro-grippers (tip-to-tip size $980\ \mu\text{m}$) inside the stomach and retrieves them after they grab tissue samples. Other researches on motorized magnet actuated propulsions include [138] and [143].

Using robotic navigation system: A magnetic shell coated capsule robot is actuated by a robotic magnetic navigation system developed by Stereotaxis in [46, 47]. The robotic system delivers a controlled magnetic field produced by two large coaxial permanent magnets arranged on both sides of the patient's table. The magnetic shell coated capsule placed within the magnetic field can experience a 360 degree omnidirectional rotation according to the orientation of the controlled magnetic field. The position of the capsule robot is continuously monitored by the fluoroscopic scanner. The size of the commercially available capsule can further be decreased for this technique as there is no need of a battery here. But the Stereotaxis system is very expensive compared to the existing capsule endoscope and it could only be performed in the healthcare centres where the system is available.

A pilot study is performed to examine human stomach using a guidance-magnet-robot controlled capsule endoscope in [144]. The capsule endoscope ($28\text{mm} \times 12\text{mm}$) has a permanent magnet inside it. 34 healthy volunteers attended the study. The volunteers swallowed gas-producing powder to distend the stomach before swallowing the capsule. The examination was well accepted by the volunteers and it took 43.8 ± 10 min to complete the examination. An actuator magnet is positioned using a Yaskawa Motoman robotic manipulator in [36] to propel a spherical device and a capsule-shaped device inside a PVC lumen during a proof-of-concept experiment. In their later work, similar actuator setup is used to control the position and orientation of a mockup capsule endoscope in fluid [12].

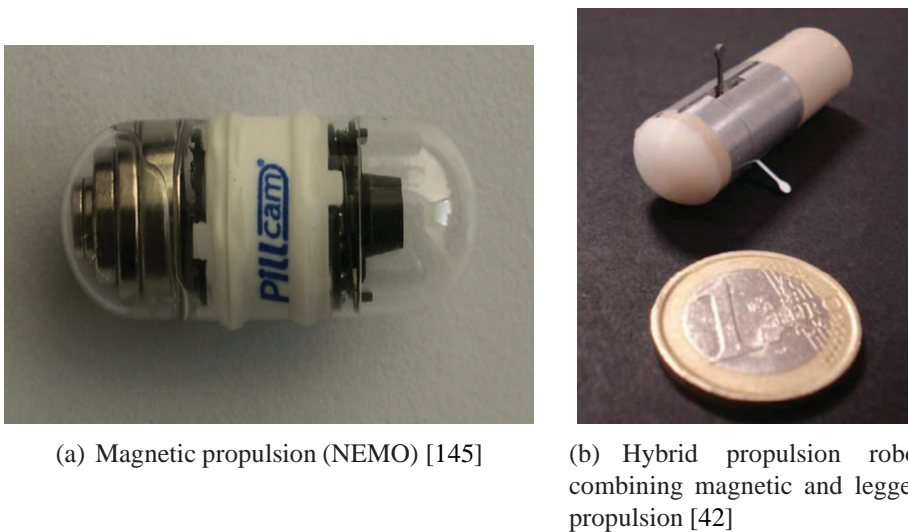


Fig. 2.9 Magnetic and hybrid propulsion endoscopic robots

External Coils Actuated Propulsion The Norika project team develops a capsule robot based on internal and external coils. It has three internal coils and is controlled by three external coils placed in a jacket worn by the patient [146].

An optimization algorithm is designed in [147] for the selection of most economical currents for the coils that generate external magnetic field for the magnetic propulsion. They propose three orthogonal coil pairs which can be placed around the abdomen. A small permanent magnet is enclosed into the capsule robot and the robot is propelled by the external orthogonal coils. Olympus develops a capsule with a permanent magnet placed inside it [146]. The capsule is controlled by a rotating magnetic field generated by three pairs of electromagnets. It can be maneuvered using a spiral ridge wrapped around its body.

An electromagnetic 3D locomotion and steering system consisting of five pairs of solenoid

components is developed in [13] for a capsule endoscope with permanent magnet to move within the digestive organs. The experiments are performed in a cubic chamber and tubular phantom filled with silicone oil. The capsule endoscope performs the translational, rotational and helical motions. An inflated bovine intestine is used in the ex-vivo experiment and the capsule endoscope performs translational and rotational motions.

Hybrid Propulsion Robot

To reduce the inherent disadvantages of both internal and external propulsion, internal and external propulsions are combined in the hybrid propulsion.

Magnetic and Motor Mechanism A hybrid robot is developed in [53] where normal locomotion is achieved by external magnetic propulsion and fine orientation is achieved by utilising a internal mechanism. An internal motor is connected to a toothed gear and the gear is glued to two small internal magnets. The external permanent magnet is moved manually or by a simple hold and the capsule robot moves along the intestinal path with the motion of the external magnet. When fine orientation is necessary the external magnet is stopped and the internal motor is activated. The interaction of the internal magnets with the external magnet while the motor applies torque to the internal magnets allows the fine adjustment of the capsule robot position from 1.8 degree to 360 degree. The principle is called magnetic internal mechanism (MIM) and is tested in free space, in a phantom and in a Pig.

Magnetic and Legged Mechanism A hybrid locomotion (Fig. 2.9(b)) is proposed in [42] combining internal legged actuation mechanisms and external magnetic dragging. The developed capsule robot is moved by magnetic dragging with the help of internal permanent magnets and external magnetic field. Whenever it gets stuck in a collapsed area of GI track, internal legged mechanism is activated remotely. The legs distend the tissue and get the capsule robot out of the collapsed region. Then the capsule robot returns to magnetic dragging mode and starts moving normally. The hybrid capsule robot achieved 8 cm/min speed in an in-vivo experiment [42].

Magnetic Torque Actuated Legged Mechanism A magnetic torque actuated legged robot is developed in [11]. Actuation of two external permanent magnets causes the rotation of an internal permanent magnet. This rotation actuates a set of legs through an internal mechanism. These legs propel the robot while distending the intestinal wall. A scaled up prototype

is developed and in-vitro experiments is conducted in a half-section intestine model where the robot moves with a speed of 5.7 mm/min.

2.7 Control of Underactuated Mechanical Systems

An underactuated mechanical system (UMS) has fewer number of control inputs than the degrees of freedom to be controlled. Control of UMSs are extremely important due to the broad range of applications of UMS such as robotics (e.g. walking robots), aerospace vehicles (e.g. helicopters), surface vessels and underwater vehicles.

2.7.1 Dynamics of UMS

The Euler-Lagrange equation of a UMS are [148]:

$$\frac{d}{dt} \frac{\partial L}{\partial \dot{q}} - \frac{\partial L}{\partial q} = F(q)\tau. \quad (2.1)$$

where $q \in \mathbb{R}^n$ is the configuration vector, $L = T - V$, T is the kinetic energy, V is the potential energy, $\tau \in \mathbb{R}^m$ is the control input, $F(q) \in \mathbb{R}^{n \times m}$ is a non-square matrix and $m < n$. For simple lagrangian systems (2.1) can be expressed as:

$$M(q)\ddot{q} + C(q, \dot{q})\dot{q} + G(q) = F(q)\tau. \quad (2.2)$$

where $M(q) \in \mathbb{R}^{n \times n}$ is the inertia matrix, $C(q, \dot{q})\dot{q} \in \mathbb{R}^n$ which contains centrifugal terms and coriolis terms, $G(q)$ is gravity term.

Assuming $F(q) = [0, I_m]^T$, the configuration vector q can be partitioned as $q = (q_1, q_2) \in \mathbb{R}^{n-m} \times \mathbb{R}^m$ where q_1 and q_2 are unactuated and actuated configuration vectors respectively. After partitioning (2.2) becomes:

$$\begin{bmatrix} m_{11}(q) & m_{12}(q) \\ m_{21}(q) & m_{22}(q) \end{bmatrix} \begin{bmatrix} \ddot{q}_1 \\ \ddot{q}_2 \end{bmatrix} + \begin{bmatrix} h_1(q, \dot{q}) \\ h_2(q, \dot{q}) \end{bmatrix} = \begin{bmatrix} 0 \\ \tau \end{bmatrix}. \quad (2.3)$$

where $\tau \in \mathbb{R}^m$. $h_1(q, \dot{q}) \in \mathbb{R}^{n-m}$ and $h_2(q, \dot{q}) \in \mathbb{R}^m$ contain centripetal, coriolis and gravitational terms.

2.7.2 Control Problems

The control problem of UMS can be divided into the following three classes [149].

- Trajectory planning: The aim here is to compute/plan a dynamically feasible trajectory from q^0 to q^d where q^0 and q^d are given initial and final configuration respectively.
- Trajectory tracking: The aim here is to compute a feedback control for a given dynamically feasible trajectory $q_d(t)$ that asymptotically stabilizes the tracking error, $e(t) = q_d(t) - q(t)$ to zero.
- Set-point regulation: The aim here is to compute a feedback control for a given desired configuration q^d that asymptotically stabilizes the equilibrium state to $q = q^d, \dot{q} = 0$.

2.7.3 Stabilization Control / Set-point Regulation

Stabilization of underactuated mechanical system can be divided into two classes:

Class I : Stabilization to a unstable equilibrium point The control aim for this class is to stabilize the system in one unstable equilibrium point from another stable or random position. The examples of this class of system are two-link manipulators (acrobot and pendubot), rotating pendulum, inverted wheel pendulum (IWP) and cart-pole system.

Class II : Stabilization to a stable equilibrium point with disturbance The control aim for this class is to stabilize the system to a stable equilibrium point overcoming disturbances from the external and internal sources and payload. The examples of the UMSs with this type stabilization are overhead crane and TORA system.

Class I : Stabilization to a unstable equilibrium point

The prevalent techniques used for stabilization of underactuated mechanical systems are energy-based control, feedback linearization, sliding mode control [150, 151], backstepping control and Lyapunov's direct method [152, 153] or their modified version or their combined version.

A vehicle position stabilization controller by utilizing partial feedback linearization were developed in [56] for wheeled inverted pendulum (wheel movement active and pendulum movement passive). A energy based control was presented in [154] for balancing a pendubot. Hybrid sliding mode based control algorithm was developed in [155] to regulate both actuated and unactuated joints to their desired positions of a 2-DOF underactuated horizontal pendulum.

Three methods (feedback linearisation, Lyapunov design and sliding mode control) were combined in [55] to achieve stabilization for underactuated systems such as pendulum on a cart where the pendulum movement is active and the wheel movement is passive. A backstepping-like adaptive controller was designed in [156] to stabilize underactuated systems such as inverted pendulum based on the function approximation technique.

Class II : Stabilization to a stable equilibrium point with disturbance

A variable structure controller was designed in [157] and sliding mode controllers were designed in [158, 159] to stabilize an overhead crane by suppressing the swings of the load. In [160] the authors designed sliding mode controller for stabilization of overhead crane where they considered suppression of load swing angles and also crane position control. A linear cascade controller and integrator back-stepping controller were presented in [161] for feedback stabilization of TORA system. In [162] a state-feedback controller was developed with experiments for a TORA system.

2.7.4 Trajectory Tracking Control

Trajectory tracking of underactuated mechanical systems such as surface vessels, VTOL aircraft, differential drive robot, underwater vehicles has attracted considerable attractions because of their wide range of applications. The control techniques includes feedback linearization [163], sliding mode control [62, 164], backstepping [165, 166], adaptive control [167], fuzzy logic control [168] and their combinations [169].

A Lyapunov-based control approach to stabilize reference trajectories of velocity, position or thrust direction was proposed in [170] for a class of underactuated systems which includes VTOL vehicles, helicopters and submarines. Surface vessels has three degrees of freedom (surge, yaw and sway) but only two control inputs (surge force and yaw moment). A state-feedback control law was developed in [171] based on cascaded approach for a surface vessel which obtained global stability for the tracking error.

Trajectory tracking of differential mobile robot was presented in [172–178]. A global trajectory tracking controller was developed using backstepping-like feedback linearization in [173] to follow various reference trajectories such as straight line, circle and sinusoidal curve. A feedback 3-D trajectory tracking controller was presented in [179] for autonomous vehicles (especially for underwater vehicles) in the presence of gravity, buoyancy and fluid dynamic forces.

Trajectory Tracking of Capsubot-type Robot Capsubot-type robot works by utilizing internal reaction force. A control law based on cluster treatment of characteristic roots (CTCR) was developed for the position trajectory tracking of an underactuated cart-pendulum i.e. actuated configuration in [180] while stabilizing the pendulum in its upward position.

2.8 Summary

This chapter has presented the robots for minimally invasive diagnosis and intervention. Table 2.1 compares among the medical robots. Though the external robots (e.g. da-Vinci robot) have been performing robot-assisted surgical procedures successfully since early 1990s, there are still needs of adding more flexibility to the surgical robot system and making it light weight. The miniature in-vivo laparoscopic and endoscopic robots are still operating in the laboratories. The in-vivo laparoscopic robots have been classified as fixed-base camera robots, wheeled robot, magnetic drive robots and suction based robots. Table 2.2 compares among the in-vivo laparoscopic robots. The in-vivo endoscopic robots are classified as external propulsion robots, internal propulsion robots and hybrid propulsion robots. Tables 2.3 to 2.5 compare among the endoscopic robots.

The fixed base laparoscopic camera robots mount themselves within the abdominal cavity using tripod or needle or suturing and help the surgeon with the video of the operating region. The driving principle of in-vivo laparoscopic magnetic drive robot and in-vivo endoscopic external drive robots are similar. For both of them an external magnetic field provides the propulsive force to move the robot inside the patient body i.e. within the abdominal cavity or gastro-intestinal (GI) track. As the propulsion force comes from external source these robots do not require internal actuators and thus no need of onboard power for the robot motion. The external magnetic field could be generated by a permanent magnet (moved by hand or robotic arm) or an electromagnet or an MRI. Some of these system e.g. the MRI guided and robotic arm guided systems are bulky and expensive whereas the hand-held magnet guided system can not perform precise robot movement.

The robots with external moving parts such as in-vivo wheeled laparoscopic robot or many in-vivo internal propulsion endoscopic robots such as legged endoscopic robot, paddling based robot and earthworm-like robot have been proved to be effective methods of propulsions. They have more precise propulsions compared to the external propulsion robots. The legged robot is able to distend the tissue in the GI track for better inspection. It can also navigate through narrow spaces by distending the tissue. However robots with external moving parts pose the risk of hurting the internal soft tissue. Furthermore

the actuation mechanism take extra space within the robot and require additional power to run it. Unlike other internal propulsion robot, the capsbot-type propulsion robots have the propulsion mechanism completely inside the robot. Thus this robot does not pose any risk of tissue damage and the robot can be made hermetically sealable i.e. the robot can be completely enclosed.

This chapter also presents control of the underactuated mechanical systems (UMSs). The UMSs have mainly two types of control aims: the stabilization control and the trajectory tracking control. Though extensive research has been done in the stabilization control of the underactuated systems, the trajectory tracking control is still challenging, specially the trajectory tracking of unactuated configuration of the underactuated systems requires further investigation and research. This research investigates the trajectory tracking of the capsule robots.

2.9 Scope of Contribution

The in-vivo laparoscopic and endoscopic robots have the potential to make the diagnostic processes such as the diagnosis of the gastro-intestinal diseases painless and, the surgical procedures such as the laparoscopic abdominal surgery less invasive. However the state of the art literature review of this chapter suggests that more researches are required to realize the full potential of the in-vivo miniature robots.

The limitations of the miniature in-vivo robots presented in this chapter justify the requirement of the design and development of novel miniature robots (propulsion systems) for in-vivo laparoscopic and endoscopic applications. Thus this thesis investigates the capsule robots and presents the 1D and 2D capsule robot because of the exceptional features of the capsule robots such as having the propulsion mechanism completely inside the robot body, having no external moving parts, having customizable outer structure, being hermitically sealable (enclosable) and being simple in structure. Furthermore to utilize the advantage of the legged propulsion robot such as the ability to distend tissue and the ability to travel through the narrow spaces, this thesis proposes a hybrid capsule robot which combines the legless capsbot propulsion and the legged propulsion. The hybrid robot has an added capability of anchoring at a place for longer observation of a suspected region within the gastro-intestinal track for improved diagnosis of the diseases. It uses same actuators for all the four modes of operation. This robot is more effective than robots with a single mode of operation as it can switch among the four modes based on the surrounding environment and situation.

The trajectory tracking control of the unactuated configuration of the capsbot-type robot such as pendulum on a cart [55] and a capsule robot (capsbot) [41] was not considered in the literature according to the author's knowledge. However the trajectory tracking control is a primary requirement for any mobile robot. Thus this thesis addresses the one and two dimensional trajectory tracking control of the capsule robot. The feedback linearization is proven to be successfully used in many underactuated systems in the literature. Thus in this thesis the feedback linearization is used for the low-level control of the inner mass (IM) of the capsule robot.

Chapter 3

1D Capsule Robot

3.1 Introduction

This chapter presents a 1D (one dimensional) capsule robot (capsubot) which is limbless (i.e. no external moving parts) and moves using internal reaction force. Fig. 3.1 shows the schematic of the 1D capsuobot. The 1D capsuobot has an inner mass (IM) that can be moved back and forth. The reaction force generated because of the IM movement can be utilized to control the capsuobot movement. The 1D capsuobot is an underactuated system as it has two degrees of freedom (one degree of freedom for the IM and one degree of freedom for the capsuobot) but only one control input which is the force on the IM. Thus the movement of the IM is active whereas the movement of the capsuobot is passive.

The main contributions of this chapter are to propose a new two-stage control strategy for the trajectory tracking control of a 1D capsuobot, to propose two acceleration profiles (utroque and contrarium) for the capsuobot motion generation, to propose a novel selection algorithm for the appropriate selection of the acceleration profile parameters and to implement the proposed control strategy in a developed capsuobot prototype.

3.2 Modelling, Problem Statement and Proposed Strategy

3.2.1 Dynamic Modelling

Fig. 3.1 shows a schematic of the capsule robot (capsuobot). The inner mass (IM) of the capsule robot can move from one end to the other end of the capsule robot. The source of the propulsion force is not shown here. By controlling the IM movement, the capsule robot

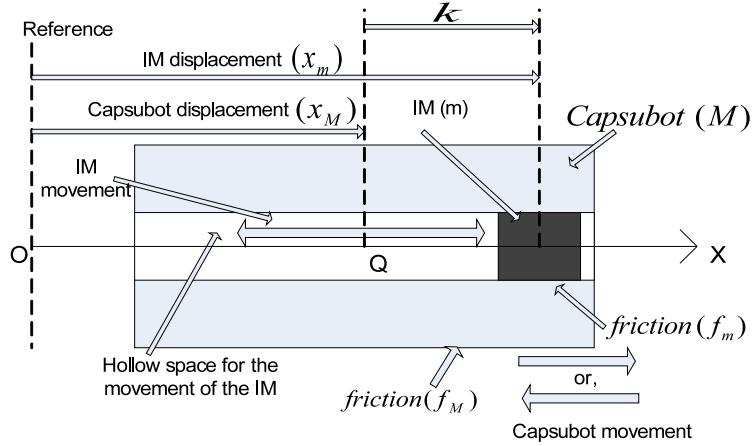


Fig. 3.1 Schematic of capsuobot with reference line

can be moved in a certain given direction. If F_m force is applied on the IM, the dynamic model of the capsule robot can be represented as:

$$F_m = m\ddot{x}_m + f_m, \quad (3.1)$$

$$F_M = -m\ddot{x}_m = M\ddot{x}_M + f_M, \quad (3.2)$$

where

- x_m and x_M are the positions of the IM and the capsuobot respectively with respect to an external reference;
- m and M are the masses of the IM and the capsuobot respectively;
- F_M is the force received by the capsuobot;
- $f_M = \text{sgn}(\dot{x}_M)\mu_M Mg$ and $f_m = \text{sgn}(\dot{x}_m - \dot{x}_M)\mu_m mg$ are the friction between the capsuobot and the surface of motion, and between the IM and the capsuobot respectively.
- μ is the coulomb friction coefficient.
- the initial position of the mid-point of the capsuobot is taken as the reference for the measurement of x_m and x_M .

3.2.2 Problem Statement and Proposed Strategy

The capsuobot is an underactuated system i.e. degrees of freedom to be controlled are greater than number of control inputs. To solve this the control problem is divided into two stages

which are described below. The schematic diagram of the complete control system is shown in Fig. 3.2.

- *Stage 1 - Desired IM Trajectory Generation:* For a given trajectory (x_{Md}, \dot{x}_{Md}) of the capsuobot, the desired trajectory $(x_{md}, \dot{x}_{md}, \ddot{x}_{md})$ of the IM is calculated.
- *Stage 2 - Control of the IM:* For the given desired trajectory $(x_{md}, \dot{x}_{md}, \ddot{x}_{md})$ of the IM, the closed-loop control is achieved by correcting the control input using the error (x_{me}, \dot{x}_{me}) which is the difference between the measured and the desired trajectories of the IM.

These two stages are discussed in details in the remaining chapter.

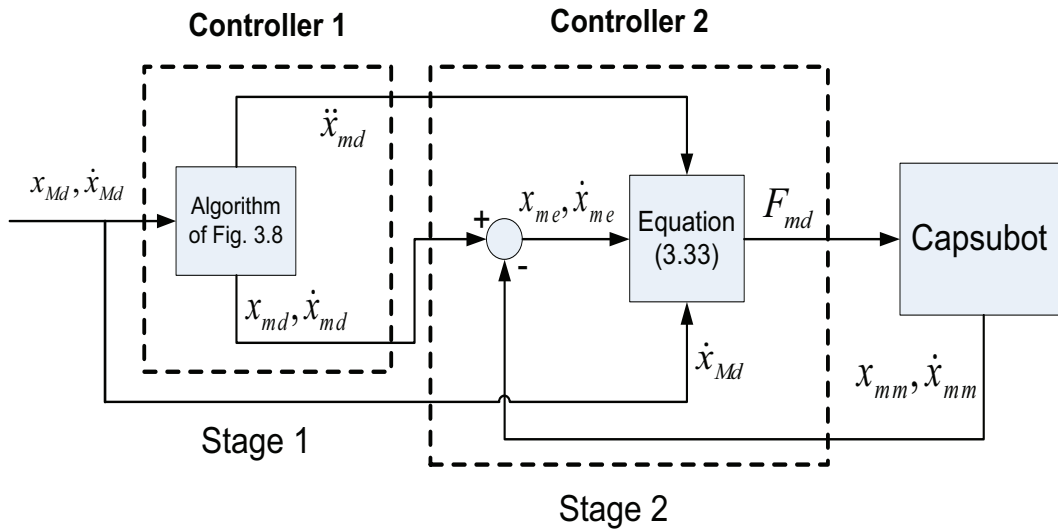


Fig. 3.2 Schematic diagram of the proposed control system of the capsuobot

3.3 Proposed Acceleration Profiles and Motion Generation

3.3.1 Proposed Acceleration Profiles

To perform trajectory tracking, the capsuobot trajectory is divided into small time segments. The IM acceleration profile parameters is tuned in every time segment to enable the capsuobot to track the trajectory. In [41], a 4-step acceleration profile of IM is proposed for the motion control of a capsuobot. The following issues arise when the acceleration profile of [41] is considered to use in capsuobot trajectory tracking.

- For a set of parameters (accelerations) of IM, the cycle time is different for cycle 1 and the other cycles.
- From cycle 2, the capsbot has a nonzero initial velocity which depends upon the previous cycle. Thus the distance travelled by the capsbot in each cycle not only depends on the IM accelerations of that particular cycle but also on the previous cycle.

Based on these observations acceleration profile of [41] is modified and two acceleration profiles namely *utroque* and *contrarium* are proposed which have the following advantages.

- Cycle times are same for all the cycles for a specific parameter (acceleration) set.
- The capsbot has a zero initial velocity in all the cycles.
- The distance travelled by the capsbot in each cycle solely depends on the IM accelerations of that cycle. This makes the trajectory tracking problem easier to solve.

Utroque is a four-step acceleration profile whereas *contrarium* is two-step acceleration profile. It is worth mentioning that steps 3 and 4 of the *utroque* profile are similar to steps 1 and 2 of the *contrarium* profile respectively apart from a nonzero initial velocity in step 3 of the *utroque* profile.

Utroque Acceleration Profile

This is a four-step acceleration profile shown in Figs. 3.3(a) and 3.3(b). The scenarios of the capsbot movement in this profile are shown in Figs. 3.4(a) and 3.4(b). In this profile, the capsbot and the IM move in the same direction in the step 2 (see Fig. 3.5(b)) and move in the opposite direction in the steps 3 and 4. The IM moves forward (forward journey) for the steps 1 and 2, and backward (return journey) for the steps 3 and 4. The capsbot moves forward for the steps 2, 3 and 4. Thus the capsbot moves forward for the IM bidirectional movements. Latin word '*utroque*' means both directions. a_{mu1} and a_{mu4} can be designed to be same in magnitude or different in magnitude. Similarly a_{mu2} and a_{mu3} can be designed to be same in magnitude or different in magnitude.

Contrarium Acceleration Profile

This is a two-step acceleration profile shown in Figs. 3.3(c) and 3.3(d). The scenarios of the capsbot movement in this profile are shown in Figs. 3.4(c) and 3.4(d). In this profile, the capsbot moves in the opposite direction of the IM (see Fig. 3.6(b)). Latin word '*contrarium*' means the opposite direction. Here the IM only performs forward journey.

3.3.2 Motion Generation

Four possible scenarios are shown in Figs. 3.4(a) to 3.4(d). Motion generation is explained for two scenarios (Figs. 3.4(a) and 3.4(c)) based on the two proposed acceleration profiles. Motion generation of the scenarios of Figs. 3.4(b) and 3.4(d) are similar in principle to the scenarios of Figs. 3.4(a) and 3.4(c) respectively.

Utroque Acceleration Profile for the Scenario of Fig. 3.4(a)

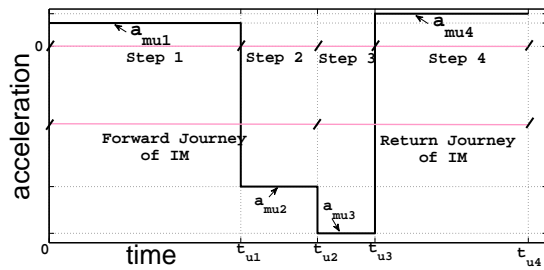
The IM is at its left end ($x_m - x_M = -k$) at the beginning of the cycle and the IM follows the acceleration profile shown in Fig. 3.3(a). Here k is the half length of the maximum relative displacement of the IM. The IM moves from the left end to the right end and then returns to the left end in this acceleration profile. The accelerations, velocities and positions of the IM and the capsbot in different steps are shown in Figs. 3.5(a) to 3.5(c) and $a_{mu1} = a_{mu4}$ and $a_{mu2} = a_{mu3}$.

Step 1 The IM moves forward slowly with a small +ve acceleration ($a_{mu1} > 0, \dot{x}_m > 0$) and, as the friction force (f_M) dominates over the reaction force (F_M) i.e. $|F_M| < |f_M|$, the capsbot remains stationary ($\ddot{x}_M = 0, \dot{x}_M = 0$).

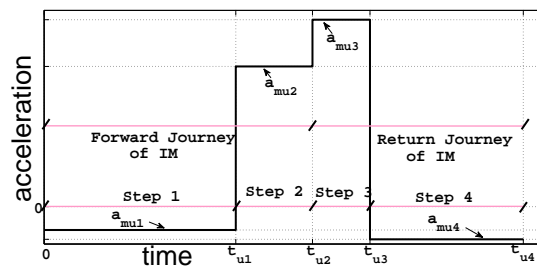
Step 2 The IM moves forward with a big -ve acceleration ($a_{mu2} \ll 0, \dot{x}_m > 0$) and the capsbot moves forward with a +ve acceleration ($a_{Mu2} > 0, \dot{x}_M > 0$) due to the reaction force (F_M) where $|F_M| > |f_M|$. The IM reaches to its right end ($x_m - x_M = k$) at the end of this step and stops.

Step 3 In this step the capsbot has a +ve initial velocity ($v_{Mu12} > 0$). The IM moves backward with a big -ve acceleration ($a_{mu3} \ll 0, \dot{x}_m < 0$) and the capsbot receives a force (F_M) in the forward direction where $|F_M| > |f_M|$. Thus the capsbot moves forward with a +ve acceleration ($a_{Mu3} > 0, \dot{x}_M > 0$). The capsbot velocity in this step is higher than in step 2.

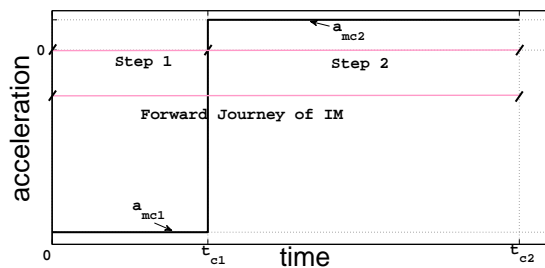
Step 4 The IM continues to move backward but with a small +ve acceleration ($a_{mu4} > 0, \dot{x}_m < 0$). The capsbot moves forward with a small -ve acceleration ($a_{Mu4} < 0, \dot{x}_M > 0$) for a part of step 4 before it stops. The capsbot remains stationary ($\ddot{x}_M = 0, \dot{x}_M = 0$) for the remaining time of step 4 as the friction force (f_M) dominates over the reaction force (F_M) i.e. $|F_M| < |f_M|$. The IM reaches to its left end ($x_m - x_M = -k$) at the end of step 4 and stops.



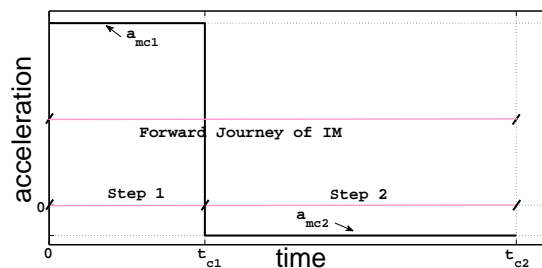
(a) Utroque acceleration profile - Scenario 1 (a_{mu1} , a_{mu2} , a_{mu3} and a_{mu4} are the IM accelerations in steps 1, 2, 3 and 4 respectively; t_{u1} , t_{u2} , t_{u3} and t_{u4} are the time after steps 1, 2, 3 and 4 respectively)



(b) Utroque acceleration profile - Scenario 2 (a_{mu1} , a_{mu2} , a_{mu3} and a_{mu4} are the IM accelerations in steps 1, 2, 3 and 4 respectively; t_{u1} , t_{u2} , t_{u3} and t_{u4} are the time after steps 1, 2, 3 and 4 respectively)

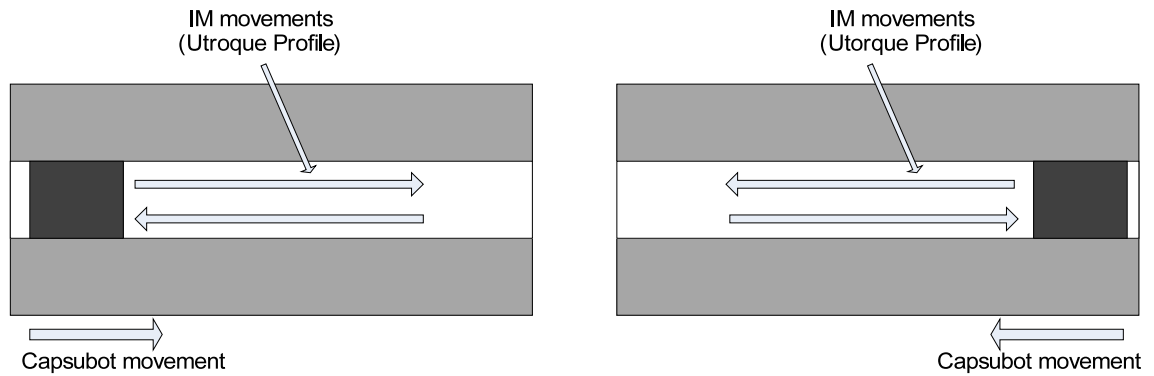


(c) Contrarium acceleration profile - Scenario 1 (a_{mc1} and a_{mc2} are the IM accelerations in steps 1 and 2 respectively; t_{u1} and t_{u2} are the time after steps 1 and 2 respectively).



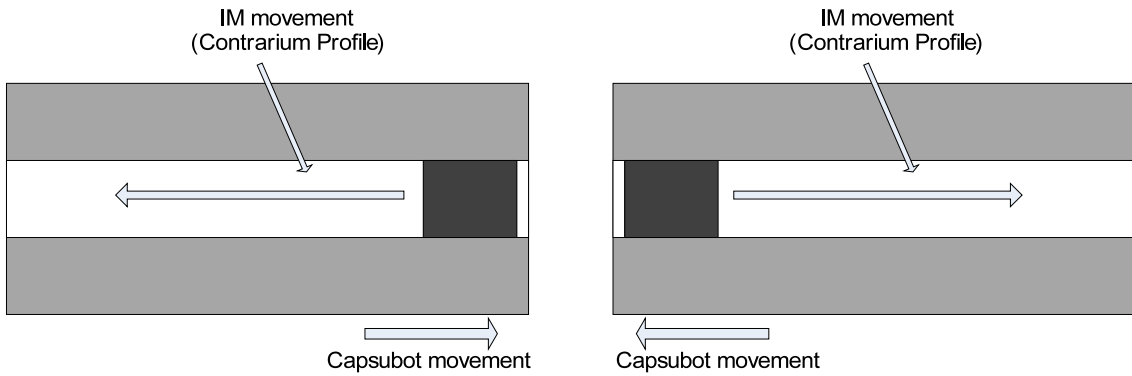
(d) Contrarium acceleration profile - Scenario 2 (a_{mc1} and a_{mc2} are the IM accelerations in steps 1 and 2 respectively; t_{u1} and t_{u2} are the time after steps 1 and 2 respectively).

Fig. 3.3 Acceleration profiles for the IM



(a) For the IM at the left end, the capsabot is moved to the right using the Utroque profile shown in Fig. 3.3(a)

(b) For the IM at the right end, the capsabot is moved to the left using the Utroque profile shown in Fig. 3.3(b)



(c) For the IM at the right end, the capsabot is moved to the right using the Contrarium profile of Fig. 3.3(c). After one cycle the IM reaches to the left end and then the IM is ready to use the Utroque profile described in Fig. 3.4(a)

(d) For the IM at the left end, the capsabot is moved to the left using the Contrarium profile of Fig. 3.3(d). After one cycle the IM reaches to the right end and then the IM is ready to use the Utroque profile described in Fig. 3.4(b)

Fig. 3.4 Four possible scenarios of the capsabot for motion generation

Figs. 3.5(a) to 3.5(c) show that, in the steps 1 and 2 the IM completes the forward journey and reaches to k position from $-k$ position. In the step 1, the IM has a small +ve acceleration ($a_{mu1} > 0$) and thus the IM slowly reaches to v_{mu12} velocity from zero velocity whereas the capsbot remains stationary for the entire step 1 and, the capsbot velocity and acceleration are zero. In the step 2, the IM has a big -ve acceleration ($a_{mu2} \ll 0$) and thus the IM velocity reaches to zero from v_{mu12} in a shorter period of time and also the IM travels shorter distance in the step 2 compared to the step 1. The capsbot moves forward with a moderate acceleration (a_{Mu2}) and it reaches to v_{Mu12} velocity from zero in the step 2.

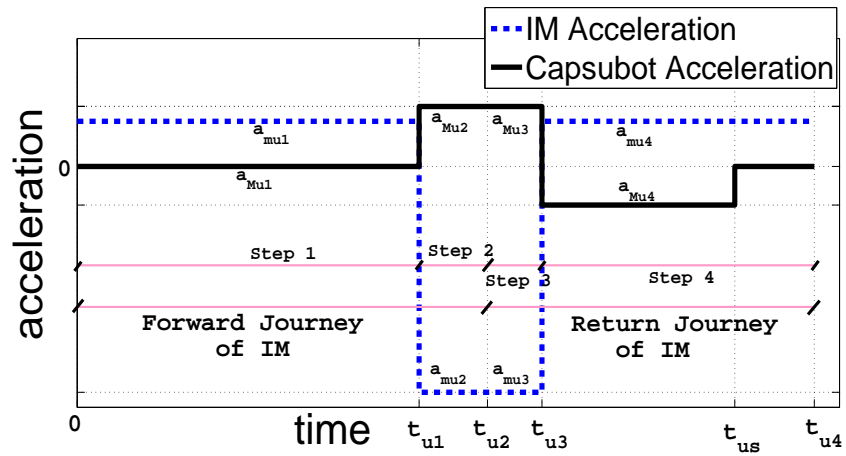
In the steps 3 and 4 the IM completes its return journey and returns to $-k$ position from k position. In the step 3 the IM moves with a big -ve acceleration and at a shorter time period, IM velocity reaches to v_{mu34} from zero. The capsbot keeps moving forward with a moderate acceleration (a_{Mu3}) and the IM velocity reaches to v_{Mu34} from v_{Mu12} in the step 3 where $v_{Mu34} > v_{Mu12}$. The capsbot average velocity in the step 3 is bigger than that in the step 2 as in the step 3 the capsbot has a non-zero initial velocity. Fig. 3.5(c) shows that the distance travelled by the capsbot in the step 3 is bigger than that in the step 2. In the step 4 the IM moves with a small +ve acceleration (a_{mu4}) and the IM velocity reaches to zero from v_{mu34} . The capsbot moves forward with a -ve acceleration (a_{Mu4}) and stops at t_{us} time. Thus the capsbot moves during the steps 1, 2 and part of step 3 and remains stationary during the rest of the time.

Contrarium Acceleration Profile for the Scenario of Fig. 3.4(c)

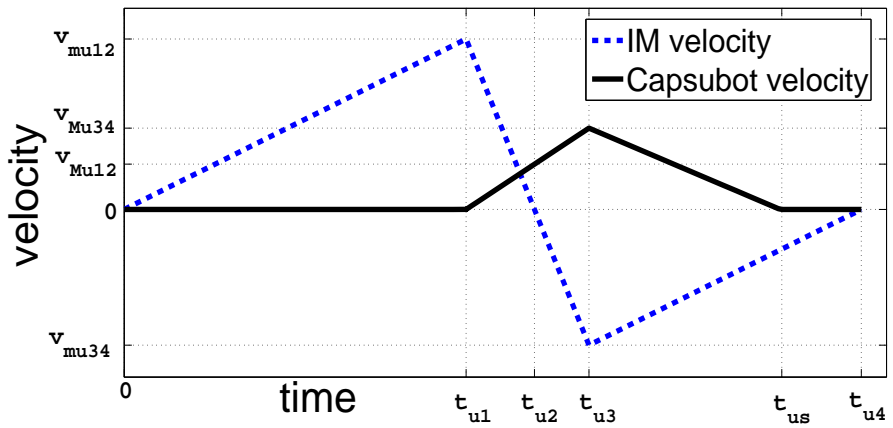
The IM is at its right end ($x_m - x_M = k$) at the beginning of the cycle and the IM follows the acceleration profile shown in Fig. 3.3(c). The IM moves from the right end to the left end in this acceleration profile. The accelerations, velocities and positions of the IM and the capsbot in the different steps are shown in Figs. 3.6(a) to 3.6(c). This is a two-step acceleration profile.

Step 1 The IM moves backward with a big -ve acceleration ($a_{mc1} \ll 0$, $\dot{x}_m < 0$) and the capsbot receives a force ($F_M > 0$) in the forward direction. Here the reaction force (F_M) is big enough to overcome the friction (f_M) i.e. $|F_M| > |f_M|$. Thus the capsbot moves forward with a +ve acceleration ($a_{Mc1} > 0$, $\dot{x}_M > 0$).

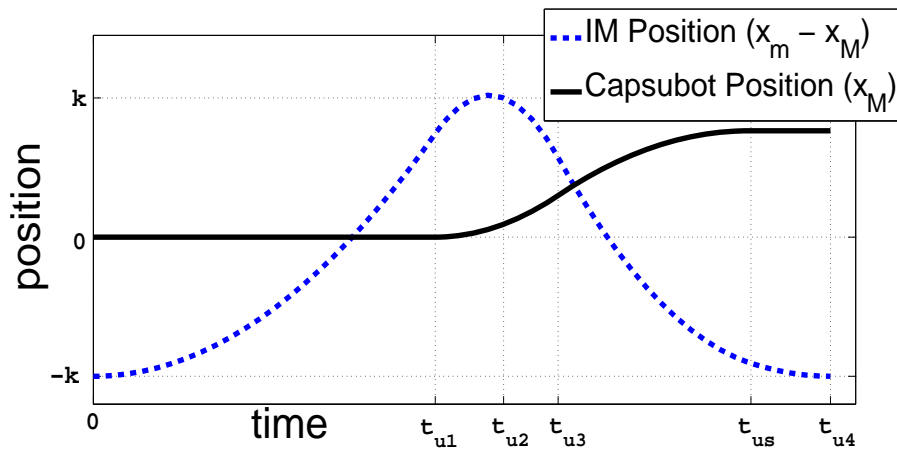
Step 2 The IM continues to move backward but with a small +ve acceleration ($a_{mc2} > 0$, $\dot{x}_m < 0$). The capsbot moves forward with a small -ve acceleration ($a_{Mc2} < 0$, $\dot{x}_M > 0$) for a part of the step 2 before it stops. The capsbot remains stationary ($\ddot{x}_M = 0$, $\dot{x}_M = 0$) for the remaining time of the step 2 as the friction force (f_M)



(a) IM and capsuobot accelerations



(b) IM and capsuobot velocities



(c) IM and capsuobot positions

Fig. 3.5 Accelerations, velocities and positions of the IM and the capsuobot for the utroque profile for the scenario of Figs. 3.4(a) and 3.3(a)

dominates over the reaction force (F_M) i.e. $|F_M| < |f_M|$. The IM reaches its left end ($x_m - x_M = -k$) at the end of the step 2 and stops.

3.3.3 Optimum Selection of Acceleration Profile Parameters

This section presents the optimum selection of acceleration profile parameters namely a_{mc1} , a_{mc2} , a_{mu1} , a_{mu2} , a_{mu3} , a_{mu4} , t_{c1} , t_{c2} , t_{u1} , t_{u2} , t_{u3} and t_{u4} of Figs. 3.3(a) and 3.3(d). a_{mc1} , a_{mu2} and a_{mu3} are big accelerations and they can be designed as big as possible (depending on the maximum force the propulsion source can provide) to get a big average velocity of the capsuobot. a_{mc2} , a_{mu1} and a_{mu4} should be small enough so that the friction force (f_M) is bigger than the reaction force (F_M), thus the capsuobot does not move reverse. Thus using (3.2) it is observed that $|a_{mc2}|$, $|a_{mu1}|$, $|a_{mu4}|$ are less than $\frac{\mu_M M g}{m}$. The following design options are available: $a_{mu1} = a_{mu4}$ and $a_{mu2} = a_{mu3}$ or, $a_{mu1} \neq a_{mu4}$ and $a_{mu2} \neq a_{mu3}$ or, $a_{mu1} = a_{mu4}$ and $a_{mu2} \neq a_{mu3}$ or, $a_{mu1} \neq a_{mu4}$ and $a_{mu2} = a_{mu3}$. In this chapter $a_{mu1} = a_{mu4}$ and $a_{mu2} = a_{mu3}$ are designed.

Utroque Profile: From Figs. 3.5(a) and 3.5(b):

$$t_{u1} = \frac{|v_{mu12}|}{|a_{mu1}|} ; t_{u2} = t_{u1} + \frac{|v_{mu12}|}{|a_{mu2}|}, \quad (3.3)$$

$$t_{u3} = t_{u2} + \frac{|v_{mu34}|}{|a_{mu3}|}; t_{u4} = t_{u3} + \frac{|v_{mu34}|}{|a_{mu4}|}, \quad (3.4)$$

$$t_{us} = t_{u3} + \frac{|v_{M34}|}{|a_{Mu4}|}, \quad (3.5)$$

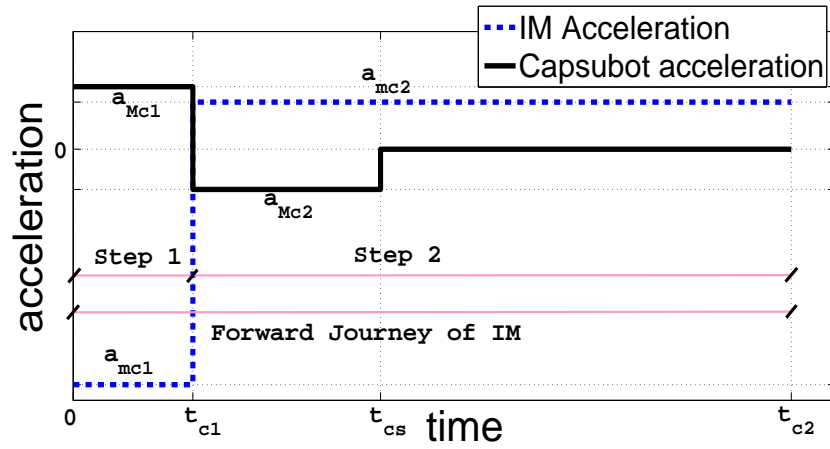
where,

$$v_{mu12} = \sqrt{\frac{4ka_{mu1}a_{mu2}^2}{a_{mu2}^2 - a_{mu1}a_{mu2} - a_{mu1}a_{Mu2}}}, \quad (3.6)$$

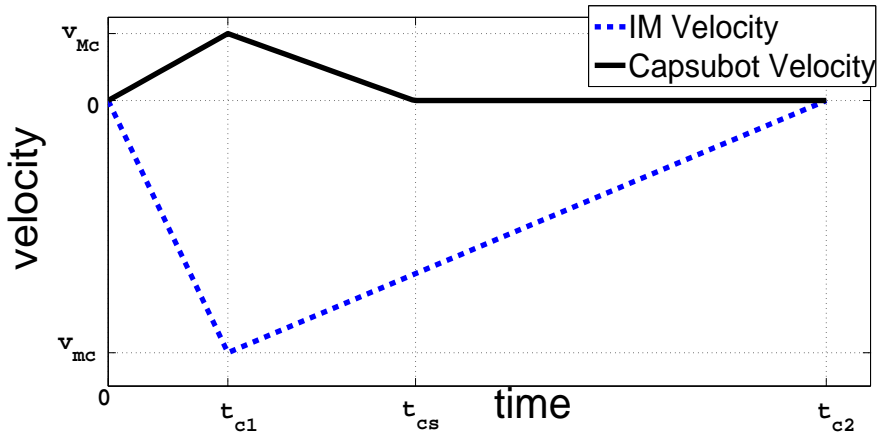
$$a_{Mui} = \frac{-ma_{mui} - \mu_M M g}{M}; i = 2, 3, 4, \quad (3.7)$$

$$v_{Mu12} = -\frac{a_{Mu2}}{a_{mu2}}v_{mu12}, \quad (3.8)$$

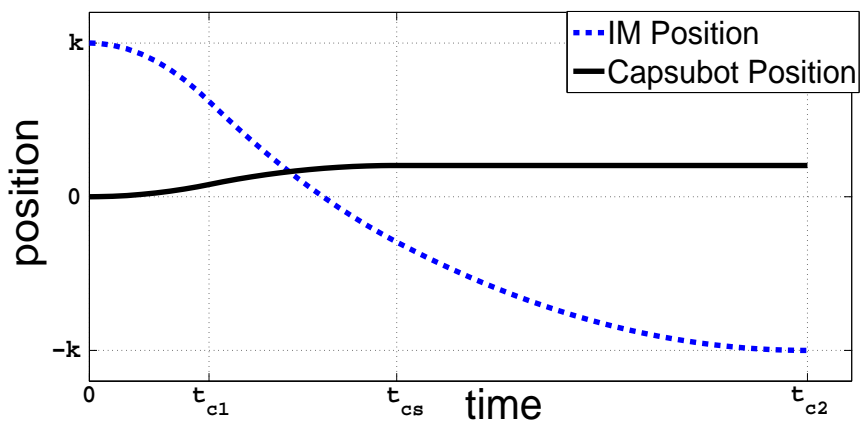
$$v_{Mu34} = \frac{a_{Mu3}}{a_{mu3}}v_{mu34} + v_{Mu12}, \quad (3.9)$$



(a) IM and capsobot accelerations



(b) IM and capsobot velocities



(c) IM and capsobot positions

Fig. 3.6 Accelerations, velocities and positions of the IM and the capsobot for the contrarium profile for the scenario of Figs. 3.4(c) and 3.3(c)

and v_{mu34} can be found by solving the quadratic equation of v_{mu34} :

$$\left(\frac{1}{a_{mu3}} - \frac{1}{a_{mu4}} + \left(\frac{1}{a_{Mu4}} - \frac{1}{a_{Mu3}}\right) \frac{a_{Mu3}^2}{a_{mu3}^2}\right) v_{mu34}^2 + 2v_{mu12} \frac{a_{Mu3} a_{Mu2}}{a_{mu3} a_{mu2}} \left(\frac{1}{a_{Mu4}} - \frac{1}{a_{Mu3}}\right) v_{mu34},$$

$$+ (4k + \frac{v_{Mu12}^2 a_{Mu2}^2}{a_{Mu4} a_{mu2}^2} v_{mu12}^2) = 0. \quad (3.10)$$

Contrarium Profile: From Figs. 3.6(a) and 3.6(b):

$$t_{c1} = \frac{|v_{mc}|}{|a_{mc1}|}; \quad t_{c2} = t_{c1} + \frac{|v_{mc}|}{|a_{mc2}|}, \quad (3.11)$$

$$t_{cs} = t_{c1} + \frac{|v_{Mc}|}{|a_{Mc2}|}, \quad (3.12)$$

where

$$v_{Mc} = \frac{a_{Mc1}}{a_{mc1}} v_{mc}, \quad (3.13)$$

$$v_{mc} = -\sqrt{\frac{-4ka_{mc1}^2 a_{mc2} a_{Mc2}}{a_{mc1} a_{Mc2} P - a_{Mc1} a_{mc2} Q}}, \quad (3.14)$$

where $P = a_{mc2} - a_{mc1}$; $Q = a_{Mc2} - a_{Mc1}$ and a_{Mc1} , a_{Mc2} can be calculated as:

$$a_{Mci} = \frac{-ma_{mci} - \mu_M M g}{M}; \quad i = 1, 2. \quad (3.15)$$

It is noted that the denominators of (3.3) to (3.14) can be avoided to become zero since a_{mc1} , a_{mc2} , a_{mu1} , a_{mu2} , a_{mu3} , and a_{mu4} are selected by the designer.

3.3.4 Comparison with Other Profiles

The references [64] and [52] analysed the motion generation of the capsbot-type robot based on velocity profiles. The reference [64] proposed a four-step velocity profile whereas reference [52] proposed a seven-step velocity profile. Through simulation and experimental results, the reference [41] demonstrated the advantages of using acceleration profile over velocity profile to analyse and control the capsbot type robot motion. The acceleration profile of the reference [41] is modified in this chapter and two new acceleration profiles are proposed.

To decide on the optimum number of steps to generate capsbot motion, previous works used various criteria. A new step is defined (i) in the reference [52] whenever there is

a change of the IM acceleration (ii) in the reference [64] whenever there is a change of the capsuot acceleration or change of the IM velocity direction (iii) in the reference [41] whenever there is a change of the IM acceleration or change of the IM velocity direction.

At least two steps are required by the IM to go from one end to the other end of the capsuot, as the IM needs to accelerate to start motion and then decelerate to stop. As in contrarium cycle the IM performs only forward journey i.e. it goes from one end to the other end, it needs at least two steps. On the other hand as in utroque profile the IM performs forward and return journey i.e. it goes from one end to the other end and then returns to its original position, it needs at least four steps.

All the previous works define the profiles for a round trip of the IM (i.e. for forward and return journey of the IM). Thus all the proposed profiles used at least four steps: the references [41, 64] used four and the reference [52] used seven. An analysis is provided below whether adding extra three steps in the reference [52] provides any added advantage. The reference [52] used three steps for the IM forward journey and four steps for the IM return journey. On the IM forward journey: step 1 uses a large IM acceleration, step 2 uses a large IM deceleration and step 3 uses a small IM deceleration. However, in the IM forward journey, the only requirement is to keep the IM acceleration such that the capsuot only moves forward. To maintain that the steps 2 and 3 can be merged to get one step. From the simulation result in the reference [52], it is seen that there is a reverse motion of the capsuot presumably in step 2 because of the large deceleration. Thus the step 2 can be removed and only the steps 1 and 3 can be kept. On the IM return journey: step 4 is motionless, step 5 has a small IM acceleration, step 6 has a constant IM velocity and step 7 has a small IM deceleration. However in the return journey the only requirement is to maintain the IM acceleration such that the capsuot does not have any reverse motion. That can be fulfilled only by using two steps.

3.4 Proposed Control Approach

The objective is to track a given trajectory (position, x_{Md}) of the capsuot. The objective is achieved using the two-stage approach of Fig. 3.2. The following steps are followed:

- Preparation Stage: Database creation (section 3.4.1)
- Stage 1: Desired IM Trajectory Generation (section 3.4.2)
 - Step 1: Generating Capsuot Trajectory Segment and Selection of Segment Period (T) (section 3.4.2)

- Step 2: Selection of Profile Parameters (Selection Algorithm) (section 3.4.2)
- Step 3: Tuning the Segment Time (section 3.4.2)
- Stage 2: Control of the IM (section 3.4.3)

3.4.1 Preparation Stage: Database creation

To track the capsbot trajectory, the projected capsbot average velocities for various IM acceleration profile parameters are required. Equations for projected average velocities are given below. The capsbot average velocity for the utroque profile is (see Fig. 3.5(c)):

$$\bar{x}_{Mu} = \frac{x_{Mu}}{t_u}, \quad (3.16)$$

where x_{Mu} is the displacement of the capsbot in utroque profile in cycle time t_u .

$$x_{Mu} = \frac{v_{Mu12}^2}{2a_{Mu2}} + \frac{v_{Mu34}^2 - v_{Mu12}^2}{2a_{Mu3}} - \frac{v_{Mu34}^2}{2a_{Mu4}}, \quad (3.17)$$

$$t_u = t_{u4} = \frac{|v_{mu12}|}{|a_{mu1}|} + \frac{|v_{mu12}|}{|a_{mu2}|} + \frac{|v_{mu34}|}{|a_{mu3}|} + \frac{|v_{mu34}|}{|a_{mu4}|}. \quad (3.18)$$

The average velocity of the capsbot for the contrarium profile is (see Fig. 3.6(c)):

$$\bar{x}_{Mc} = \frac{x_{Mc}}{t_c}, \quad (3.19)$$

where x_{Mc} is the displacement of the capsbot in contrarium profile in cycle time t_c .

$$x_{Mc} = \frac{v_{Mc}^2}{2a_{Mc1}} - \frac{v_{Mc}^2}{2a_{Mc2}}, \quad (3.20)$$

$$t_c = t_{c2} = \frac{|v_{mc}|}{|a_{mc1}|} + \frac{|v_{mc}|}{|a_{mc2}|}. \quad (3.21)$$

Four parameters (a_{mu1} , a_{mu2} , a_{mu3} and a_{mu4}) can be changed for the utroque profile to get different capsbot average velocities. In this chapter, $a_{mu2} = a_{mu3}$ and $a_{mu1} = a_{mu4}$ are designed. Also a fixed value for $a_{mu1} = a_{mu4}$ (maintaining $|a_{mu1}| = |a_{mu4}| < \frac{\mu_M Mg}{m}$) is chosen. Only $a_{mu2} = a_{mu3}$ are tuned to get different capsbot average velocities. If a_{mumax} is the maximum acceleration, a_{mumin} is the minimum acceleration and a_{mudiff} is the difference between two consecutive profile parameter sets, then total number of acceleration profile

sets for the utroque profile is:

$$n_u = \text{floor}\left(\frac{|a_{mumax}| - |a_{mumin}|}{a_{mudiff}}\right) + 1. \quad (3.22)$$

Two parameters (a_{mc1} and a_{mc2}) can be changed for the contrarium profile to get different capsbot average velocities. A fixed value for a_{mc2} (maintaining $|a_{mc2}| < \frac{\mu_M Mg}{m}$) is chosen. Only a_{mc1} is tuned to get different capsbot average velocities. If a_{mcmax} is the maximum acceleration, a_{mcmin} is the minimum acceleration and a_{mcdiff} is the difference between two consecutive profile parameter sets, then total number of profile parameter sets for the contrarium profile is:

$$n_c = \text{floor}\left(\frac{|a_{mcmax}| - |a_{mcmin}|}{a_{mcdiff}}\right) + 1. \quad (3.23)$$

The maximum capsbot average velocity will be:

$$\bar{x}_{Mmax} = \max(\max(\bar{x}_{Mc}), \max(\bar{x}_{Mu})), \quad (3.24)$$

where

$$\max(\bar{x}_{Mc}) = \max((\bar{x}_{Mc})_1, (\bar{x}_{Mc})_2, \dots, (\bar{x}_{Mc})_{n_c}), \quad (3.25)$$

$$\max(\bar{x}_{Mu}) = \max((\bar{x}_{Mu})_1, (\bar{x}_{Mu})_2, \dots, (\bar{x}_{Mu})_{n_u}). \quad (3.26)$$

The average velocities of the capsbot for different profile parameter sets for the two acceleration profiles are calculated and stored in the database.

3.4.2 Stage 1: Desired IM Trajectory Generation

The control requirement is that the capsbot tracks a given trajectory. As the capsbot is an underactuated system, the movements of the capsbot cannot be controlled directly (i.e. x_M is uncontrollable directly). The capsbot movements are controlled indirectly by controlling the movements of the IM (x_m is controllable directly). The capsbot average velocity can be tuned by changing the parameters of the IM acceleration profile ($\bar{x}_M = f(x_m, \ddot{x}_m)$). Let the capsbot track the position trajectory shown in Fig. 3.7. The desired capsbot velocity changes throughout the trajectory. Thus to track the trajectory, the IM acceleration profile parameters need to be tuned so that the capsbot average velocity changes according to the desired value. To track the capsbot trajectory primarily the utroque profile is used. The

contrarium profile is used for one cycle when the capsbot velocity changes from negative to positive or positive to negative. Then the IM continues to follow the utroque profile. In the desired trajectory for path A-B the capsbot velocity is positive and for path B-C the capsbot velocity is negative. Thus the IM follows the utroque profile of Fig. 3.3(a) for A-B path (but changes the parameters to tune the capsbot average velocity to track the trajectory) and then uses the contrarium profile of Fig. 3.3(d) for one cycle and after that follows the utroque profile of Fig. 3.3(b) for B-C path (but changes the parameters to tune the capsbot average velocity to track the trajectory).

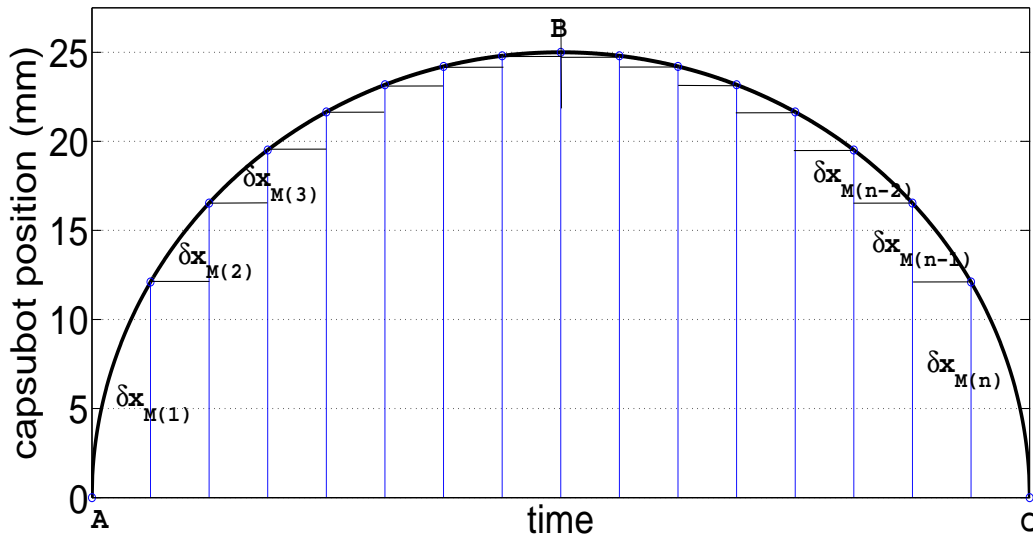


Fig. 3.7 Desired trajectory for the 1D capsbot trajectory tracking (segment-wise tracking)

Step 1: Generating Capsbot Trajectory Segment and Selection of Segment Period (T):

Segments (shown in Fig. 3.7) are designed based on the desired trajectory. T is the time period of each segment. $\delta x_M(i)$ is the required displacement in the i th segment. The desired average velocity in the i th segment is:

$$\bar{x}_{Md}(i) = \frac{\delta x_M(i)}{T}. \quad (3.27)$$

A smaller T provides smoother tracking of trajectory. However, the T cannot be infinitesimally small as the IM has to complete at least one cycle with one profile parameter set once it starts, before it can start another cycle with different acceleration profile parameters. Thus

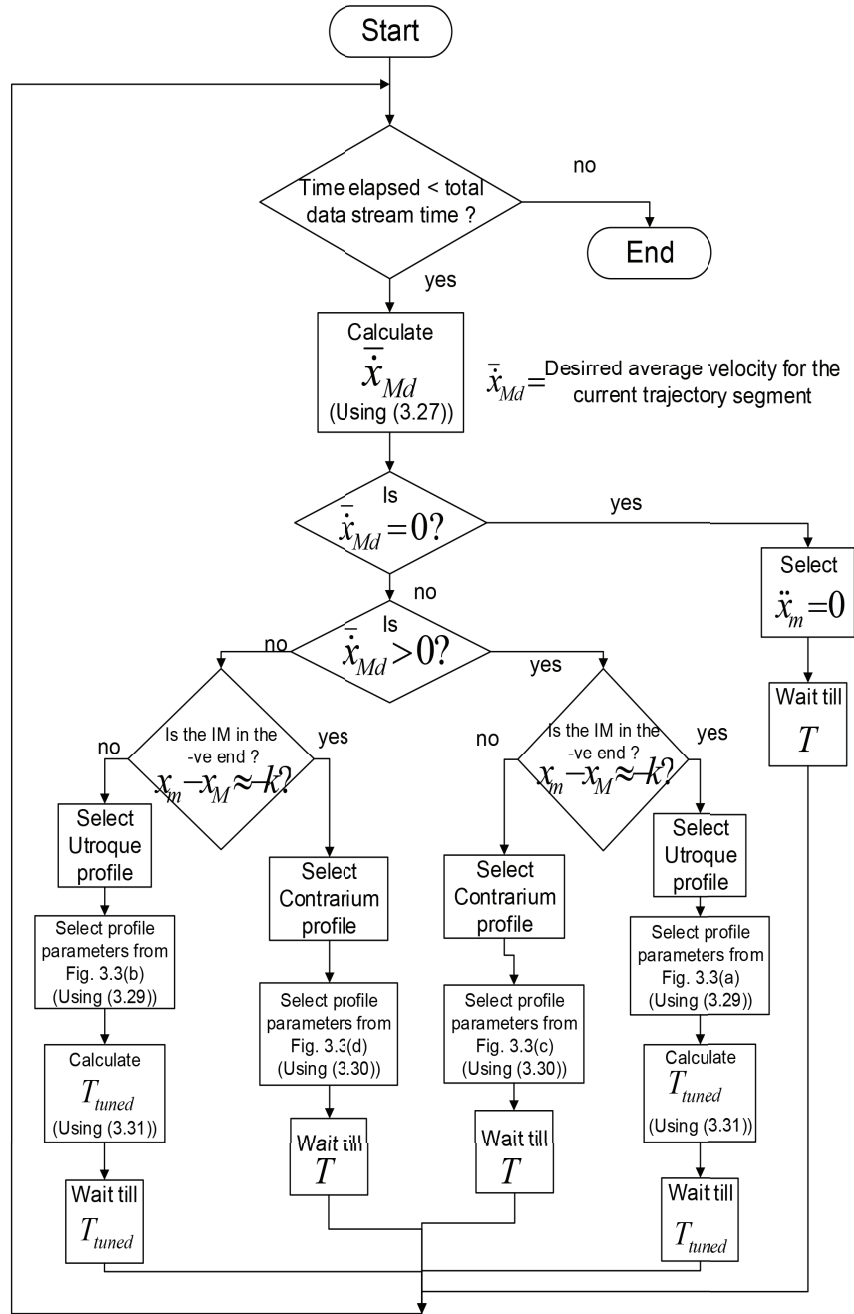


Fig. 3.8 Flow chart of the selection algorithm for the 1D capsbot trajectory tracking

the minimum segment period is:

$$T_{min} = \max(\max(t_c), \max(t_u)), \quad (3.28)$$

where, t_c and t_u are the cycle times of the contrarium profile and the utroque profile respectively.

Step 2: Selection of Profile Parameters (Selection Algorithm):

\bar{x}_{Md} is compared with the database created in the preparation stage of section 3.4.1 for each segment of the capsbot trajectory. Following two steps are followed:

1. One profile is selected from the four profiles described in Fig. 3.3. Normally one of the two utroque acceleration profiles is used: profile of Fig. 3.3(a) for positive \bar{x}_{Md} and profile of 3.3(b) for negative \bar{x}_{Md} . In the utroque acceleration profile the IM returns to its initial position at the end of each cycle. Thus one of the two contrarium acceleration profiles (Figs. 3.3(c) or 3.3(d)) is used whenever a switching between the two utroque acceleration profiles is required.
2. For the utroque profile, two profile parameters namely a_{mu1} , a_{mu2} , a_{mu3} and a_{mu4} need to be selected which will generate the required desired average velocity (\bar{x}_{Md}). All the possible profile parameters and corresponding projected average velocities i.e. $\bar{x}_{Mu}(p)$, $p = 1, 2, \dots, n_u$ can be found from the created database. The desired average velocity (\bar{x}_{Md}) is compared with projected average velocities as shown in (3.29). The profile parameter-set corresponding to minimum error of (3.29) is selected.

$$\dot{x}_{diff} = \min((|\bar{x}_{Md}| - |\bar{x}_{Mu}(1)|), (|\bar{x}_{Md}| - |\bar{x}_{Mu}(2)|), \dots, (|\bar{x}_{Md}| - |\bar{x}_{Mu}(n_u)|)). \quad (3.29)$$

For the contrarium cycle, two profile parameters namely a_{mc1} and a_{mc2} need to be selected which will generate the required desired average velocity (\bar{x}_{Md}). All the possible profile parameters and corresponding projected average velocities i.e. $\bar{x}_{Mc}(p)$, $p = 1, 2, \dots, n_c$ can be found from the crated database. The desired average velocity (\bar{x}_{Md}) is compared with projected average velocities as shown in (3.30). The profile parameter set corresponding to minimum error of (3.30) is selected.

$$\dot{x}_{diff} = \min((|\bar{x}_{Md}| - |\bar{x}_{Mc}(1)|), (|\bar{x}_{Md}| - |\bar{x}_{Mc}(2)|), \dots, (|\bar{x}_{Md}| - |\bar{x}_{Mc}(n_c)|)). \quad (3.30)$$

The segment is taken from the desired trajectory with a segment period (T) considering the constraint of (4.24). In each segment the IM is required to follow a specific acceleration profile with a specific profile parameter set to track the desired trajectory. This research proposes a selection algorithm to select the right acceleration profile with right profile parameters in each segment. The selection algorithm is presented in Fig. 3.8. The selection algorithm incorporates all the logical development presented in section 3.4.2. It also uses database created in section 3.4.1 and, equations developed in sections 3.4.2 and 3.4.3.

Step 3: Tuning the Segment Time:

An acceleration profile with a profile parameter set cannot be operated for a discrete amount of time but for a multiple of the cycle time of that acceleration profile with that parameter set. The selected parameter set will be used for the following time span:

$$T_{tuned} = t_{sel} \times \text{floor}\left(\frac{T}{t_{sel}}\right), \quad (3.31)$$

where, t_{sel} is the cycle time of the selected utroque profile; $\text{floor}(A)$ rounds the elements of A to the nearest integers less than or equal to A.

3.4.3 Stage 2 : Control of the IM

Open loop control law of the IM is:

$$F_{md} = m\ddot{x}_{md} + \text{sgn}(\dot{x}_{md} - \dot{x}_{Md})\mu_m mg. \quad (3.32)$$

The closed-loop control law can be selected, using partial feedback linearization [51]:

$$F_{md} = \alpha \tau_{md} + \beta, \quad (3.33)$$

where $\alpha = m$ and $\beta = \text{sgn}(\dot{x}_{md} - \dot{x}_{Md})\mu_m mg$.

Let $\tilde{x}_m = x_{me} = x_{mm} - x_{md}$ be the tracking error; choosing the linear control law $\tau_{md} = \ddot{x}_m - k_1 \dot{\tilde{x}}_m - k_2 \tilde{x}_m$ and applying the control law of (3.33) to (3.2) the error equation:

$$\ddot{\tilde{x}}_m + k_1 \dot{\tilde{x}}_m + k_2 \tilde{x}_m = 0. \quad (3.34)$$

The values of k_1 and k_2 can properly be selected using the standard linear control theory. Then by using the control law of (3.33) the IMs can be made to follow the desired accelera-

tions, velocities and positions.

3.5 Simulation, Experiments and Analysis

This section presents the simulation and experimental results and provides analysis.

3.5.1 Simulation Setup and Results

Simulation Setup

The simulation is performed in the Simulink environment, and the data in Table 3.1 is used. The data is taken from the prototype implemented in section 3.5.2. For simulation and experimentation $T=1\text{sec}$ is used. The Ode45 (Dormand-Prince) solver is used with a variable step. The maximum step size is 1 ms and the minimum step size is 0.0001 ms and the initial step size is 1 ms. The simulink model is provided in the appendix A.

Table 3.1 Parameters of the developed 1D capsuobot

M	m	μ_M	μ_m	k
0.396kg	0.05kg	0.1	0.2	9mm

Simulation Results

The 1D capsuobot uses the proposed trajectory tracking control to track the desired trajectory of 3.7. Fig. 3.9(a) shows the desired and simulated trajectories of the capsuobot in the same graph for the ease of comparison.

From Fig. 3.9(a), it is observed that the capsuobot moves from starting position (0cm) to position 2.5cm in the first 8s and then it returns to starting position (0cm) from position 2.5cm in the second 8s. Thus the capsuobot moves with high positive velocity at the beginning of the trajectory and then the velocity decreases with time and become zero at 8s. After that the capsuobot moves with negative velocity and the magnitude of the velocity increases with time and reaches to maximum in magnitude at the end of the trajectory. Fig. 3.9(a) also shows that the simulated trajectory is not smooth rather stepwise as the capsuobot tracks the trajectory segment by segment where the segment time (T) is 1s. Fig. 3.9(b) shows the position trajectory tracking error in the simulation. From Fig. 3.9(b), it is observed that the error

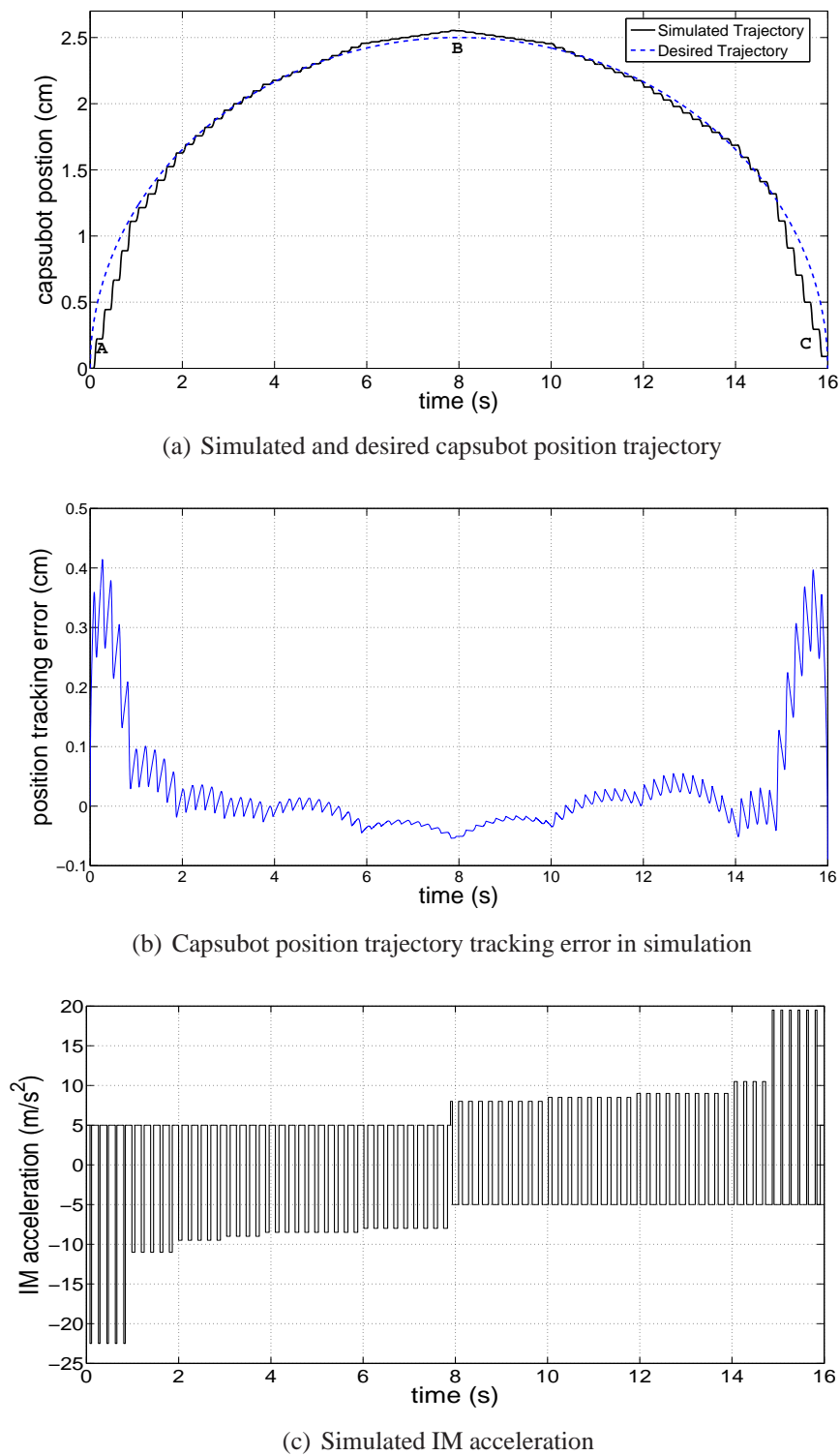


Fig. 3.9 Simulated results for the capsobot trajectory tracking using the proposed control

is big at the beginning and ending of the trajectory i.e. when the magnitude of the capsbot velocity requirement is high. Fig. 3.9(c) shows the simulated IM acceleration. From Fig. 3.9(c), it is observed that the IM follows the utroque acceleration profile of Fig. 3.3(a) for the first 8s and then it follows the contrarium acceleration profile of Fig. 3.3(d) for 1 cycle and after that it follows the utroque acceleration profile of Fig. 3.3(b) for the second 8s. The contrarium profile is necessary to switch from one utroque profile (Fig. 3.3(a)) to another utroque profile (Fig. 3.3(b)). In the first 8s the magnitude of the capsbot velocity decreases with time. Thus the magnitudes of the acceleration profile parameters (a_{mu2} and a_{mu3}) for the IM also decrease gradually in the first 8s which can be observed from Fig. 3.9(c). In the second 8s the magnitude of the capsbot velocity increases with time. Thus the magnitudes of the acceleration profile parameters (a_{mu2} and a_{mu3}) for the IM also increase gradually in the second 8s which can be observed from Fig. 3.9(c).

3.5.2 Experimental Setup and Results

Experimental Setup and Physical Constraints

The 3D CAD design of the Capsbot (without Capsbot-shell) is shown in Fig. 3.10(a). A prototype shown in Figs. 3.10(b) and 3.10(c) is developed based on the design and the proposed trajectory tracking control is implemented in the developed prototype. In the experimentation, segment time $T=1s$ is used. The main components of the developed capsbot system are a linear DC motor (QUICKSHAFT LM1247-020-01), a motion controller [181], two batteries and a capsbot-shell to hold all the components. The linear motor is comprised of a motor-housing which houses the coil, three hall sensors and a cylindrical rod which is capable of moving back and forth within the capsbot. The motion controller provides power to the linear motor and controls the movement of the cylindrical rod by controlling the current flow to the motor coil. The coil is placed inside the motor housing and peripheral to the cylindrical rod. Two batteries provide power to the motion controller. The motion controller is programmed using the Motion Manager Software [181] and then can be disconnected from the PC. The capsbot is 20cm in length and 8cm in diameter. The cylindrical rod works as the Inner Mass (IM) of the capsbot.

It is noted that the IM includes the cylindrical rod and two extra masses (adhesive tack) at both ends of the cylindrical rod. The extra masses are added to increase IM to capsbot mass ratio. The parameters of the capsbot are listed in Table 3.1. The Hall sensors are used to determine the position of the cylindrical rod (IM). The linear motor data (i.e. IM position and velocity, and current through the coil) can be logged using the Motion Man-

ager software. To obtain the data for capsbot movements the motion of the capsbot are recorded using a video camera and then a video analysis software Quintic Biomechanics [182] is used. It determines the position, velocity and acceleration of the capsbot.

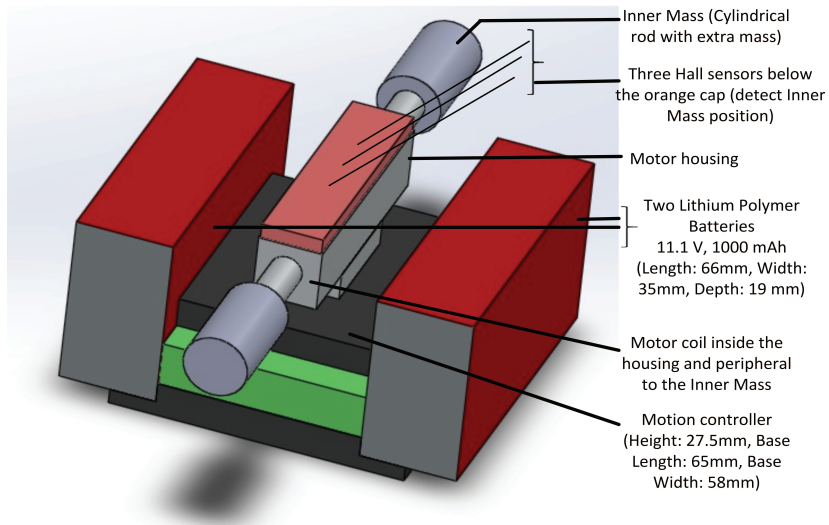
The capsbot has the following physical constraints:

- The stroke length of the IM is 20mm [181] (Figs. 3.10(a) and 3.10(c)). In the experimentation and simulation stroke length of 18 mm ($-k \leq x_m - x_M \leq k$ where $k = 9\text{mm}$) was used to avoid the collision. This constraint was considered while designing the profile parameters t_{c1} , t_{c2} , t_{u1} , t_{u2} , t_{u3} and t_{u4} of Fig. 3.3.
- The maximum achievable continuous acceleration of the IM is $\pm 30\text{ms}^{-2}$. This limit was considered while designing the profile parameters a_{mu2} , a_{mu3} and a_{mc1} of Fig. 3.3.
- The maximum static friction force of the capsbot is $\mu_M Mg$. This constraint was considered while designing the profile parameters a_{mu1} , a_{mu4} and a_{mc2} of Fig. 3.3(a) and 3.3(c).
- Other constraints of the linear motor (LM 1247-0201-01) from the data sheet [181]:
 - Maximum continuous force on the IM : 3.09 N
 - Peak force on the IM : 9.26 N
 - Maximum continuous current through the motor coil: 0.48 A
 - Peak current through the motor coil : 1.44 A

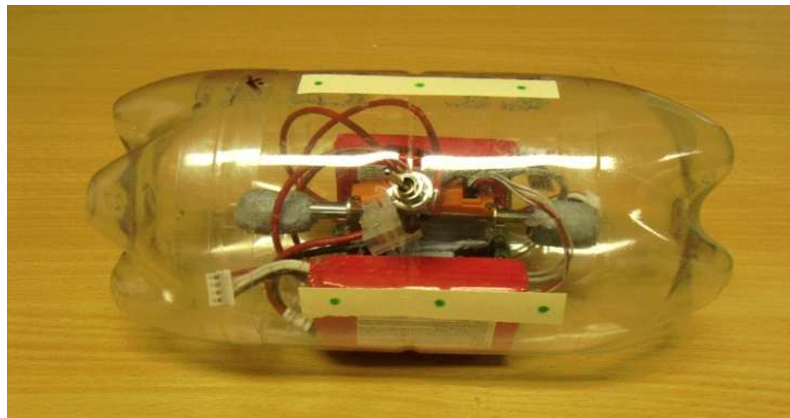
The above mentioned constraints are met when acceleration is used within the limit $\pm 30\text{ms}^{-2}$.

System Calibration

The components of the capsbot that are involved in the calibration process are the motion controller, the linear DC motor (QUICKSHAFT LM1247-020-01) [181] and the hall sensors. To calibrate the hall sensor signals the built-in capability of the motion manager software [181] is used. Calibration of the hall sensor signals is necessary to optimally adjust the motion controller to the connected linear motor. The linear DC motor is connected to a PC through the motion controller where the motion manager software is installed. Before starting the calibration, it is ensured that the rod is in the middle of its traversing path and can be freely moved over the whole traversing range. Then the motion manager software is



(a) 3D CAD design of the Capsubot (without Capsubot-shell)



(b) Implemented Capsubot: With capsubot-shell (Length: 20cm, Diameter: 8cm)



(c) Implemented Capsubot: Without capsubot-shell (Extra masses - blue tack - are added to the cylinder to increase IM to capsobot mass ratio)

Fig. 3.10 CAD design and implemented capsobot

asked to calibrate the hall sensor signals. During the calibration process the cylindrical rod (IM) of the linear DC motor is positioned several times within its range limits. The software shows a message after successful completion of the calibration of the hall sensor signals. The optimized system parameters are saved in the motion controller memory by using the "EEPSAV" command in the motion manager software.

When the calibration is completed few test measurements are taken to verify the calibration. The motion manager software is given the command "POS" which shows the current position of the cylindrical rod measured by the hall sensors. Then the cylindrical rod is asked to move to "+9mm" by using the command "LA". Then the command "POS" is used to know the position of the cylindrical rod after the movement measured by the hall sensors. From the two measured positions the travelled distance by the cylindrical rod is calculated. The travelled distance is also measured by using a vernier caliper. The measured values are within " $9 \pm 0.02mm$ " for both the hall sensors and the vernier caliper measurements. The complete process is repeated for five times and the measured values lie within " $9 \pm 0.02mm$ ". The process is then repeated for a movement of "-9mm". The measured values lie within " $-9 \pm 0.02mm$ ". Thus the calibration of hall sensors along with the linear DC motor and the motion controller are verified.

Creation and Use of the Database

The equations presented in section 3.4.1 are used to create the database for the implementation. The parameters are used from Table 3.1. The other parameters which are required for the creation of the database are presented in Table 3.2. Using all the above information a database is created which have the format presented in Tables 3.3 and 3.4 for the utroque and contrarium profiles respectively. The selection algorithm is used for the selection of the acceleration parameter set from the database of Tables 3.3 and 3.4 to track the capsuot trajectory. This chapter proposes a segment-wise trajectory tracking and thus the complete trajectory is divided into many trajectory segments. The selection algorithm firstly calculates the required capsuot average velocity ($\bar{x}_{Md}(i)$) for the current trajectory segment. Then it selects the required profile (utroque or contrarium) to track the current trajectory segment. After that the selection algorithm compares $\bar{x}_{Md}(i)$ with all the \bar{x}_{Mu} (Table 3.3) for the utroque profile and selects the parameter-set corresponding to that particular \bar{x}_{Mu} for which $\bar{x}_{Md}(i)$ is the closest in magnitude. Same procedure is followed for the contrarium profile. Then the inner mass uses the selected parameter set and thus capsuot tracks the current trajectory segment. For each trajectory segment the above procedures are repeated. When all the trajectory segments are tracked, the capsuot completes the trajectory tracking.

Table 3.2 Parameters of the developed capsbot to create the database

$ a_{mumax} $	$ a_{mumin} $	a_{mudiff}	$ a_{mu1} = a_{mu4} $	g
$30ms^{-2}$	$8ms^{-2}$	$0.5ms^{-2}$	$5ms^{-2}$	$9.8ms^{-2}$
$ a_{mcmax} $	$ a_{mcmin} $	a_{mcdiff}	$ a_{mc2} $	
$30ms^{-2}$	$8ms^{-2}$	$0.5ms^{-2}$	$5ms^{-2}$	

Table 3.3 Database for the utroque profile

Serial number	\bar{x}_{Mu}	a_{mu1}	a_{mu2}	a_{mu3}	a_{mu4}
1					
2					
..					
n_u					

Experimental Results

The capsbot tracks a semi-circular position trajectory on a plywood table. Fig. 3.11(a) shows the experimental position of the IM for the capsbot trajectory tracking. From Fig. 3.11(a), it is observed that the IM moves within the limit i.e. $[-k, k]$ where k is 9mm. Fig. 3.11(b) shows the experimental position trajectory of the capsbot. From Fig. 3.11(b), it is observed that the capsbot trajectory is not smooth rather it goes step by step. The reason behind this is the very nature of the capsbot movement principle where capsbot moves part of each cycle and remains stationary for the remaining time of the cycle. If a smaller segment time is used, the smoothness of the trajectory tracking will improve.

3.5.3 Analysis

Comparison Analysis

Fig. 3.12(a) shows the experimental and simulation positions of the IM for 1s for the position trajectory tracking. From Fig. 3.12(a), it is observed that the simulation and experimental results have the same pattern. However there are differences between the curves. The experimental result is delayed compared to the simulation result.

Fig. 3.12(b) shows the experimental, simulation and desired (target) position trajectories

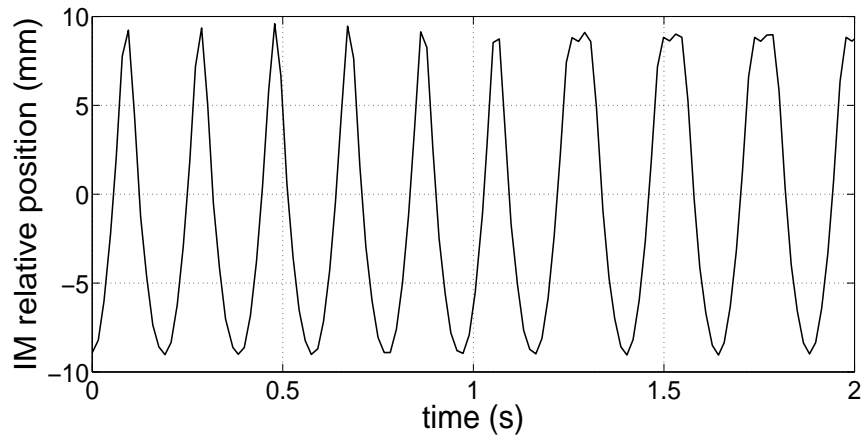
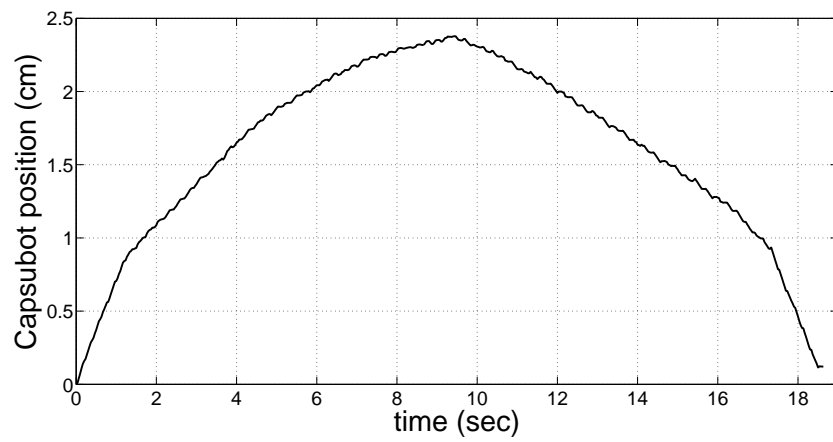
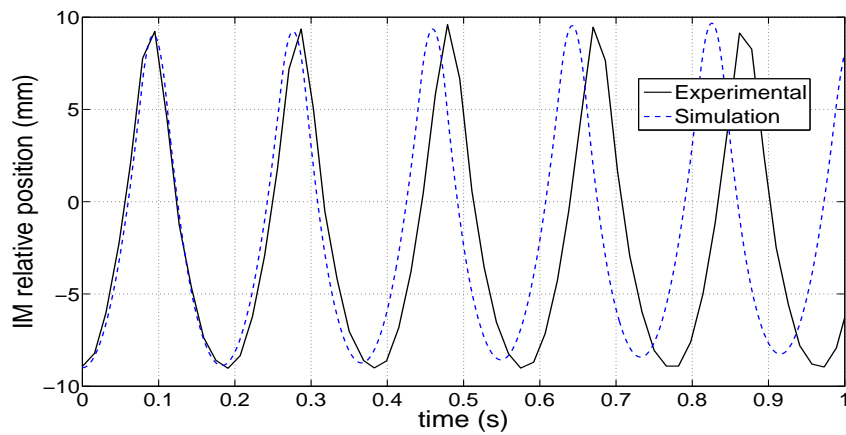
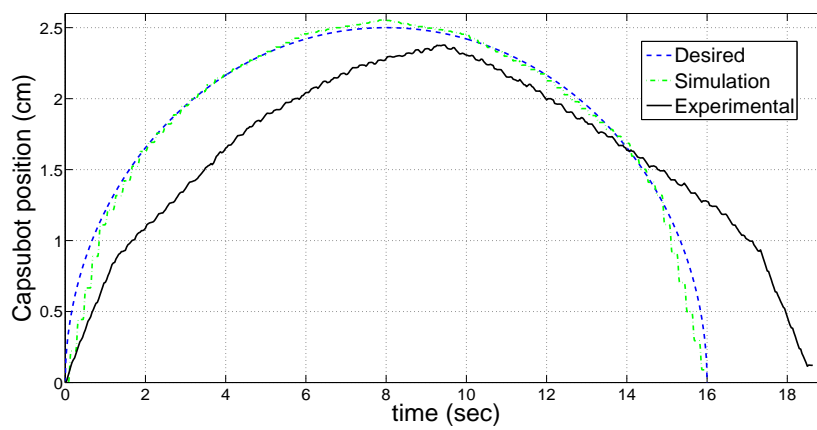
(a) Experimental IM relative position ($x_m - x_M$)(b) Experimental capsobot position (x_M)

Fig. 3.11 Experimental results for position trajectory tracking using proposed control approach



(a) Experimental and simulation IM position ($x_m - x_M$) for position trajectory tracking for 1 sec



(b) Experimental and simulation capsuobot position (x_M) for position trajectory tracking

Fig. 3.12 Experimental and simulation results for position trajectory tracking using proposed control approach

Table 3.4 Database for the contrarium profile

Serial number	\bar{x}_{Mc}	a_{mc1}	a_{mc2}
1			
2			
..			
n_c			

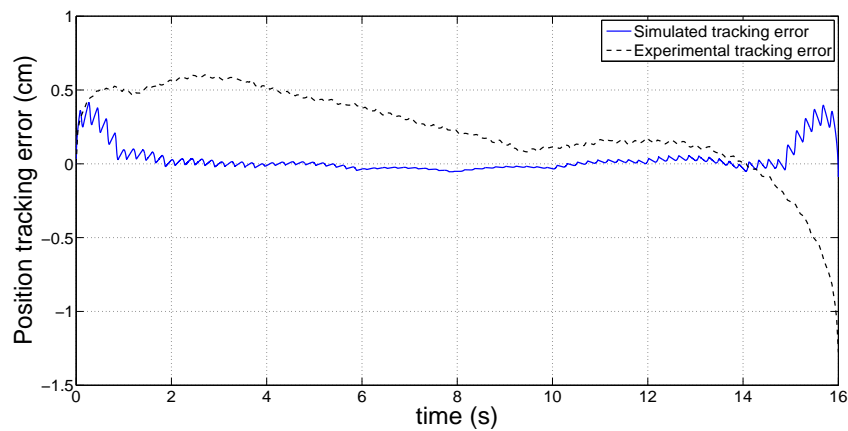


Fig. 3.13 Experimental and simulation capsuobot position trajectory tracking error using proposed control approach

of the capsuobot. From Fig. 3.12(b), it is observed that the capsuobot experiences 2.5s delay in total in the experiments than the desired and simulation results. However the experimental capsuobot trajectory has a similar pattern as the desired and simulation trajectories.

One possible reason which leads to this difference is that only the capsuobot dynamics is considered and the dynamics of the linear motor is ignored. Actually, the IM is actuated by energising the coil placed inside the motor housing and peripheral to the IM. The terminal inductance (phase-phase) of the coil is $820\mu H$. The current provided to the coil cannot be changed abruptly because of the dynamics of the linear motor. Thus the force applied to the IM and subsequently the acceleration of the IM cannot be changed abruptly. This makes the developed capsuobot response in the experiment slower than that in the simulation and subsequently a delay is occurred in the experimental trajectory.

Fig. 3.13 shows the position trajectory tracking error in the simulation and experimentation. Table 3.5 presents the maximum absolute tracking error, mean absolute error and relative mean absolute error of the trajectory tracking. The simulation position trajectory

tracking error is small (relative mean absolute error: 2.62%) whereas the experimental position trajectory tracking error is big (relative mean absolute error: 16.06%). One main reason of this big error is the delay in the experiments which is explained above. The other factors which might contribute to the error are measurement noise, friction uncertainty (simple coulomb friction model is used here) and other disturbances.

In future research the actuator dynamics can be incorporated into the model and a sophisticated friction model can be used. Other areas of improvements are to choose the segment time optimally and incorporate capsulot position feedback into the control loop.

Table 3.5 Comparison of the algorithm performance for simulation and experiments

Position Trajectory Tracking	Maximum absolute error (cm)	Mean absolute error (cm)	Relative mean absolute error* (%)
Simulation	0.41	0.05	2.62
Experimentation	1.28	0.31	16.06

* Relative mean absolute error =
(mean absolute error / mean absolute desired value)100%

Repeatability and Reproducibility

The repeatability and reproducibility are discussed below:

1. Repeatability: The trajectory tracking experiment was performed on a plywood table. The experiment was repeated on the same table and the results were also repeated. When the experiment was performed on a different table with different friction coefficient, the results were not repeated. To get a repeated result the database was recreated considering the new friction coefficient and then trajectory tracking was performed.
2. Reproducing the simulation: Standard simulation tool Matlab/Simulink was used for the simulation of this research. The simulink model is provided in the appendix A. The parameters used in the simulation is also mentioned in the thesis. By following the description in the thesis the simulation results could be reproduced. Furthermore several articles has been published by the author based on the research of this thesis which are listed in Chapter 1. Those resources also can be used to get help for the reproduction of the simulation.

3. Reproducing the capsbot prototype: Many off-the-shelf components such as linear DC motor, motion controller and batteries were used to develop the capsbot prototype for this research. These components are available in the market and by following the description in the thesis the capsbot prototype can be reproduced. Several times during the research the capsbot prototype was disintegrated into individual components and then reassembled. The assembled capsbot was able to reproduce the results. The key things to consider while assembling all the components are:
 - To keep the axis of movement of the inner mass (cylindrical rod) in the horizontal plane.
 - To keep the axis of movement of the inner mass (cylindrical rod) parallel to the sides of the robot shell.
 - To ensure the distances of the inner mass (cylindrical rod) from both the sides of the robot shell are equal .
4. Reproducing the experiment: Once the capsbot prototype is developed the experiment can be reproduced by following the description in the thesis. The programming instruction of a motion controller used in the developed prototype can be found in the Faulhaber website [181]. Furthermore the published articles by the author can be used to get help for the reproduction of the experiment.

Drift, Overshoot and Noise

In Figs. 3.12(a) and 3.12(b) drifts are seen in the experimental results compared to the simulation results. One possible reason for the drift could be the dynamics of the linear motor which is explained above in the "Comparison Analysis" section. The control of the trajectory tracking in this thesis is not fully closed loop rather semi-closed loop. This could be another reason for the drift. By modifying the control to fully closed loop system the amount of drift could be reduced. The modification to fully closed loop control is discussed below in the "Fully Closed-loop System" section. The other factors which might have contributed to the drift are measurement noise and friction uncertainty. Hall sensors are used for the measurement of the inner mass position. The capsbot movement is measured by taking a video of the robot movement and then analysing the video using a Quintic video analysis software [182]. Measurement noises may have been introduced during the above mentioned measurements.

Overshoots are also seen in the simulation and experimental results shown in Fig. 3.12(b).

One of the main reasons behind this is the segment-wise trajectory tracking control used in this thesis. To reduced the overshoots a smaller segment-time can be used.

Fully Closed-loop System

The control system developed in this thesis is semi-closed loop. The control of the inner mass is closed loop where partial feedback linearization has been used. By controlling the inner mass movements, the capsbot trajectory tracking is performed while using a segment-wise approach. The feedback from the capsbot actual position has not been used in the control i.e. the control is not fully closed loop. Due to the time constraint this thesis has not implemented the fully closed loop control of the capsbot. However a guideline is provided below to perform the fully closed loop control. To make the capsbot trajectory tracking fully closed loop an on-board sensor such as accelerometer is required. Feedback should be taken from the capsbot position (the on-board accelerometer can provide this) and the control input should be corrected according to the error (x_{Me}) value for tracking the position of the capsbot more accurately:

$$x_{Me}(i) = x_{Md}(i) - x_{Mm}(i). \quad (3.35)$$

where x_{Md} and x_{Mm} are desired and measured capsbot positions respectively.

x_{Me} of (3.35) should be utilized to modify desired average velocity (\bar{x}_{Md}) at the start of each segment. (3.27) of section 3.4.2 should be modified as below:

$$\bar{x}_{Md}(i) = \frac{\delta x_M(i) + x_{Me}(i-1)}{T}. \quad (3.36)$$

The fully closed loop control can be implemented using an arduino or a raspberry pi along with the existing motion controller.

Capsbot Demonstration

A video is attached with the thesis (see the attached DVD) where the demonstration of the position trajectory tracking is shown accompanied by a capsbot position (desired, simulation and experimental) vs time plot.

In the video demonstration, it is seen that the capsbot shakes while moving. To have a smooth movement, the capsbot centre of mass should stay on the IM axis of movement. It ensures that no torque is applied on the robot. For the implemented prototype of this chapter, the centre of mass does not reside on the axis of movement of the IM as off-the-shelf linear

motor and controller are used manufactured by Faulhaber [181]. Rather the centre of mass resides below the axis of movement of the IM. Thus the IM movement produces a torque which tries to roll over the capsbot. The torque is not big enough to roll over the capsbot. However these repetitive attempts are responsible for the shaking of the capsbot. A custom built capsbot can be made where the centre of mass resides on the axis of movement of the IM as done in [64] and the shaking issue may be resolved.

The robot structure also might have contributed to the shaking of the capsbot. Here the cylindrical structure robot is moving on a flat surface. If the robot is used inside a cylindrical structure e.g. inside a pipe the shaking may reduce. On the other hand if the outer cover of the robot is changed to a parallelepiped and the robot is used on a flat surface the shaking may reduce.

Scalability of the Capsbot

The dimension of commercially available smallest linear motor is: diameter 8 mm and length 58mm whereas the diameter and length of the cylindrical rod (which works as IM) are 4mm and 58mm respectively. The robot used in [64] is custom-built and the dimension is: diameter 7mm and length 40mm. It demonstrates that the capsbot can be miniaturized to be integrated with a capsule endoscope. The size of a commercially available capsule endoscope is 11mm in diameter and 26mm in length [183].

3.6 Summary

This chapter has presented the modelling, theoretical analysis, trajectory tracking control, simulation and experimentation of the 1D capsule robot (capsbot). It has addressed the trajectory tracking control of the capsbot-type underactuated system for the first time. A two-stage control strategy for the trajectory tracking of the underactuated 1D capsbot has been presented. Two modified acceleration profiles (utroque and contrarium) have been proposed which removes the limitations of the previously proposed acceleration profile in [41]. The profile parameters for the newly proposed acceleration profiles have been optimally selected considering the physical constraints. It has proposed a novel selection algorithm for the proper selection of the acceleration profile (i.e. utroque or contrarium) and also to select the correct acceleration profile parameters (acceleration values). The trajectory tracking control strategy has been implemented on a developed prototype. The simulation and experimental results have validated the trajectory tracking control strategy. This chapter has

discussed the repeatability and reproducibility of the simulation and experimental results. It has also explained the drift, overshoot and noise which are present in the experimental results. It has presented an approach to develop a fully closed-loop trajectory tracking control which may improve the trajectory tracking performance of the semi-closed loop trajectory tracking control which has been proposed and developed in this thesis. Finally this chapter has presented the scalability of the developed capsbot prototype.

Chapter 4

2D Capsule Robot

4.1 Introduction

This chapter presents a 2D (two dimensional) capsule robot (capsubot) which can perform linear, rotational and 2D motions. The 2D capsuobot shown in Fig. 4.1(a), has the shape of a parallelepiped. The two inner masses (IMs) are placed in the hollow spaces within the capsuobot. The hollow spaces are identical and placed symmetrically within the capsuobot, IMs are also identical. IMs can move along the hollow spaces. By controlling the movements of IMs the capsuobot can be moved on a plane. The sources of the propulsion forces of the IMs are not shown in Fig. 4.1(a). The 2D capsuobot is an underactuated system as it has five degrees of freedom (two degrees of freedom for two IMs and three degrees of freedom for the capsuobot) but only two control inputs which are the forces on the IMs.

The main contributions of this chapter are to propose a trajectory tracking control algorithm for an underactuated 2D capsuobot by combining segment-wise and behaviour-based control, defining various basis behaviours for the 2D capsuobot, to develop a selection algorithm for the proper selection of the behavior-set and to propose the rules for implementing each behaviour. Other contributions include implementing the closed-loop control strategy for the IMs of the 2D capsuobot in a developed prototype and conducting simulation and experimentation to demonstrate the proposed capsuobot movability.

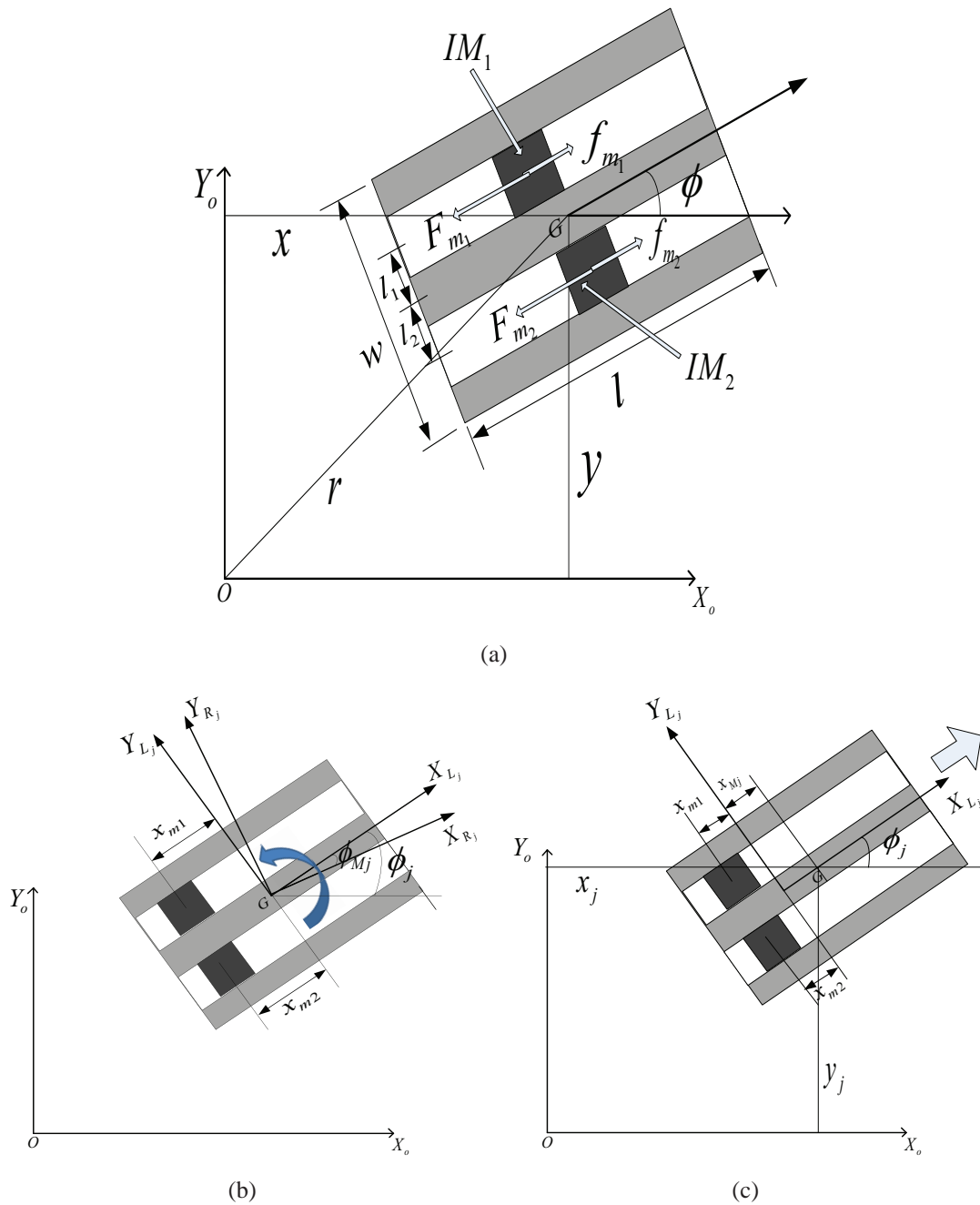


Fig. 4.1 Top view of the 2D capsutbot (a) x , y and ϕ are generalised coordinate and measured with respect to the fixed reference frame $O(X_0, Y_0)$ (b) Rotation ϕ_{Mj} is measured with respect to the local frame R_j - frame L_j rotates with the capsutbot during rotation (here positive direction of rotational motion is shown) (c) Translation x_{Mj} and x_{mi} are measured with respect to the local frame L_j (here positive direction of linear motion is shown)

4.2 System Description and Defining the Behaviours

4.2.1 System Description: 2D Capsubot Model

F_{m_i} force shown in Fig. 4.1(a) is applied on the IM_i along the hollow space and creates a motion whereas f_{m_i} is the friction force. IM_i applies equal and opposite forces on the capsubot. The sources of the forces which are not shown in the figure could be linear motors as used in chapter 3. From the Fig. 4.1(a), the capsubot dynamic model is:

$$F_{m_i} - f_{m_i} = m_i \ddot{x}_{m_i} \quad \forall i = 1, 2, \quad (4.1)$$

$$\sum F_x = M \ddot{x} = (F_r - f_M) \cos(\phi) = (-F_{m_1} + f_{m_1} - F_{m_2} + f_{m_2} - f_M) \cos(\phi), \quad (4.2)$$

$$\sum F_y = M \ddot{y} = (F_r - f_M) \sin(\phi) = (-F_{m_1} + f_{m_1} - F_{m_2} + f_{m_2} - f_M) \sin(\phi), \quad (4.3)$$

$$\sum M_G = I \ddot{\phi} = M_r - M_f = (-F_{m_2} + f_{m_2}) l_2 - (-F_{m_1} + f_{m_1}) l_1 - M_f, \quad (4.4)$$

where

- \ddot{x}_{m_i} is the acceleration of the IM_i ;
- x, y and ϕ are generalised coordinates of the capsubot with respect to the fixed frame $O(X_O, Y_O)$;
- m_i and M are the IM_i mass and capsubot mass respectively;
- F_r is the total reaction forces of the IMs on the capsubot;
- M_r is the total moment due to reaction forces of the IMs on the capsubot about z-axis through the mass centre of the capsubot;
- l_i is the perpendicular distance of the direction of the force F_{m_i} from the axis of rotation;
- f_M is the friction force on the capsubot with the surface of motion - $f_M = 0$ if $F_r = 0$ and $|f_M|$ increases when $|F_r|$ increases with a maximum value of $f_{MM} = \text{sgn}(\dot{r}) \mu M g$,
 - \dot{r} is the linear velocity of the capsubot,
 - μ is translational friction coefficient,
 - g is gravitational constant;

- M_f is the frictional moment of the capsbot about z-axis through the mass centre of the capsbot - $M_f = 0$ if $M_r = 0$ and $|M_f|$ increases when $|M_r|$ increases with a maximum value of $M_{fM} = \text{sgn}(\dot{\phi}) \frac{2}{3} \mu_r M g (r_2 + \frac{wl - \pi r_2^2}{\pi r_1})$,
 - $r_2 = \frac{w}{2}$, $r_1 = \frac{\sqrt{l^2 + w^2}}{2}$ [184]),
 - μ_r is rotational friction coefficient,
 - l and w are the length and width of the capsbot respectively, and
 - $I = \frac{1}{12} M (l^2 + w^2)$ is the moment of inertia of the capsbot about z-axis through the mass centre of the capsbot.

4.2.2 System Description: Motion Generation and Switching

The capsbot has one switching mode and two motion modes namely linear motion mode and rotational motion mode depending on the forces applied on the IMs. For easy implementation, the capsbot is designed with $m_1 = m_2 = m$ and $l_1 = l_2$. The mass centre of the capsbot is assumed to stay at a fixed point within the capsbot and the natural mass centre of a parallelepiped i.e. G of Fig. 4.1. The IMs follows the following four-step acceleration profile in linear and rotational motion modes. One example of the acceleration profile is shown in Fig. 4.2(a).

$$\ddot{x}_{mid} = \begin{cases} a_{mi1} & 0 \leq t < t_{i1}; \quad \forall i = 1, 2 \quad \text{Step 1: Forward journey of } IM_i, \\ a_{mi2} & t_{i1} \leq t < t_{i2}; \quad \forall i = 1, 2 \quad \text{Step 2: Forward journey of } IM_i, \\ a_{mi3} & t_{i2} \leq t < t_{i3}; \quad \forall i = 1, 2 \quad \text{Step 3: Return journey of } IM_i, \\ a_{mi4} & t_{i3} \leq t < t_{i4}; \quad \forall i = 1, 2 \quad \text{Step 4: Return journey of } IM_i. \end{cases} \quad (4.5)$$

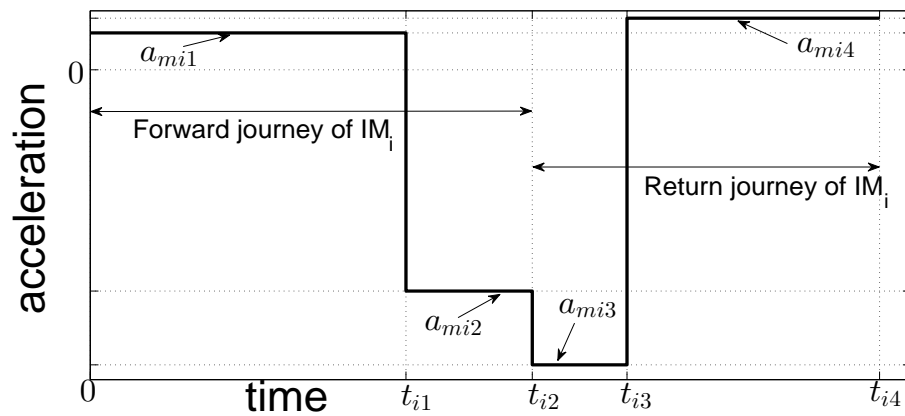
After choosing a_{mi1} to a_{mi4} based on the desired capsbot velocities, t_{i1} to t_{i4} can be found as:

$$t_{i1} = \frac{|v_{mi1}|}{|a_{mi1}|}; \quad t_{i2} = t_{i1} + \frac{|v_{mi1}|}{|a_{mi2}|}; \quad t_{i3} = t_{i2} + \frac{|v_{mi3}|}{|a_{mi3}|}; \quad t_{i4} = t_{i3} + \frac{|v_{mi3}|}{|a_{mi4}|}, \quad (4.6)$$

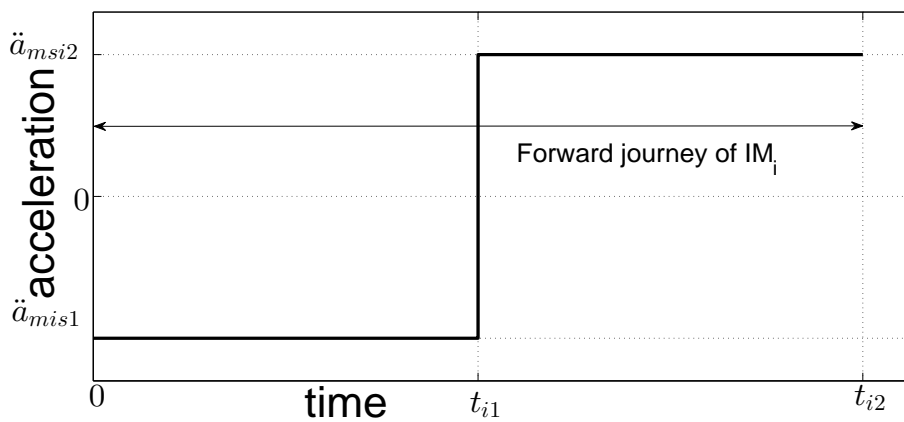
where v_{mi1} and v_{mi3} are the IM_i velocities at the end of steps 1 and 3 respectively.

The IMs follow the following two-step acceleration profile in switching mode:

$$\ddot{x}_{mid} = \begin{cases} a_{msi1} & 0 \leq t < t_{i1}; \quad \forall i = 1 \text{ and/or } 2 \quad \text{Step 1: Forward journey of } IM_i, \\ a_{msi2} & t_{i1} \leq t < t_{i2}; \quad \forall i = 1 \text{ and/or } 2 \quad \text{Step 2: Forward journey of } IM_i. \end{cases} \quad (4.7)$$



(a)



(b)

Fig. 4.2 Examples of acceleration profile for the (a) Motion modes (linear and rotational) (b) Switching mode

A convenient choice for switching accelerations are $a_{msi1} = -a_{msi2}$. Then t_{i1} and t_{i2} can be found as:

$$t_{i1} = \sqrt{\frac{2k}{|a_{msi1}|}}; \quad t_{i2} = 2t_{i1}, \quad (4.8)$$

where k = maximum stroke length of IM_i .

Linear Motion Mode: If forces of same magnitude and direction are applied to both the IMs i.e. $F_{m1} = F_{m2}$ ($\ddot{x}_{m1d} = \ddot{x}_{m2d}$) then from (4.2), (4.3) and (4.4) :

$$F_r \neq 0$$

$$M_r = 0 \text{ and } \sum M_G = 0$$

As $\sum M_G = 0$, the capsbot has no rotational motion. From (4.2) and (4.3), it can be said that if the capsbot has a zero initial velocity and $|F_r| > |f_{MM}|$, the capsbot starts a linear motion. An example of acceleration for the linear motion mode is shown in 4.2(a). The 2D capsbot performs the linear motion in steps 2, 3 and part of step 4.

Rotational Motion Mode: If forces of same magnitude but opposite directions are applied to the IMs i.e. $F_{m1} = -F_{m2}$ ($\ddot{x}_{m1d} = -\ddot{x}_{m2d}$) then from (4.2), (4.3) and (4.4):

$$F_r = 0 \text{ and } \sum F_x = \sum F_y = 0$$

$$M_r \neq 0$$

As $\sum F_x = \sum F_y = 0$, the capsbot has no linear motion. From (4.4), it can be said that if the capsbot has a zero initial velocity and $|M_r| > |M_{fM}|$, the capsbot starts a rotational motion. An example of acceleration for the rotation motion mode is shown in 4.2(a). The 2D capsbot performs the rotational motion in steps 2, 3 and part of step 4.

Switching Mode: The 2D capsbot uses this mode to switch from one motion to another. In this mode the IM/IMs changes/change its/their position from one end to other but the capsbot remains stationary. Here the forces applied on the IMs are small enough so that $|F_r| < |f_{MM}|$ and $|M_r| < |M_{fM}|$. Thus the IMs' accelerations maintain following constraint: $|\ddot{x}_{mid}| < \min(\frac{|f_{MM}|}{2m_i}, \frac{|M_{fM}|}{2m_i l_i})$. An example of acceleration for the switching mode is shown in 4.2(b).

4.2.3 System Description: Basis Behaviours

The following nine basis behaviours are defined based on the above switching and motion modes. These behaviours are followed for the trajectory tracking.

1. Forward (FW) linear motion: The IMs' initial and final positions are the rear end of the capsobot; the capsobot moves forward. The movements of the IMs are shown in Fig. 4.3(a) for this behaviour.
2. Backward (BW) linear motion: The IMs' initial and final positions are the front end of the capsobot; the capsobot moves backward. The movements of the IMs are shown in Fig. 4.3(b) for this behaviour.
3. Clock-wise (CW) rotational motion: The initial and final positions of the IM_1 are the rear end of the capsobot and of the IM_2 are the front end; the capsobot rotates clockwise. The movements of the IMs are shown in Fig. 4.3(c) for this behaviour.
4. Counter clock-wise (CCW) rotational motion: The initial and final positions of the IM_1 are the front end of the capsobot and of the IM_2 are the rear end; the capsobot rotates clockwise. The movements of the IMs are shown in Fig. 4.3(d) for this behaviour.
5. Switching to FW linear motion: Using this behaviour both the IMs reach to the rear end of the capsobot and ready to start FW linear motion.
6. Switching to BW linear motion: Using this behaviour both the IMs reach to the front end of the capsobot and ready to start BW linear motion.
7. Switching to CW rotational motion: Using this behavior IM_1 and IM_2 reach to the rear and front end of the capsobot respectively and ready to start CW rotational motion.
8. Switching to CCW rotational motion: Using this behavior IM_1 and IM_2 reach to the front and rear end of the capsobot respectively and ready to start CCW rotational motion.
9. Stationary: Both the IMs remain stationary and thus the capsobot also remains stationary.

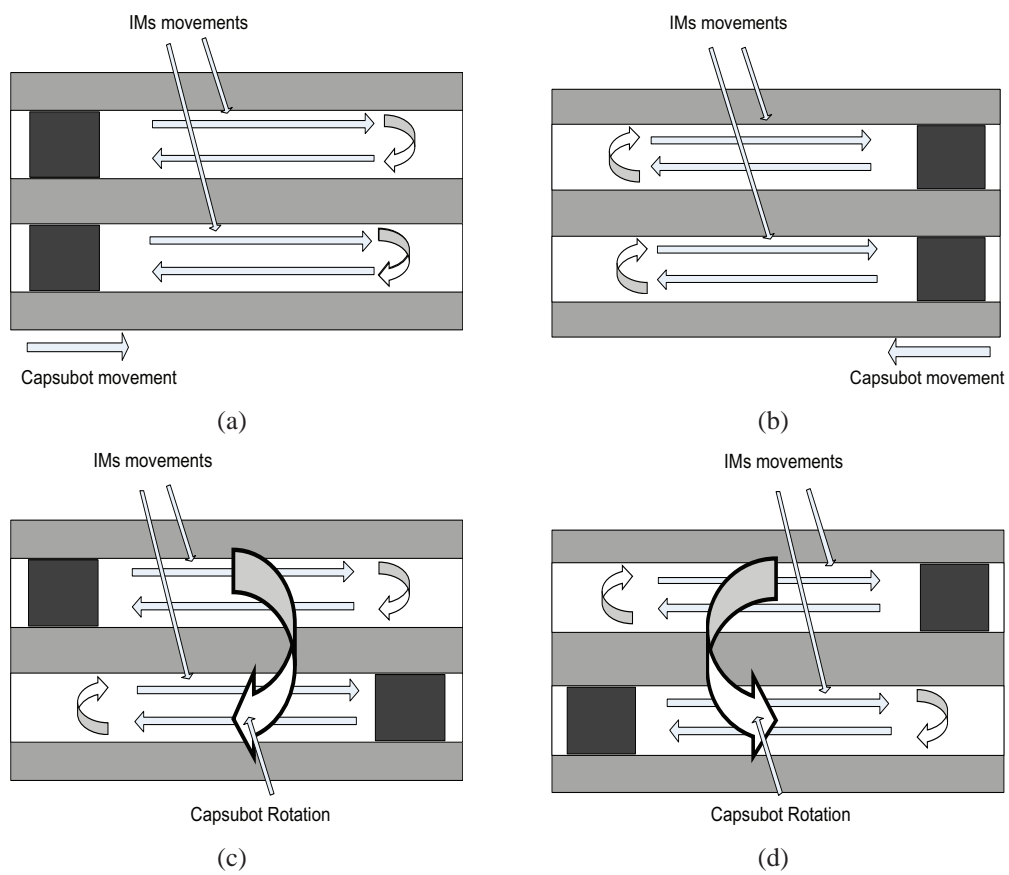


Fig. 4.3 Movements of the IMs for various motion behaviours (a) Linear (FW) (b) Linear (BW) (c) Rotational (CW) (d) Rotational (CCW)

4.2.4 Reference Frame Allocation

A fixed reference frame $O(X_O, Y_O)$ and the following local frames are assigned with the robot and the IMs while the robot moves (shown in Fig. 4.1). Two local frames: $R_j(X_{R_j}, Y_{R_j})$ and $L_j(X_{L_j}, Y_{L_j})$ are assigned on the mass centre of the capsobot. The robot performs only one behaviour at a time. When the capsobot needs to move from one point to another, it uses rotational motion to align itself with the straight line joining current position and destination; then it uses linear motion to move to the destination. When the capsobot rotates R_j remains stationary with respect to O and, L_j moves with the capsobot. Then L_j also become stationary with respect to O and the capsobot performs linear motion. When the robot moves to the next destination two more local frames are assigned. The current orientation and position of the capsobot with respect to O are:

$$\phi_j = \phi_{j-1} + \phi_{Mj}, \quad (4.9)$$

$$x_j = x_{j-1} + x_{Mj} \cos(\phi_j), \quad (4.10)$$

$$y_j = y_{j-1} + x_{Mj} \sin(\phi_j), \quad (4.11)$$

where ϕ_{Mj} is the rotation of the capsobot with respect to R_j and x_{Mj} is the translation of the capsobot with respect to L_j .

When the capsobot switches from one motion behaviour to another it uses the switching mode while the capsobot remains stationary but the IM/IMs moves/move.

Linear Motion Mode: In the local frame (L_j) the motion equations (1)-(4) become:

$$F_{m_1} - f_{m_1} = m_1 \ddot{x}_{m1} = F_{m_2} - f_{m_2} = m_2 \ddot{x}_{m2}, \quad (4.12)$$

$$\sum F_x = M \ddot{x}_M = -2F_{m_1} + 2f_{m_1} - f_M, \quad (4.13)$$

where $f_{m_i} = \text{sgn}(\dot{x}_{m_i} - \dot{x}_M) \mu_i m_i g \ \forall i = 1, 2$ and $f_M = \text{sgn}(\dot{x}_M) \mu M g$, x_{m_i} and x_M are the displacement of the IM_i and the capsobot respectively measured in the local frame (L_j).

The average linear velocity of the capsobot \bar{x}_M is:

$$\bar{x}_M = \frac{x_M}{t_l}, \quad (4.14)$$

where x_M is the linear displacement of the capsbot in the cycle time t_l .

$$x_M = \frac{v_{M2}^2}{2a_{M2}} + \frac{v_{M3}^2 - v_{M2}^2}{2a_{M3}} - \frac{v_{M3}^2}{2a_{M4}}, \quad (4.15)$$

$$t_l = t_{i4} = \frac{|v_{mi1}|}{|a_{mi1}|} + \frac{|v_{mi1}|}{|a_{mi2}|} + \frac{|v_{mi3}|}{|a_{mi3}|} + \frac{|v_{mi3}|}{|a_{mi4}|}, \quad (4.16)$$

where a_{Mq} is the capsbot acceleration in step q , v_{M2} and v_{M3} are the capsbot velocities at the end of steps 2 and 3 respectively.

$$v_{M2} = a_{M2}(t_{i2} - t_{i1}); \quad v_{M3} = a_{M2}(t_{i2} - t_{i1}) + a_{M3}(t_{i3} - t_{i2}),$$

$$a_{Mq} = \frac{-m_1 a_{m1q} - m_2 a_{m2q} - \mu M g}{M}; \quad q = 1, 2, 3, 4,$$

Rotational Motion Mode: In the local frames (L_j, R_j) the motion equations (1)-(4) become:

$$F_{m_i} - f_{m_i} = m_i \ddot{x}_{m_i} \quad \forall i = 1, 2, \quad (4.17)$$

$$\sum M_G = I \ddot{\phi}_M = (2F_{m_1} - 2f_{m_1})l_1 - M_f, \quad (4.18)$$

where $f_{m_i} = \text{sgn}(\dot{x}_{m_i})\mu_i m_i g$, $M_{fM} = \text{sgn}(\dot{\phi}_M) \frac{2}{3} \mu_r M g (r_2 + \frac{wl - \pi r_2^2}{\pi r_1})$ [184], ϕ_M is the orientation of the capsbot in the local frame.

The average angular velocity of the capsbot $\bar{\dot{\phi}}_{Mi}$ is:

$$\bar{\dot{\phi}}_{Mi} = \frac{\phi_{Mi}}{t_r}, \quad (4.19)$$

where ϕ_{Mi} is the angular displacement of the capsbot in the cycle time t_r .

$$\phi_M = \frac{\omega_{M2}^2}{2\alpha_{M2}} + \frac{\omega_{M3}^2 - \omega_{M2}^2}{2\alpha_{M3}} - \frac{\omega_{M3}^2}{2\alpha_{M4}}, \quad (4.20)$$

$$t_r = t_{i4} = \frac{|v_{mi1}|}{|a_{mi1}|} + \frac{|v_{mi1}|}{|a_{mi2}|} + \frac{|v_{mi3}|}{|a_{mi3}|} + \frac{|v_{mi3}|}{|a_{mi4}|}, \quad (4.21)$$

where α_{Mq} is the capsbot angular acceleration in step q , ω_{M2} and ω_{M3} are the capsbot angular velocities after steps 2 and 3 respectively.

$$\begin{aligned}\omega_{M2} &= \alpha_{M2}(t_{i2} - t_{i1}); \quad \omega_{M3} = \alpha_{M2}(t_{i2} - t_{i1}) + \alpha_{M3}(t_{i3} - t_{i2}), \\ \alpha_{Mq} &= (m_2 a_{m2q} l_2 - m_1 a_{m1q} l_1 - M_f) / I \quad q = 1, 2, 3, 4.\end{aligned}$$

Switching Mode: In the local frame (L_j) the motion equations (1) to (4) become:

$$F_{m_i} - f_{m_i} = m_i \ddot{x}_{mi} \quad \forall i = 1, 2,$$

where $f_{m_i} = \text{sgn}(\dot{x}_{mi}) \mu_i m_i g$.

4.3 Trajectory Tracking of 2D Capsubot

4.3.1 Proposed Trajectory Tracking Algorithm

Let the capsubot follow the planar position trajectory shown in Fig. 4.4(a) which is a sinusoidal trajectory. This trajectory reflects necessary complexity to test the performance of the proposed trajectory tracking algorithm. This research proposes the following algorithm (trajectory tracking control algorithm) to solve the trajectory tracking problem with the details in section 4.3.2.

Preparation Step: Database creation: To track the trajectory, change the capsubot velocity by tuning the acceleration parameters of the IMs. Hence a database is created by computing capsubot linear and angular velocities for different profile parameters to feed into step 2.3.

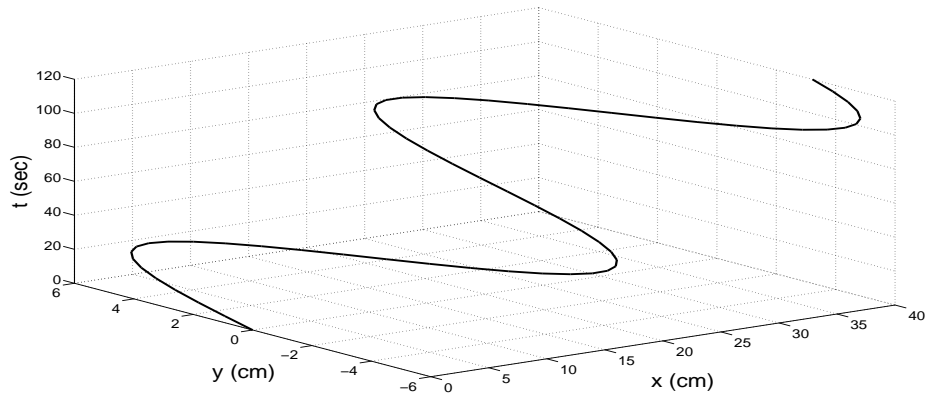
Step 1: Generating trajectory segment: Divide the trajectory into small segments as shown in Fig. 4.4(b), and compute the desired angular and linear velocities of the capsubot to track each segment.

Step 2: Behaviour-based control: A behaviour-based control approach tracks each segment from step 1.

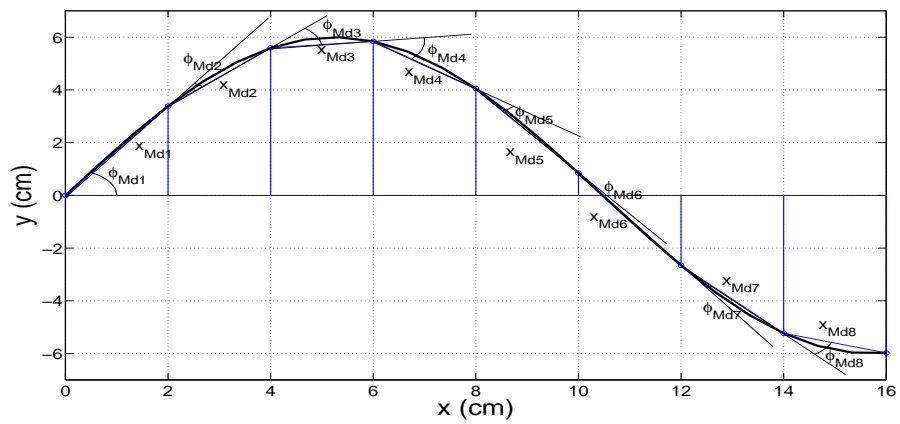
Step 2.1: Behaviour sets: Define nine basis behaviours. Several behaviour sets (A to I in Fig. 4.5) comprising one or more basis behaviours are formed. These behaviour sets include all necessary combinations of behaviours to track each segment of trajectory.

Step 2.2: Selection algorithm: A selection algorithm shown in Fig. 4.6 is used to select appropriate behaviour set for each trajectory segment.

Step 2.3: Selection of profile parameters: The desired velocity is compared with the database and the appropriate profile parameters are selected. The acceleration sets for which



(a)



(b)

Fig. 4.4 (a) Desired position trajectory with time axis ($x = At, y = B\sin(\Omega t)$); where, $A = \frac{1}{3}, B = 6, \Omega = \frac{1}{10}$ (b) Taking segments from the desired position trajectory (part of the trajectory is shown)

(4.31) and (4.32) give the minimum value, are selected for rotational and linear motion modes respectively. To switch among various motion modes, switching modes are used.

Step 2.4: Tuning the segment time: Tune the segment time based on the selected parameters.

Step 2.5: Modification of the desired angular and linear velocities: The desired linear and angular velocities for each segment are modified based on the projected position of the capsubot before the start of the tracking of the segment.

Step 2.6: Rules for behaviours: Develop rules to implement behaviours of selected behaviour sets.

Step 3: Low-level control: IMs movements for each behaviour is performed using partial feedback linearization control.

Summary of the Algorithm: Step 1 is used to generate segments from the desired trajectory. Step 2.1 is used to define behaviours and behaviour sets. Step 2.2 is used to select appropriate behaviour-set to track the trajectory in a segment. Then in step 2.3 appropriate profile parameters are selected for the selected behaviour set. These profile parameters are the desired accelerations of the IMs $\ddot{x}_{mid}, \forall i = 1, 2$. In step 3 the low-level IMs controller tracks the desired IMs accelerations \ddot{x}_{mid} and eventually track the capsubot trajectory in a segment. The process will be repeated for the rest of the segments.

4.3.2 Methods for Implementing the Proposed Trajectory Tracking Algorithm

Preparation Step: Database creation

For the acceleration profiles, the tunable variables are a_{mi1} , a_{mi2} , a_{mi3} and a_{mi4} (where $i = 1, 2$) to get various average velocities of the capsubot. For simplicity, $a_{mi2} = a_{mi3}$ and $a_{mi1} = a_{mi4}$ are designed and a fixed value for $a_{mi1} = a_{mi4}$ (maintaining $|a_{mi1}| = |a_{mi4}| < \min(\frac{|f_{MM}|}{2m_i}, \frac{|M_{fM}|}{2m_i l_i})$) is used. Only $a_{mi2} = a_{mi3}$ are tuned to get various average velocities of the capsubot. It is noted that if $a_{miu2} \neq a_{miu3}$ and $a_{miu1} \neq a_{mi4}$ are chosen, the database size will be larger.

A parameter set includes a_{mi1} , a_{mi2} , a_{mi3} and a_{mi4} (where $i = 1, 2$). Total number of

acceleration profile parameter sets for linear motion (n_l) and rotational motion (n_r) are:

$$n_l = \text{floor}\left(\frac{|a_{mmax}(l)| - |a_{mmin}(l)|}{a_{mdiff}(l)}\right) + 1, \quad (4.22)$$

$$n_r = \text{floor}\left(\frac{|a_{mmax}(r)| - |a_{mmin}(r)|}{a_{mdiff}(r)}\right) + 1, \quad (4.23)$$

where $\text{floor}(A)$ rounds the elements of A to the nearest integers less than or equal to A ; l and r refers to linear and rotational; $|a_{mmax}(l)|$ and $|a_{mmax}(r)|$ are maximum accelerations, $|a_{mmin}(l)|$ and $|a_{mmin}(r)|$ are minimum accelerations, $a_{mdiff}(l)$ and $a_{mdiff}(r)$ are differences between accelerations of two consecutive profile parameter sets.

The average linear and angular velocities of the capsuobot for all possible profile parameter sets are calculated using (4.14) and (4.19) respectively and stored in the database.

Step 1: Generating Trajectory Segment

The trajectory tracking is performed in a segment-wise manner. The desired trajectory of Fig. 4.4(a) is divided into small segments with a segment time T , as shown in Fig. 4.4(b). The capsuobot follows the straight lines connecting the start and end points of the segments. Firstly the capsuobot aligns itself with the straight line by using one of the rotational behaviours i.e. the capsuobot corrects its steering angle. Then the capsuobot uses one of the switching behaviours to switch from rotational to linear motion mode. Finally the capsuobot travels the distance of the straight line using one of the linear behaviours.

The smaller the segment time, the smoother the tracked trajectory. However as the capsuobot may need to complete the behaviour set comprising up to four behaviours (switching to rotation, rotation, switching to linear and linear motion) to track the trajectory in a segment, the capsuobot should satisfy:

$$T \geq t_s + t_{rm} + t_s + t_{lm}, \quad (4.24)$$

where t_s = time to complete the switching cycle, t_{rm} = maximum time to complete a rotation cycle, t_{lm} = maximum time to complete a linear cycle.

Step 2: Tracking using Behaviour-Based Control

Step 2.1: Behaviour sets: Nine basis behaviours are defined in section 4.2.3. A to I shown in Fig. 4.5 are all the possible behaviour sets to follow certain segment of trajectory. E is used when the capsuobot doesn't change its position and orientation in the trajectory

segment. A or B is used when the capsubot only changes its orientation whereas C or D is used when it only changes its position in the trajectory segment. F, G, H or I is used when the capsubot changes both of its position and orientation in the trajectory segment.

Step 2.2: Selection algorithm: The selection algorithm shown in Fig. 4.6 is used to select the right behaviour set - A to I - to track each trajectory segment. At the beginning of the tracking the IMs are placed at the rear end of the capsubot. The variable P is used to keep record of the behaviour of the capsubot - P = 1, 2, 3 or 4 means the previous behaviour executed is FW linear, BW linear, CCW rotational or CW rotational respectively. The rules developed in the step 2.6 are used to implement behaviours of the selected behaviour sets.

Step 2.3: Selection of Profile Parameters The segment time, T is decided from the desired trajectory by satisfying the constraint of (4.24). In each segment the capsubot needs to follow a behaviour set from Fig. 4.5. The desired velocity, $\bar{x}_{Md(j)}$ and desired angular velocity, $\bar{\phi}_{Md(j)}$ can be calculated as:

$$x_{Md(j)} = \sqrt{(x_j - x_{j-1})^2 - (y_j - y_{j-1})^2}, \quad (4.25)$$

$$\phi_{Md(j)} = \tan^{-1} \frac{y_j - y_{j-1}}{x_j - x_{j-1}} \quad \forall j = 1, 2, \dots, n, \quad (4.26)$$

$$\bar{x}_{Md(j)} = \frac{x_{Md(j)}}{\frac{T}{2} - t_s}, \quad (4.27)$$

$$\bar{\phi}_{Md(j)} = \frac{\phi_{Md(j)} - \phi_{Md(j-1)}}{\frac{T}{2} - t_s} \quad \forall j = 1, 2, \dots, n, \quad (4.28)$$

where n is the number of segments; (x_0, y_0) and $\phi_{Md(0)}$ are the initial capsubot position and orientation.

For A and B (Fig. 4.5), $|\bar{x}_{Md(i)}| \leq \varepsilon_2$ (ε_2 is a small number), thus $\bar{\phi}_{Md(j)}$ is modified as:

$$\bar{\phi}_{Md(j)} = \frac{\phi_{Md(j)} - \phi_{Md(j-1)}}{T - t_s} \quad \forall j = 1, 2, \dots, n. \quad (4.29)$$

For C and D (Fig. 4.5), $|\bar{\phi}_{Md(j)}| \leq \varepsilon_1$ (ε_1 is a small number), thus $\bar{x}_{Md(j)}$ is modified as:

$$\bar{x}_{Md(j)} = \frac{x_{Md(j)}}{T - t_s} \quad \forall j = 1, 2, \dots, n. \quad (4.30)$$

Selection: If $\bar{\phi}_{Md}$ is negative (CW rotational motion) IM_2 follows the profile of Fig. 4.2(a) whereas IM_1 follows $\ddot{x}_{m1d} = -\ddot{x}_{m2d}$. If $\bar{\phi}_{Md}$ is positive (CW rotational motion) IM_1

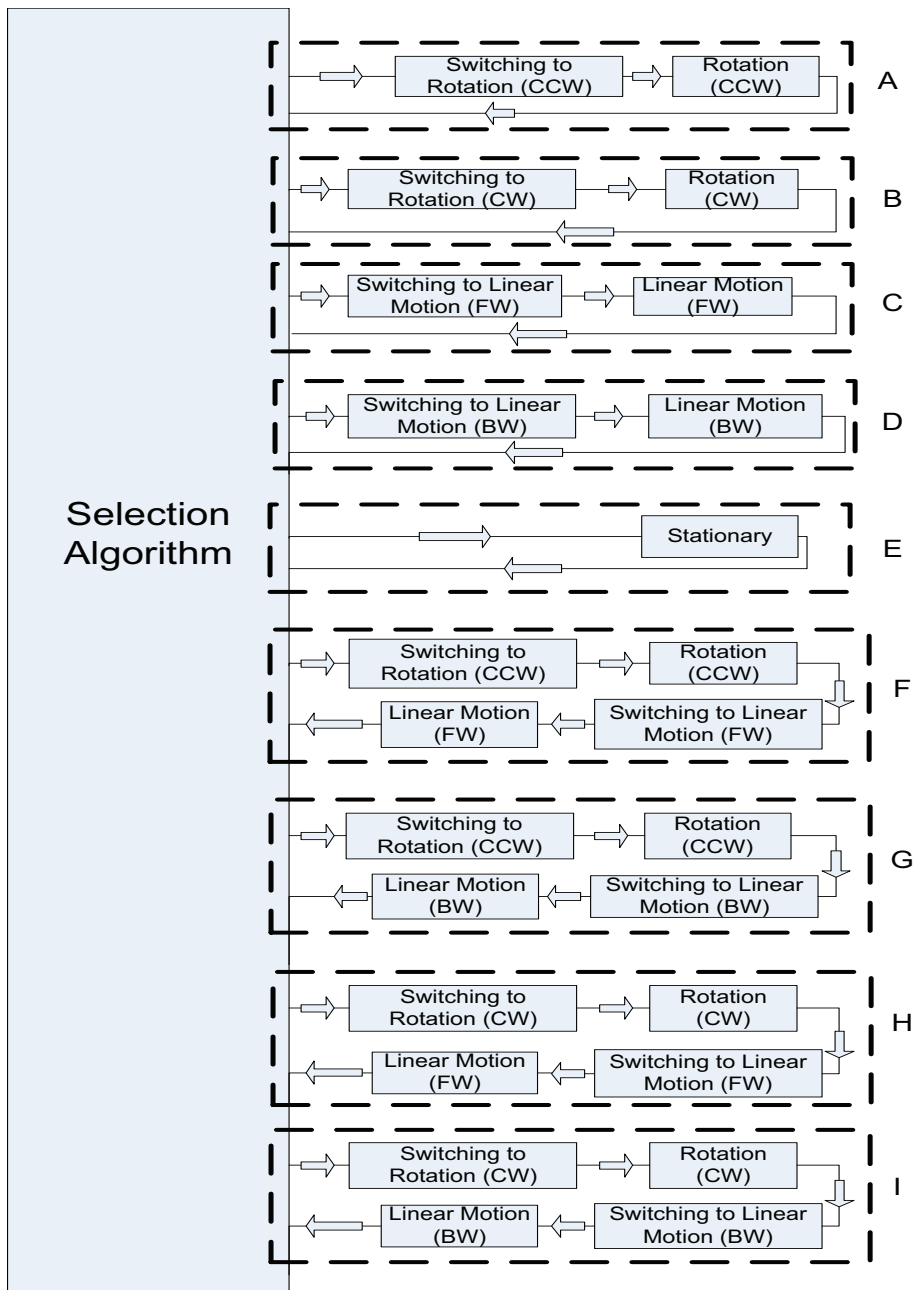


Fig. 4.5 Block diagram of the behaviour-based control of the 2D capsutbot (one of the behaviour set from A to I is used to track a segment)

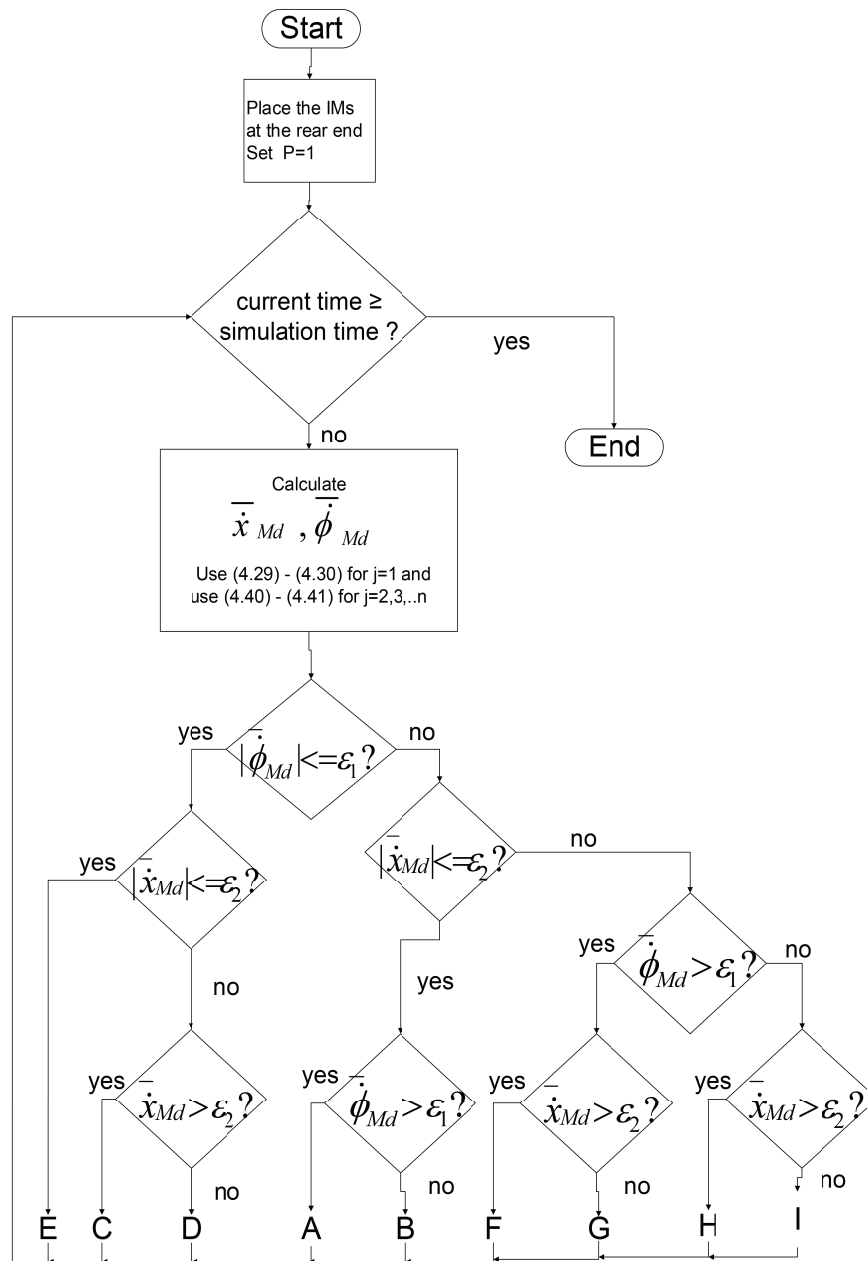


Fig. 4.6 Selection algorithm for Fig. 4.5 (ϵ_1 and ϵ_2 are small positive numbers)

follows the profile of Fig. 4.2(a) whereas IM_2 follows $\ddot{x}_{m2d} = -\ddot{x}_{m1d}$. Now the profile parameters (a_{mi1} , a_{mi2} , a_{mi3} and a_{mi4}) need to be selected which will generate the desired $\bar{\phi}_{Md}$. All the possible profile parameter sets and corresponding average angular velocities i.e. $\bar{\phi}_M(q)$, $q = 1, 2, \dots, n_r$ are found from the database created in the preparation stage. The minimum error $\dot{\phi}_{diff}$ can be obtained from (4.31). The profile parameter set corresponding to minimum error in (4.31) is selected.

$$\dot{\phi}_{diff} = \min(|\bar{\phi}_{Md}| - |\bar{\phi}_M(1)|), (|\bar{\phi}_{Md}| - |\bar{\phi}_M(2)|), \dots, (|\bar{\phi}_{Md}| - |\bar{\phi}_M(n_r)|). \quad (4.31)$$

If \bar{x}_{Md} is positive (FW linear motion) both IMs follow the profile of Fig. 4.2(a). If \bar{x}_{Md} is negative (BW linear motion) IMs follow accelerations with the equal magnitude as in Fig. 4.2(a) but opposite in direction. All the possible profile parameter sets and corresponding average linear velocities i.e. $\bar{x}_M(p)$, $p = 1, 2, \dots, n_l$ are found from the database. The minimum error \dot{x}_{diff} can be obtained from (4.32). The profile parameter set corresponding to minimum error in (4.32) is selected.

$$\dot{x}_{diff} = \min(|\bar{x}_{Md}| - |\bar{x}_M(1)|), (|\bar{x}_{Md}| - |\bar{x}_M(2)|), \dots, (|\bar{x}_{Md}| - |\bar{x}_M(n_l)|). \quad (4.32)$$

Step 2.4: Tuning the Segment Time The segment time is tuned based on the selected profile parameter sets. The selected parameter set can only be used for a multiple of cycle time¹ i.e. one cycle or two cycles or three cycles or so on. To satisfy this constraint the segment time T is tuned as follows:

$$\text{Rotation: } T_{R(tuned)} = t_{r(sel)} \times \text{floor}\left(\frac{T - t_s}{t_{r(sel)}}\right), \quad (4.33)$$

$$\text{Linear: } T_{l(tuned)} = t_{L(sel)} \times \text{floor}\left(\frac{T - t_s}{t_{l(sel)}}\right), \quad (4.34)$$

$$\text{For A and B: } T_{tuned} = T_{r(tuned)} + t_s, \quad (4.35)$$

$$\text{For C and D: } T_{tuned} = T_{l(tuned)} + t_s, \quad (4.36)$$

$$\text{For F, G, H and I: } T_{tuned} = T_{l(tuned)} + T_{r(tuned)} + 2t_s, \quad (4.37)$$

where $t_{l(sel)}$ and $t_{r(sel)}$ are the cycle times of the selected acceleration profiles for linear and rotational motions respectively and t_s is the cycle time for switching mode.

¹cycle time is the time to complete all the steps (four steps for linear and rotational mode and two steps for switching mode) of the acceleration profile.

Step 2.5: Modification of the desired angular and linear velocities The desired angular and linear velocities are modified iteratively using the error in each segment. The expected position of the capsubot after completing each segment is calculated based on the selected profile parameters and tuned segment time. This position is used to modify the desired angular and linear velocities for the next segment. Thus the modified desired velocities $\bar{x}_{Md(j)}$ and $\bar{\phi}_{Md(j)}$ are:

$$x_{Md(j)} = \sqrt{(x_j - x_{c(j-1)})^2 - (y_j - y_{c(j-1)})^2} \quad \forall j = 2, 3, \dots, n, \quad (4.38)$$

$$\phi_{Md(j)} = \tan^{-1} \frac{y_j - y_{c(j-1)}}{x_j - x_{c(j-1)}} \quad \forall j = 2, 3, \dots, n, \quad (4.39)$$

$$\bar{x}_{Md(j)} = \frac{x_{Md(j)}}{\frac{T}{2} - t_s} \quad \forall j = 2, 3, \dots, n, \quad (4.40)$$

$$\bar{\phi}_{Md(j)} = \frac{\phi_{Md(j)} - \phi_{Md(j-1)}}{\frac{T}{2} - t_s} \quad \forall j = 2, 3, \dots, n, \quad (4.41)$$

where $(x_{c(j-1)}, y_{c(j-1)})$ is the current position of the capsubot before the tracking of the j th segment of trajectory and can be calculated iteratively as:

$$x_{c(j-1)} = x_{c(j-2)} + s_{j-1} \cos(\theta_{j-1}), \quad (4.42)$$

$$y_{c(j-1)} = y_{c(j-2)} + s_{j-1} \sin(\theta_{j-1}), \quad (4.43)$$

where θ_{j-1} is the current orientation with respect to O before tracking starts at the j th segment; s_{j-1} is the displacement of the capsubot at the $(j-1)$ th segment.

$$\theta_{j-1} = \theta_{j-2} + T_{R(tuned)} \bar{\phi}_{Mu(j-1)sel}, \quad (4.44)$$

$$s_{j-1} = T_{R(tuned)} \bar{x}_{Mu(j-1)sel}, \quad (4.45)$$

where $\bar{\phi}_{Mu(j-1)sel}$ and $\bar{x}_{Mu(j-1)sel}$ are the capsubot angular and linear average velocities respectively of the $(j-1)$ th segment for the selected parameters.

Step 2.6: Rules for Implementing the Behaviours The following rules are developed to implement each of the behaviour:

FW linear motion:

1. Select profile parameters
2. Calculate the corresponding $T_{L(tuned)}$

3. Execute the IMs movement till $T_{elapsed} \leq T_{L(tuned)}$

4. Set P=1

BW linear motion:

1. Select profile parameters

2. Calculate the corresponding $T_{L(tuned)}$

3. Execute the IMs movement till $T_{elapsed} \leq T_{L(tuned)}$

4. Set P=2

CW rotational motion:

1. Select profile parameters

2. Calculate the corresponding $T_{R(tuned)}$

3. Execute the IMs movement till $T_{elapsed} \leq T_{R(tuned)}$

4. Set P=3

CCW rotational motion:

1. Select profile parameters

2. Calculate the corresponding $T_{R(tuned)}$

3. Execute the IMs movement till $T_{elapsed} \leq T_{R(tuned)}$

4. Set P=4

Switching to FW linear motion:

1. Decide on the last behaviour ²

2. (a) If P=1 then $\ddot{x}_{m1d} = \ddot{x}_{m2d} = 0$ for IM_1 and IM_2

(b) Elseif P=2 then switching mode ($a_{ms11} = -a_{ms12}$; $a_{ms21} = -a_{ms22}$ and $\ddot{x}_{m1d} = \ddot{x}_{m2d}$) for both the IMs,

(c) Elseif P=3 then switching mode ($a_{ms11} = -a_{ms12}$) for IM_1 and $\ddot{x}_{m2d} = 0$ for IM_2

²P=1, 2, 3 or 4 means the previous behaviour executed is FW linear, BW linear, CCW rotational or CW rotational respectively

- (d) Elseif P=4 then switching mode ($a_{ms21} = -a_{ms22}$) for IM_2 and $\ddot{x}_{m1} = 0$ for IM_1 ,
3. Execute one switching cycle with selected parameters.

Switching to BW linear motion:

1. Decide on the last behaviour
2. (a) If P=1 then switching mode ($a_{ms11} = -a_{ms12}$; $a_{ms21} = a_{ms22}$ and $\ddot{x}_{m1d} = \ddot{x}_{m2d}$) for both the IMs
 - (b) Elseif P=2 then $\ddot{x}_{m1d} = \ddot{x}_{m2d} = 0$ for IM_1 and IM_2
 - (c) Elseif P=3 then switching mode ($a_{ms21} = -a_{ms22}$) for IM_2 and $\ddot{x}_{m1d} = 0$ for IM_1
 - (d) Elseif P=4 then switching mode ($a_{ms11} = -a_{ms12}$) for IM_1 and $\ddot{x}_{m2d} = 0$ for IM_2
3. Execute one switching cycle with selected parameters.

Switching to CW rotational motion:

1. Decide on the last behaviour
2. (a) If P=1 then switching mode ($a_{ms21} = a_{ms22}$) for IM_2 and $\ddot{x}_{m1} = 0$ for IM_1
 - (b) Elseif P=2 then switching mode ($a_{ms11} = a_{ms12}$) for IM_1 and $\ddot{x}_{m2d} = 0$ for IM_2
 - (c) Elseif P=3 then switching mode ($a_{ms11} = -a_{ms12}$; $a_{ms21} = -a_{ms22}$ and $\ddot{x}_{m1d} = -\ddot{x}_{m2d}$) for both the IMs,
 - (d) Elseif P=4 then $\ddot{x}_{m1d} = \ddot{x}_{m2d} = 0$ for IM_1 and IM_2
3. Execute one switching cycle with selected parameters.

Switching to CCW rotational motion:

1. Decide on the last behaviour
2. (a) If P=1 then switching mode ($a_{ms11} = -a_{ms12}$) for IM_1 and $\ddot{x}_{m2} = 0$ for IM_2
 - (b) Elseif P=2 then switching mode ($a_{ms21} = -a_{ms22}$) for IM_2 and $\ddot{x}_{m1d} = 0$ for IM_1
 - (c) Elseif P=3 then $\ddot{x}_{m1d} = \ddot{x}_{m2d} = 0$ for IM_1 and IM_2
 - (d) Elseif P=4 then switching mode ($a_{ms11} = -a_{ms12}$; $a_{ms21} = -a_{ms22}$ and $\ddot{x}_{m1d} = -\ddot{x}_{m2d}$) for both the IMs
3. Execute one switching cycle with selected parameters.

Stationary: Wait for one segment time.

Step 3: Low-level Control of the IMs

The open loop control laws of the IMs are:

$$F_{m_{id}} = m_i \ddot{x}_{mid} + \text{sgn}(\dot{x}_{mid} - \dot{r}_d) \mu_i m_i g \quad \forall i = 1, 2, \quad (4.46)$$

where $\dot{r}_d = \dot{x}_{Md}$ for linear motion mode and, $\dot{r}_d = 0$ for switching mode and rotational motion mode.

The closed loop control law can be selected, using partial feedback linearization [51]

$$F_{m_{id}} = \alpha_i \tau_{id} + \beta_i, \quad (4.47)$$

where $\alpha_i = m_i$, $\beta_i = \text{sgn}(\dot{x}_{mid} - \dot{r}_d) \mu_i m_i g$.

Let $\tilde{x}_i = x_{mi} - x_{mid}$ be the tracking error; choosing the linear control law $\tau_{id} = \ddot{x}_{mid} - k_1 \dot{\tilde{x}}_i - k_2 \tilde{x}_i$ and applying the control law (4.47) to (4.1):

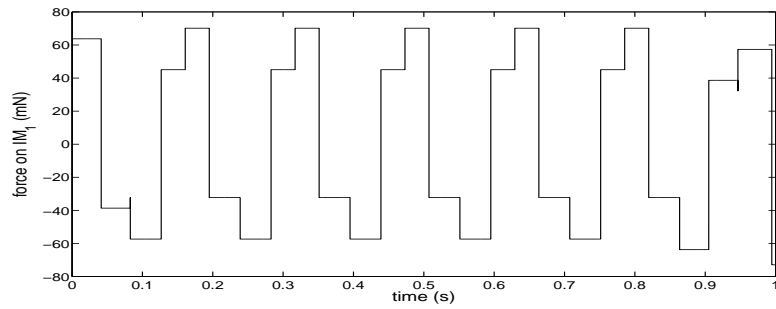
$$\ddot{\tilde{x}}_i + k_{i1} \dot{\tilde{x}}_i + k_{i2} \tilde{x}_i = 0. \quad (4.48)$$

The values of k_{i1} and k_{i2} can properly be selected using the standard linear control theory. Then by using the control laws (4.47) the IMs can be made to track the IMs' desired trajectories.

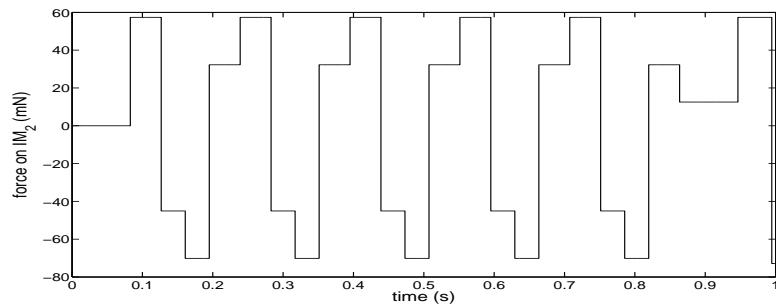
4.3.3 Simulation Results and Discussion

The simulation is performed in the Simulink/Matlab environment. The simulink model is provided in the appendix B. The parameters used for simulation are taken from the prototype developed in this research (presented in the section 4.4): $m_1 = m_2 = 6.4gm$, $\mu_1 = \mu_2 = 0.2$, $\mu_r = 0.08$, $\mu = 0.28$, $F_{m1(max)} = F_{m2(max)} = 1.03N$, $l_1 = l_2 = 11.5mm$, $M = 42.9gm$, $g = 9.8ms^{-2}$, $w = 7cm$, $l = 8.7cm$ and $k = 6mm$. The acceleration profile parameters used to create the database for the trajectory tracking algorithm are: Linear: $|a_{mmax(l)}| = 20ms^{-2}$, $|a_{mmin(l)}| = 10ms^{-2}$, $a_{mdiff(l)} = 0.05ms^{-2}$, $|a_{mi1}| = |a_{mi4}| = 7ms^{-2}$; Rotation: $|a_{mmax(r)}| = 20ms^{-2}$, $|a_{mmin(r)}| = 9ms^{-2}$, $a_{mdiff(r)} = 0.1ms^{-2}$ and $|a_{mi1}| = |a_{mi4}| = 7ms^{-2}$. The minimum segment time (T) is 0.47s which is calculated from the constraint of (4.24) and the above mentioned parameters. The segment time (T) of 1s, 2s and 4s are used in the simulation to evaluate the impact of the segment time (T) to the control performance. The initial position and orientation of the capsbot are assumed to be (0, 0) and 1 rad respectively.

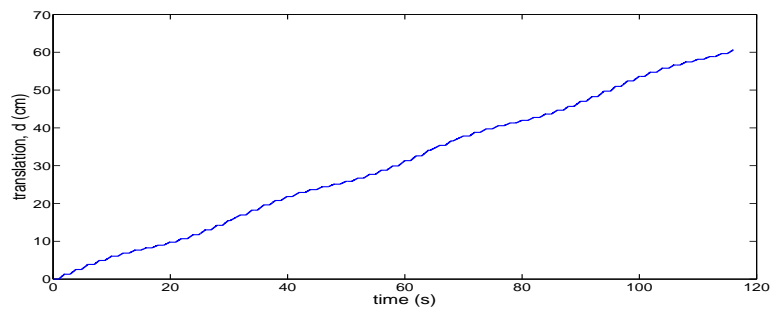
Figs. 4.7 to 4.8 show the simulation results for the trajectory tracking using the proposed



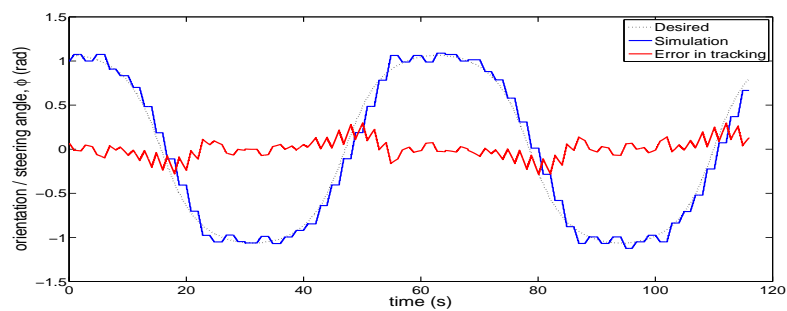
(a)



(b)



(c)



(d)

Fig. 4.7 Simulated control forces on the IMs for the segment time, $T=2s$ (a) IM_1 (b) IM_2 ; Trajectories of the 2D capsobot for $T = 2s$ (c) Segment-wise translation trajectory (d) Orientation/ steering angle trajectory

approach for the segment time (T) of 2s. Figs. 4.7(a) and 4.7(b) show the force applied on the inner masses for the first one second of the trajectory tracking while the capsbot firstly performs "switching to CCW rotation" behaviour (until 0.09s) and then performs "CCW rotation" behaviour (until 0.86s) and after that performs "switching to FW linear motion" behaviour. During the "switching to CCW rotation" behaviour, the IM_2 remains stationary and thus the forces on the IM_2 is zero as can be seen in Fig. 4.7(b). The IM_1 follows a two-step acceleration profile as described in (4.7) and thus the force on the IM_1 also has the same two-step pattern as can be seen in Fig. 4.7(a). During the "CCW rotational motion" behaviour, forces of same magnitude but opposite directions are applied to the IMs which can be observed from Figs. 4.7(a) and 4.7(b).

From Figs. 4.7(c) and 4.7(d), the impact of the segment-wise tracking is observed in the simulated translation and steering angle. In every segment the capsbot firstly corrects the orientation and then it travels the line joining the start and end points of the segment. Thus from Fig. 4.7(c), it is observed that the translation graph remains flat (translation zero) at the beginning of the segment and then increases whereas the steering angle graph changes for the first portion of the segment and then remains flat (rotation zero) for the rest of the segment. The steering angle tracking error remains within a limit (between -0.29 rad to 0.30 rad). The mean absolute error of steering angle tracking is 0.07 rad. The error can further be reduced by decreasing the segment time.

The simulated trajectories of Fig. 4.8 are obtained by using the following equations:

$$x_j = x_{j-1} + (d_j - d_{j-1})\cos(\phi_j), \quad (4.49)$$

$$y_j = y_{j-1} + (d_j - d_{j-1})\sin(\phi_j). \quad (4.50)$$

It is noted from Fig. 4.8 that the capsbot follows the trajectory quite accurately. Fig. 4.9 provides a comparison of the errors in the trajectory tracking using various segment times. From Figs. 4.8(a) and 4.9(b) (the curve for T=2s) the error in x trajectory tracking increases at the beginning of each segment and then goes to close to zero at the end of the segment. The capsbot corrects its steering angle in the first portion of the segment when it does not have any translation and thus the x trajectory tracking error increases. In the second portion the capsbot performs translation and thus the error in x trajectory tracking decreases. Fig. 4.8(b) compares the desired and simulated y trajectory and shows the error in trajectory tracking. From Figs. 4.9(b) and 4.9(c) (the curve for T=2s) the error patterns are same for both the x and y trajectory tracking. The error in the y trajectory tracking increases at the beginning of each segment and then decreases to close to zero at the end of the segment for

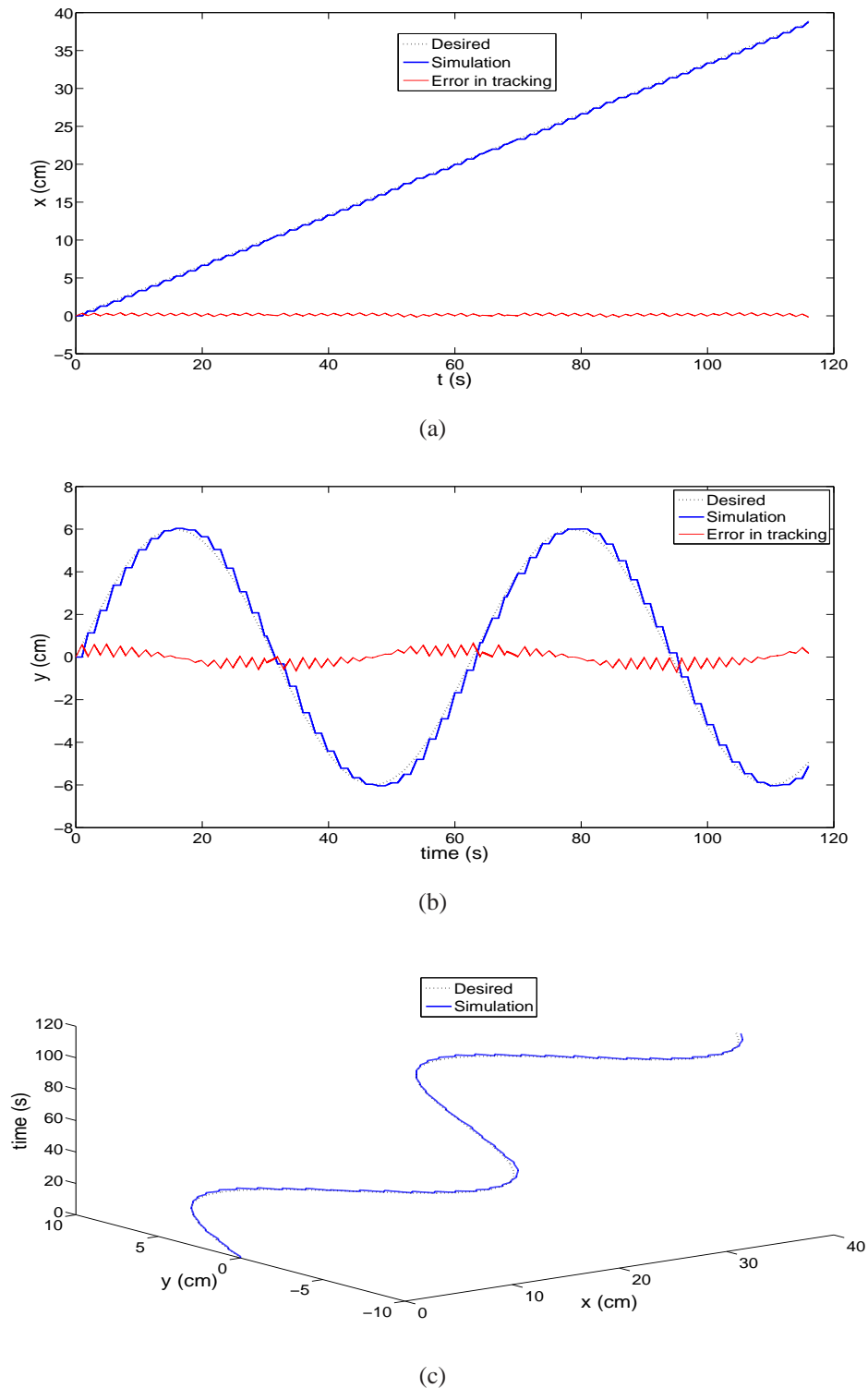


Fig. 4.8 Trajectories of the 2D capsubot for the segment time, $T = 2$ s (a) x trajectory (by using $x_j = x_{j-1} + (d_j - d_{j-1})\cos(\phi_j)$) (b) y trajectory (by using $y_j = y_{j-1} + (d_j - d_{j-1})\sin(\phi_j)$) (c) Position trajectory on $x - y$ plane with time axis

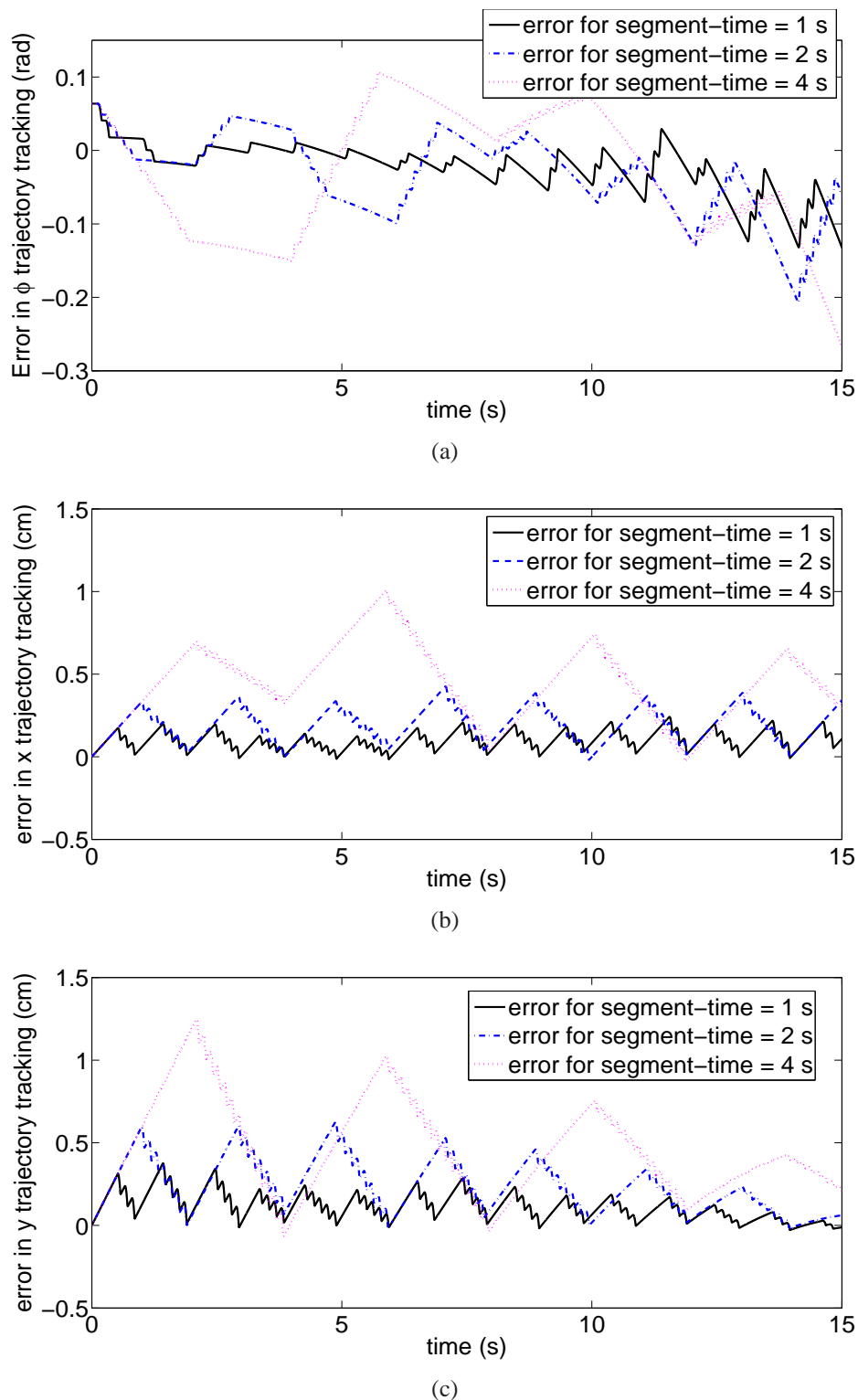


Fig. 4.9 Comparison of the trajectory tracking errors for various segment times (a) steering angle (ϕ) trajectory (b) x trajectory (c) y trajectory

the same reason as the x trajectory tracking. The error range for the x trajectory tracking is -0.18 cm to 0.44 cm whereas the error range for the y trajectory tracking is -0.73 cm to 0.67 cm. The mean absolute error of the x trajectory tracking is 0.16 cm whereas mean absolute error of y trajectory tracking is 0.23 cm.

From Fig. 4.8(c), it is observed that the capsubot can follow the desired trajectory. However the simulated trajectory is not smooth as the capsubot follows the trajectory in a segment-wise manner. However, this simulation result demonstrates the feasibility of the segment-wise trajectory tracking algorithm for the capsubot-type underactuated robots.

Table 4.1 presents a comparison of the algorithm performance for various segment times. From Fig. 4.9 and Table 4.1, it is observed that the errors in x, y, and steering angle increase if the segment time (T) increases. On the other hand, computation time decreases if the segment time (T) increases.

The uncertainties and disturbances have an impact on the trajectory tracking performance of the algorithm. The parameter uncertainty of the friction is considered which is one of the dominated uncertainties. Table 4.2 provides the tracking errors of the algorithm for various friction uncertainties (0% – $\pm 15\%$). It is seen from Table 4.2 that the errors increase with increasing uncertainty. From Table 4.2, it can be seen that the performance of the algorithm is acceptable as long as the uncertainties remain within -10% to $+10\%$. One way to increase the robustness of the algorithm with respect to the friction uncertainty is to modify the friction model in each segment using the measured data and then use it in the next segment. Other control methods such as adaptive control and robust control can be explored to improve the sensitivity and robustness of the tracking algorithm to model uncertainties and disturbances in the future research.

Table 4.1 Comparison of the algorithm performance for various segment times

T (s)	Maximum absolute tracking error			Mean absolute error			Computation Time (ms)
	x (cm)	y (cm)	ϕ (rad)	x (cm)	y (cm)	ϕ (rad)	
1	0.27	0.41	0.23	0.09	0.13	0.05	67
2	0.44	0.73	0.30	0.16	0.23	0.07	59
4	1.09	1.31	0.46	0.40	0.37	0.11	55

Table 4.2 Comparison of the algorithm performance for various friction changes where the segment time = 1s

Friction variation (%)		Maximum absolute error			Mean absolute error			Relative mean absolute error* (%)		
Translational (μ)	Rotational (μ_r)	x (cm)	y (cm)	ϕ (rad)	x (cm)	y (cm)	ϕ (rad)	x (cm)	y (cm)	ϕ (rad)
0	0	0.27	0.41	0.23	0.09	0.13	0.05	0.48	3.42	4.54
-10 to 10	0	0.42	0.60	0.23	0.15	0.18	0.05	0.79	4.59	4.54
0	-10 to 10	0.96	0.77	0.23	0.33	0.30	0.05	1.68	7.64	4.86
-10 to 10	-10 to 10	0.83	0.94	0.23	0.32	0.38	0.05	1.65	9.63	4.86
-15 to 15	0	0.42	0.73	0.23	0.13	0.26	0.05	0.68	6.60	4.54
0	-15 to 15	1.89	1.19	0.24	0.77	0.56	0.07	3.98	14.2	5.93
-15 to 15	-15 to 15	1.94	1.61	0.24	0.84	0.74	0.07	4.36	18.8	5.93

* Relative mean absolute error = $\left(\frac{\text{mean absolute error}}{\text{mean absolute desired value}} \right) \times 100\%$

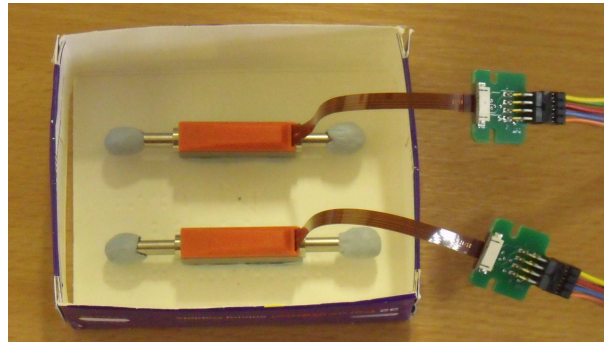
4.4 Experimentation

4.4.1 Experimental Setup

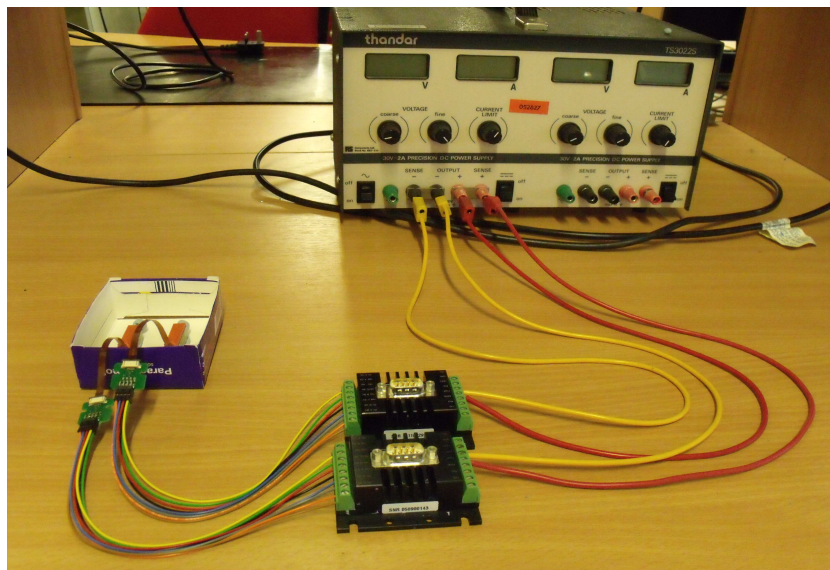
A prototype shown in Fig. 4.10(a) has been developed for the 2D capsbot. Here the cylindrical rods of the two linear DC motors (LM0830-015-01) [181] (Fig. 4.11(A)) are used as the two IMs. The linear DC motors (LMs) are placed and attached using adhesive on a housing made of thin paperboard and thus forms the prototype. Each of the linear DC motor is connected to a motion controller through wires.

The main components of the linear DC motor (LM) (Fig. 4.11(A)) are a housing or motor shell which houses the coil, hall sensors, a PCB (printed circuit board) and a cylindrical rod which is a permanent magnet. The cylindrical rod can move back and forth through the housing. The cylindrical rod can move 7.5mm in each direction from its middle position. In the experiment the cylindrical rod is moved 6 mm in each direction and the rest is left as a clearance. Extra masses (blue tack) are added to the both ends of the cylindrical rod to increase the IM mass to capsbot mass ratio. The term IM (inner mass) will be used for the cylindrical rod with extra mass in the remaining chapter.

The motion of the IM is controlled by a motion controller shown in Fig. 4.11(B). A linear force is applied to the IM when the coil in the motor shell is energised by the motion controller. The linear DC motor can be connected to the motion controller through wires and a connector. The motion controller provides power to the linear DC motor. The hall sensors sense the position of the IM and feed the data to the motion controller to form a



(a) Capsubot prototype



(b) Capsubot prototype with controllers and power supply

Fig. 4.10 Implemented capsubot

closed loop system.

The controller is programmed to move the IM from one location to another location by using a given acceleration and deceleration. The controller by itself calculates the time that it has to use for acceleration and then deceleration to reach the desired location. The controller uses three hall sensors on each linear DC motor to take position feedback of the IM and corrects the input to the IM accordingly to maintain the desired acceleration or deceleration and velocity.

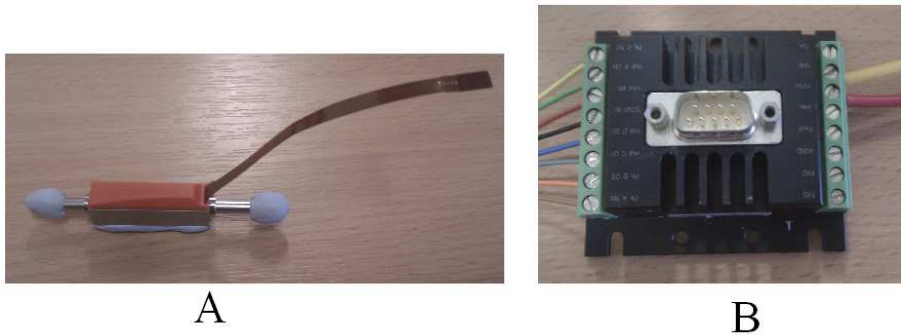


Fig. 4.11 A) Modified linear DC motor (LM) B) Motion controller

The motion controller is driven by 12V - 30V DC which is taken from a DC power supply. The motion controller of the capsbot system is programmed using the Motion Manager software [181] and the program is transferred from the PC to the motion controller by a RS-232 cable and stored in the EEPROM of the motion controller. Then the motion controller can be disconnected from the PC. When the motion controller is powered the stored program is executed and the IMs move accordingly. If the motion controller is connected to the PC, the Motion Manager software logs the data of the linear DC motor.

4.4.2 Control Strategy

Control strategy presented in section 3.2.2 for the 1D capsbot is modified for 2D capsbot and described below:

- *Stage 1:* For a given trajectory of the 2D capsbot, desired trajectories of the IMs are calculated.
- *Stage 2:* For the desired trajectories of the IMs, the control inputs i.e. the forces are calculated (open-loop). The closed-loop control is achieved by correcting the control inputs using the error which is the difference between the measured and the desired trajectories of the IMs.

In the experimentation, stage 2 of the control strategy is evaluated i.e. experimentation of the closed loop control of the IMs are performed. The schematic diagram of the control system for the stage 2 is shown in Fig. 4.12. By implementing this stage the capsuobot can perform linear and rotational motions and by combining these two motions, can perform 2D motion. If the IMs follow a fixed set of accelerations the capsuobot would have a constant average linear or rotational velocity in every cycle. To change the velocity a different set of acceleration has to be chosen.

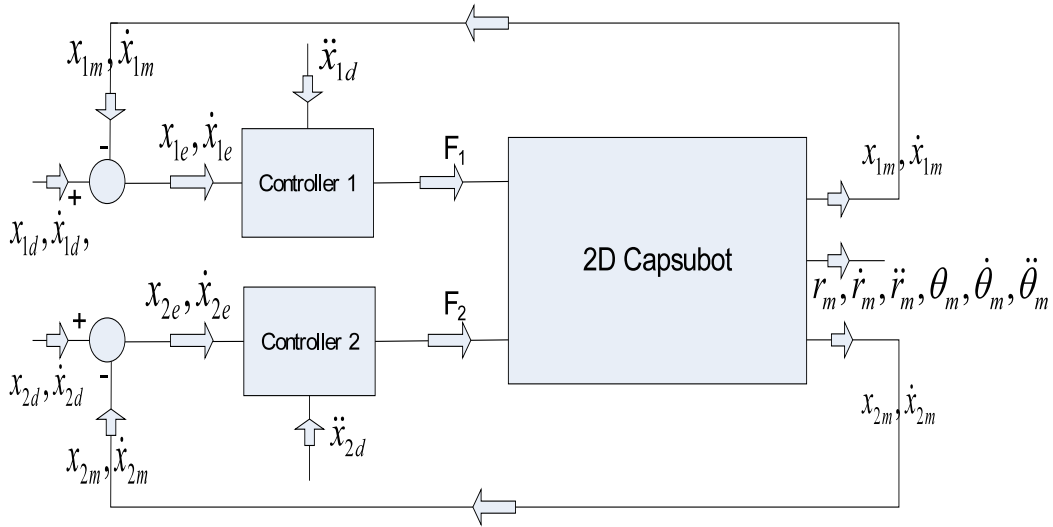


Fig. 4.12 Schematic diagram of stage 2 of the control system

Low-level Control of the IMs

Low-level Control of the IMs are described in the step 3 of the section 4.3.2.

All the simulations in this section are performed using Matlab and Simulink with the help of the control law of (4.47) and motion equations (4.1) to (4.4).

4.4.3 Experimental Results and Analysis

The acceleration of the IM_i is constrained by $\ddot{x}_i \leq \min(\ddot{x}_{imax}, \frac{F_{icmax}}{m_i})$. Here \ddot{x}_{imax} is the $30ms^{-2}$ which is a physical constraint of the IM_i . F_{icmax} is the maximum force that can be applied on the IM_i continuously. On the other hand F_{ipmax} is the maximum force that the IM_i can sustain for a short time. In this experiment, the maximum used acceleration is $20ms^{-2}$. The parameters of the capsuobot are listed in Table 4.3.

Table 4.3 Parameter values of the 2D capsbot

m_1, m_2	μ_1, μ_2	k	w	l	h
6.4gm	0.2	6mm	7cm	8.7cm	3.2cm
g	M	F_{max}	l_1, l_2	μ_r	μ
$9.8ms^{-2}$	42.9gm	1.03N	11.5mm	0.08	0.28
F_{ipmax}	F_{icmax}		Linear Motion	a_{mi1}, a_{mi4}	a_{mi2}, a_{mi3}
2.74N	1.03N			$-20ms^{-2}$	$5ms^{-2}$
Rotational Motion	a_{m11}, a_{m14}	a_{m21}, a_{m24}	a_{m12}, a_{m13}	a_{m22}, a_{m23}	
	$-20ms^{-2}$	$20ms^{-2}$	$5ms^{-2}$	$-5ms^{-2}$	

The data of the *IMs* are obtained from the Motion Manager software and then the curves are plotted using Matlab. To obtain the data for capsbot movements, the motion of the capsbot is recorded using a video camera and then a video analysis software Quintic Biomechanics [182] is used. The software provides the position, velocity and acceleration of the 2D capsbot.

Experimental Results

Fig. 4.13(a) shows the positions of the IM_1 and IM_2 , and Fig. 4.13(b) shows the currents of the LM_1 (linear motor 1) and LM_2 (linear motor 2) for the linear motion. From Fig. 4.13(a), it is observed that the *IMs* move in the range of -6 mm to 6 mm with a cycle period of 0.15s. The shape of the curves for IM_1 and IM_2 positions are similar. From Fig. 4.13(b), it is observed that the shape of the curves for the motor currents are similar in pattern though there is a difference in magnitude between them. The coils inside the linear motors are not fully identical. Thus the current flow through the coils that is required for the two linear motors to generate same motion are also different.

Fig. 4.14(a) shows the positions of the IM_1 and IM_2 , and Fig. 4.14(b) shows the currents of the LM_1 (linear motor 1) and LM_2 (linear motor 2) for the rotational motion. From Fig. 4.14(a), it is seen that the two *IMs* move in the range of -6 mm to 6 mm in the opposite direction with a cycle period of 0.15s. From Fig. 4.14(b), it is observed that the shape of the curves for the motor currents are similar in pattern even though the *IMs* are moving in the opposite direction as the magnitudes of the accelerations for both the *IMs* are same.

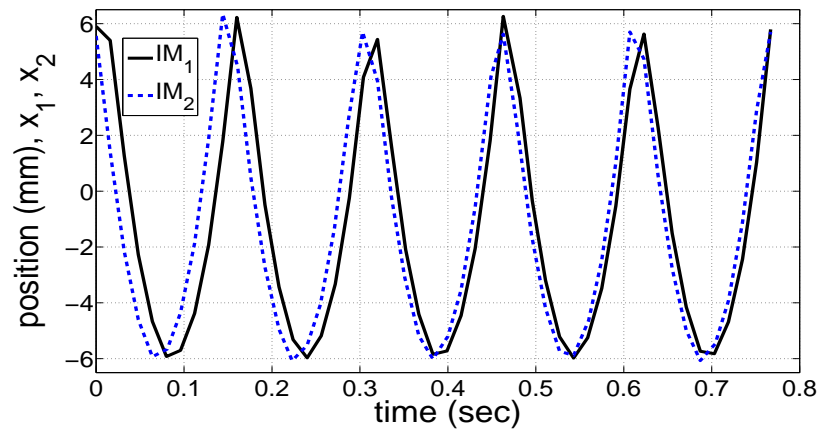
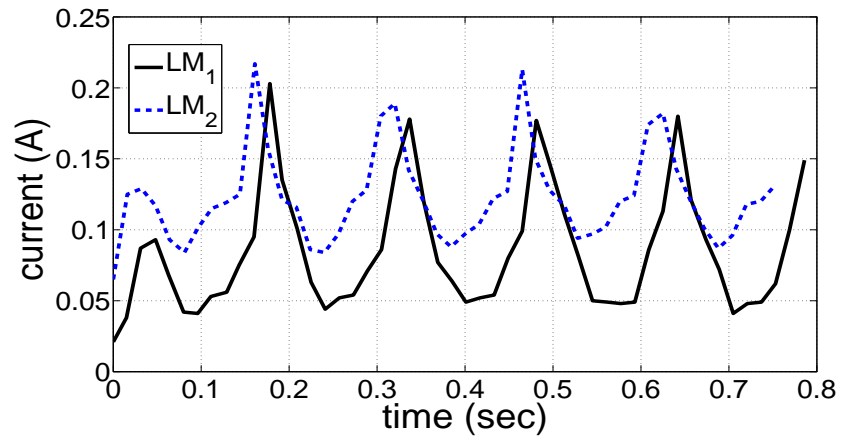
(a) IM_1 and IM_2 positions for the linear motion(b) Currents of the LM_1 (linear motor 1) and LM_2 (linear motor 2) for the linear motion

Fig. 4.13 Experimental results for the linear motion

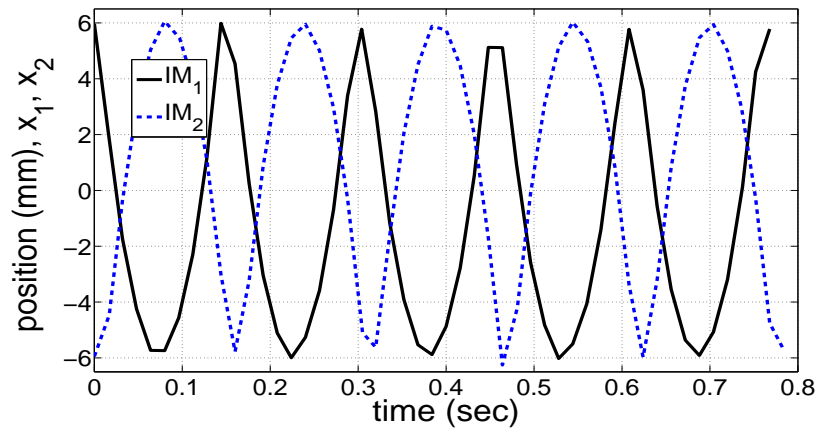
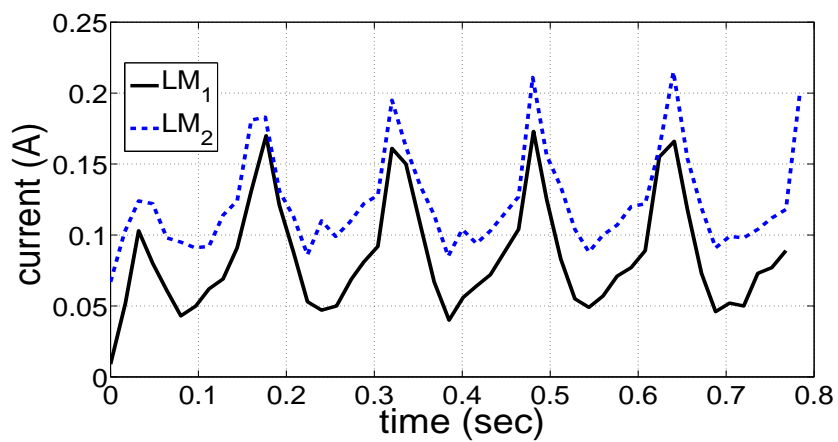
(a) IM_1 and IM_2 positions for the rotational motion(b) Currents of the LM_1 (linear motor 1) and LM_2 (linear motor 2) for the rotational motion

Fig. 4.14 Experimental results for the rotational motion

Comparison with Simulation

The parameters for the simulation of the capsbot is taken from the developed prototype and are listed in Table 4.3.

Figs. 4.15(a)-4.15(d) and 4.16(a)-4.16(d) show the comparison between the experimental and simulation results for the linear motion and rotational motion. For the linear motion both IMs has the same acceleration profile. Thus comparison for only IM_1 is shown in Figs. 4.15(a)-4.15(d). For the rotational motion one of the IMs follows the same acceleration profile as the linear motion and the other IM follows an acceleration profile that is same in magnitude but opposite in direction. Thus for the rotational motion comparison for IM that has the opposite acceleration profile i.e. IM_2 is shown in the Figs. 4.16(a)-4.16(d).

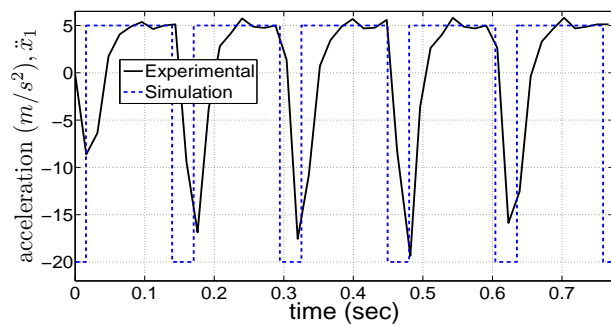
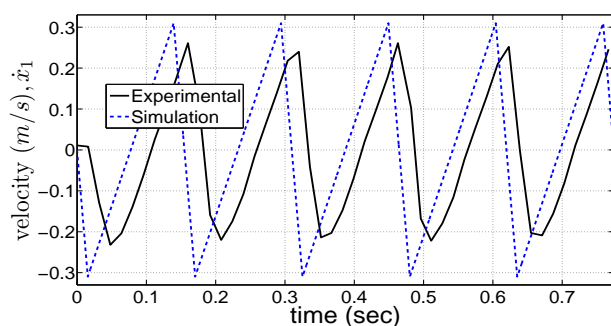
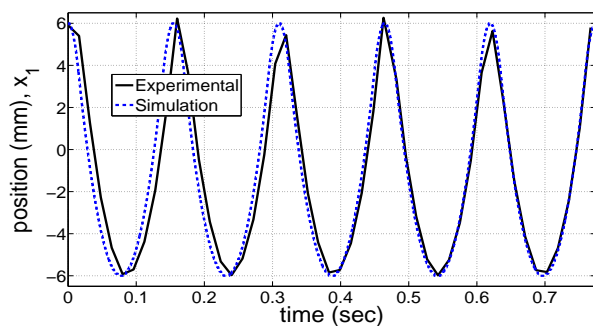
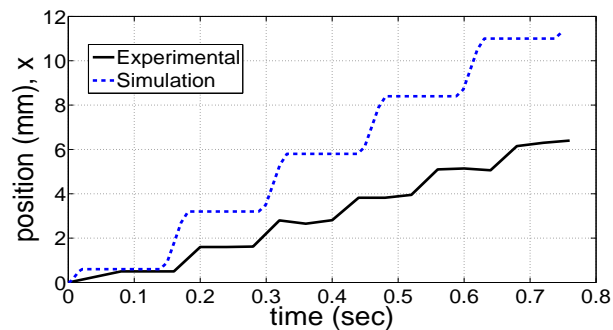
Although there are differences between the experimental and simulation results, their trends are similar. The reasons for the differences could be motor dynamics, sensor dynamics and other disturbances which are not considered in the simulation. These issues could further be investigated in the future research.

From Fig. 4.15(d), it is observed that the capsbot moves with a average velocity of 8.4 mm/s in the linear motion mode. To move the capsbot in the opposite direction, the acceleration of the IMs need to be changed to the opposite direction. From Fig. 4.16(d), it is observed that the capsbot moves with a CCW average angular velocity of 13 degrees/s in the rotational motion. To rotate the capsbot in the opposite direction (CW), the acceleration profiles need to be swapped between the IMs .

4.5 Summary

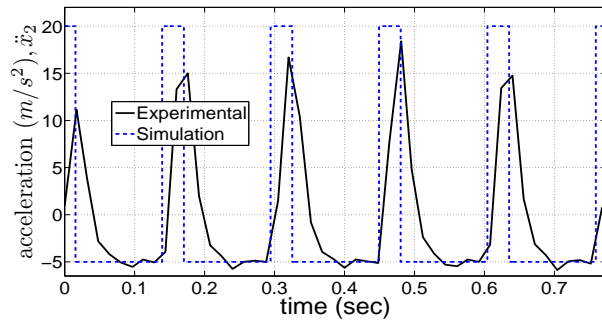
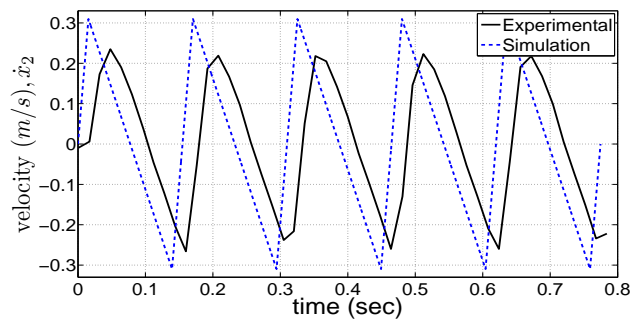
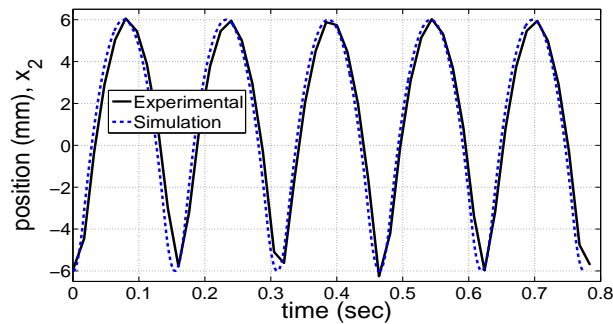
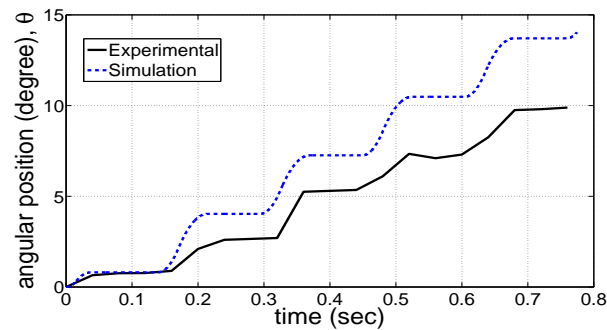
This chapter has presented a 2D capsule robot (capsbot), its modelling, motion generation, theoretical analysis, trajectory tracking control, simulation and experimentation. It has proposed a trajectory tracking control algorithm combining segment-wise and behaviour-based control to solve the trajectory tracking problem of an underactuated 2D capsbot. The basis behaviours have been defined and behaviour sets needed to track the trajectory have been formed. The selection algorithm chooses the appropriate behaviour set to track each segment of the trajectory. The rules have been used to execute individual behaviours of the selected behaviour set. The partial feedback linearization control has been used for the low level IMs ' motion control. The simulation results has shown the feasibility of the proposed trajectory tracking algorithm and the rules.

The simulation results for various segment time has been presented which has shown

(a) Acceleration of the IM_1 for the linear motion(b) Velocity of the IM_1 for the linear motion(c) Position of the IM_1 for the linear motion

(d) Position of the capsobot for the linear motion

Fig. 4.15 Comparison between the experimental and simulation results for the linear motion

(a) Acceleration of the IM_2 for the rotational motion(b) Velocity of the IM_2 for the rotational motion(c) Position of the IM_2 for the rotational motion

(d) Angular position of the the capsbot for the rotational motion

Fig. 4.16 Comparison between the experimental and simulation results for the rotational motion

that the trajectory tracking performance improves as the segment time decreases (e.g. the mean absolute error for the x trajectory tracking decreases to 0.09cm from 0.40cm when the segment time decreases from 4s to 1s). Also the simulation results for various friction uncertainties has been presented which has shown that the trajectory tracking performance declines as the friction uncertainty increases (e.g. the relative mean absolute error in the x trajectory tracking increases from 0.48% to 4.96% when the uncertainty in the linear and rotational frictions increase from 0% to $\pm 15\%$). This chapter has developed a 2D capsuobot prototype and implemented the closed loop control strategy for the IMs in the prototype. It has presented the experimentation of the 2D capsuobot where it has shown the linear and rotational motion generation of the 2D capsuobot.

Chapter 5

Hybrid Robot

5.1 Introduction

This chapter presents a hybrid capsule robot which combines the legless and legged propulsion mechanism. It has four modes of operation namely legless mode, legged mode, hybrid mode and anchoring mode. Fig. 5.1 shows the design of the hybrid robot and Fig. 5.2 shows a partially exploded view of the robot. The robot comprises of a housing closed by two end caps, a pair of linear actuators and two sets of legs. The actuators may be solenoids or linear motors and releasably coupled to the legs via grippers which can be electromagnets. When the grippers are disengaged the actuators provide an inertial drive and the robot works in the legless motion mode. On the other hand when the grippers are engaged, the actuators can extend the legs through the slots in the housing and the robot works in the legged motion mode.

The main contributions of this chapter are to design a novel hybrid robot for the medical applications comprising four modes of operation, to develop an anchoring method and three other methods of moving the robot within the channel of a tubular environment in three motion modes, all by using the same set of actuators and, to model the hybrid robot in all the modes of operation.

5.2 Hybrid Robot Design

Fig. 5.1 shows a perspective view of the hybrid robot. The hybrid robot has two sets of projecting legs. Each set consists of six legs. The robot is formed of an elongate cylindrical housing and a pair of hemispherical end caps being a front end cap and a rear end cap. The

housing of the hybrid robot has a longitudinal axis A-A' and six axis-parallel slots within which two leg-sets are operable to slide in a longitudinal direction. The legs are operable both to retract through the slots so as to be entirely contained within the housing and to project through the slots. The leg-sets are identical.

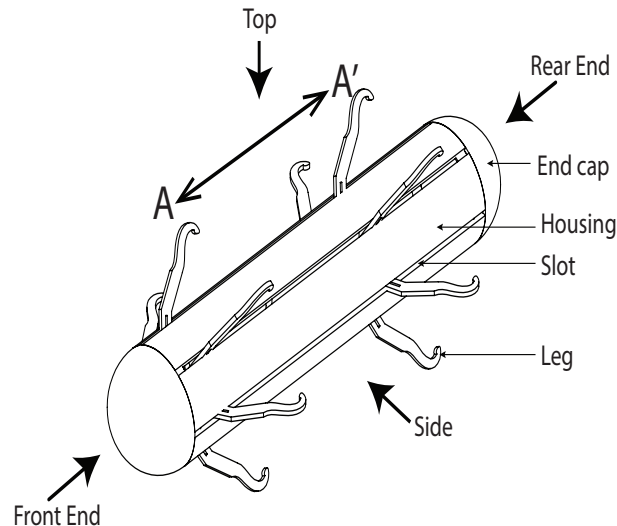


Fig. 5.1 A perspective view of a hybrid robot having two sets of projecting legs.

Fig. 5.2 shows a partially exploded perspective view of the hybrid robot of Fig. 5.1. In Fig. 5.2, it can be seen that the housing is substantially hollow and is arranged to house a pair of actuators. Each actuator is arranged to move its associated rod in the axial direction. Each set of legs is pivotally coupled to a respective nut, and each nut is coupled respectively to an associated gripper mechanism. Each gripper mechanism is arranged to be able to both grip and release an associated rod.

In Fig. 5.2, each gripper is activated and engaged with the corresponding rod so as to mechanically couple the rod to the corresponding set of legs. Thus, the actuation of each actuator that is arranged to move the corresponding rod moves not only the rod, but also the corresponding gripper, nut, and leg-set in a parallel direction to the robot axis.

When the first and/or second set of legs project through the slots and the grippers engage the rods, actuation of the respective actuators causes the sets of legs to slide in the slots. Thereby enables the sets of legs to push and/or pull the hybrid robot relative to matter surrounding the hybrid robot. For example, when the hybrid robot is located in a bodily lumen, the legs may push or pull the hybrid robot along that lumen. In the example of Figs. 5.1 and 5.2, the actuators are linear motors or solenoids such as Quickshaft Linear DC-Servomotor as produced by Faulhaber [181] and the grippers have electromagnets (not

shown) that can be energised to enable the gripper to hold the respective rod.

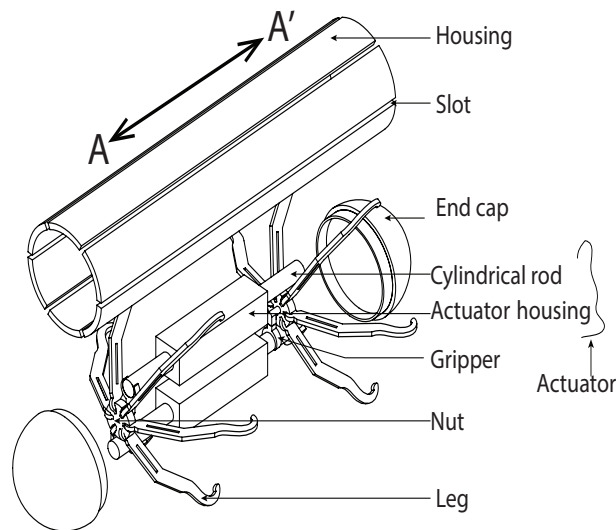


Fig. 5.2 A partially exploded perspective view of the hybrid robot of Fig. 5.1 where the leg-sets are coupled with the cylindrical rods.

Fig. 5.3 shows an end elevation of a gripper, leg, and nut assembly of the hybrid robot. Each gripper has an arcuate gripping face for gripping the corresponding rod, the arcuate surface being profiled to correspond to the profile of the corresponding rod to facilitate gripping thereof.

Fig. 5.4 shows a perspective view of a gripper, leg, and nut assembly of the hybrid robot. In Figs. 5.3 and 5.4, the legs are of unitary structure and each leg is planar. Each leg consists of a first straight elongate portion (a) extending from a pivot region (b) by which it is pivotally secured to the nut. At the distal region of the first portion (a), it extends into a second straight elongate portion (c) that is raked backwardly by an angle of about 40 degrees. The first straight elongate portion has a central elongate slot (d) extending along most of its length to receive a pin. The second straight elongate portion (c) extends into a hooked end region (e). The hooked end region (e) has an inner curved edge region (f) that extends on the backward side of the leg (to the right as seen in Fig. 5.3). The inner curved edge region (f) extends via an outer curved edge region (g) to the outer straight edge (h) of the second straight elongate portion (c). In this example, all the legs are of identical length. The free end of the leg with a hook-like structure is to make sure that the legs movement makes the hybrid robot move in one direction.

In Figs. 5.3 and 5.4, each of the six legs is coupled to the nut via a respective pin (Fig. 5.5) about which that leg is rotatable. It enables the retraction of that leg through the slot so

that the leg lies entirely within the housing. Likewise, each leg is also rotatable by means of the associated constraining pin (Fig. 5.4). It enables that leg to be deployed from the retracted configuration, through the slot, so as to project therefrom. The two leg-sets can be independently actuated using the respective rod without any collision between the rods or leg-sets.

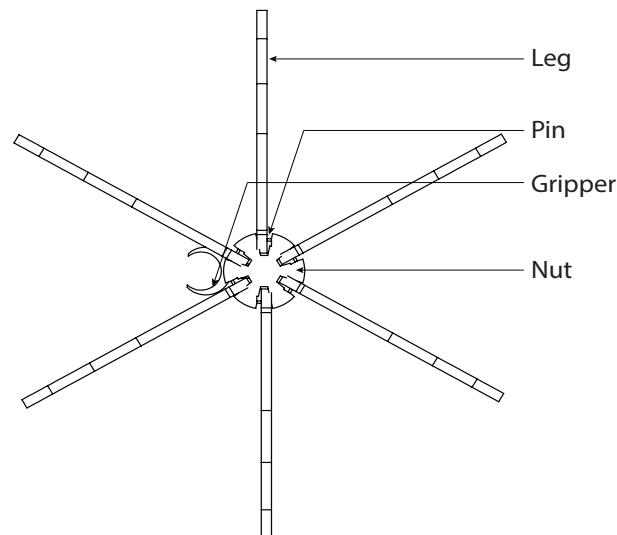


Fig. 5.3 A rear end view of a gripper, leg, and nut assembly of a hybrid robot

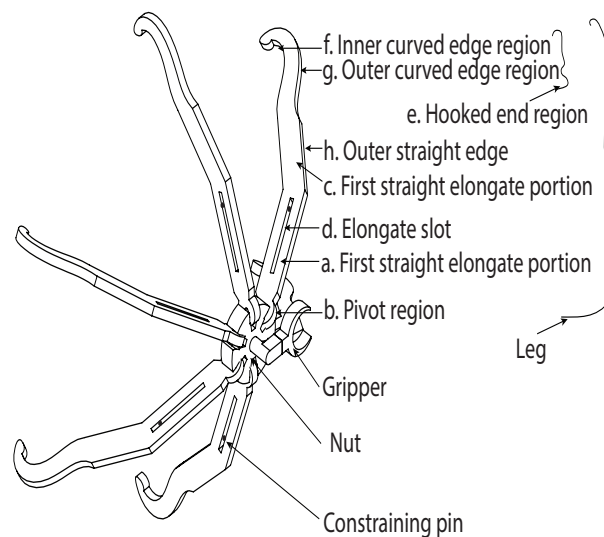


Fig. 5.4 A perspective view of a gripper, leg, and nut assembly of a hybrid robot

Fig. 5.5 shows a close up end view of a nut and the pins for coupling legs to the nut. Figs. 5.6 shows side views of an actuator, a leg and nut assembly of a hybrid robot in two

different positions. Here the gripper is engaged with the rod. The leg is coupled to the nut as explained above with reference to Fig. 5.4. Furthermore, a constraining pin that is fixed relative to the housing is disposed in the slot of the leg. Here one constraining pin per leg is provided. To move between the first (Fig. 5.6(a)) and second (Fig. 5.6(b)) configurations, the actuator is actuated in order to move the rod so as to move the nut away from the actuator. The leg is coupled to the nut by the pin and the leg is free to rotate about the pin subject to the constraints of the constraining pin. The constraining pin is fixedly coupled to the housing and passes through the slot in the leg. The movement of the nut draws the end of the leg that is coupled to the nut inwardly towards the actuator. The constraining pin rides in the slot in the leg so as to cause rotation of the leg in the counter-clockwise direction as illustrated. Thus the combination of the pin, the constraining pin and the slot in the leg act to translate linear motion of the actuator into rotational motion of the leg.

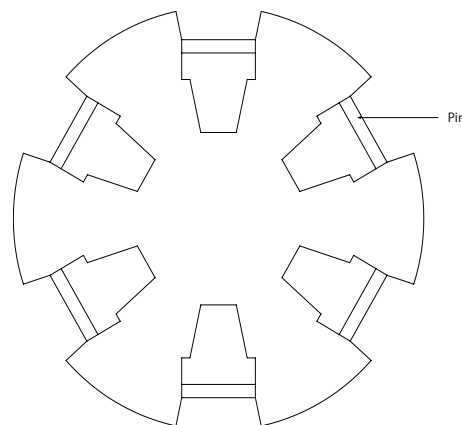


Fig. 5.5 End view of a nut and pin assembly of a hybrid robot

Fig. 5.7 shows a rear end view of the actuator, leg, and nut assembly in which the pin that connects the nut to the leg can clearly be seen. Furthermore, Fig. 5.7 also shows the gripper engaged with the rod to enable a legged mode of operation.

5.3 Working Principle

The hybrid robot has four modes of operation: legless motion mode, legged motion mode, hybrid motion mode and anchoring mode. Same actuators create motion in all the motion modes.

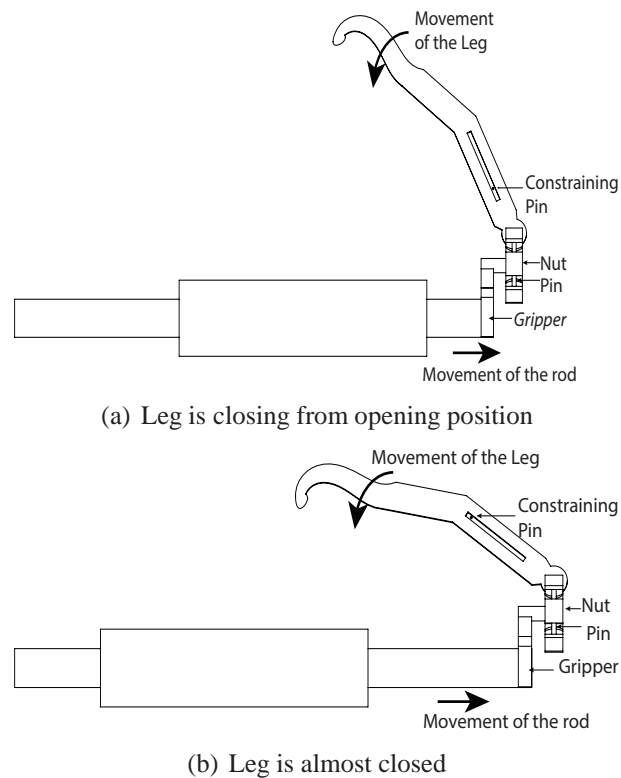


Fig. 5.6 First and second configurations, a side view of a linear actuator, leg, and nut assembly of the hybrid robot when configured for legged motion

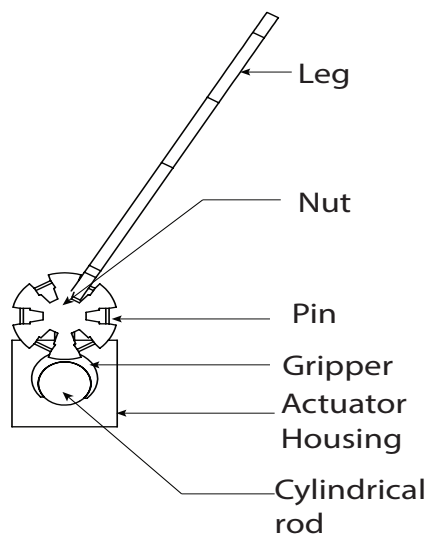


Fig. 5.7 A rear end view of one of the linear actuator, leg, and nut assembly in legged mode

5.3.1 Legless Mode

This is the primary propulsion mode. In this mode the cylindrical rods act as inertial masses (IMs) to cause propulsion. The leg-sets are disengaged from the cylindrical rods and retracted inside the robot body. Thus the movement of the cylindrical rod does not cause any movement of the leg-sets. By controlling the acceleration of the cylindrical rods, the robot can i) move forward or backward and ii) rotate clockwise or counter clockwise. In legless mode the hybrid robot can be compared with the 2D capsbot described in chapter 4. Thus the working principle in legless mode is same as described in 4.2.2. The mass of the leg-nut-gripper assemblies are added to the mass of the robot.

5.3.2 Legged Mode

This is secondary propulsion mode. This mode is only activated when the robot can not pass some path using legless mode. In legged mode (Fig. 5.8) the grippers are engaged with the cylindrical rod and thus the leg-sets are connected with cylindrical rods through the gripper-nut assemblies. When the cylindrical rod moves linearly, the corresponding gripper-nut assembly moves linearly with it. As the constraining pin is fixed on the robot cover, thus the legs rotate and slide with respect to the constraining pins. The repeated leg movement can be utilized to move the robot forward. The closing and opening can be controlled in the following control sequences so that the robot only moves in the forward direction.

- Cycle 1: At the beginning of the legged locomotion, both the leg sets are closed.
 - Step 1: In this step the rear leg-set starts opening. During this step the robot experiences a small backward force and thus moves backward.
 - Step 2: The front leg-set starts opening. The robot experiences a small backward force. But as the hook of the front leg set locks the robot and opposes any backward movement, the robot remains stationary.
 - Step 3: The front leg set starts closing. The robot experiences a forward force from the reaction from the surrounding and the robot moves forward. Because of the hook-like structure, the opened rear leg set creates very low resistance in the forward movement of the robot.
- Repeated cycle: By repeating steps 2 and 3 the robot moves forward.

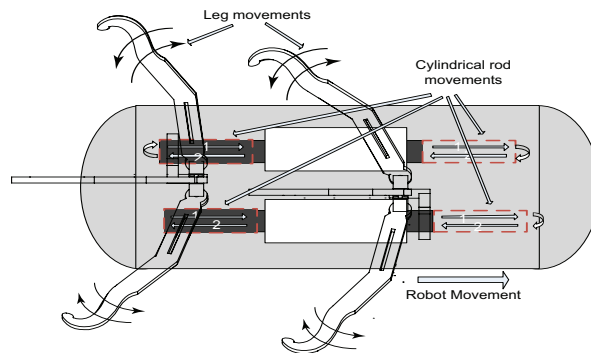


Fig. 5.8 Leg and cylindrical rod movements in Legged mode

5.3.3 Hybrid Mode

In this mode one of the leg-set is kept always open and other leg-set is disengaged from the cylindrical rod and retracted inside the robot body. The free cylindrical rod is operated in legless mode. Thus in hybrid motion mode one of the actuator is used to ensure that one leg-set is open to make path for the robot. The other actuator works in legless motion mode to provide force to move the robot forward. It helps to open an occlusion or to widen a narrowing.

The hybrid motion can be divided into two types: 1) Hybrid translation-anti-clockwise rotation (Fig. 5.9(a)) and 2) Hybrid translation-clockwise rotation (Fig. 5.9(b)).

Hybrid translation-anti-clockwise rotation

The first leg-set is kept open and second cylindrical rod (inertial mass/ inner mass - IM_2) follows the acceleration profile shown in Fig. 4.2(a) in chapter 4. The reaction force urges the robot to move forward. Moreover as the reaction force does not go through the mass centre of the robot, it creates a torque with respect to the mass centre of the robot. The torque urges the robot to rotate counter-clockwise.

Hybrid translation-clockwise rotation

The second leg-set is kept open and first cylindrical rod (inertial mass/ inner mass - IM_1) follows the acceleration profile shown in Fig. 4.2(a) in chapter 4. The reaction force urges the robot to move forward. Moreover as the reaction force does not go through the mass centre of the robot, it creates a torque which urges the robot to rotate clockwise.

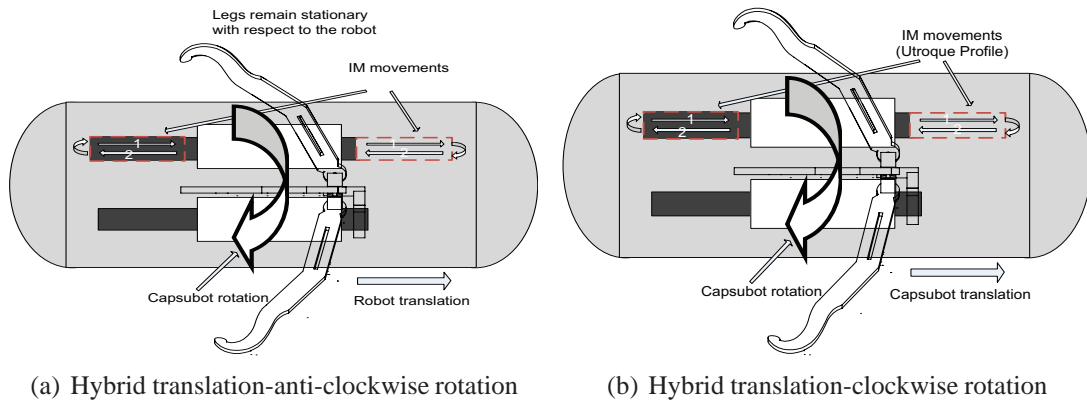


Fig. 5.9 IM movements in hybrid mode

5.3.4 Anchoring Mode

In anchoring mode (Fig. 5.10) the robot stays in a certain position to do a certain task e.g. delivering treatments and taking video for longer time for better observation. Both the actuators are used to keep both the leg-sets open. The actuators oppose any movement tendency of the legs by any external force e.g. visceral peristalsis. Thus the features of the anchoring mode are: i) the robot does not move and ii) both of the leg-sets are opened to anchor the robot in certain position to do a certain task (take video and deliver treatment).

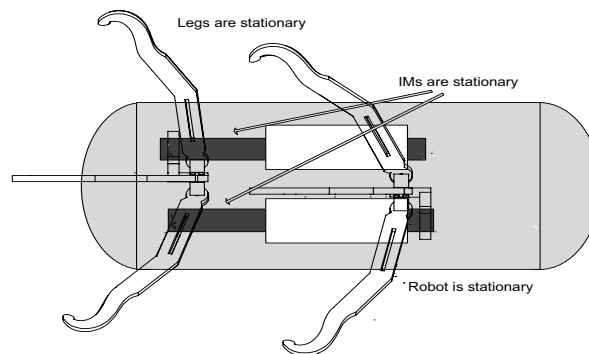


Fig. 5.10 Hybrid robot in anchoring mode

5.4 Modelling of the Hybrid Robot

5.4.1 Modelling of the Legless Mode

In legless mode the hybrid robot can be compared with the 2D capsuobot described in chapter 4. Thus the working principle and modelling in legless mode is same as described in chapter 4. The mass of the leg-nut-gripper assemblies are added to the mass of the robot.

5.4.2 Modelling of the Legged Mode

By controlling the movements of the cylindrical rods the leg-sets can be opened and closed. The leg has good contact with colon while the opening of the leg is $140^\circ - 110^\circ$ [48]. Thus the working angle for the leg is kept $140^\circ - 110^\circ$. The closing of the leg is defined as moving the leg-set from leg-opening 140° to 110° as shown in Figs. 5.12 and 5.13. The opening of the leg is defined as moving the leg-set from leg-opening 110° to 140° as shown in Fig. 5.14. In one cycle the leg performs closing and opening i.e. moves from 140° to 110° and then returns to 140° from 110° . To help the reader to follow modelling of the legged mode a notation list is provided in Table 5.1.

Table 5.1 Description of the notation used in this chapter

Notation	Description
F_{act}	Force on the cylindrical rod by the Motor housing
F_{leg}	Force on the colon wall by the leg-tip
l_1	Length of the first link of the leg
l_2	Length of the second link of the leg
θ	Angle between the first link and the robot body
θ_M	Maximum leg-opening, 140°
θ_m	Minimum leg-opening, 110°
δ	Angle between the first and second links = -15°
p'	Straight line distance between the constraining pins (on the cover and on the nut)
q'	Straight line distance between the constraining pin on the cover and leg-tip (contact point with the surrounding)
$x_{leg-tip}$	Horizontal position of the leg-tip
$y_{leg-tip}$	Vertical position of the leg-tip
(x_F, y_F)	Position of the pin on the robot cover, F
(x_m, y_m)	Position of the cylindrical rod (inertial mass)
(x_M, y_M)	Position of the robot

When the leg-set is closing from 140° to 110° and leg-tips have no contact with the surrounding

Fig. 5.12 shows the scenario where the leg-set is closing from 140° to 110° and leg-tips have no contact with the surrounding. Here the cylindrical rod moves towards left from A' to A'' position, θ changes from 140° to 110°, the leg moves from red dotted to blue solid position and the leg-tip moves from C' to C'' position. The position of leg-tip for Fig. 5.12:

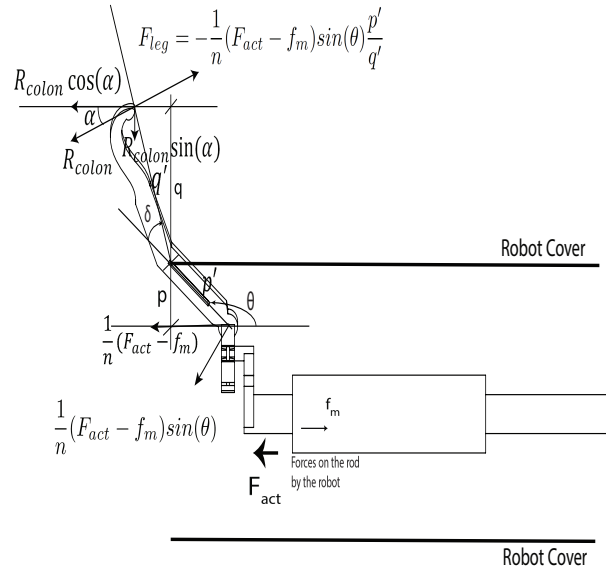


Fig. 5.11 Leg-opening 140 degrees - the robot is stationary

$$x_{leg-tip} = l_1 \cos(\theta) + l_2 \cos(\theta + \delta) + x_m, \quad (5.1)$$

$$y_{leg-tip} = l_1 \sin(\theta) + l_2 \sin(\theta + \delta) + y_m, \quad (5.2)$$

where $\delta = -15^\circ$, $l_1 = 4mm$ and $l_2 = 8mm$. These are constants for a specific leg.

$$\theta(x_m) = \tan^{-1} \frac{l_1 \sin(\theta_M)}{l_1 \cos(\theta_M) - x_m}, \quad (5.3)$$

$$x_M = 0. \quad (5.4)$$

Thus:

- From (5.3) and (5.1) if $\theta = \theta_M$ then $x_m = 0$ and $x_{leg-tip} = -7.6528mm$.
- Similarly from (5.3) and (5.1) if $\theta = \theta_m$ then $x_m = -2.1284mm$ and $x_{leg-tip} = -4.1937mm$.

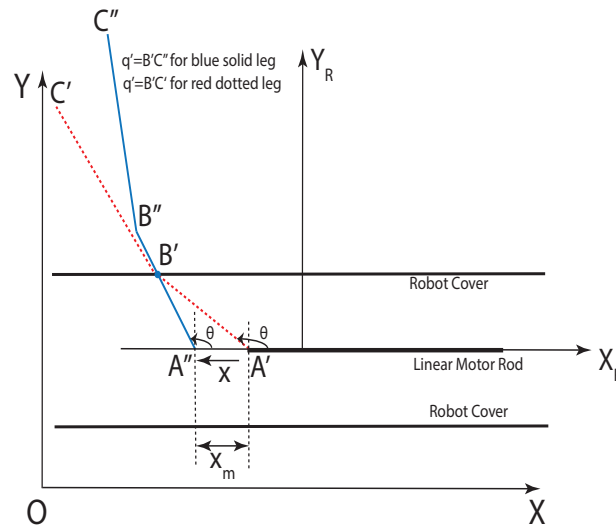


Fig. 5.12 Leg closing: the leg (red dotted and blue solid) in two positions (140° and 110°) when the leg is not facing any obstacle - the robot does not move

When the leg-set is closing from 140° to 110° and leg-tips have contacts with tubular surrounding e.g. colon wall

Fig. 5.11 shows the force balance where the cylindrical rod tries to move left. F_{act} force is applied by the housing of the linear motor on the rod. The rod and the robot are stationary. Friction f_m opposes the movement tendency. The rod applies " $-F_{act}$ " reaction force on the housing of the linear motor which is attached to the outer cover of the robot. The rod applies F_{leg} force on the leg-tip of each leg by lever action - the pin on slot (on the robot cover) of each leg works as a crum and forms a lever. The reaction by the colon wall on the leg-tip is $R_{colon} = -F_{leg}$. The rod and the robot are still stationary. The force on the leg-tip is:

$$F_{leg} = -\frac{1}{n}(F_{act} - f_m) \sin(\theta) \frac{p'}{q'}, \quad (5.5)$$

where $R_{colon} = -F_{leg}$, $f_m = \sin(\dot{x}_m) \mu_m m g$, $p' = \frac{p}{\sin(\theta)}$,
 $q' = \sqrt{(y_{leg-tip} - y_F)^2 + (x_{leg-tip} - x_F)^2}$.

The forces considered in (5.5) are perpendicular to the lever arm. The force $\frac{1}{n}(F_{act} - f_m)$ which is applied to the leg is not perpendicular to the lever arm. Thus the component

of $\frac{1}{n}(F_{act} - f_m)$ force is taken along the perpendicular direction of the lever arm which is $\frac{1}{n}(F_{act} - f_m) \sin(\theta)$. Thus the force on the leg-tip which is perpendicular to other lever arm is $-\frac{1}{n}(F_{act} - f_m) \sin(\theta) \frac{p'}{q'}$. Where p' is straight line distance between the constraining pins (on the cover and on the nut) and q' is the straight line distance between the constraining pin on the cover and leg-tip.

When all parts and the robot are stationary, there is a force balance. As two forces are acting on the leg horizontally (towards left in Fig. 5.11): one by the rod $\frac{1}{n}(F_{act} - f_m)$ and another by the colon wall $R_{colon} \cos(\alpha)$ and, the leg is stationary, thus the pin (cram) of lever must apply $\frac{1}{n}(F_{act} - f_m) + R_{colon} \cos(\alpha)$ (towards right in Fig. 5.11) force on each leg. Each leg applies $\frac{1}{n}(F_{act} - f_m) + R_{colon} \cos(\alpha)$ reaction force (towards left in Fig. 5.11) on the pin (cram). The pin on each slot of the leg are fixed to the robot cover, thus the force by all the legs $(F_{act} - f_m) + nR_{colon} \cos(\alpha)$ are applied to the robot cover and tries to move the robot. Again the cylindrical rod applies $F_{act} - f_m$ force (towards right in Fig. 5.11) on the robot. Thus the total force acting on the robot is $(F_{act} - f_m) + nR_{colon} \cos(\alpha) - (F_{act} - f_m) = nR_{colon} \cos(\alpha)$ (towards left in Fig. 5.11). Initially the robot does not move as $nR_{colon} \cos(\alpha)$ is small. Also $\sum R_{colon} \sin(\alpha) = 0$ as there are three pairs of legs and the legs in each pair cancels each others vertical component of reaction forces.

Now if F_{act} on the rod is increased, it tries to move the leg; but the leg cannot move as the colon wall resists the movement. From (5.5) it is observed that if F_{act} increases, then $|nR_{colon} \cos(\alpha)|$ also increases. Thus the robot starts moving when this force exceeds the friction of the robot ($|f_M| = |\mu_M F_{NM}|$, where F_{NM} is the normal force). To maintain this $|nR_{colon} \cos(\alpha)|$ force, the leg-tip needs to have contact with the colon-wall all the time. So the rod needs to move slightly faster to maintain the reaction force; thus the rod has a relative velocity with respect to the robot.

To fulfill the above mentioned constraints: the robot moves left, the rod moves left which causes leg-tip to stay in the same horizontal position but leg-tip vertical position changes. Thus in one closing cycle the rod moves left so that the angle θ goes from 140° to 110° and to keep the leg-tip in the same horizontal position the distance travelled by the robot in one cycle is (from Fig. 5.13):

$$x_M = (l_1 \cos(\theta) + l_2 \cos(\theta + \delta) + x_m) \text{ for } \theta_M - (l_1 \cos(\theta) + l_2 \cos(\theta + \delta) + x_m) \text{ for } \theta_m. \quad (5.6)$$

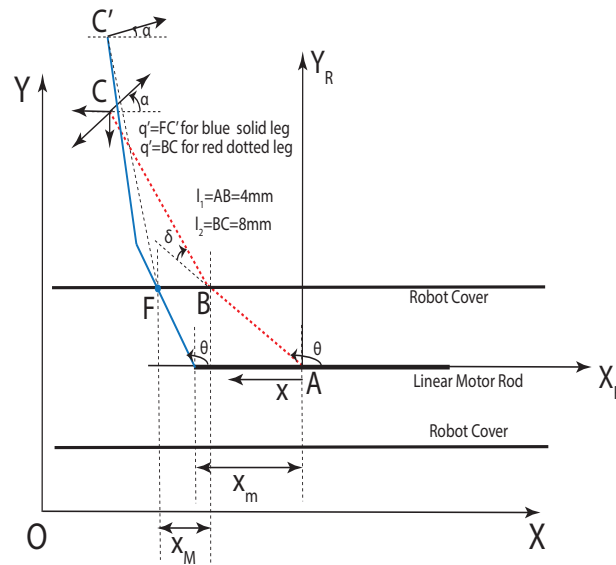


Fig. 5.13 Leg closing: the leg (red dotted and blue solid) in two positions (140° and 110°) if the robot moves

When both the rod and robot moves, $\theta(x_m, x_M)$ is:

$$\theta(x_m, x_M) = \tan^{-1} \frac{l_1 \sin(\theta_M)}{l_1 \cos(\theta_M) - x_m + x_M}, \quad (5.7)$$

and the leg-tip position is:

$$x_{leg-tip} = l_1 \cos(\theta) + l_2 \cos(\theta + \delta) + x_m, \quad (5.8)$$

$$y_{leg-tip} = l_1 \sin(\theta) + l_2 \sin(\theta + \delta) + y_m. \quad (5.9)$$

Thus:

- From (5.7) and (5.8) if $x_{leg-tip} = -7.65mm$ and $\theta = 140^\circ$ then $x_m = 0$ and $x_M = 0$.
- From (5.7) and (5.8) if $x_{leg-tip} = -7.65mm$ and $\theta = 110^\circ$ then $x_m = -5.59$ and $x_M = -3.46$.

Thus in one closing cycle the rod moves from $x_m = 0$ position to $x_m = -5.59mm$ position; the angle changes from $\theta = 140^\circ$ to $\theta = 110^\circ$; the robot moves from $x_M = 0$ to $x_M = -3.46mm$. However the horizontal position of the leg-tip remains unchanged i.e. $x_{leg-tip} = -7.65mm$.

The dynamic equations are:

$$\begin{aligned} nR_{colon} \cos(\alpha) &= f_M + M\ddot{x}_M, \\ R_{colon} &= \frac{1}{n}(F_{act} - f_m - m\ddot{x}_m) \sin(\theta) \frac{p'}{q'}, \end{aligned} \quad (5.10)$$

where

$$\begin{aligned} p' &= \frac{P}{\sin(\theta)}, \quad q' = \sqrt{(y_{leg-tip} - y_F)^2 + (x_{leg-tip} - x_F)^2}, \\ \theta(x_m, x_M) &= \tan^{-1} \frac{l_1 \sin(\theta_M)}{l_1 \cos(\theta_M) - x_m + x_M}, \\ y_F = p &= l_1 \sin(\theta_M), \quad x_F = x_m + \frac{P}{\tan(\theta)}, \\ x_{leg-tip} &= l_1 \cos(\theta) + l_2 \cos(\theta + \delta) + x_m, \\ \alpha &= \tan^{-1} \frac{y_{leg-tip} - y_F}{x_{leg-tip} - x_F} - \frac{\pi}{2}, \\ x_m &= x_{leg-tip} - l_1 \cos(\theta) - l_2 \cos(\theta + \delta), \\ x_M &= \frac{l_1 \sin(\theta_M)}{\tan(\theta)} - l_1 \cos(\theta_M) + x_m, \\ f_M &= \text{sgn}(\dot{x}_M) \mu_M F_{NM}, \quad F_{NM} = Mg. \end{aligned}$$

Modifying (5.10), finally the dynamic equation is:

$$M\ddot{x}_M = (F_{act} - f_m - m\ddot{x}_m) \cos(\alpha) \frac{p}{q'} - f_M. \quad (5.11)$$

When the leg-set is opening from 110° to 140°

At the end of closing cycle the robot is stationary, the front leg-set is partially open (110°) and the rear leg-set is fully open (140°). The rear leg-set maintains its open position. The rod associated with the front leg-set tries to move in. Here the forces are same as forces during leg closing but opposite in direction. Unlike leg closing, here the leg faces little resistance while trying to move and, thus the reaction force is also small. Thus the force $nR_{colon} \cos(\alpha)$ is not enough to move the robot. So the robot remains stationary when the leg opens from 110° to 140° (Fig. 5.14).

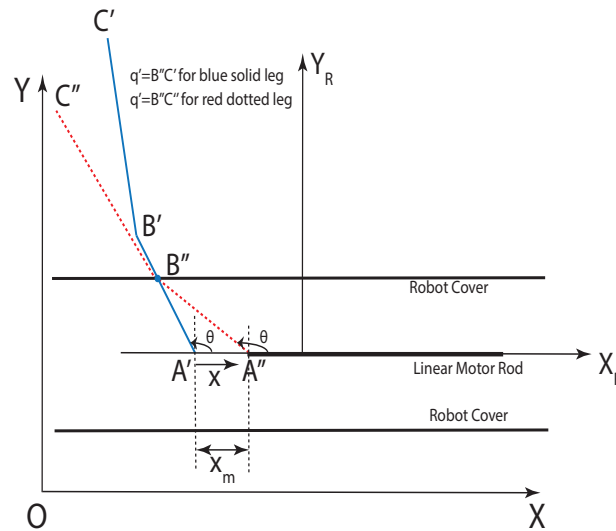


Fig. 5.14 Leg opening: the leg (blue solid and red dotted) in two positions (110° and 140°) - the robot remains stationary

Repeated cycle

Thus to keep the robot moving the rear leg-set is kept open and, the front leg-set opens and closes repetitively. The robot moves during the closing cycle and remains stationary during the opening cycle.

5.4.3 Modelling of the Hybrid Mode

In this mode the hybrid robot performs a hybrid translation-rotation because of the reaction force from the IM that moves using the acceleration profile shown in 4.2(a) in chapter 4. As the robot moves, the legs experience an external force. Thus the actuator that is used to keep the leg-set open, has to apply a force to balance the external force so that the leg-set remains open. Let us consider the external force on each leg is F_{ext} and the limiting friction of each leg is f_{leg} . Fig. 5.15 shows the acting forces for one leg in hybrid mode. From Fig. 5.15 the required force for the actuator is:

$$F_{act} = -n \cos \alpha \sin \theta (F_{ext} - f_{leg}) \frac{q'}{p'} + f_m. \quad (5.12)$$

The dynamic model of the robot and the IM which works in legless mode is as follows (from chapter 4):

$$F_{m_i} - f_{m_i} = m_i \ddot{x}_{m_i} \quad i = 1, 2, \quad (5.13)$$

$$M \ddot{x} = (-F_{m_i} + f_{m_i} - f_M) \cos(\phi) \quad i = 1, 2, \quad (5.14)$$

$$M \ddot{y} = (-F_{m_i} + f_{m_i} - f_M) \sin(\phi) \quad i = 1, 2, \quad (5.15)$$

$$I \ddot{\phi} = (-1)^i [(-F_{m_i} + f_{m_i}) d_i - M_f] \quad i = 1, 2, \quad (5.16)$$

where x , y and ϕ are generalised coordinates of the robot with respect to fixed frame $O(X_O, Y_O)$; m_i and M are the IM_i mass and robot mass respectively; d_i is the perpendicular distance of the direction of forces F_{m_i} and f_{m_i} and, the axis of rotation; f_M is the friction force on the capsbot; M_f is the frictional moment of the capsbot about z-axis through the mass centre of the capsbot.

Model for two hybrid motions are provided below.

Hybrid translation-anti-clockwise rotation

Here the first cylindrical rod is used to keep open the first leg-set. The cylindrical rod will oppose any radial movement of the leg-sets. However the robot as a whole can move forward. The extended leg will increase the friction. Here IM_2 (second cylindrical rod) is dis-engaged from the leg-set to perform legless motion. Thus (5.13)-(5.16) become:

$$F_{m_2} - f_{m_2} = m_2 \ddot{x}_2, \quad (5.17)$$

$$M \ddot{x} = -F_{m_2} - (-f_{m_2}) - f_M, \quad (5.18)$$

$$I \ddot{\phi} = (-F_{m_2} + f_{m_2}) d_2 - M_f. \quad (5.19)$$

Thus the robot moves forward and rotates anti-clockwise.

Hybrid translation-clockwise rotation

Here the second cylindrical rod is used to keep open the second leg-set. Here IM_1 (first cylindrical rod) is dis-engaged from the leg-set to perform legless motion. Thus (5.13)-

(5.16) become:

$$F_{m_1} - f_{m_1} = m_1 \ddot{x}_1, \quad (5.20)$$

$$M \ddot{x} = -F_{m_1} - (-f_{m_1}) - f_M, \quad (5.21)$$

$$I \ddot{\phi} = -(-F_{m_1} + f_{m_1}) d_1 + M_f. \quad (5.22)$$

5.4.4 Modelling of the Anchoring Mode

In this mode each of the leg-set is engaged with the corresponding cylindrical rod by the gripper and the leg-set is kept wide open all the time.

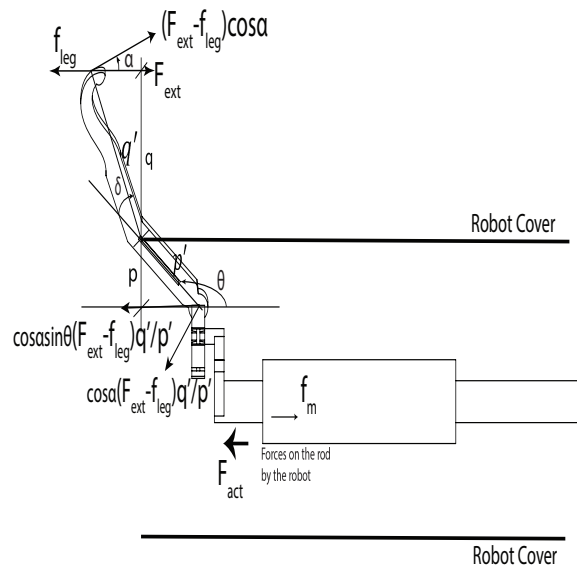


Fig. 5.15 Acting forces for one leg when F_{ext} exceeds the limiting value of f_{leg} (applicable to both hybrid and anchoring mode)

If any external force (e.g. peristalsis) try to move the robot, the friction of the legs will stop the robot from moving. The external force is assumed to be acting uniformly on all the legs. If F_{ext} is working on each leg and f_{leg} is the limiting friction of each leg then:

$$F_{ext} \leq f_{leg}. \quad (5.23)$$

If the external force exceeds the limiting friction force of the leg, the actuators need to provide force to stop the robot from moving. Fig. 5.15 shows the acting forces for one leg in anchoring mode. From Fig. 5.15, the required actuator force:

$$F_{act} = -ncos\alpha sin\theta(F_{ext} - f_{leg})\frac{q'}{p'} + f_m. \quad (5.24)$$

5.5 Simulation Results and Discussion

Simulation is performed in Matlab/Simulink environment and the data in Table 5.2 is used. Some of these parameters are design parameters such as n , δ , l_1 , l_2 , m , M and μ_m . They are chosen by the designer. Some other parameters are operating parameters such as θ_m and θ_M . They are chosen as 110° and 140° as the leg has good contact with colon while the opening of the leg is $140^\circ - 110^\circ$ [48]. The equations developed in modelling section are used for the simulation. The Ode45 (Dormand-Prince) solver is used with a variable step.

Table 5.2 Parameters for the hybrid robot

n	g	δ	l_1	l_2	m
6	9.8	-15°	4mm	8mm	25gm
M	μ_m	μ_M	θ_m	θ_M	
100gm	0.2	0.3	110°	140°	

5.5.1 Legless Mode

The simulation for legless motion is similar to that of chapter 4.

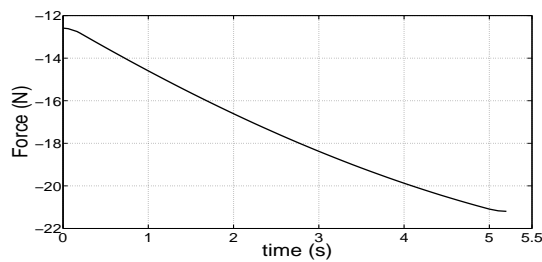
5.5.2 Legged Mode

The simulation results for legged motion for one closing cycle are shown in Fig. 5.16. Fig. 5.16(a) shows the force on the IM required to generate robot movement in legged mode while the legs are closing. Fig. 5.16(a) shows that the force required to generate the motion is $-12.5N$ to $-21N$. Various parameters of the robot design can be modified to improve the force requirement. One of the scope of improvement is the ratio q'/p (Fig. 5.11). It can be done by increasing the length of the leg from constraining pin to the leg-tip. By decreasing this ratio, the force requirement can be decreased.

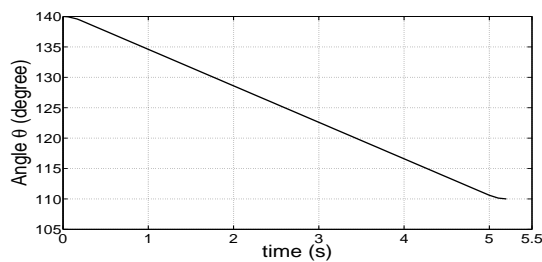
Fig. 5.16(b) shows the angle of the leg with the robot body while the robot and the IM is moving. The angle decreases from 140° to 110° . From Figs. 5.16(a) and 5.16(b) it can be

concluded that as the leg closes the required force increases and reaches to maximum when the leg-closing is 110° .

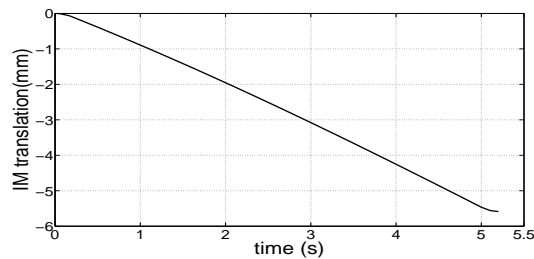
Figs. 5.16(c) and 5.16(d) show the IM and the robot translation respectively. It can be seen from the figures that the IM travels -5.5 mm whereas the robot travels -3.4 mm in one closing cycle. Thus the IM moves faster than the robot. This is necessary to maintain a contact between the the leg-tip and the surrounding environment.



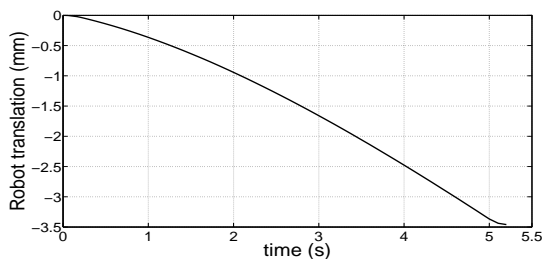
(a) Force applied on the IM



(b) Angle of the leg with the robot body in legged mode



(c) IM translation in legged mode



(d) Robot translation in legged mode

Fig. 5.16 Legged movement in one closing cycle -

5.5.3 Hybrid Mode

Hybrid translation-clockwise rotation

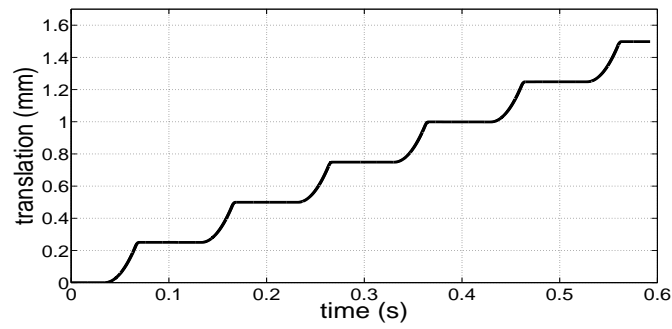
The simulation results for hybrid translation-clockwise rotation are shown in Fig. 5.17. Figs. 5.17(a) and 5.17(b) show the translation and rotation of the hybrid robot. The figures show the step-wise movement of the robot i.e. the robot moves for part of the each cycle and remains stationary for the rest of the cycle. It is because of the acceleration profile which the IM followed. Fig. 5.17(c) shows the hybrid translation-clockwise rotation in x-y plane. It is also seen that the rotation performed by the robot is very small and it is less than -2° in one cycle. Thus in Fig. 5.17(c) the translation in along y axis is very minimal compare to the translation along x axis.

Hybrid translation-anti-clockwise rotation

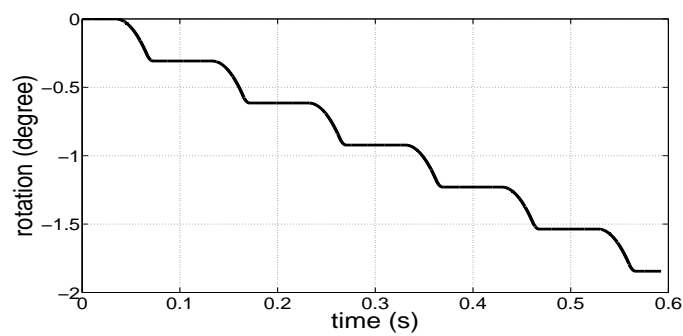
The simulation results for hybrid translation-anti-clockwise rotation are shown in Fig. 5.17. The figures are similar to that of 5.17 except that the robot rotates anti-clockwise. Like the Fig. 5.17(c), in Fig. 5.18(c) the robot translates smaller distance along the y axis compare to along the x axis.

5.6 Summary

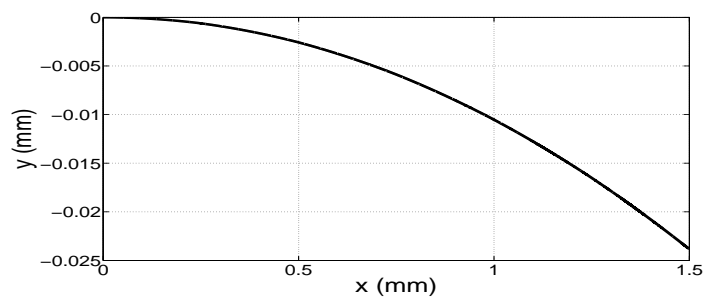
This chapter has presented the detailed design, working principle, modelling and simulation of a novel hybrid capsule robot. The designed hybrid robot is an effective solution for in-vivo active locomotion for the diagnostic purposes. The design incorporates four operating modes in a single unit. Moreover, the use of the same actuators for all four operating modes reduces complexity. The most appropriate operating mode can be selected based on the situation to minimize the chance to cause harm to internal tissues. The chapter has presented the detailed design of the hybrid robot where it has described all the components of the robot and their usage in executing the modes of operation. It has also analyzed the working principles of the hybrid robot in all the modes of operation. This chapter has presented the modelling of the robot for all the operating modes considering all the internal and external forces while the robot is within a tuber environment. The simulation results has shown the feasibility of the hybrid robot design and propulsion principles. There is no existing robot design in the literature which incorporates all the functionalities of the designed hybrid robot in one unit.



(a) Forward translation

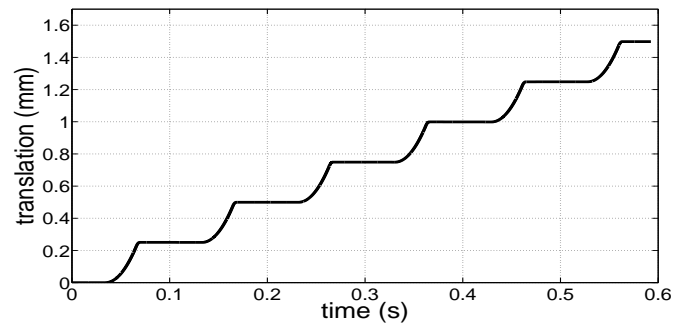


(b) Clockwise rotation

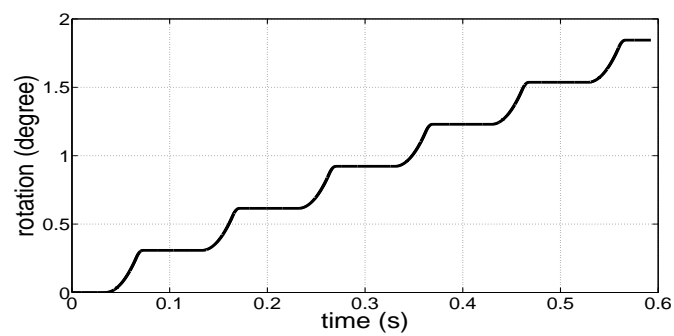


(c) Hybrid translation-clockwise rotation

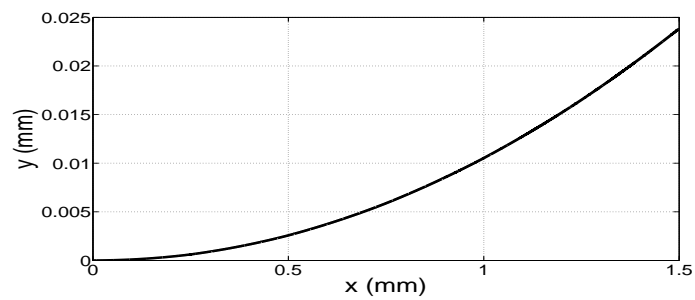
Fig. 5.17 Simulation results for hybrid translation-clockwise rotation



(a) Forward translation



(b) Anticlockwise rotation



(c) Hybrid translation-anti-clockwise rotation

Fig. 5.18 Simulation results for hybrid translation-anti-clockwise rotation

Chapter 6

Conclusions and Future Works

6.1 Conclusions

This research has performed the design, modelling and trajectory tracking control of underactuated mobile capsule robots and has implemented the trajectory tracking control algorithm in a developed prototype. The proposed robots have the potential to be used in medical applications (e.g. capsule endoscopy and surgery assistant).

This research has presented three underactuated capsule robots: 1D capsule robot, 2D capsule robot, 2D hybrid capsule robot. The 1D and 2D capsule robots have been designed and implemented in this thesis. Two new modified acceleration profiles (utroque and contrarium) for the inner mass have been proposed, analysed and implemented for the motion generation of the capsule robots. These acceleration profiles have removed the limitations of the previously proposed acceleration profiles presented in [41]. The 1D capsule robot can move along a straight line (forward and backward) with variable speed. The 2D capsule robot can perform linear motion, rotational motion and combining these can move on a surface. This thesis has proposed a two-stage control strategy for the motion control of an underactuated capsule robot. A segment-wise trajectory tracking control has been developed for the 1D capsule robot. A novel selection algorithm for the selection of appropriate acceleration profile (i.e. utroque and contrarium) and acceleration profile parameters has been proposed for 1D capsule robot. The simulation has been performed in the Matlab/Simulink environment and the algorithm has been implemented in the developed 1D capsule robot prototype. The experiments has been conducted where the robot tracks a semi-circular trajectory on a plywood table.

A trajectory tracking algorithm combining segment-wise and behaviour-based control has been proposed for the 2D capsule robot. Various basis behaviours for the 2D capsule

robot has been defined, a selection algorithm for the proper selection of the behavior-set has been developed, the rules for implementing each behaviour have been proposed. The effect of uncertainty and disturbances on the trajectory tracking performance has been analysed by introducing friction variation. The simulation results have shown the feasibility of the algorithm. As the propulsion mechanism is totally internal the capsule robot outer-structure can be made according to the requirement of the application and also it is hermetically sealable. These features are useful in the in-vivo applications.

A novel 2D hybrid robot with four modes of operation - legless motion mode, legged motion mode, hybrid motion mode and anchoring mode - has also been designed. The methods of moving the robot in three different modes and an anchoring method have been presented, all using a single set of actuators. Also the modelling of the robot in various operating modes has been presented. The legless mode is the primary motion mode and the robot switches to legged mode if it is stuck within the GI (gastro-intestinal) track. The robot returns to legless mode when the robot rescues itself using the legged mode. The robot uses anchoring mode when it needs to be stationary for longer observation in a suspected region, overcoming the force from visceral peristalsis within the GI (gastro-intestinal) track.

This thesis has demonstrated effective ways of propulsion for in-vivo applications and presented three capsule robots. The designed hybrid capsule robot has combined the legless and the legged motion. This thesis has addressed the trajectory tracking of the capsule-type underactuated system for the first time. The theoretical analysis, simulation studies and experimental results have validated the proposed trajectory tracking control.

6.2 Aims and Objectives Revisited

This research aimed to design and analyse underactuated mobile capsule robots. This research also aimed to develop and implement the trajectory tracking control for the capsule robots. This research has successfully designed a hybrid 2D capsule robot with four modes of operation. It has analysed three underactuated mobile capsule robots namely 1D capsule robot, 2D capsule robot and 2D hybrid capsule robot. This research has developed the trajectory tracking controls for the 1D and 2D capsule robots. It has performed the simulation and implemented the trajectory tracking control in a developed prototype.

The objectives of this research are revisited individually below.

- To identify the challenges of the miniature in-vivo robots for the medical diagnosis and interventions: The challenges have been identified and presented in the section 2.2.2 of the chapter 2. Among the challenges this thesis has focused on the design

- and control of the robots, encapsulation (hermetically sealable feature) of the robot and stopping/anchoring capability.
- To review designs and working principles of the miniature in-vivo robots for the medical diagnosis and interventions: The designs and working principles of the robots for the medical diagnosis and interventions have been reviewed in the sections 2.5 (in-vivo laparoscopic robots) and 2.6 (in-vivo endoscopic robots) of the chapter 2. Tables 2.1 - 2.5 have compared among various robot designs. The robots with external moving parts such as the wheeled robot and legged robot pose risk of hurting the internal soft tissue whereas the external magnetic drive robots such as MRI guided robot require large operating room.
 - To propose a design of the miniature in-vivo mobile robot for the medical diagnosis and interventions: This research has designed a novel 2D hybrid capsule robot combining the best aspects of the legless and legged motion. The details of the design has been presented in the section 5.2 of the chapter 5. The robot design combines four modes of operation namely legless mode, legged mode, hybrid mode and anchoring mode. Only one set of actuators has been used for all the operating modes. The robot can switch among the modes based on the situation. The hybrid robot operates in legless mode in normal situation, switches to legged mode if it needs to travel through narrow path, switches to hybrid mode if it needs to open an occlusion and switches to anchoring mode if it needs to stay stationary on a position for a longer period of time for a detailed observation for diagnosis. These are the unique capabilities of the designed robot and existing robot designs in the literature do not have these capabilities together in one unit.
 - To develop mathematical models of the underactuated mobile capsule robots (capsubots): The mathematical models for the 1D capsule robot, 2D capsule robot and 2D hybrid capsule robot have been developed and presented in the section 3.2.1 of the chapter 3, the section 4.2.1 of the chapter 4 and the section 5.4 of the chapter 5 respectively. The mathematical models have been used to design the control systems for the capsule robots. The models have also been used to perform the simulation.
 - To propose a control strategy for the trajectory tracking of the capsuobot-type underactuated systems: A two-stage control strategy has been proposed for the trajectory tracking control of the capsuobot-type underactuated systems. The control strategies for the 1D and 2D capsule robots have been presented in the section 3.2.2 of the chap-

ter 3 and the section 4.4.2 of the chapter 4 respectively. In the first stage the desired trajectory for the IM is generated from the desired trajectory of the capsbot. In the second stage the closed loop control of the desired IM trajectory tracking is achieved. The literature review of the chapter 2 suggests that no research was conducted to address the trajectory tracking of the capsbot-type underactuated systems.

- To conduct the theoretical analysis of the working principles of the capsule robots: The theoretical analysis of the working principle of the 1D, 2D and hybrid capsule robots have been presented in the section 3.3 of the chapter 3, the section 4.2.2 of the chapter 4 and the section 5.3 of the chapter 5 respectively. Two new acceleration profiles namely *utroque* and *contrarium* have been proposed for the motion generation of the capsbot. The *utroque* profile is used for the normal motion generation whereas *contrarium* profile is used to change the direction of motion in the 1D capsbot. The capsbot can move faster using these acceleration profiles compared to other profiles proposed in the literature. The comparison with previous profiles has been presented in the section 3.3.4 of the chapter 3.
- To conduct the theoretical analysis of the proposed control strategy: The theoretical analysis of the proposed trajectory tracking control strategy has been presented in the section 3.4 of the chapter 3 and the section 4.3 of the chapter 4 for the 1D and 2D capsule robots respectively. A segment-wise trajectory tracking control has been used for the 1D capsule robot whereas a combination of the segment-wise and behaviour-based trajectory tracking control has been used for the 2D capsule robot. The selection algorithms have been proposed for the selection of the profile parameters for the capsbot.
- To conduct the simulation of the trajectory tracking control and to investigate the robustness of the trajectory tracking control with uncertainties: The simulation has been performed in the Matlab/Simulink environment. The simulation studies for the trajectory tracking control for the 1D and 2D capsbots have been presented in the section 3.5.1 of the chapter 3 and the section 4.3.3 of the chapter 4 respectively. To investigate the effect of the segment time on the trajectory tracking performance the simulation has been performed for various segment times (1s, 2s and 3s). The results of Table 4.1 have shown that the tracking errors increases if the segment time increases (e.g. the mean absolute error for the x trajectory tracking increases from 0.09cm to 0.40cm when the segment time increases from 1s to 4s). The simulation has also been performed to analyze the robustness of the trajectory tracking with the friction

uncertainty. The results of Table 4.2 has shown that the performance declines if the uncertainty increases (e.g. the relative mean absolute error in the x trajectory tracking increases from 0.48% to 4.96% when the uncertainty in the linear and rotational frictions increase from 0% to $\pm 15\%$).

- To develop the capsbot prototypes and demonstrate the motion generation of the capsbot: One 1D capsbot prototype (Fig. 3.10) and one 2D capsbot prototype (Fig. 4.10) have been developed. Off-the-shelf components have been used to develop the prototypes. The section 4.4 of the chapter 4 has presented the experimentation of the 2D capsbot where it has shown the linear and rotational motion generation of the 2D capsbot.
- To implement the trajectory tracking control in the developed capsbot prototype: The developed trajectory tracking control has been implemented in the developed prototype and presented in the section 3.5.2 of the chapter 3. The motion manager [181] software has been used to program the motion controller [181] for the trajectory tracking.
- To perform the experiments to demonstrate the performance of the proposed trajectory tracking control: The section 3.5.2 of the chapter 3 has presented the experimentation of the trajectory tracking of the 1D capsule robot. The capsule robot tracks a semi-circular trajectory. A delay is seen in the experimental results. However the experimental trajectory has similar pattern as the desired trajectory.

6.3 Future Works

Future works along the direction of this research are described below:

Control In this research trajectory tracking controls for the 1D and 2D capsule robots have been developed. The following future works can be conducted to improve the trajectory tracking performance of the capsbots.

- Optimally select and tune the segment time T .
- Feedback should be taken from the capsbot position and the control input should be corrected according to the error value for the tracking of the capsbot position more accurately. This will make the trajectory tracking control fully closed loop whereas the developed trajectory tracking control is semi-closed loop.

- The motion controller provided by the Faulhaber [181] provides limited access to the control design. A custom controller can be utilized to improve the performance of the system.
- To improve the robustness of the control algorithms, investigation of the impact of the actuator dynamics, modelling uncertainties and other disturbances on the control performance should be carried out.
- Adaptive control can be developed to enable the robot to navigate through unknown environments. Adaptive control would be able to adapt when the friction coefficient changes dynamically.

Miniaturization The size of the developed stand-alone 1D capsbot prototype is 8 cm in diameter and 20 cm in length which includes the controller and batteries. The size of the developed 2D capsbot prototype is 8.5cm in length, 7cm in width and 3 cm in height which does not include controller and power supply. Off-the-shelf components such as Faulhaber [181] linear motors and motion controllers have been used to build these prototypes. Thus the developed prototypes are bigger compared to the required size of an in-vivo capsule endoscope or an in-vivo laparoscopic robot - the size of a commercially available capsule endoscope is 11mm in diameter and 26mm in length [183]. Custom-built components can be used to scale the robot size down to the required size of an in-vivo capsule endoscope or an in-vivo laparoscopic robot.

Prototype Development and Experiments In this research the 1D and 2D capsule robot prototypes have been developed. A 2D hybrid robot prototype can also be developed. To develop a hybrid robot prototype Faulhaber [181] linear motors can be used as actuators as have been used to develop the 1D and 2D capsule robot prototypes in this research. The legs, nut-gripper assembly of the hybrid robot can be developed using a microwire electrical discharge machine (EDM), a sink EDM and a micro-CNC machining center as was used in [40] to develop a legged micro robot.

More experiments can be performed using the 1D, 2D and hybrid capsule robot prototypes such as:

- trajectory tracking of the robots on the surfaces with various friction coefficients.
- trajectory tracking of the robots in the tubular environments e.g. gas and water pipes.
- trajectory tracking of the robots in an artificial GI track phantom and

- trajectory tracking of the robots in the ex-vivo and in-vivo environments.

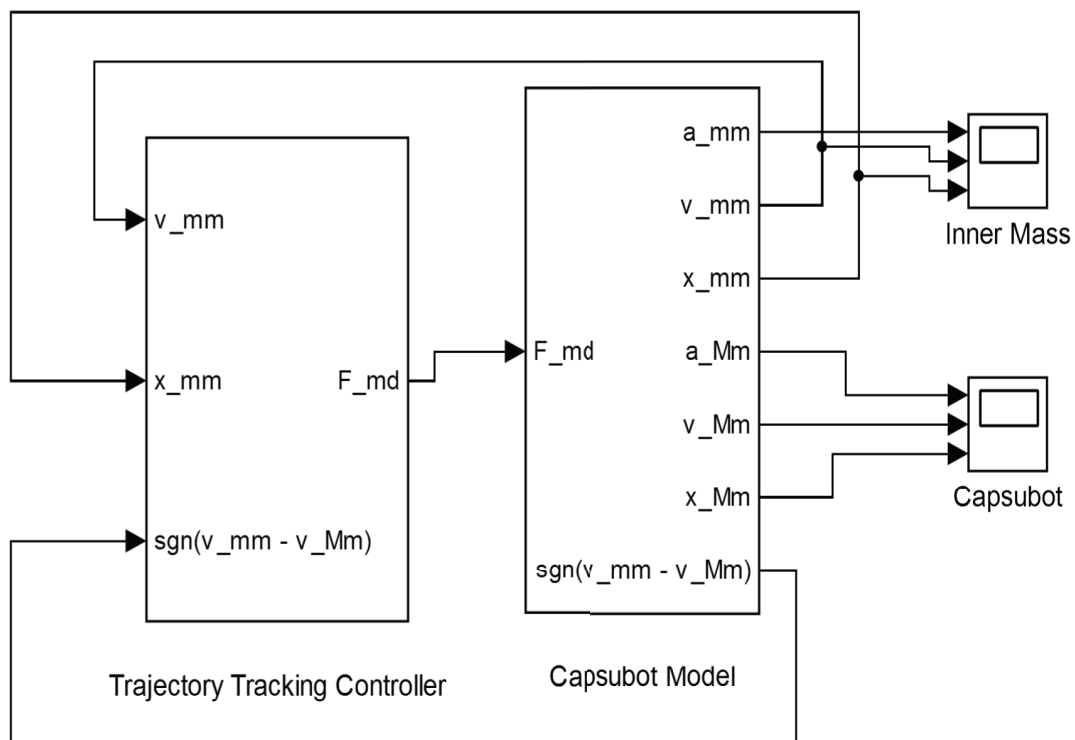
3D Capsubot Design A 3D capsubot will be useful for in-vivo applications such as medical inspection inside a stomach. It can be designed using three parallel inner masses (IMs) placed inside three parallel hollow spaces of a cylindrical housing. The IMs could be solenoids or linear motors. By controlling the movements of the three IMs, the 3D capsubot can move in a fluid environment inside a liquid-distended stomach. Fluid dynamics has to be considered to model the environment and to design a controller for the 3D capsubot.

Appendix A

A.1 Simulink Model of 1D Capsubot

Appendix A presents the Simulink model of the 1D capsubot. Fig. A.1 shows the complete Simulink model for the trajectory tracking control of the 1D capsubot. It consists of the following subsystems:

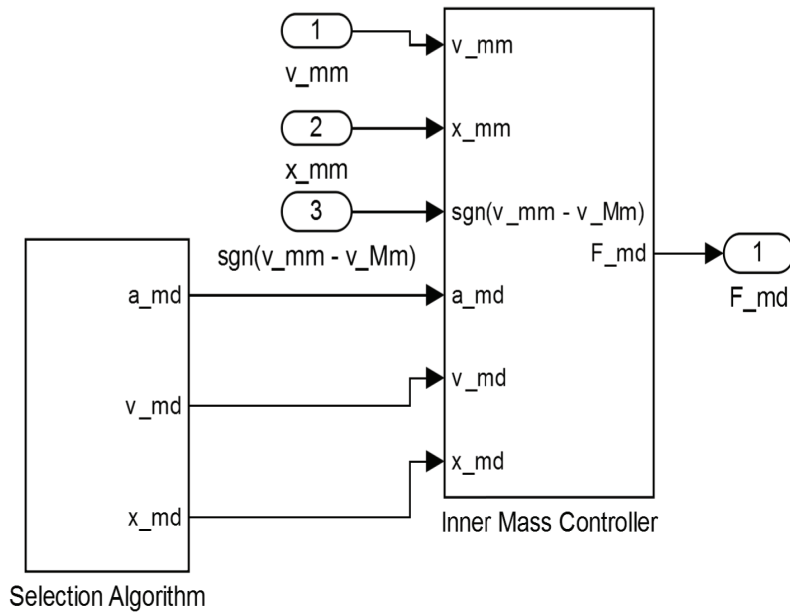
- Trajectory tracking controller (Fig. A.2(a))
 - Selection algorithm (Fig. A.3(a))
 - Inner Mass controller (Fig. A.3(b))
- Capsubot model (Fig. A.2(b))
 - Simulink model for equation (3.1) (Fig. A.4(a))
 - Simulink model for equation (3.2) (Fig. A.4(b))



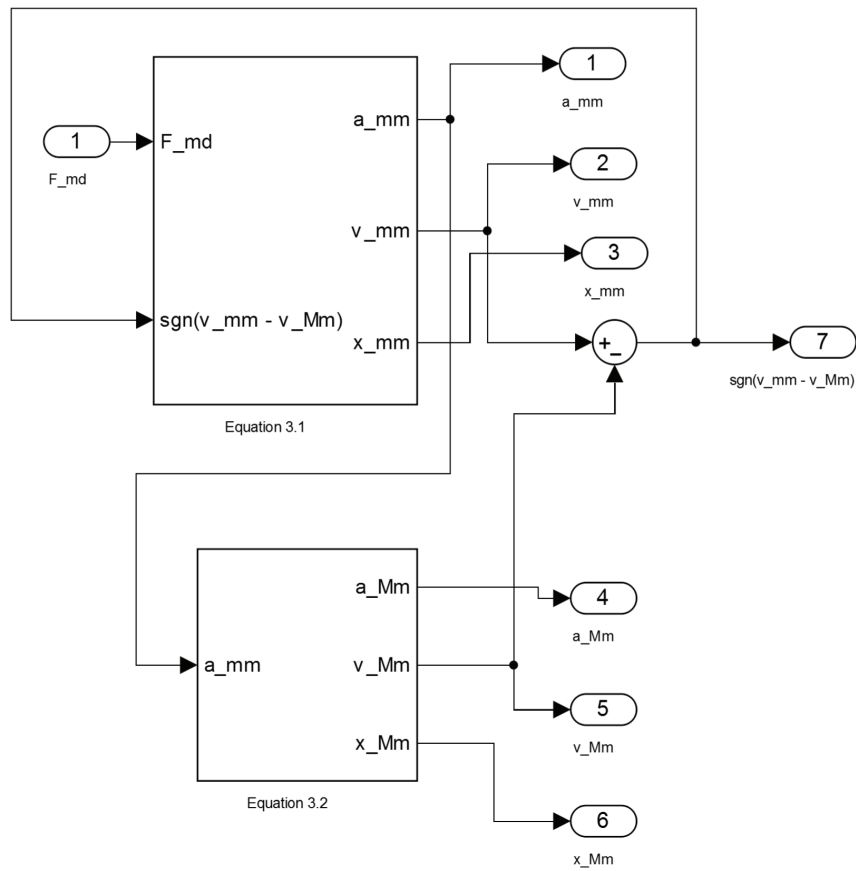
mm => First m indicates Inner Mass, second m indicates measured
 md => m indicates Inner Mass, d indicates desired
 Mm => M indicates Capsuobot, m indicates measured
 Md => M indicates Capsuobot, d indicates desired

a indicates acceleration
 v indicates velocity
 x indicates position

Fig. A.1 Simulink model of the 1D capsuobot trajectory tracking

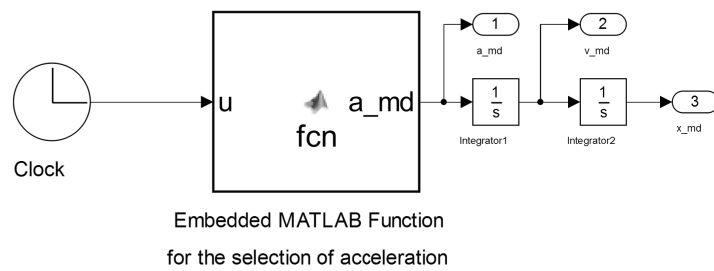


(a) Subsystem - trajectory tracking controller



(b) Subsystem - capsbot model

Fig. A.2 Subsystems of the Simulink model of the 1D capsbot trajectory tracking control of A.1



(a) Subsystem - selection algorithm

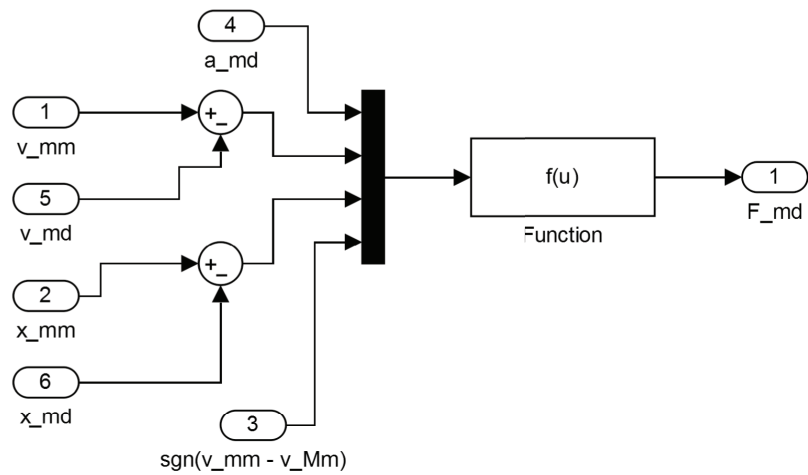
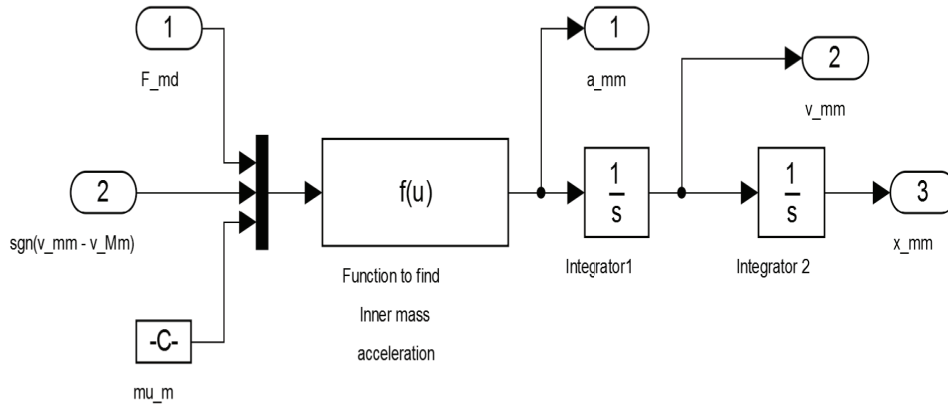
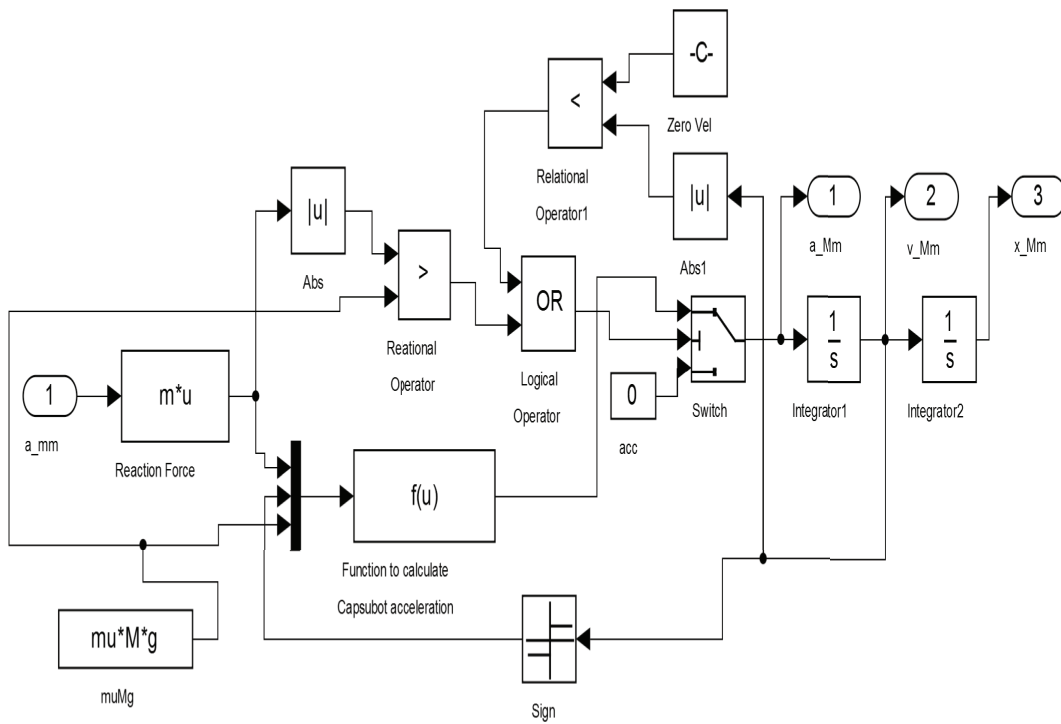


Fig. A.3 Subsystems of the trajectory tracking controller subsystem of Fig. A.2(a)



(a) Subsystem - Simulink model for equation (3.1)



(b) Subsystem - Simulink model for equation (3.2)

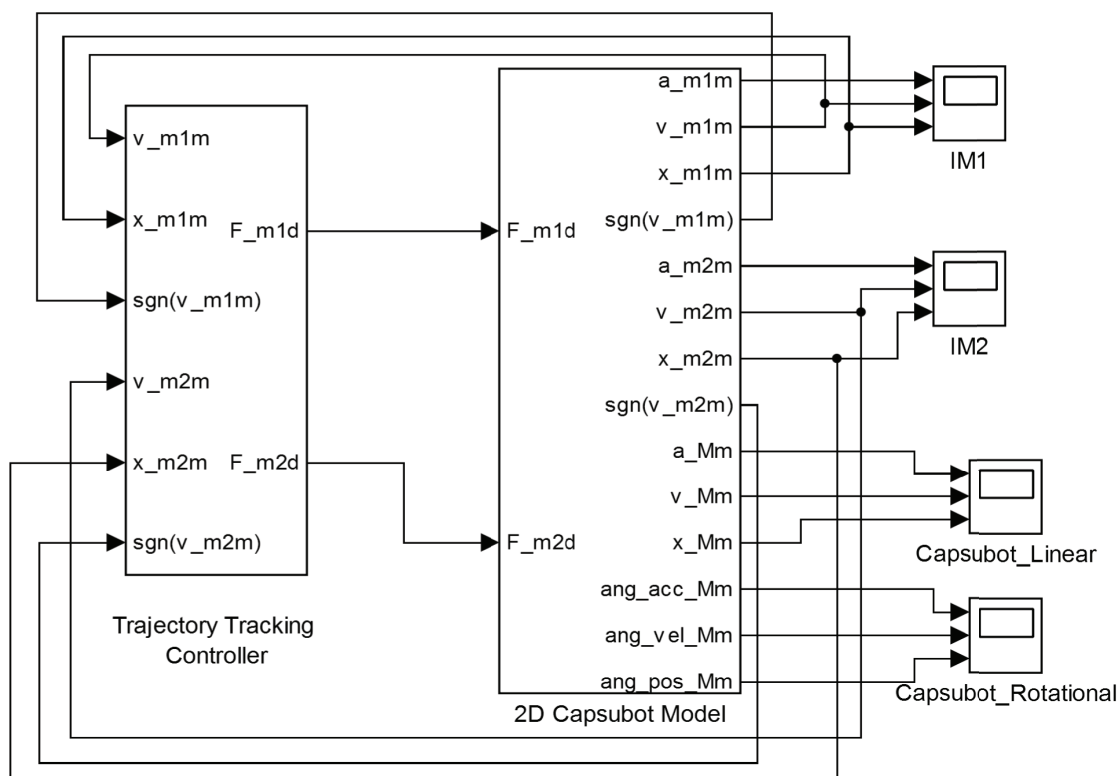
Fig. A.4 Subsystems of the capsubot model subsystem of Fig. A.2(b)

Appendix B

B.1 Simulink Model of 2D Capsubot

Appendix B presents the Simulink model of 2D capsubot. Fig. B.1 shows the complete Simulink model for the trajectory tracking control of the 2D capsubot. It consists of the following subsystems.

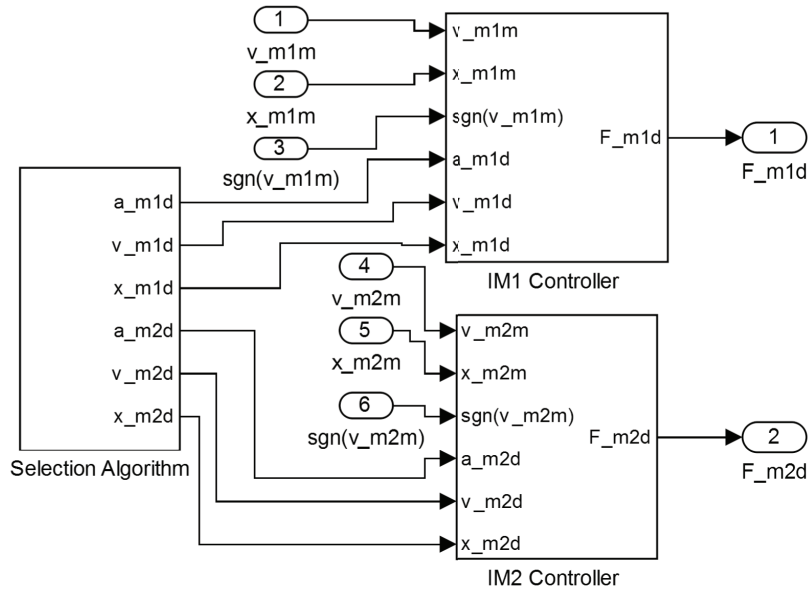
- Trajectory tracking controller (Fig. B.2(a))
 - Selection algorithm (Fig. B.3(a))
 - IM_1 controller (Fig. B.3(b))
 - IM_2 controller (Fig. B.3(c))
- Capsubot Model (Fig. B.2(b))
 - Simulink model for equation (4.1) (Fig. B.4)
 - Simulink model for equations (4.2) and (4.3) (Fig. B.5)
 - Simulink model for equation (4.4) (Fig. B.6)



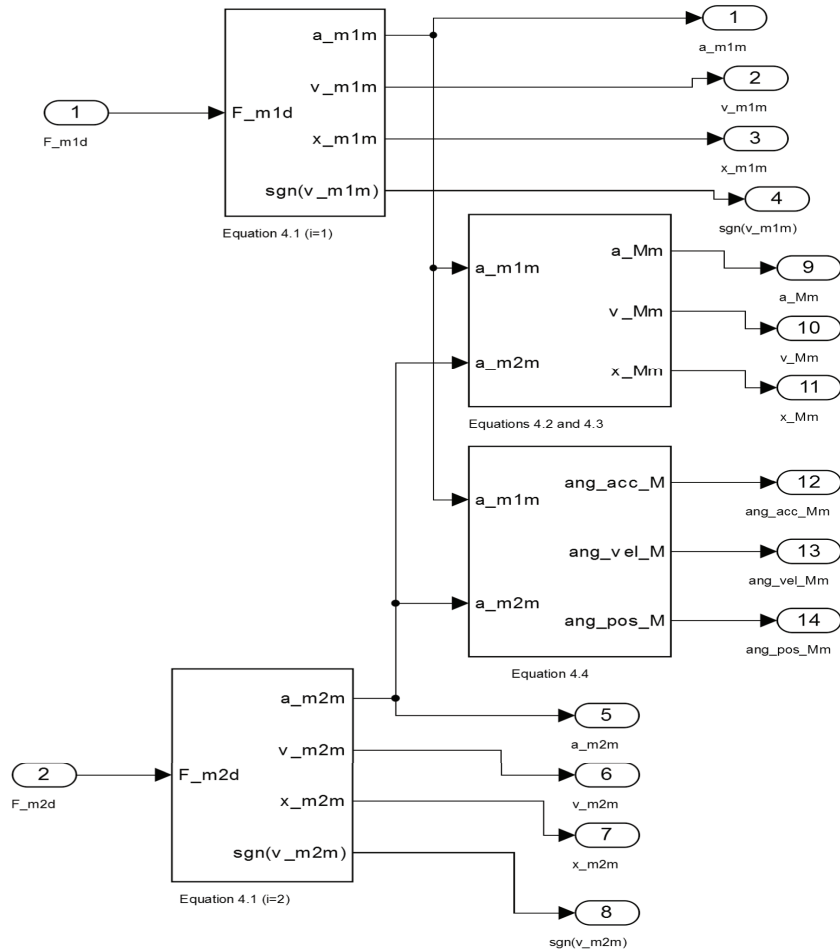
mim => m_i indicates Inner Mass i , second m indicates measured
 mid => m_i indicates Inner Mass i , d indicates desired
 Mm => M indicates Capsubot, m indicates measured
 Md => M indicates Capsubot, d indicates desired

a and acc indicate acceleration
 v and vel indicate velocity
 x and pos indicate position
 ang indicates angular

Fig. B.1 Simulink model of the 2D capsobot trajectory tracking control

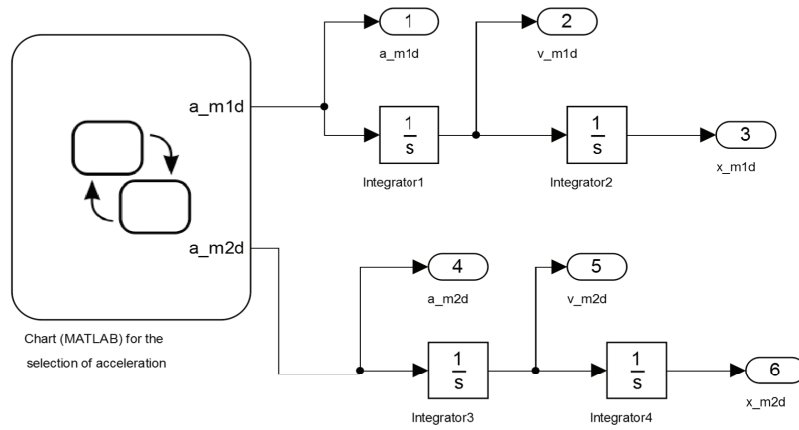


(a) Subsystem - trajectory tracking controller

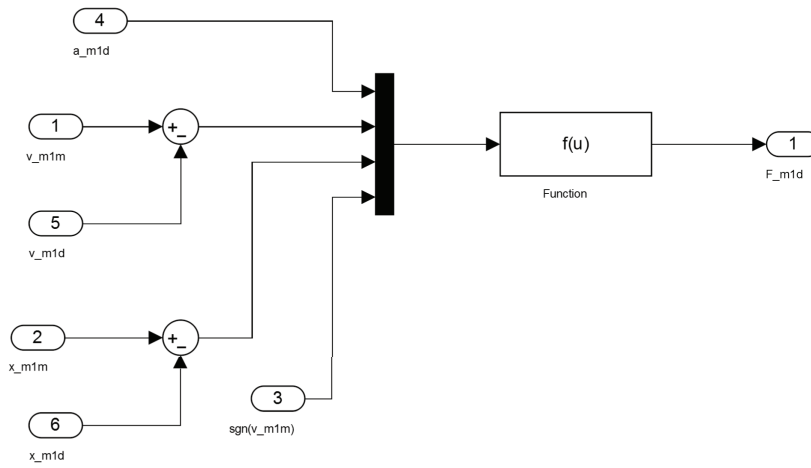


(b) Subsystem - capsubot model

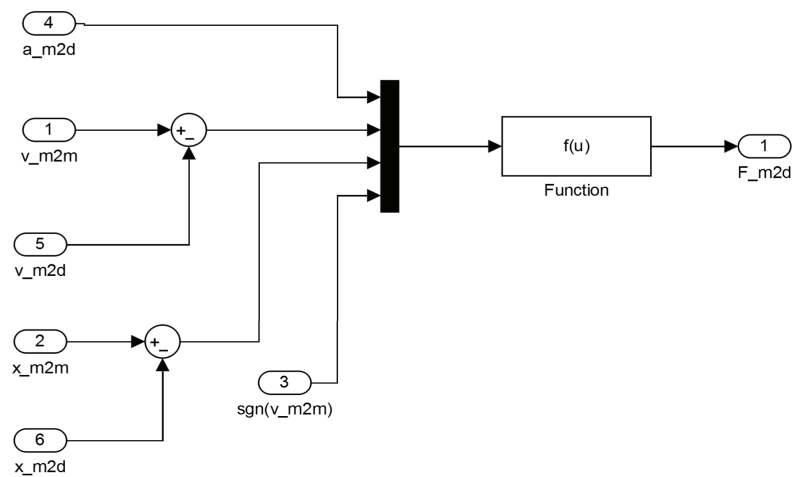
Fig. B.2 Subsystems of the Simulink model of the 2D capsubot trajectory tracking control of B.1



(a) Subsystem - selection algorithm



(b) Subsystem - IM_1 controller



(c) Subsystem - IM_2 controller

Fig. B.3 Subsystems of the trajectory tracking controller subsystem of Fig. B.2(a)

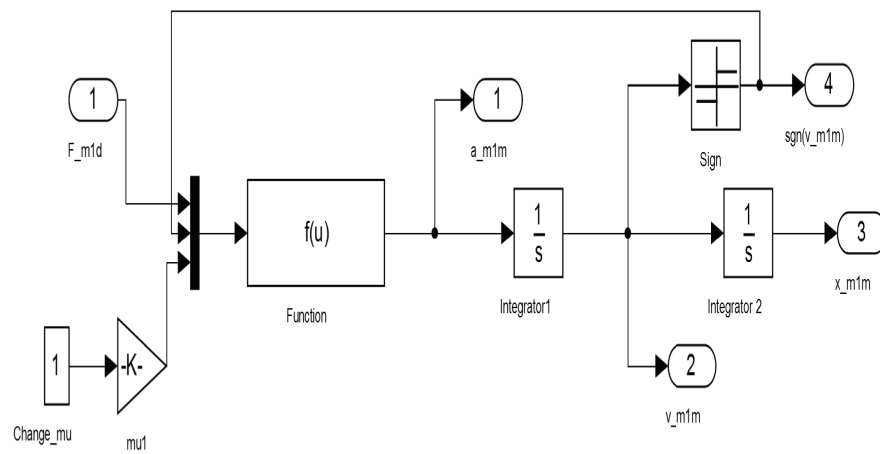


Fig. B.4 Simulink model for equation (4.1) - a subsystem of the capsbot model subsystem of Fig. B.2(b)

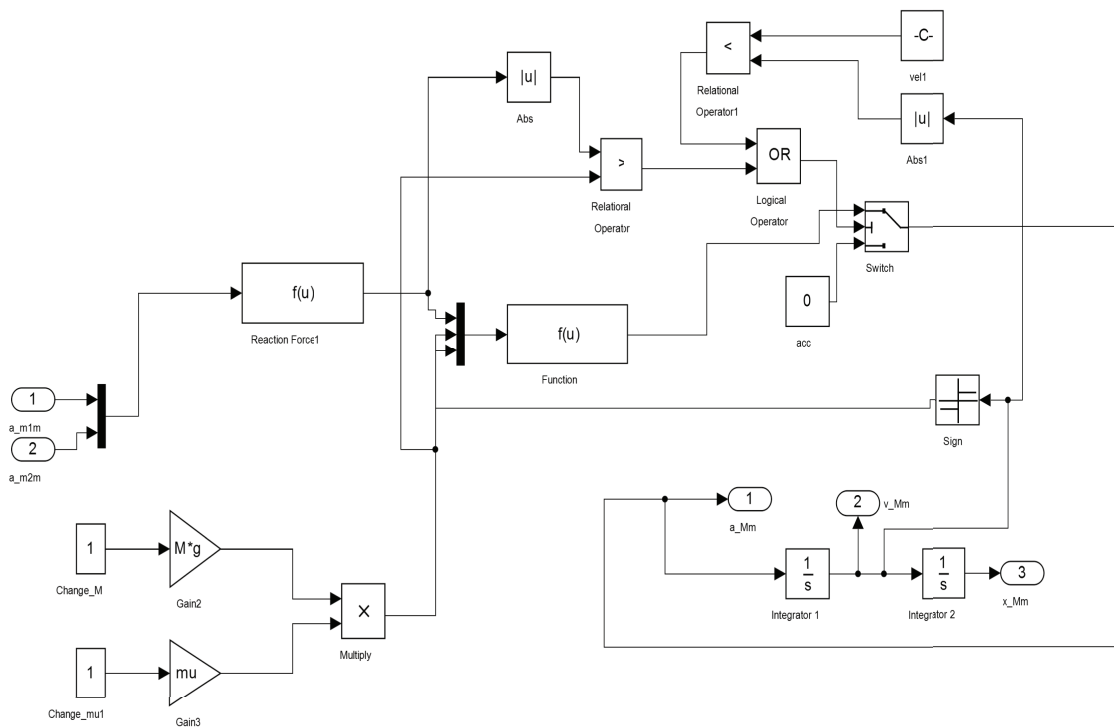


Fig. B.5 Simulink model for equations (4.2) and (4.3) - a subsystem of the capsbot model subsystem of Fig. B.2(b)

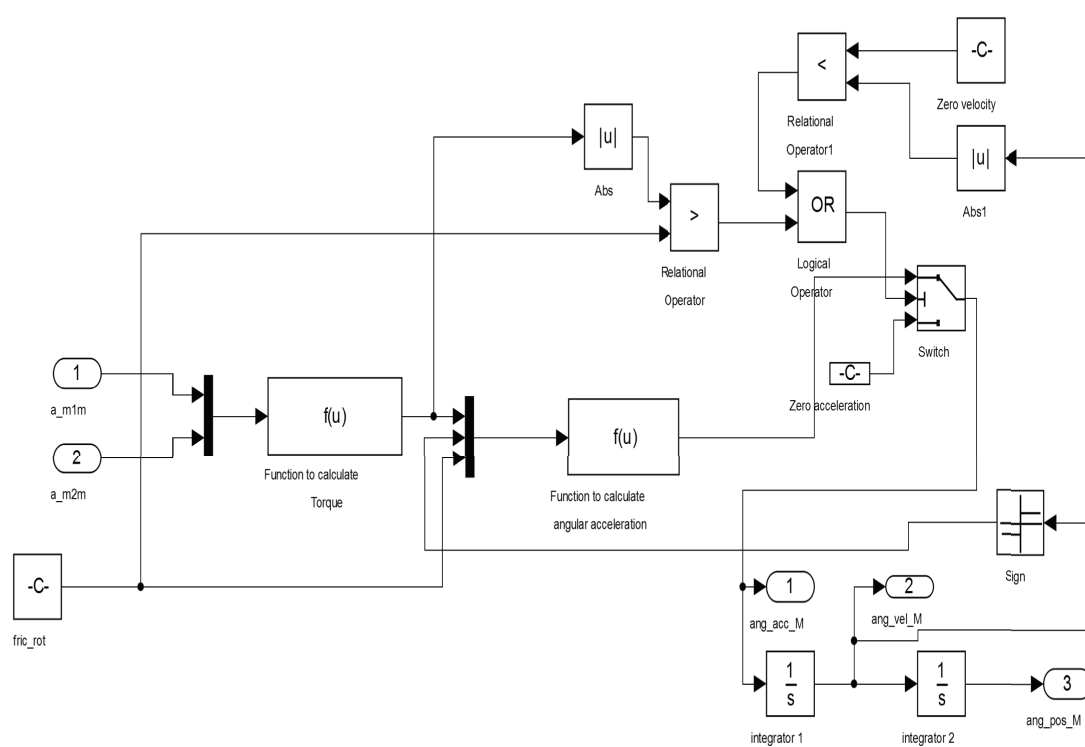


Fig. B.6 Simulink model for equations (4.4) - a subsystem of the capsbot model subsystem of Fig. B.2(b)

References

- [1] C. Braumann, C. Jacobi, C. Menenakos, M. Ismail, J. Rueckert, and J. Mueller, "Robotic-assisted laparoscopic and thoracoscopic surgery with the da vinci system: a 4-year experience in a single institution," *Surgical Laparoscopy Endoscopy & Percutaneous Techniques*, vol. 18, no. 3, p. 260, 2008.
- [2] C. Tsui, R. Klein, and M. Garabrant, "Minimally invasive surgery: national trends in adoption and future directions for hospital strategy," *Surgical endoscopy*, pp. 1–5, 2013.
- [3] V. Vitiello, S.-L. Lee, T. P. Cundy, and G.-Z. Yang, "Emerging robotic platforms for minimally invasive surgery," *IEEE Reviews in Biomedical Engineering*, vol. 6, pp. 111–126, 2013.
- [4] B. Cheon, E. Gezgin, D. K. Ji, M. Tomikawa, M. Hashizume, H.-J. Kim, and J. Hong, "A single port laparoscopic surgery robot with high force transmission and a large workspace," *Surgical endoscopy*, pp. 1–11, 2014.
- [5] S. Yim, E. Gultepe, D. H. Gracias, and M. Sitti, "Biopsy using a magnetic capsule endoscope carrying, releasing, and retrieving untethered microgrippers," *IEEE Transactions on Biomedical Engineering*, vol. 61, no. 2, pp. 513–521, 2014.
- [6] P. Dario, B. Hannaford, and A. Menciassi, "Smart surgical tools and augmenting devices," *IEEE Transactions on Robotics and Automation*, vol. 19, no. 5, pp. 782–792, 2003.
- [7] N. A. Patronik, T. Ota, M. A. Zenati, and C. N. Riviere, "A miniature mobile robot for navigation and positioning on the beating heart," *IEEE Transactions on Robotics*, vol. 25, no. 5, pp. 1109–1124, 2009.
- [8] C. Briggs, C. Mann, G. Irving, C. Neal, M. Peterson, I. Cameron, and D. Berry, "Systematic review of minimally invasive pancreatic resection," *Journal of Gastrointestinal Surgery*, vol. 13, no. 6, pp. 1129–1137, 2009.
- [9] P. Gomes, "Surgical robotics: Reviewing the past, analysing the present, imagining the future," *Robotics and Computer-Integrated Manufacturing*, vol. 27, no. 2, pp. 261–266, 2011.
- [10] S. Tognarelli, M. Salerno, G. Tortora, C. Quaglia, P. Dario, M. O. Schurr, and A. Menciassi, "A miniaturized robotic platform for natural orifice transluminal endoscopic surgery: in vivo validation," *Surgical endoscopy*, vol. 29, no. 12, pp. 3477–3484, 2015.

- [11] Z.-J. Sun, B. Ye, Y. Qiu, X.-G. Cheng, H.-H. Zhang, and S. Liu, "Preliminary study of a legged capsule robot actuated wirelessly by magnetic torque," *IEEE Transactions on Magnetics*, vol. 50, no. 8, pp. 1–6, 2014.
- [12] A. W. Mahoney and J. J. Abbott, "Five-degree-of-freedom manipulation of an untethered magnetic device in fluid using a single permanent magnet with application in stomach capsule endoscopy," *The International Journal of Robotics Research*, 2015.
- [13] C.-K. Lee, H.-S. Choi, G. Go, S. Jeong, S. Y. Ko, J. Park, and S. Park, "Active locomotive intestinal capsule endoscope (alice) system: A prospective feasibility study," *IEEE/ASME Transactions on Mechatronics*, vol. 20, no. 5, pp. 2067–2074, 2015.
- [14] A. C. Lehman, K. A. Berg, J. Dumpert, N. A. Wood, A. Q. Visty, M. E. Rentschler, S. R. Platt, S. M. Farritor, and D. Oleynikov, "Surgery with cooperative robots," *Computer Aided Surgery*, vol. 13, no. 2, pp. 95–105, 2008.
- [15] A. C. Lehman, M. E. Rentschler, S. M. Farritor, and D. Oleynikov, "The current state of miniature in vivo laparoscopic robotics," *Journal of Robotic Surgery*, vol. 1, no. 1, pp. 45–49, 2007.
- [16] S. Ohno, C. Hiroki, and W. Yu, "Design and manipulation of a suction-based micro robot for moving in the abdominal cavity," *Advanced Robotics*, vol. 24, no. 12, pp. 1741–1761, 2010.
- [17] S. R. Platt, J. A. Hawks, and M. E. Rentschler, "Vision and task assistance using modular wireless in vivo surgical robots," *IEEE transactions on bio-medical engineering*, vol. 56, no. 6, p. 1700, 2009.
- [18] M. E. Rentschler, J. Dumpert, S. R. Platt, D. Oleynikov, S. M. Farritor, and K. Iagnemma, "Mobile in vivo biopsy robot," in *2006 IEEE International Conference on Robotics and Automation*, 2006, pp. 4155–4160.
- [19] M. E. Rentschler, S. R. Platt, K. R. Berg, J. Dumpert, D. Oleynikov, and S. M. Farritor, "Miniature in vivo robots for remote and harsh environments," *IEEE Transactions on Information Technology in Biomedicine*, vol. 12, no. 1, pp. 66–75, 2008.
- [20] USGIMedical, "<http://www.usgimedical.com/news>," online, accessed: 10.06.2009.
- [21] A. Forgione, "In vivo microrobots for natural orifice transluminal surgery. current status and future perspectives," *Surgical Oncology*, vol. 18, no. 2, pp. 121–129, 2009.
- [22] C. Castro, A. Alqassis, S. Smith, T. Ketterl, Y. Sun, S. Ross, A. Rosemurgy, P. P. Savage, R. D. Gitlin *et al.*, "A wireless robot for networked laparoscopy," *IEEE Transactions on Biomedical Engineering*, vol. 60, no. 4, pp. 930–936, 2013.
- [23] C. Castro, S. Smith, A. Alqassis, T. Ketterl, Y. Sun, S. Ross, A. Rosemurgy, P. P. Savage, R. D. Gitlin *et al.*, "Marvel: A wireless miniature anchored robotic video-scope for expedited laparoscopy," in *IEEE International Conference on Robotics and Automation (ICRA)*, 2012, pp. 2926–2931.
- [24] D. Oleynikov, S. M. Farritor, M. E. Rentschler, S. R. Platt, J. Dumpert *et al.*, "Surgical camera robot," Mar. 2008, uS Patent 7,339,341.

- [25] M. E. Rentschler, J. Dumpert, S. R. Platt, K. Lagnernma, D. Oleynikov, and S. M. Farritor, "Modeling, analysis, and experimental study of in vivo wheeled robotic mobility," *IEEE Transactions on Robotics*, vol. 22, no. 2, pp. 308–321, 2006.
- [26] I. Rivas-Blanco, P. del Saz-Orozco, I. Garcia-Morales, and V. Muñoz, "Robotic system for single incision laparoscopic surgery," in *IECON-38th Annual Conference on IEEE Industrial Electronics Society*, 2012, pp. 2774–2779.
- [27] B. S. Terry, Z. C. Mills, J. Schoen, M. E. Rentschler *et al.*, "Single-port-access surgery with a novel magnet camera system," *IEEE Transactions on Biomedical Engineering*, vol. 59, no. 4, pp. 1187–1193, 2012.
- [28] M. Nokata, S. Kitamura, T. Nakagi, T. Inubushi, and S. Morikawa, "Capsule type medical robot with magnetic drive in abdominal cavity," in *2nd IEEE RAS & EMBS International Conference on Biomedical Robotics and Biomechatronics*, 2008, pp. 348–353.
- [29] G. Tortora, P. Dario, and A. Menciassi, "Array of robots augmenting the kinematics of endocavitary surgery," *IEEE/ASME Transactions on Mechatronics*, vol. 19, no. 6, pp. 1821–1829, 2014.
- [30] G. Tortora, A. Dimitracopoulos, P. Valdastri, A. Menciassi, and P. Dario, "Design of miniature modular in vivo robots for dedicated tasks in minimally invasive surgery," in *IEEE/ASME International Conference on Advanced Intelligent Mechatronics (AIM)*, 2011, pp. 327–332.
- [31] S. Ohno, J. Tachikawa, and W. Yu, "Development of a micro mobile robot in the abdominal cavity," in *IEEE/RSJ International Conference on Intelligent Robots and Systems*, 2009, pp. 4707–4711.
- [32] Given-Imaging, "<http://www.givenimaging.com>," online, accessed: 02.07.2014.
- [33] Y. Kusuda, "A further step beyond wireless capsule endoscopy," *Sensor Review*, vol. 25, no. 4, pp. 259–260, 2005.
- [34] G. Ciuti, A. Menciassi, and P. Dario, "Capsule endoscopy: from current achievements to open challenges," *IEEE Reviews in Biomedical Engineering*, no. 99, pp. 1–1, 2011.
- [35] J. L. Toennies, G. Tortora, M. Simi, P. Valdastri, and R. J. Webster, "Swallowable medical devices for diagnosis and surgery: the state of the art," *Proceedings of the Institution of Mechanical Engineers, Part C: Journal of Mechanical Engineering Science*, vol. 224, no. 7, pp. 1397–1414, 2010.
- [36] A. W. Mahoney and J. J. Abbott, "Generating rotating magnetic fields with a single permanent magnet for propulsion of untethered magnetic devices in a lumen," *IEEE Transactions on Robotics*, vol. 30, no. 2, pp. 411–420, 2014.
- [37] I. Rahman, N. A. Afzal, and P. Patel, "The role of magnetic assisted capsule endoscopy (mace) to aid visualisation in the upper gi tract," *Computers in biology and medicine*, vol. 65, pp. 359–363, 2015.

- [38] I. De Falco, G. Tortora, P. Dario, and A. Menciassi, "An integrated system for wireless capsule endoscopy in a liquid-distended stomach," *IEEE Transactions on Biomedical Engineering*, vol. 61, no. 3, pp. 794–804, 2014.
- [39] R. Carta, M. Sfakiotakis, N. Pateromichelakis, J. Thoné, D. Tsakiris, and R. Puers, "A multi-coil inductive powering system for an endoscopic capsule with vibratory actuation," *Sensors and Actuators A: Physical*, vol. 172, no. 1, pp. 253–258, 2011.
- [40] P. Valdastrì, R. Webster, C. Quaglia, M. Quirini, A. Menciassi, and P. Dario, "A new mechanism for mesoscale legged locomotion in compliant tubular environments," *IEEE Transactions on Robotics*, vol. 25, no. 5, pp. 1047–1057, 2009.
- [41] H. Yu, M. N. Huda, and S. Wane, "A novel acceleration profile for the motion control of capsulobots," in *2011 IEEE International Conference on Robotics and Automation*, 2011, pp. 2437–2442.
- [42] M. Simi, P. Valdastrì, C. Quaglia, A. Menciassi, and P. Dario, "Design, Fabrication, and Testing of a Capsule With Hybrid Locomotion for Gastrointestinal Tract Exploration," *IEEE/ASME Transactions on Mechatronics*, vol. 15, no. 2, 2010.
- [43] L. Liu, S. Towfighian, and A. Hila, "A review of locomotion systems for capsule endoscopy," *IEEE Reviews in Biomedical Engineering*, vol. 8, pp. 138–151, 2015.
- [44] G. Kósa, P. Jakab, F. Jólesz, and N. Hata, "Swimming capsule endoscope using static and RF magnetic field of MRI for propulsion," in *Proceedings of the IEEE International Conference on Robotics and Automation*, 2008, pp. 2922–2927.
- [45] J.-F. Rey, H. Ogata, N. Hosoe, K. Ohtsuka, N. Ogata, K. Ikeda, H. Aihara, I. Pangtay, T. Hibi, S.-E. Kudo *et al.*, "Blinded nonrandomized comparative study of gastric examination with a magnetically guided capsule endoscope and standard videoendoscope," *Gastrointestinal endoscopy*, vol. 75, no. 2, pp. 373–381, 2012.
- [46] F. Carpi and C. Pappone, "Magnetic maneuvering of endoscopic capsules by means of a robotic navigation system," *IEEE transactions on biomedical engineering*, vol. 56, no. 5, pp. 1482–1490, 2009.
- [47] F. Carpi, N. Kastelein, M. Talcott, and C. Pappone, "Magnetically controllable gastrointestinal steering of video capsules," *IEEE Transactions on Biomedical Engineering*, vol. 58, no. 2, pp. 231–234, 2011.
- [48] M. Quirini, S. Scapellato, A. Menciassi, P. Dario, F. Rieber, C. Ho, S. Schostek, and M. Schurr, "Feasibility proof of a legged locomotion capsule for the GI tract," *Gastrointestinal endoscopy*, 2008.
- [49] P. R. Slawinski, K. L. Obstein, and P. Valdastrì, "Capsule endoscopy of the future: What's on the horizon?" *World journal of gastroenterology: WJG*, vol. 21, no. 37, pp. 10 528–10 541, 2015.
- [50] J. Gao, G. Yan, Z. Wang, S. He, F. Xu, P. Jiang, and D. Liu, "Design and testing of a motor-based capsule robot powered by wireless power transmission," *IEEE/ASME Transactions on Mechatronics*, no. 99, 2015.

- [51] H. Yu, Y. Liu, and T. Yang, "Closed-loop tracking control of a pendulum-driven cart-pole underactuated system," *Proceedings of the Institution of Mechanical Engineers, Part I: Journal of Systems and Control Engineering*, vol. 222, no. 2, pp. 109–125, 2008.
- [52] Y. Liu, H. Yu, and T. Yang, "Analysis and Control of a Capsbot," in *Proceedings of the 17th IFAC (International Federation of Automatic Control) World Congress*, 2008, pp. 756–761.
- [53] A. Menciassi, P. Valdastri, C. Quaglia, E. Buselli, and P. Dario, "Wireless steering mechanism with magnetic actuation for an endoscopic capsule," in *Annual International Conference of the IEEE Engineering in Medicine and Biology Society*, 2009, pp. 1204–1207.
- [54] Y. Liu and H. Yu, "A survey of underactuated mechanical systems," *IET Control Theory & Applications*, vol. 7, no. 7, pp. 921–935, 2013.
- [55] M. Lo'pez-Mart'nez, J. Acosta, and J. Cano, "Non-linear sliding mode surfaces for a class of underactuated mechanical systems [brief paper]," *IET Control Theory & Applications*, vol. 4, no. 10, pp. 2195–2204, 2010.
- [56] K. Pathak, J. Franch, and S. Agrawal, "Velocity and position control of a wheeled inverted pendulum by partial feedback linearization," *IEEE Transactions on Robotics*, vol. 21, no. 3, pp. 505–513, 2005.
- [57] J. Huang, F. Ding, T. Fukuda, and T. Matsuno, "Modeling and velocity control for a novel narrow vehicle based on mobile wheeled inverted pendulum," *IEEE Transactions on Control Systems Technology*, vol. 21, no. 5, pp. 1607–1617, 2013.
- [58] R. Xu and Ü. Özgüner, "Sliding mode control of a class of underactuated systems," *Automatica*, vol. 44, no. 1, pp. 233–241, 2008.
- [59] K. Do, Z.-P. Jiang, and J. Pan, "Global output-feedback tracking control of a vtol aircraft," in *42nd IEEE Conference on Decision and Control*, vol. 5, 2003, pp. 4914–4919.
- [60] A. P. Aguiar and J. P. Hespanha, "Trajectory-tracking and path-following of underactuated autonomous vehicles with parametric modeling uncertainty," *IEEE Transactions on Automatic Control*, vol. 52, no. 8, pp. 1362–1379, 2007.
- [61] F. Bi, Y. Wei, J. Zhang, and W. Cao, "Position-tracking control of underactuated autonomous underwater vehicles in the presence of unknown ocean currents," *IET Control Theory & Applications*, vol. 4, no. 11, pp. 2369–2380, 2010.
- [62] H. Ashrafiuon, K. R. Muske, L. C. McNinch, and R. A. Soltan, "Sliding-mode tracking control of surface vessels," *IEEE Transactions on Industrial Electronics*, vol. 55, no. 11, pp. 4004–4012, 2008.
- [63] F. Chernous'ko, "The optimum rectilinear motion of a two-mass system," *Journal of applied Mathematics and Mechanics*, vol. 66, no. 1, pp. 1–7, 2002.

- [64] N. Lee, N. Kamamichi, H. Li, and K. Furuta, "Control system design and experimental verification of capsbot," in *IEEE/RSJ International Conference on Intelligent Robots and Systems*, 2008, pp. 1927–1932.
- [65] R. H. Taylor, A. Menciassi, G. Fichtinger, and P. Dario, "Medical robotics and computer-integrated surgery," *Springer Handbook of Robotics*, pp. 1199–1222, 2008.
- [66] M. Butter, A. Rensma, J. van Boxsels, S. Kalisingh, M. Schoone, M. Leis, G. Gelderblom, G. Cremers, M. de Wilt, W. Kortekaas *et al.*, "Robotics for health-care. final report," *Leiden: TNO, Quality of Life*, 2008.
- [67] P. Kazanzides, G. Fichtinger, G. D. Hager, A. M. Okamura, L. L. Whitcomb, and R. H. Taylor, "Surgical and interventional robotics-core concepts, technology, and design [tutorial]," *IEEE Robotics & Automation Magazine*, vol. 15, no. 2, pp. 122–130, 2008.
- [68] A. M. Okamura, M. J. Mataric, and H. I. Christensen, "Medical and health-care robotics," *Robotics and Automation Magazine*, vol. 17, no. 3, pp. 26–27, 2010.
- [69] J. D. MacDonald, "Learning to perform microvascular anastomosis," *Skull Base*, vol. 15, no. 3, p. 229, 2005.
- [70] A. DiGioia, *Computer and robotic assisted hip and knee surgery*, 2004.
- [71] A. R. Lanfranco, A. E. Castellanos, J. P. Desai, and W. C. Meyers, "Robotic surgery: a current perspective," *Annals of surgery*, vol. 239, no. 1, p. 14, 2004.
- [72] J. Rosen, B. Hannaford, and R. M. Satava, *Surgical Robotics: Systems Applications and Visions*, 2011.
- [73] K. Ahmed, M. S. Khan, A. Vats, K. Nagpal, O. Priest, V. Patel, J. A. Vecht, H. Ashrafian, G.-Z. Yang, T. Athanasiou *et al.*, "Current status of robotic assisted pelvic surgery and future developments," *International Journal of Surgery*, vol. 7, no. 5, pp. 431–440, 2009.
- [74] A. Lehman, N. Wood, J. Dumpert, D. Oleynikov, and S. Farritor, "Robotic natural orifice transluminal endoscopic surgery," in *IEEE International Conference on Robotics and Automation*, 2008, pp. 2969–2974.
- [75] G. H. Ballantyne, "Robotic surgery, telerobotic surgery, telepresence, and telementoring," *Surgical Endoscopy and Other Interventional Techniques*, vol. 16, no. 10, pp. 1389–1402, 2002.
- [76] M. Rentschler, J. Dumpert, S. Platt, S. Farritor, and D. Oleynikov, "Natural orifice surgery with an endoluminal mobile robot," *Surgical endoscopy*, vol. 21, no. 7, pp. 1212–1215, 2007.
- [77] H. Marcus, D. Nandi, A. Darzi, and G.-Z. Yang, "Surgical robotics through a key-hole: from today's translational barriers to tomorrow's "disappearing" robots." *IEEE transactions on bio-medical engineering*, vol. 60, no. 3, pp. 674–681, 2013.

- [78] D. Di Marco, G. Chow, M. Gettman, and D. Elliott, "Robotic-assisted laparoscopic sacrocolpopexy for treatment of vaginal vault prolapse," *Urology*, vol. 63, no. 2, pp. 373–376, 2004.
- [79] S. Lucak, "Handbook of gastroenterologic procedures," *Gastroenterology*, vol. 130, no. 2, pp. 617–618, 2006.
- [80] M. Rentschler and D. Oleynikov, "Recent in vivo surgical robot and mechanism developments," *Surgical endoscopy*, vol. 21, no. 9, pp. 1477–1481, 2007.
- [81] A. Moglia, A. Menciacchi, P. Dario, and A. Cuschieri, "Capsule endoscopy: progress update and challenges ahead," *Nature Reviews Gastroenterology and Hepatology*, 2009.
- [82] G. T. Sung and I. S. Gill, "Robotic laparoscopic surgery: a comparison of the da vinci and zeus systems," *Urology*, vol. 58, no. 6, pp. 893–898, 2001.
- [83] R. Satava, "Surgical robotics: the early chronicles: a personal historical perspective," *Surgical Laparoscopy Endoscopy & Percutaneous Techniques*, vol. 12, no. 1, p. 6, 2002.
- [84] G. H. Ballantyne and F. Moll, "The da vinci telerobotic surgical system: the virtual operative field and telepresence surgery," *Surgical Clinics of North America*, vol. 83, no. 6, pp. 1293–1304, 2003.
- [85] Y. S. Kwok, J. Hou, E. A. Jonckheere, and S. Hayati, "A robot with improved absolute positioning accuracy for ct guided stereotactic brain surgery," *IEEE Transactions on Biomedical Engineering*, vol. 35, no. 2, pp. 153–160, 1988.
- [86] S. Ho, R. Hibberd, and B. Davies, "Robot assisted knee surgery," *IEEE Engineering in Medicine and Biology Magazine*, vol. 14, no. 3, pp. 292–300, 1995.
- [87] J. Cobb, J. Henckel, P. Gomes, S. Harris, M. Jakopec, F. Rodriguez, A. Barrett, and B. Davies, "Hands-on robotic unicompartmental knee replacement a prospective, randomised controlled study of the acrobot system," *Journal of Bone & Joint Surgery, British Volume*, vol. 88, no. 2, pp. 188–197, 2006.
- [88] A. Barrett, B. Davies, M. Gomes, S. Harris, J. Henckel, M. Jakopec, V. Kannan, F. R. y Baena, and J. Cobb, "Computer-assisted hip resurfacing surgery using the acrobot® navigation system," *Proceedings of the Institution of Mechanical Engineers, Part H: Journal of Engineering in Medicine*, vol. 221, no. 7, pp. 773–785, 2007.
- [89] A. Barrett, B. Davies, M. Gomes, S. Harris, J. Henckel, M. Jakopec, F. R. y Baena, and J. Cobb, "Preoperative planning and intraoperative guidance for accurate computer-assisted minimally invasive hip resurfacing surgery," *Proceedings of the Institution of Mechanical Engineers, Part H: Journal of Engineering in Medicine*, vol. 220, no. 7, pp. 759–773, 2006.
- [90] B. Davies, "A review of the state-of-the-art of" smart" systems in surgery," in *15th International Conference on Mechatronics and Machine Vision in Practice*, 2008, pp. 151–155.

- [91] W. Siebert, S. Mai, R. Kober, and P. F. Heeckt, "Technique and first clinical results of robot-assisted total knee replacement," *The Knee*, vol. 9, no. 3, pp. 173–180, 2002.
- [92] W. Siebert, S. Mai, R. Kober, P. Heekt, A. DiGioia III, B. Jaramaz, F. Picard, and L. Nolte, "Total knee replacement: robotic assistive technique," *Computer and Robotic Assisted Hip and Knee Surgery*, p. 127, 2004.
- [93] B. Davies, F. R. y Baena, A. Barrett, M. Gomes, S. Harris, M. Jakopec, and J. Cobb, "Robotic control in knee joint replacement surgery," *Proceedings of the Institution of Mechanical Engineers, Part H: Journal of Engineering in Medicine*, vol. 221, no. 1, pp. 71–80, 2007.
- [94] B. D. Mittelstadt, P. Kazanzides, J. F. ZUHARS, B. Williamson, P. Cain, F. Smith, and W. L. Bargar, "The evolution of a surgical robot from prototype to human clinical use," *Computer-Integrated Surgery: Technology and Clinical Applications*, pp. 397–407, 1996.
- [95] M. Jakopec, S. Harris, F. Rodriguez y Baena, P. Gomes, J. Cobb, and B. Davies, "The first clinical application of a "hands-on" robotic knee surgery system," *Computer Aided Surgery*, vol. 6, no. 6, pp. 329–339, 2001.
- [96] M. Jakopec, S. J. Harris, P. Gomes, J. Cobb, B. L. Davies *et al.*, "The hands-on orthopaedic robot" acrobot": Early clinical trials of total knee replacement surgery," *IEEE Transactions on Robotics and Automation*, vol. 19, no. 5, pp. 902–911, 2003.
- [97] J. Cobb, J. Henckel, F. Rodriguez, and B. Davies, "Accuracy improves outcome in knee arthroplasty: five-year results of a prospective randomised controlled trial of robotic unicompartmental knee replacement," in *Proceedings of the IMechE Conference on Knee arthroplasty*, 2009, pp. 210–213.
- [98] P.-L. Yen and B. Davies, "Active constraint control for image-guided robotic surgery," *Proceedings of the Institution of Mechanical Engineers, Part H: Journal of Engineering in Medicine*, vol. 224, no. 5, pp. 623–631, 2010.
- [99] W. P. Geis, H. C. Kim, E. Brennan, P. C. McAfee, and Y. Wang, "Robotic arm enhancement to accommodate improved efficiency and decreased resource utilization in complex minimally invasive surgical procedures," *Studies in health technology and informatics*, pp. 471–481, 1996.
- [100] G. Ballantyne, P. Merola, A. Weber, and A. Wasielewski, "Robotic solutions to the pitfalls of laparoscopic colectomy," *Osp Ital Chir*, vol. 7, pp. 405–412, 2001.
- [101] N. Hockstein, C. Gourin, R. Faust, and D. Terris, "A history of robots: from science fiction to surgical robotics," *Journal of robotic surgery*, vol. 1, no. 2, pp. 113–118, 2007.
- [102] Da-Vinci-Surgery, "<http://www.davincisurgery.com/>," online, accessed: 24.01.2014.
- [103] K. Bhattacharya, "Kurt semm: A laparoscopic crusader," *Journal of minimal access surgery*, vol. 3, no. 1, p. 35, 2007.

- [104] P. Mouret, "How i developed laparoscopic cholecystectomy." *Annals of the Academy of Medicine, Singapore*, vol. 25, no. 5, p. 744, 1996.
- [105] T. Hu, P. K. Allen, T. Nadkarni, N. J. Hogle, and D. L. Fowler, "Insertable stereoscopic 3d surgical imaging device with pan and tilt," in *2nd IEEE RAS & EMBS International Conference on Biomedical Robotics and Biomechatronics*, 2008, pp. 311–316.
- [106] T. Hu, P. K. Allen, N. J. Hogle, and D. L. Fowler, "Insertable surgical imaging device with pan, tilt, zoom, and lighting," *The International Journal of Robotics Research*, 2009.
- [107] C. Hiroki, S. Ohno, Y. Ikemoto, and W. Yu, "A study on wire-wire driven abdominal cavity mobile micro robot," in *2010 IEEE/RSJ International Conference on Intelligent Robots and Systems (IROS)*, 2010, pp. 2816–2821.
- [108] D. Oleynikov, M. Rentschler, A. Hadzialic, J. Dumpert, S. Platt, and S. Farritor, "Miniature robots can assist in laparoscopic cholecystectomy," *Surgical Endoscopy And Other Interventional Techniques*, vol. 19, no. 4, pp. 473–476, 2005.
- [109] J. Hawks, J. Kunowski, and S. Platt, "In vivo demonstration of surgical task assistance using miniature robots," *IEEE Transactions on Biomedical Engineering*, vol. 59, no. 10, pp. 2866–2873, 2012.
- [110] S. Gorini, M. Quirini, A. Menciassi, G. Pernorio, C. Stefanini, and P. Dario, "A novel sma-based actuator for a legged endoscopic capsule," in *The First IEEE/RAS-EMBS International Conference on Biomedical Robotics and Biomechatronics*, 2006, pp. 443–449.
- [111] M. Quirini, A. Menciassi, S. Scapellato, C. Stefanini, and P. Dario, "Design and fabrication of a motor legged capsule for the active exploration of the gastrointestinal tract," *IEEE/ASME Transactions on Mechatronics*, vol. 13, no. 2, pp. 169–179, 2008.
- [112] M. Quirini, S. Scapellato, P. Valdastri, A. Menciassi, and P. Dario, "An approach to capsular endoscopy with active motion," in *29th Annual International Conference of the IEEE Engineering in Medicine and Biology Society*, 2007, pp. 2827–2830.
- [113] P. Glass, E. Cheung, and M. Sitti, "A legged anchoring mechanism for capsule endoscopes using micropatterned adhesives," *IEEE Transactions on Biomedical Engineering*, vol. 55, no. 12, pp. 2759–2767, 2008.
- [114] P. Glass, E. Cheung, H. Wang, R. Appasamy, and M. Sitti, "A motorized anchoring mechanism for a tethered capsule robot using fibrillar adhesives for interventions in the esophagus," in *2nd IEEE RAS & EMBS International Conference on Biomedical Robotics and Biomechatronics*, 2008, pp. 758–764.
- [115] B. Kim, S. Lee, J. Park, and J. Park, "Design and fabrication of a locomotive mechanism for capsule-type endoscopes using shape memory alloys (SMAs)," *IEEE/ASME transactions on mechatronics*, vol. 10, no. 1, pp. 77–86, 2005.

- [116] B. Kim, S. Park, C. Y. Jee, and S.-J. Yoon, "An earthworm-like locomotive mechanism for capsule endoscopes," in *2005 IEEE/RSJ International Conference on Intelligent Robots and Systems*, 2005, pp. 2997–3002.
- [117] B. Kim, S. Lee, J. H. Park, and J.-O. Park, "Inchworm-like microrobot for capsule endoscope," in *IEEE International Conference on Robotics and Biomimetics*, 2004, pp. 458–463.
- [118] B. Kim, S. Park, and J.-O. Park, "Microrobots for a capsule endoscope," in *IEEE/ASME International Conference on Advanced Intelligent Mechatronics*, 2009, pp. 729–734.
- [119] L. Kim, S. C. Tang, and S.-S. Yoo, "Prototype modular capsule robots for capsule endoscopies," in *13th International Conference on Control, Automation and Systems (ICCAS)*, 2013, pp. 350–354.
- [120] H. Fang, C. Wang, S. Li, K. Wang, and J. Xu, "A comprehensive study on the locomotion characteristics of a metameric earthworm-like robot," *Multibody System Dynamics*, vol. 35, no. 2, pp. 153–177, 2014.
- [121] W. Li, W. Guo, M. Li, and Y. Zhu, "A novel locomotion principle for endoscopic robot," in *Proceedings of the 2006 IEEE International Conference on Mechatronics and Automation*, 2006, pp. 1658–1662.
- [122] Y. Feng, W. Li, M. Li, and L. Sun, "Structure optimization of the endoscopic robot ciliary leg based on dimensional analysis," in *IEEE International Conference on Robotics and Biomimetics*, 2007, pp. 109–114.
- [123] G. Kósa, M. Shoham, and M. Zaaroor, "Propulsion method for swimming micro-robots," *IEEE Transactions on Robotics*, vol. 23, no. 1, pp. 137–150, 2007.
- [124] G. Kósa, P. Jakab, N. Hata, F. Jólesz, Z. Neubach, M. Shoham, M. Zaaroor, and G. Székely, "Flagellar swimming for medical micro robots: theory, experiments and application," in *2nd IEEE RAS & EMBS International Conference on Biomedical Robotics and Biomechatronics*, 2008, pp. 258–263.
- [125] S. Park, H. Park, S. Park, and B. Kim, "A paddling based locomotive mechanism for capsule endoscopes," *Journal of mechanical science and technology*, vol. 20, no. 7, pp. 1012–1018, 2006.
- [126] H. Park, S. Park, E. Yoon, B. Kim, J. Park, and S. Park, "Paddling based microrobot for capsule endoscopes," in *2007 IEEE International Conference on Robotics and Automation*, 2007, pp. 3377–3382.
- [127] C. A. Mosse, T. N. Mills, M. N. Appleyard, S. S. Kadiramanathan, and C. P. Swain, "Electrical stimulation for propelling endoscopes," *Gastrointestinal endoscopy*, vol. 54, no. 1, pp. 79–83, 2001.
- [128] S. Woo, J. Jang, E. Jung, J. Lee, Y. Moon, T. Kim, C. Won, H. Choi, and J. Cho, "Electrical stimuli capsule for control moving direction at the small intestine," in *Proceedings of the 24th IASTED International Conference on Biomedical Engineering*, 2006, pp. 311–316.

- [129] S. H. Woo, T. W. Kim, J. H. Lee, P. U. Kim, C. H. Won, and J. H. Cho, "Implemented edge shape of an electrical stimulus capsule," *The International Journal of Medical Robotics and Computer Assisted Surgery*, vol. 5, no. 1, pp. 59–65, 2009.
- [130] S. H. Woo, T. W. Kim, Z. Mohy-Ud-Din, I. Y. Park, and J.-H. Cho, "Small intestinal model for electrically propelled capsule endoscopy," *Biomedical engineering online*, vol. 10, no. 1, p. 1, 2011.
- [131] G. Tortora, P. Valdastri, E. Susilo, A. Menciassi, P. Dario, F. Rieber, and M. O. Schurr, "Propeller-based wireless device for active capsular endoscopy in the gastric district," *Minimally Invasive Therapy & Allied Technologies*, vol. 18, no. 5, pp. 280–290, 2009.
- [132] X. Zabulis, M. Sfakiotakis, and D. P. Tsakiris, "Effects of vibratory actuation on endoscopic capsule vision," in *30th Annual International Conference of the IEEE on Engineering in Medicine and Biology Society*, 2008, pp. 5901–5904.
- [133] A. Menciassi, P. Valdastri, K. Harada, and P. Dario, "Single and multiple robotic capsules for endoluminal diagnosis and surgery," in *2nd IEEE RAS & EMBS International Conference on Biomedical Robotics and Biomechatronics*, 2008, pp. 238–243.
- [134] R. Carta, G. Tortora, J. Thoné, B. Lenaerts, P. Valdastri, A. Menciassi, P. Dario, and R. Puers, "Wireless powering for a self-propelled and steerable endoscopic capsule for stomach inspection," *Biosensors and Bioelectronics*, vol. 25, no. 4, pp. 845–851, 2009.
- [135] Y. Yamagata and T. Higuchi, "A micropositioning device for precision automatic assembly using impact force of piezoelectric elements," in *1995 IEEE International Conference on Robotics and Automation*, vol. 1, 1995, pp. 666–671.
- [136] H. Li, K. Furuta, and F. Chernousko, "Motion generation of the capsobot using internal force and static friction," in *45th IEEE Conference on Decision and Control*, 2006, pp. 6575–6580.
- [137] —, "A pendulum-driven cart via internal force and static friction," in *2005 International Conference Physics and Control*, 2005, pp. 15–17.
- [138] M. Gao, C. Hu, Z. Chen, H. Zhang, and S. Liu, "Design and fabrication of a magnetic propulsion system for self-propelled capsule endoscope," *IEEE Transactions on Biomedical Engineering*, vol. 57, no. 12, pp. 2891–2902, 2010.
- [139] F. Volke, J. Keller, A. Schneider, J. Gerber, M. Reimann-Zawadzki, E. Rabinovitz, C. Mosse, and P. Swain, "In-vivo remote manipulation of modified capsule endoscopes using an external magnetic field," *Gastrointestinal Endoscopy*, vol. 67, no. 5, 2008.
- [140] S. Yim and M. Sitti, "Design and analysis of a magnetically actuated and compliant capsule endoscopic robot," in *IEEE International Conference on Robotics and Automation (ICRA)*, 2011, pp. 4810–4815.
- [141] —, "Design and rolling locomotion of a magnetically actuated soft capsule endoscope," *IEEE Transactions on Robotics*, vol. 28, no. 1, pp. 183–194, 2012.

- [142] S. Yim, K. Goyal, and M. Sitti, "Magnetically actuated soft capsule with the multimodal drug release function," *IEEE/ASME Transactions on Mechatronics*, vol. 18, no. 4, pp. 1413–1418, 2013.
- [143] G.-S. Lien, C.-W. Liu, J.-A. Jiang, C.-L. Chuang, and M.-T. Teng, "Magnetic control system targeted for capsule endoscopic operations in the stomach—design, fabrication, and in vitro and ex vivo evaluations," *IEEE Transactions on Biomedical Engineering*, vol. 59, no. 7, pp. 2068–2079, 2012.
- [144] Z. Liao, X.-D. Duan, L. Xin, L.-M. Bo, X.-H. Wang, G.-H. Xiao, L.-H. Hu, S.-L. Zhuang, and Z.-S. Li, "Feasibility and safety of magnetic-controlled capsule endoscopy system in examination of human stomach: a pilot study in healthy volunteers," *Journal of interventional gastroenterology*, vol. 2, no. 4, pp. 155–160, 2012.
- [145] J. Keller, C. Fibbe, F. Volke, J. Gerber, A. C. Mosse, M. Reimann-Zawadzki, E. Rabinovitz, P. Layer, and P. Swain, "Remote magnetic control of a wireless capsule endoscope in the esophagus is safe and feasible: results of a randomized, clinical trial in healthy volunteers," *Gastrointestinal endoscopy*, vol. 72, no. 5, pp. 941–946, 2010.
- [146] A. Moglia, A. Menciassi, M. Schurr, and P. Dario, "Wireless capsule endoscopy: from diagnostic devices to multipurpose robotic systems," *Biomedical microdevices*, vol. 9, no. 2, pp. 235–243, 2007.
- [147] X. Wang and M. Meng, "A magnetic stereo-actuation mechanism for active capsule endoscope," in *29th Annual International Conference of the IEEE Engineering in Medicine and Biology Society*, 2007, pp. 2811–2814.
- [148] R. Olfati-Saber, "Nonlinear control of underactuated mechanical systems with application to robotics and aerospace vehicles," Ph.D. dissertation, Massachusetts Institute of Technology, 2000.
- [149] A. de Luca, S. Iannitti, R. Mattone, and G. Oriolo, "Control problems in underactuated manipulators," in *IEEE/ASME International Conference on Advanced Intelligent Mechatronics*, vol. 2, 2001, pp. 855–861.
- [150] W. Wang, J. Yi, D. Zhao, and D. Liu, "Design of a stable sliding-mode controller for a class of second-order underactuated systems," *IEE Proceedings-Control Theory and Applications*, vol. 151, no. 6, pp. 683–690, 2004.
- [151] M.-S. Park and D. Chwa, "Swing-up and stabilization control of inverted-pendulum systems via coupled sliding-mode control method," *IEEE Transactions on Industrial Electronics*, vol. 56, no. 9, pp. 3541–3555, 2009.
- [152] W. N. White, M. Foss, J. Patenaude, X. Guo, and D. García, "Improvements in direct lyapunov stabilization of underactuated, mechanical systems," in *Proc. of the 2008 American Control Conference*, 2008, pp. 11–13.
- [153] W. N. White, M. Foss, and X. Guo, "A direct lyapunov approach for stabilization of underactuated mechanical systems," in *American Control Conference, 2007*, 2007, pp. 4817–4822.

- [154] I. Fantoni, R. Lozano, M. W. Spong *et al.*, “Energy based control of the pendubot,” *IEEE Transactions on Automatic Control*, vol. 45, no. 4, pp. 725–729, 2000.
- [155] R. Martinez, J. Alvarez, and Y. Orlov, “Hybrid sliding-mode-based control of underactuated systems with dry friction,” *IEEE Transactions on Industrial Electronics*, vol. 55, no. 11, pp. 3998–4003, 2008.
- [156] Y. Chen and A. Huang, “Controller design for a class of underactuated mechanical systems,” *Control Theory & Applications, IET*, vol. 6, no. 1, pp. 103–110, 2012.
- [157] M. A. Karkoub and M. Zribi, “Robust control schemes for an overhead crane,” *Journal of Vibration and Control*, vol. 7, no. 3, pp. 395–416, 2001.
- [158] G. Bartolini, N. Orani, A. Pisano, and E. Usai, “Load swing damping in overhead cranes by sliding mode technique,” in *Proceedings of the 39th IEEE Conference on Decision and Control*, vol. 2, 2000, pp. 1697–1702.
- [159] K.-K. Shyu, C.-L. Jen, and L.-J. Shang, “Design of sliding-mode controller for anti-swing control of overhead cranes,” in *31st Annual Conference of IEEE Industrial Electronics Society*, 2005, pp. 147–152.
- [160] N. B. Almutairi and M. Zribi, “Sliding mode control of a three-dimensional overhead crane,” *Journal of vibration and control*, vol. 15, no. 11, pp. 1679–1730, 2009.
- [161] M. Jankovic, D. Fontaine, and P. V. Kokotović, “A example: Cascade-and passivity-based control designs,” *IEEE Transactions on Control Systems Technology*, vol. 4, no. 3, p. 293, 1996.
- [162] A. Pavlov, B. Janssen, N. van de Wouw, and H. Nijmeijer, “Experimental output regulation for a nonlinear benchmark system,” *IEEE Transactions on Control Systems Technology*, vol. 15, no. 4, pp. 786–793, 2007.
- [163] D.-H. Kim and J.-H. Oh, “Tracking control of a two-wheeled mobile robot using input–output linearization,” *Control Engineering Practice*, vol. 7, no. 3, pp. 369–373, 1999.
- [164] R. Yu, Q. Zhu, G. Xia, and Z. Liu, “Sliding mode tracking control of an underactuated surface vessel,” *IET Control Theory & Applications*, vol. 6, no. 3, pp. 461–466, 2012.
- [165] K. D. Do, Z.-P. Jiang, and J. Pan, “Underactuated ship global tracking under relaxed conditions,” *IEEE Transactions on Automatic Control*, vol. 47, no. 9, pp. 1529–1536, 2002.
- [166] K. D. Do and J. Pan, “Robust path-following of underactuated ships: Theory and experiments on a model ship,” *Ocean Engineering*, vol. 33, no. 10, pp. 1354–1372, 2006.
- [167] A. Roberts and A. Tayebi, “Adaptive position tracking of vtol uavs,” *IEEE Transactions on Robotics*, vol. 27, no. 1, pp. 129–142, 2011.
- [168] T. Das and I. N. Kar, “Design and implementation of an adaptive fuzzy logic-based controller for wheeled mobile robots,” *IEEE Transactions on Control Systems Technology*, vol. 14, no. 3, pp. 501–510, 2006.

- [169] F. Raimondi and M. Melluso, "Fuzzy adaptive ekf motion control for non-holonomic and underactuated cars with parametric and non-parametric uncertainties," *IET Control Theory & Applications*, vol. 1, no. 5, pp. 1311–1321, 2007.
- [170] M.-D. Hua, T. Hamel, P. Morin, and C. Samson, "A control approach for thrust-propelled underactuated vehicles and its application to VTOL drones," *IEEE Transactions on Automatic Control*, vol. 54, no. 8, pp. 1837–1853, 2009.
- [171] E. Lefeber, K. Y. Pettersen, and H. Nijmeijer, "Tracking control of an underactuated ship," *IEEE transactions on control systems technology*, vol. 11, no. 1, pp. 52–61, 2003.
- [172] X. Chen, Y. Jia, and F. Matsuno, "Tracking control for differential-drive mobile robots with diamond-shaped input constraints," *IEEE Transactions on Control Systems Technology*, no. 99, 2014.
- [173] D. Chwa, "Tracking control of differential-drive wheeled mobile robots using a backstepping-like feedback linearization," *IEEE Transactions on Systems, Man and Cybernetics, Part A: Systems and Humans*, vol. 40, no. 6, pp. 1285–1295, 2010.
- [174] H. Dong, D. Sun, and S. K. Tso, "Tracking control of differential mobile robots using adaptive coupling scheme," in *7th International Conference on Control, Automation, Robotics and Vision*, vol. 3, 2002, pp. 1138–1143.
- [175] D. Sun, H. Dong, and S. K. Tso, "Tracking stabilization of differential mobile robots using adaptive synchronized control," in *IEEE International Conference on Robotics and Automation*, vol. 3, 2002, pp. 2638–2643.
- [176] W. Dong, "Tracking control of multiple-wheeled mobile robots with limited information of a desired trajectory," *IEEE Transactions on Robotics*, vol. 28, no. 1, pp. 262–268, 2012.
- [177] C.-L. Hwang and H.-M. Wu, "Trajectory tracking of a mobile robot with frictions and uncertainties using hierarchical sliding-mode under-actuated control," *IET Control Theory & Applications*, vol. 7, no. 7, pp. 952–965, 2013.
- [178] Z.-P. Jiang, E. Lefeber, and H. Nijmeijer, "Saturated stabilization and tracking of a nonholonomic mobile robot," *Systems & Control Letters*, vol. 42, no. 5, pp. 327–332, 2001.
- [179] A. Sanyal, N. Nordkvist, and M. Chyba, "An almost global tracking control scheme for maneuverable autonomous vehicles and its discretization," *IEEE Transactions on Automatic Control*, vol. 56, no. 2, pp. 457–462, 2011.
- [180] M. Cavdaroglu and N. Olgac, "Trajectory tracking of cart-pendulum dynamics using multiple time-delayed feedback," *IET Control Theory & Applications*, vol. 2, no. 6, pp. 458–466, 2008.
- [181] Minimotor, "<http://www.faulhaber-group.com/>," online, accessed: 02.07.2014.
- [182] Quintic-Biomechanics, "<http://www.quintic.com/>," online, accessed: 02.07.2014.

-
- [183] Olympus, “Endocapsule system. [http://www.olympus.co.uk/;](http://www.olympus.co.uk/)” online, accessed: 02.07.2014.
- [184] M. N. Huda and H. Yu, “Modelling and motion control of a novel double parallel mass capsbot,” in *18th World Congress of the International Federation of Automatic Control (IFAC)*, 2011, pp. 8120–8125.

